Remote sensing of boreal forest phenology: methods and applications

Dissertation

zur Erlangung des

Doktorgrades der Naturwissenschaften (Dr. rer. nat.)

Der

Naturwissenschaftlichen Fakultät III

Agrar- und Ernährungswissenschaften, Geowissenschaften und Informatik

der Martin-Luther-Universität

Halle-Wittenberg

vorgelegt

von Frau Kristin Böttcher

Gutacher:

Prof. Dr. Cornelia Gläßer

Prof. Dr. Patrick Hostert

Halle (Saale), 26.06.2019 (Tag der Verteidigung)

Acknowledgements

Zusammenfassung

Das Potential von Ökosystemen zur Bereitstellung von Leistungen, z.B. Kohlenstoff zu binden, wird vom phänologischen Zyklus der Vegetation stark beeinflusst. Informationen zum Zeitpunkt der Phänophasen werden daher benötigt, um den Einfluss des Klimawandels auf die boreale Nadelwaldzone, das größte Landökosystem der Erde, zu verstehen und vorherzusagen. Die meisten Fernerkundungsuntersuchungen zur Bestimmung von Phänophasen konzentrierten sich auf die Blattentfaltung und Blattverfärbung der laubabwerfenden Vegetation. Die entwickelten Verfahren beruhten zumeist auf der Nutzung von Vegetationsindizes, wie z.B. dem *Normalised Difference Vegetation Index*. Allerdings sind diese Verfahren zur Beobachtung des saisonalen Zyklus von Wachstum und Photosynthese in immergrünen Nadelwäldern der borealen Zone nur eingeschränkt nutzbar. Darüber hinaus sind optische Fernerkundungsverfahren bei zu geringem Sonnenstand im Herbst und Winter nicht anwendbar. Faktoren, die mit der Photosynthese korrelieren, wie Schneebedeckung und Bodenfrost, sind aus Fernerkundungsdaten ableitbar und könnten alternativ genutzt werden.

Diese Arbeit zielte daher auf die Entwicklung von Methoden zur Bestimmung des Zeitpunktes des Beginns und der Einstellung der photosynthetischen Aktivität immergrüner Nadelwälder auf der Basis von Satellitendaten zur Schneebedeckung und zum Bodenfrost. Aus MODIS (*Moderate Resolution Imaging Spectroradiometer*)-Daten abgeleitete Zeitserien zur prozentualen Schneebedeckung und auf SMOS (*Soil Moisture and Ocean Salinity*)-Daten basierende Informationen zum Bodenfrost wurden dafür erstmals eingesetzt. Messungen des Kohlenstoffflusses an drei Standorten in Finnland dienten als Referenz. Zur Bestimmung des Zeitpunktes des Endes der photosynthetischen Aktivität wurden zusätzlich Daten von drei Standorten in Kanada genutzt. Zum Vergleich mit Satellitendaten zum Bodenfrost wurde der Zeitpunkt des Luftfrosts aus ERA-Interim Reanalyse Daten abgeleitet. Ein, auf dem NDWI (*Normalised Difference Water Index*) basierendes, Verfahren zur Bestimmung der Blattentfaltung der Laubwälder wurde für Finnland angepasst und mit phenologischen Beobachtungen der Blattentfaltung ausgewertet.

Es wurde ein enger Zusammenhang des Beginns der photosynthetischen Aktivität mit der Schneeschmelze, und des Endes der photosynthetischen Aktivität mit dem Auftreten des ersten Luft-und Bodenfrostes festgestellt. Daher konnten diese Phänophasen aus den Zeitserien der prozentualen Schneebedeckung und des Bodenfrostes bestimmt werden. Im Vergleich zu den Satellitendaten zum Bodenfrost, wurde mit dem Tag des ersten Luftfrostes eine etwas höhere Genauigkeit für die Standorte erreicht. Der aus Satellitendaten abgeleitete Tag der Blattentfaltung zeigte eine gute Übereinstimmung mit den phänologischen Beobachtungen. Mit den Methoden konnten der Beginn und das Ende der photosynthetischen Aktivität über einen Zeitraum von 17, beziehungsweise, 6 Jahren in Finnland dargestellt werden.

Die für die Nadelwälder entwickelten Methoden schließen Lücken in der Beobachtung der Phänologie der borealen Zone und ergänzen damit vorhandene Methoden für die laubabwerfende Vegetation. Die Daten sind wichtig für die Einschätzung von Ökosystemleistungen und die Beobachtung der Biodiversität. Dies wurde in dieser Arbeit mit zwei Anwendungsbeispielen gezeigt, in denen die Daten zur Bewertung modellierter Phänophasen eines Biosphärenmodells und zur Vorhersage der Phänologie von pflanzenfressenden Insekten genutzt wurden.

Abstract

The phenological cycle of vegetation strongly influences the potential of ecosystems to provide services, e.g. to sequester carbon. To understand and to predict the impact of climate change on the boreal forest zone, the largest terrestrial biome, information on the timing of phenological events is needed. Most remote sensing studies have focussed on the detection of vegetation greening-up and senescence. However, methods based on vegetation indices, such as the normalised difference vegetation index, have limited use for monitoring the phenology of photosynthesis and growth in the evergreen forest type. Low illumination poses an additional challenge to optical remote sensing in autumn and winter. Alternatively, environmental variables that are correlated with photosynthesis, such as snow cover and soil freeze, can be observed with remote sensing.

Hence, this work focussed on the development of methods for the determination of the timing of recovery and cessation of photosynthesis in the evergreen boreal forest based on satellite observations of snow cover and soil freeze, respectively. For this, the applicability of the time series of fractional snow cover from the Moderate Resolution Imaging Spectroradiometer and soil freeze state from the Soil Moisture and Ocean Salinity mission were tested for the first time. The references for the start and end of the vegetation active period (VAPstart, VAPend) were obtained from three CO_2 flux measurements sites in Finland. Additionally, three sites from Canada were employed in the development of indicators for the VAPend. The date of first autumnal freeze from a reanalysis of the air temperature was investigated in comparison to satellite obtained soil freeze data. For the detection of vegetation greening in the deciduous forest, a method based on the normalised difference water index was applied and evaluated with birch bud breaking observations in Finland.

It was found that the recovery of photosynthesis in boreal evergreen forests is coupled with the timing of the snow melt. The VAPstart could be extracted from a snow cover time series with good accuracy on Finnish sites (R^2=0.89, root mean squared error (RMSE)=5.3 days). In autumn, the observed strong relationship between autumn air and soil freeze with the VAPend can be utilised to determine this event from the satellite-observed date of partially frozen soil (R^2=0.84, RMSE=7.5 days) but with lower accuracy than for the air temperature indicator (R^2=0.92, RMSE=5.2 days). The satellite-observed vegetation greening date showed good agreement with the birch bud breaking (R^2=0.75, RMSE=7.3 days). Methods were utilised to generate national-scale maps of the VAPstart and VAPend covering a period of 17 and 6 years, respectively.

The developed methods for the evergreen forest fill observational gaps in the monitoring of the phenology of the boreal forest zone and complement existing ones, targeting deciduous vegetation. The maps provide relevant information for the assessment of ecosystem services and the monitoring of biodiversity. This was demonstrated in two applications, the evaluation of the phenology of a biosphere model and the prediction of the phenology of herbivorous insects.

Contents

List of original publications and author's contribution

This thesis consists of an introductory overview and synthesis of the research reported in four articles (Appendices I-IV), which are referred to in the text by Roman numerals:

I. Böttcher, K., Aurela, M., Kervinen, M., Markkanen, T., Mattila, O.-P., Kolari, P., Metsämäki, S., Aalto, T., Arslan, A.N., Pulliainen, J. (2014). MODIS time-series-derived indicators for the beginning of the growing season in boreal coniferous forest — A comparison with CO_2 flux measurements and phenological observations in Finland. *Remote Sensing of Environment*, 140, 625-638.

II. Böttcher, K., Rautiainen, K., Aurela, M., Kolari, P., Mäkelä, A., Arslan, A.N., Black, T.A., Koponen, S. (2018). Proxy indicators for mapping the end of the vegetation active period in boreal forests inferred from satellite-observed soil freeze and ERA-Interim reanalysis air temperature. *Journal of Photogrammetry, Remote Sensing and Geoinformation Science,* 86 (3-4), 169–185.

III. Böttcher, K., Markkanen, T., Thum, T., Aalto, T., Aurela, M., Reick, C., Kolari, P., Arslan, A., Pulliainen, J. (2016). Evaluating biosphere model estimates of the start of the vegetation active season in boreal forests by satellite observations. *Remote Sensing*, 8, 580.

IV. Pöyry, J., Böttcher, K., Fronzek, S., Gobron, N. Leinonen, R., Metsämäki, S., Virkkala, R. (2018). Predictive power of remote sensing versus. temperature-derived variables in modelling of herbivorous insects. *Remote sensing in Ecology and Conservation*, 4, 113-126.

Supplementary materials for articles II−IV are provided in the Appendices SII-SIV.

In **Paper I,** K. Böttcher conceived and designed the study with participation of co-authors, developed the remote sensing method for the start of the vegetation active period in evergreen needle-leaved forest, made all data analysis, led the writing of the paper and prepared all figures, except Figure 2.

In **Paper II,** K. Böttcher conceived and designed the study with participation of co-authors, made the main part of the data analysis, led the writing of the paper and prepared all figures, except Figure 2.

In **Paper III,** K. Böttcher conceived and designed the study together with co-authors, adapted the remote sensing methods, analysed the remote sensing data and made comparisons with in situ observations and model results and interpreted results mainly together with T. Markkanen and T. Thum. K. Böttcher led the writing of the paper and prepared all figures, except Figures 4 and 5 by T. Thum.

In **Paper IV,** K. Böttcher participated in the study design, prepared the remote sensing observations on greening date, applied spatial prediction models to remote sensing and temperature data and prepared the maps. K.B. contributed to the writing of the paper, specifically to the remote sensing literature and methodology.

List of acronyms and symbols

AVHRR	Advanced Very High Resolution Radiometer
CA-Obs	Saskatchewan, Southern Old Black Spruce
CA-Ojp	Saskatchewan, Old Jack Pine
CA-Qfo	Quebec, Eastern Old Black Spruce
Doy	Day of year
EBV	Essential biodiversity variable
EVI	Enhanced vegetation index
FI-Hyy	Hyytiälä
FI-Ken	Kenttärova
FI-Sod	Sodankylä
FSC	Fractional snow cover
GPI	Gross photosynthesis index
GPP	Gross primary production
JSBACH	Jena scheme for biosphere-atmosphere coupling in Hamburg
MODIS	Moderate Resolution Imaging Spectroradiometer
NDVI	Normalised difference vegetation index
NDWI	Normalised difference water index
NEE	Net ecosystem exchange
SMOS	Soil Moisture and Ocean Salinity
SYKE	Finnish Environment Institute
UAV	Unmanned aerial vehicle
VAPend	End of the vegetation active period
VAPstart	Start of the vegetation active period
CBD	Convention of Biological Diversity (CBD)
RMSE	Root mean squared error

a	Slope parameter of the linear regression model for VAPend
b	Offset parameter of the linear regression model for VAPend
FSC_f	Interpolated FSC by fitting a sigmoid function to the time series
$NDVImin$	Minimum of the annual NDWI
R^2	Coefficient of determination
t	Time variable (doy)
x_1	Inflection point of sigmoid function
x_2	Parameter that controls the rate of change of the sigmoid function
ε	Estimate of the noise level in NDWI time series

1 Introduction

1.1 Phenology of boreal forests

The boreal zone is the largest terrestrial biome; it covers about 13% of the land area of the earth (Schultz 1995). Its subarctic climate is characterised by strong seasonality with long cold winters and short summers. The boreal zone is found throughout the northern hemisphere and is mainly characterised by needle-leaved trees (spruce, pine, larch and fir) and partly mixed forest, lakes, wetland and mires. The amount of stored carbon in the boreal zone is estimated to be larger than in the temperate and tropical forest (Ruckstuhl et al. 2008). A large part of it is stored in permafrost soil and wetlands. The boreal forests contribute 22% of the global forest carbon sink and were a consistent sink of carbon for two decades 1990-2007 (Pan et al. 2011).

Plant species in the boreal zone are adapted to extreme conditions, cold temperatures, limited nutrients, frost and snow cover. Evergreen and deciduous trees have adapted differently to cope with the climate conditions and to maximise carbon gains. To prevent frost damage in winter, trees go through biochemical modifications and enter winter dormancy. In evergreen trees, the recovery of photosynthetic activity in spring occurs before visual signs of growth (Suni et al. 2003a). In contrast, the photosynthetic recovery in the deciduous broad-leaved forest is closely linked to the development of the leaves (Baldocchi et al. 2005). For both, deciduous and evergreen trees, the main driver of spring development is the increase in the air temperature (Linkosalo et al. 2009; Suni et al. 2003b). The response to the temperature and photoperiod varies according to the species, provenance, geographic location and tree age. Prevalent deciduous tree species in the boreal forest zone are pioneer species, such as birch and poplars, which are less photo-sensitive than tree species which occur further south in the temperate zone (Körner and Basler 2010). The relative importance of the temperature, photoperiod and other factors on leaf senescence, cessation of growth and downregulation of photosynthesis are still under debate. Evergreen trees develop frost hardiness and enter dormancy to avoid frost damage in the winter. The shortening of the photoperiod and decreasing temperature are the main drivers for the decrease in photosynthetic capacity and the cessation of growth (Bauerle et al. 2012; Öquist and Huner 2003; Sevanto et al. 2006; Suni et al. 2003a; Vesala et al. 2010; Vogg et al. 1998).

The seasonal cycle of vegetation plays an important role in ecosystem processes; it directly influences the water, carbon and nutrient cycle and is thus important for many ecosystem services, such as carbon sequestration and forest timber production. It has been found that the description of vegetation phenology needs improvement in global earth system models (Mahowald et al. 2015)

and more validation and calibration for the boreal zone (Melaas et al. 2013b; Richardson et al. 2012) to accurately simulate carbon balances. Shortcomings in the description of the phenological cycle in the models have a considerable impact on the predicted gross primary production (Jeong et al. 2012; Picard et al. 2005; Richardson et al. 2012).

Furthermore, vegetation feedback to the climate system is strongly linked to phenology through changes in albedo, surface roughness length, canopy conductance and the water and surface energy budget (Figure 1, Peñuelas et al. 2009; Richardson et al. 2013). The timing of the spring recovery of forests is important also for the formation of aerosols. Dal Maso et al. (2009) found that during the spring recovery of photosynthesis, biogenic volatile compound emissions from the boreal ecosystems have a larger potential to form atmospheric aerosol particles than later in the year. Phenology is also important for the distribution and survival of species (Chuine 2010). It has been proposed as one of the essential biodiversity variables (EBVs) (Pereira et al. 2013) that will support the monitoring of changes in biodiversity and progress towards global conservation targets set by the Convention of Biological Diversity (CBD) at the Aichi conference (O'Connor et al. 2015; Secades et al. 2014; Skidmore et al. 2015; Vihervaara et al. 2017).

Because of its sensitivity to changes in the climate, phenology is utilised as an indicator for the long-term biological impacts of climate change on terrestrial ecosystems (Menzel and Fabian 1999; Menzel et al. 2006; Richardson et al. 2013; Schwartz 1998). In the northern latitudes, the increase in observed annual mean temperatures for the period 1901-2005 (Räisänen and Tuomenvirta 2009) and the projected 21st century change in surface temperature were higher than the annual mean global warming (IPCC 2013). For most parts of the boreal zone a long-term increase in precipitation is projected (Räisänen and Tuomenvirta 2009). The projected changes are not spatially uniform. The warming climate and the increasing atmospheric CO_2 concentrations have already affected and will affect biophysical processes in boreal forests in the future, since the photosynthesis rate increases with the increase in CO_2 concentrations and the regulation of the annual cycle of vegetation, and the decomposition of soil organic matter are strongly influenced by temperature (Hari et al. 2009). Already today, the boreal region is an area which is undergoing fast phenological change (Buitenwerf et al. 2015). The timing and the length of the snow melt has changed (Anttila et al. 2018; Metsämäki et al. 2018). The growing season has extended, but the nature of the underlying phase shifts have varied from region to region (Buitenwerf et al. 2015). In the boreal areas in Europe, both satellite and in situ observations have shown a trend towards an earlier start of the growing season (Delbart et al. 2008; Ivits et al. 2012; Linkosalo et al. 2009; Pudas et al. 2008) with the exception of some areas (e.g. Shutova et al. 2006). Warmer spring temperatures have caused an earlier onset of photosynthesis in evergreen forests, which has

resulted in enhanced carbon sequestration (Black et al. 2000; Pulliainen et al. 2017; Richardson et al. 2009). Trends in autumn phenology and their effect on the carbon balance are less certain.
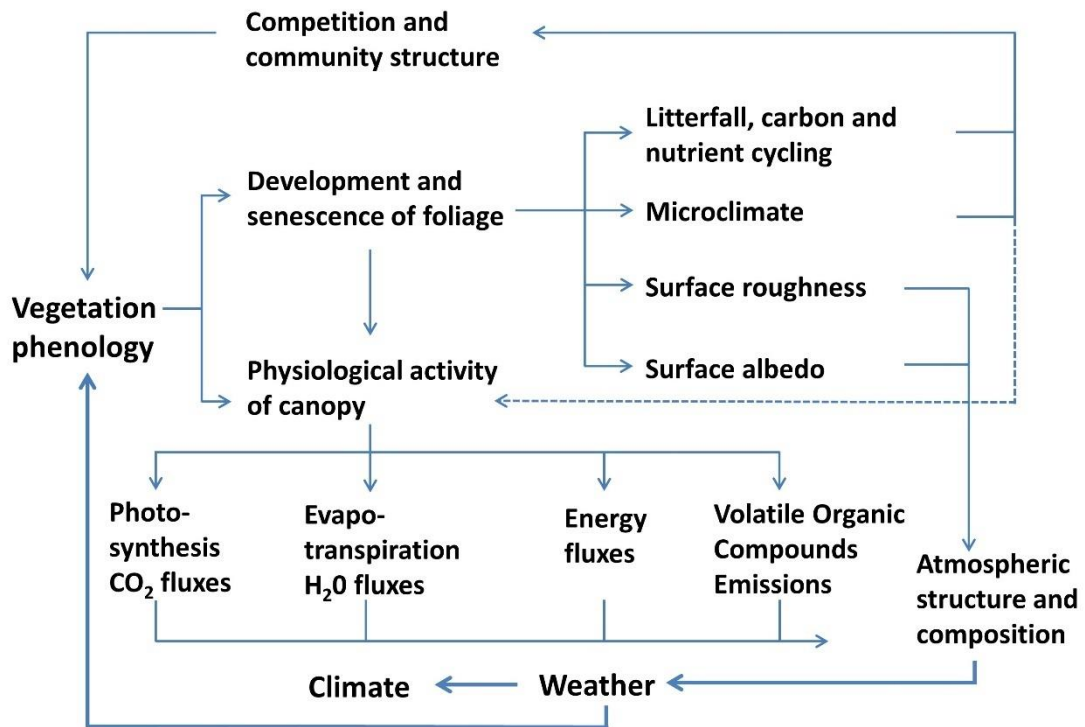
Figure 1. Feedback between vegetation and the climate system that are influenced by the vegetation phenology (redrawn from Richardson et al. 2013).

Furthermore, plant and animal species respond to changes in climate with changes in their range and abundance (Fitchett et al. 2015, Pecl et al. 2017). For example, some species may adapt to warmer climates through spatial migration (Jeganathan et al. 2014), such as a northward shift of the tree line or range shifts of insect communities (Pöyry et al. 2009). Potentially, such changes may lead to mismatches of animal production and the availability of food (Fitchett et al. 2015; Ruckstuhl et al. 2008). A better trophic match between insects and the host plants may lead to a higher risk of insect damage. These phenological mismatches are of concern for the survival of some species and will result in changes in the ecosystem composition and processes (Foster et al. 2013; Pureswaran et al. 2015).

1.2   Observation of vegetation phenology and the contributions of remote sensing

Phenology is defined as "*the study of the timing of recurring biological events, the causes of their timing with regard to biotic and abiotic forces and the interrelation among phases of the same or different species*" (Lieth 1974). Plant phenology has traditionally been studied by observing visual signs of plant development, such as bud break and leaf senescence. As an extension to the traditional concept, *vegetation photosynthetic phenology* can be studied on the ecosystem scale based on eddy covariance measurements of the exchange of carbon between the land surface and the atmosphere (Gu et al. 2009; Gu et al. 2003). The eddy covariance method measures the net ecosystem exchange (NEE) of CO_2, i.e. the difference between ecosystem gross primary production (GPP) and respiration. To describe the seasonal dynamics of plant community photosynthesis, phenological indicators have been determined from the measured NEE or GPP (Gu et al. 2009; Gu et al. 2003; Richardson et al. 2010; Suni et al. 2003b). These indicators can be used to analyse differences in the seasonal cycle of photosynthesis of different vegetation types and their responses to climate conditions.

Recently, digital repeat photography has been established as a method for monitoring phenological events (Richardson et al. 2007; Sonnentag et al. 2012) and as a ground truth source for remote sensing observations (Hufkens et al. 2012; Klosterman et al. 2014). Web camera networks have been set up in different parts of the world, for example in North America (Richardson et al. 2018) and Finland (Peltoniemi et al. 2018b). These near-surface observations with networked digital cameras (webcams) provide images of the vegetation at regular intervals at a high temporal resolution and, hence, allow for consistent and objective analyses of phenological changes in vegetation and snow cover.

Still, such ground observations are available only in certain locations and do not represent the boreal forest zone adequately (Falge et al. 2017). Instead, satellite remote sensing provides a means to extrapolate information from scarce ground-based observations across large geographical areas. It can provide observations in regions where ground-based observations are challenging or not feasible (Bonan 2008; Yang et al. 2012). The scale of medium (100 m−1 km) to low resolution (<1 km) satellite observations corresponds to that of the climatological drivers of phenology and is applicable for global climate and biosphere models. Hence, satellite-observed phenology can provide valuable information for the improvement of the description of the phenology in global terrestrial biosphere models (Richardson et al. 2012) and can also contribute to a more accurate presentation of the annual carbon balance and its response to climate variability (Dalmonech and Zaehle 2013; Luo et al. 2012). Satellite-observed vegetation phenology is potentially useful also for studying connections between vegetation and animal phenology. So far very few studies have

used such information for the prediction of animal phenology. Studies using remote sensing have mostly focussed on the spatial prediction of species occurrence (Leyequien et al. 2007; Pettorelli et al. 2014) with some exceptions that have targeted the temporal occurrence of insect abundances (Jepsen et al. 2009; Olsson et al. 2016; Spruce et al. 2011).

Satellite remote sensing of vegetation phenology differs from traditional observations of phenological events of specific plant species that are made in situ (e.g. the bud break of leaves), since it integrates information across the pixel footprint. To account for this difference, the term *land surface phenology* has been introduced and is defined as *"the seasonal pattern of variation in vegetated land surfaces observed from remote sensing"* (Friedl et al. 2006). Satellite observations have been utilised to monitor land surface phenology since the 1980s using observations from the Advanced Very-High-Resolution Radiometer (AVHRR). For this, mainly the normalised difference vegetation index (NDVI) has been applied (Goward et al. 1985; Justice et al. 1985; Moulin et al. 1997; Reed et al. 1994; Reed et al. 2009; White et al. 1997). The NDVI is calculated by rationing the difference between observed reflectances in the near-infrared and red bands to the sum of the two reflectance values (Deering (1978) in Jackson and Huete 1991). The enhanced vegetation index (EVI) was developed to improve the low sensitivity of the index in high biomass regions and to reduce the influence of the soil and atmospheric background on the vegetation signal (Huete et al. 2002). The EVI has served as baseline index for the operational global Land Cover Dynamics product (MCD12Q2) from the Moderate Resolution Imaging Spectrometer (MODIS) (Ganguly et al. 2010). The functionally equivalent two-band EVI (EVI2) is applied to derive global land surface phenology products from the Visible Infrared Imaging Radiometer Suite (VIIRS) data that is used to continue the MODIS time series (Zhang et al. 2018b; Zhang et al. 2017).

A range of methods have been developed to extract phenological events from time series of vegetation indices. They consist of two main types:

(i) The seasonal cycle of vegetation is approximated by mathematical functions, e.g. a logistic function, and phenological events are extracted from the modelled seasonal cycle (Beck et al. 2006; Fischer 1994; Gonsamo et al. 2012; Hmimina et al. 2013; Jönsson and Eklundh 2004; Soudani et al. 2008; Zhang et al. 2006).

(ii) Absolute or relative vegetation index threshold values of the annual amplitude (Badeck et al. 2004; White and Nemani 2006; White et al. 1997) or pixel-based threshold values (Karlsen et al. 2006; Karlsen et al. 2008) are utilised to determine phenological events.

A direct linkage between satellite and phenological observations is challenging (White et al. 1997). Type (i) methods assume that true vegetation phenological development can be described by a mathematical function. This may not be achievable for different vegetation types and when making assessments on a regional and even global scale (Cong et al. 2012). In addition, vegetation disturbances can alter the vegetation index temporal profile considerably (Potter et al. 2003). Similarly, the ecological meaning of a vegetation index threshold value for type (ii) methods may vary for different vegetation types and ecosystems. Furthermore, the comparison between ground observations and medium- and low-resolution satellite observations is handicapped by a mismatch in scale. This mismatch has been recognised as a major source of uncertainty in the detection of phenological events from satellite observations (Badeck et al. 2004; Doktor et al. 2009; Liang et al. 2011).

Additional challenges for the observation of phenology using vegetation indices in the boreal region are: the short vegetation growing period, the dominance of evergreen trees, seasonal snow cover, long periods of cloud cover and the low solar elevation in autumn. The short growing period limits the time frame for observations. The change from the dormant to the active period usually occurs very fast and photosynthesis recovers in coniferous forest before the snow is completely melted (Thum et al. 2009). Snow strongly alters the surface reflectance and affects vegetation indices, such as NDVI. In deciduous boreal forest, the vegetation greening may be detected too early from the NDVI signal because of its increase during snow melt (Delbart et al. 2005; Moulin et al. 1997; White et al. 1997). In evergreen forests in Sweden, snow dynamics explained about 90% of the change in the vegetation index compared to 10% for changes in needle biomass. New buds in spring account only for a very small proportion of the overall green biomass and vegetation index thresholds were not useful for the detection of phenological events in evergreen trees (Jönsson et al. 2010).

As a consequence of limitations of the NDVI in the boreal region, methods have been proposed to reduce the effect of snow on the vegetation index signal (Delbart et al. 2005; Gonsamo et al. 2012; Karlsen et al. 2006, Jin and Eklundh 2014) and to track the leaf area index of evergreen forests (e.g. Jin and Eklundh 2014; Stenberg et al. 2004). Based on the separation of snow dynamics from the vegetation cycle, e.g. by using the normalised difference water index (NDWI), good agreement has been achieved between ground observations of leaf unfolding of deciduous trees and the satellite-detected greening-up of vegetation in boreal regions (Delbart et al. 2006; Gonsamo and Chen 2016). The NDWI is calculated as the normalised difference of reflectances in the near-infrared and the shortwave infrared bands (Gao 1996) and allows to distinguish snow melt and greening-up (Delbart et al. 2005). The detection of autumn senescence has been found to be less accurate when compared to phenological observations, although reasonable agreement has been

achieved in comparison to carbon flux measurements (Gonsamo et al. 2012). The lower performance for the detection of autumn phenological events may be due to the higher spatial heterogeneity of autumn senescence compared to the green-up and to low illumination and frequent overcast conditions. In addition, pest outbreaks may cause defoliation of trees in large areas that could be falsely detected as leaf fall from satellite observations. While the above methods are applicable for the detection of greening-up and leaf senescence in deciduous vegetation, they showed large deviations to observations from eddy covariance measurement sites for evergreen forest (Melaas et al. 2013b; Richardson et al. 2010).

Photosynthetic activity in evergreen needle-leaved forests starts before changes in the canopy structure and ends later than growth. With regard to the monitoring of photosynthesis, satellite observations of sun-induced chlorophyll fluorescence offer new opportunities compared to traditional vegetation indices. It has been shown that satellite-observed sun-induced chlorophyll fluorescence is linked to gross photosynthesis of ecosystems (Frankenberg et al. 2014; Joiner et al. 2014; Walther et al. 2016). Currently, observations have a large footprint and furthermore the noise in the signal increases with low solar elevation, which limits the application in the autumn in boreal regions. Alternatively, environmental variables that correlate with photosynthesis, such as temperature (Sims et al. 2008), soil freeze (Barichivich et al. 2013; Barr et al. 2009; Jarvis and Linder 2000), snow cover, and incoming radiation could help to track seasonal changes in photosynthesis in boreal evergreen forests with satellite observations. In this respect, the strong albedo (the fraction of the incoming solar radiation that is reflected hemispherically by the surface) change due to the spring snow melt has been suggested as an indicator for detection of the onset of photosynthesis (Thum et al. 2009). The spring snowmelt controls the soil temperature and moisture and, therefore, has a direct influence on the recovery of photosynthesis (Monson et al. 2005). Thus, snow melt may serve as an indicator of the start of vegetation activity in boreal evergreen forests. Snow cover can be observed with optical satellite instruments due to its high reflectance in the visible wavelength range. The reflectance difference between visible (green) and the shortwave-infrared wavelength regions is widely utilised for snow detection with the normalised difference vegetation index (NDSI) (Hall et al. 1995). For the boreal forest and tundra belt, a method for the detection of fractional snow cover (FSC) was developed by Metsämäki et al. (2012) and was later adapted for continental and global snow mapping (Metsämäki et al. 2012; Metsämäki et al. 2015). The method accounts for the forest canopy effect on the observed reflectance and thus, it provides high retrieval accuracies for boreal forests (Metsämäki et al. 2012; Metsämäki et al. 2015) and allows the monitoring of spring snow melt in boreal areas.

In the autumn, low solar elevation restricts observations with optical instruments. Additionally, frequent cloud cover prevents observation of the surface conditions at this time of the year. Very

few studies have used satellite observations outside the optical wavelength range for the detection of phenology events based on satellite-observed landscape freeze (Bartsch et al. 2007; Kimball et al. 2004). Soil freeze blocks the water transport from the soil to the trees and could therefore have a more direct effect on photosynthesis (Hölttä et al. 2017). Soil freeze can be detected from active and passive microwave observations (Bartsch et al. 2007; Derksen et al. 2017; Kim et al. 2011; Kimball et al. 2004; Rautiainen et al. 2016; Roy et al. 2015; Smith et al. 2004), which are independent of weather conditions and the low solar elevation. New observations on the soil freeze state from L-band (1−2 GHz) active radar and passive microwave radiometers (Derksen et al. 2017; Rautiainen et al. 2016; Roy et al. 2015) have a higher emission depth, and lower sensitivity to vegetation and snow cover compared to observations from higher frequency bands (Kim et al. 2011; Kimball et al. 2004) and, therefore, they provide good possibilities for monitoring the soil freeze.

2   Objectives of this work

This work contributes to the development of remote sensing methods for the monitoring of the phenology of photosynthesis in evergreen needle-leaved forests. Current operational satellite methods based on vegetation indices, show large biases against in situ carbon flux measurements for this forest type. This work focussed, therefore, on the usability of remote sensing observations of environmental factors that influence photosynthesis for the detection of the start and end dates of the vegetation active period. The vegetation active period is defined as the time period when the vegetation assimilates carbon through photosynthesis. Satellite observed FSC and soil freeze were analysed in comparison to reference dates for the start (VAPstart) and end (VAPend) of the vegetation active period from carbon flux measurement sites. The observed relationships were utilised to build proxy indicators for the mapping of the VAPstart and VAPend. Further, a method for the detection of the greening-up of vegetation was adapted and evaluated for the Finnish area. Hereafter, derived map products for the VAPstart were applied in two important areas: carbon balance modelling and biodiversity monitoring.

The specific objectives of this work were:

1. The development of remote sensing methods for the determination of the VAPstart and VAPend in evergreen needle-leaved forest in the boreal forest region;
    a) Analysis of the usability of satellite-observed snow cover for the detection of the VAPstart;
    b) Analysis of the usability of satellite-observed soil freeze for the detection of the VAPend;
2. Evaluation of the NDWI-based method for the detection of the greening-up of deciduous broad-leaved forest in Finland;
3. Assessment of the performance of a simulated VAPstart from a large-scale biosphere model with remote sensing observations in Finland;
4. Investigation of the benefits of using satellite-observed vegetation greening-up to predict animal phenology.

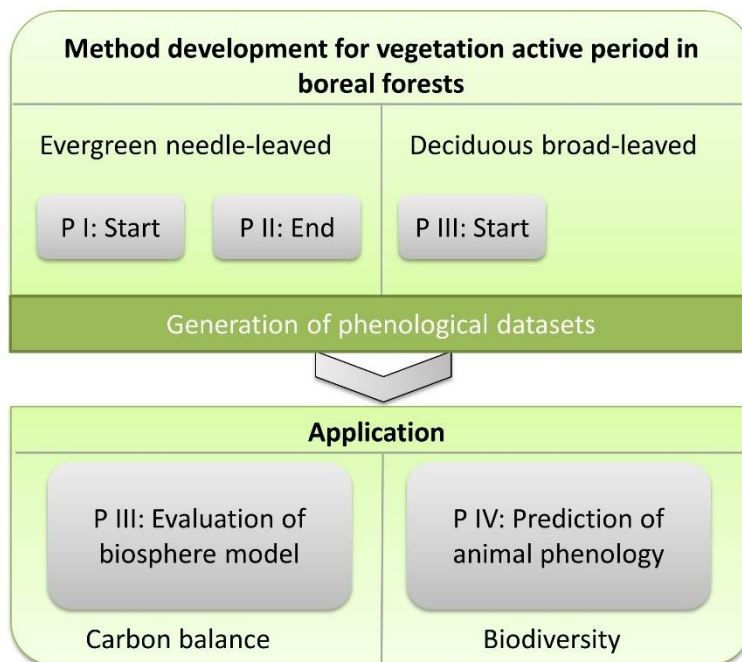**Figure 2. Relation of research papers (P). Roman numerals for the papers correspond to the list of original publications.**

The first objective was addressed with two research articles (Figure 2). Paper **I** responds to objective 1a. The feasibility of snow cover as a proxy indicator for mapping the VAPstart was assessed at three eddy covariance sites in Finland. For this, an FSC time series, calculated from

MODIS observations, was utilised. The performance of the indicator based on the FSC data was compared to commonly used vegetation indices.

In Paper **II** (objective 1b), the soil freeze state detected from SMOS L-Band passive microwave observations was tested as an indicator for the VAPend in evergreen needle-leaved forests. CO_2 flux measurement sites in Finland and Canada were employed in this study. The results were compared to an autumnal freeze indicator from ERA-Interim reanalysis air temperature data. In Paper **III**, the applicability of the NDWI-method (Delbart et al. 2005) for the detection of the greening-up in Finland was evaluated with bud break observations of birch trees (objective 2).

The developed methods for detecting the VAPstart in boreal forests (objective 1a and 2) were utilised to generate maps for the Finnish area. These data sets formed the base for responding to objectives 3 and 4. Paper **III** addresses the need to evaluate simulated phenology in global biosphere models. The simulated VAPstart in the Jena scheme for biosphere-atmosphere coupling in Hamburg (JSBACH) model was assessed. In Paper **IV**, satellite observations on the timing of the vegetation greening-up were utilised, among other explanatory variables, for spatial predictions of the peak flying period of nocturnal moths. Nocturnal moths are an important part of global biodiversity. They provide food for many other species and pollinate plants but can also act as pests.

The contributions of the research papers to the objectives are compiled in the following chapters. In Chapter 3 the materials and methods are briefly introduced. The main results related to the four objectives are presented in Chapter 4. This is followed by a discussion of the implications of the research results, their reliability and validity and recommendations for future work in Chapter 5. The overall conclusions are presented in Chapter 6.

3   Material and methods

3.1   Study area and measurement sites

The main study area for this thesis is the area of Finland, located at 60-70°N, 20-30°E (Figure 3). The average temperature of the coldest month is below -2°C and the average temperature of the warmest month is above 10°C (Pirinen et al. 2012). Seasonal snow cover settles during November to December and covers northern and southern Finland for six and four months (Kuusisto 1984), respectively. Most of the area belongs to the boreal forest zone, except the southern coastal areas and the hemi-arctic areas in northern Lapland. The dominant land cover type is forest, covering

44% of the area, followed by shrubs and herbaceous vegetation, inland waters and wetlands and agricultural land (Härmä et al. 2005). Evergreen needle-leaved forests are the major forest type with dominant tree species Scots pine (*Pinus sylvestris* L., 67%) and Norway spruce (*Picea abies* L., 22%). The main deciduous species is birch (10%, *Betula pendula* Roth *and pubescens* Ehrh.). Deciduous broad-leaved forests are common in the southwestern coastal areas and in the northern fell areas where mountain birch forest is common.

Three eddy covariance measurement sites in evergreen forests in Finland were used in this work (Paper **I−III**): Hyytiälä, Kenttärova and Sodankylä (Figure 3, Table 1, Figure 4). Additionally, three measurement sites in the southern boreal zone in Canada were utilised in Paper **II** to obtain a wider spatial coverage within the boreal forest zone (Table 1). Visual phenological observations concerning pine (4 sites) and birch (8 sites) trees were obtained from the Natural Resources Institute Finland.
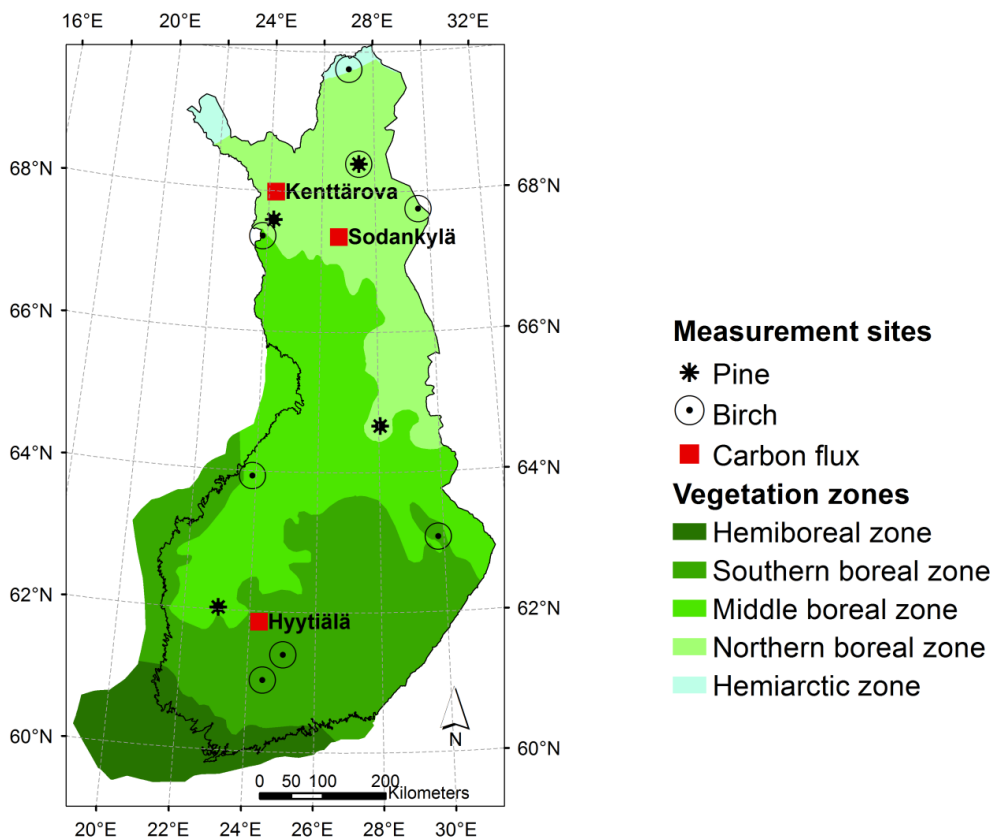
Figure 3. CO₂ flux measurement and phenological sites in Finland (data sources: Vegetation zones © SYKE 2015).

Table 1. CO$_2$ flux measurement sites that were used in this work and the papers in which they were employed (extract from Table 1 in Paper II).

Site	Name	Latitude, longitude (decimal degrees)	Altitude above sea (m)	Forest type	Paper
FI-Hyy	Hyytiälä	61.85 N, 24.29 E	170	Scots pine/ Norway spruce	**I, II, III**
FI-Ken	Kenttärova	67.99 N, 24.24 E	347	Norway spruce	**I, II**
FI-Sod	Sodankylä	67.36 N, 26.64 E	179	Scots pine	**I, II, III**
CA-Obs	Saskatchewan, Southern Old Black Spruce	53.99 N, 105.12 W	629	Mature black spruce	**II**
CA-Ojp	Saskatchewan, Old Jack Pine	53.92 N, 104.69 W	579	Mature jack pine	**II**
CA-Qfo	Quebec, Eastern Old Black Spruce	49.69 N, 74.34 W	382	Mature black spruce	**II**

(a)

(b)

(c)

(d)

Figure 4. Typical landscape view at the CO$_2$ flux measurement sites at Sodankylä (a, b) and Kenttärova (c), and the forest canopy view at Hyytiälä (d). At Sodankylä, the pictures were taken on 22 March 2010 (a) and during snow melt on 05 May 2011 (b). At Kenttärova, the image was taken from the eddy covariance tower on 8 June 2013. The Hyytiälä web camera image was taken on 28 October 2014.

3.2 Ground reference data

For evergreen needle-leaved forests, the VAPstart and VAPend were defined from eddy covariance measurements. The day on which the CO_2 uptake exceeded or fell below a certain threshold level of the growing season maximum was defined as the VAPstart and VAPend (Paper **I**, Paper **II**). In practice, the dates were obtained from the annual cycle of the gross photosynthesis index (GPI) (Aurela et al. 2001), which indicates the photosynthetic capacity of the ecosystem on a daily time scale. The photosynthetic recovery and downregulation are gradual processes and it is, therefore, difficult to define specific dates for these events from carbon flux measurements. In Paper **I**, a threshold level of 15% of the GPI was utilised to define the VAPstart. In Paper **II**, two additional threshold values for the determination of the VAPend (5% and 10%), were included in the analysis (Table 2). Visual phenological observations of pine growth (May shoot) were utilised in addition to the VAPstart in Paper **I** (Table 2). Supplementary meteorological measurements (air and soil temperature, soil water content, snow depth) were obtained from CO_2 flux sites, meteorological stations and the distributed network of soil moisture and soil temperature observations at the Sodankylä research station (Ikonen et al. 2016).

Eddy covariance measurements are not available for deciduous forest ecosystems in Finland. For this reason, bud break observations of birch (*Betula pubescens* Ehrh.) trees were utilised for the evaluation of satellite observations for the vegetation greening-up of deciduous vegetation in Paper **III**.

3.3 Spatial data sets

MODIS and SMOS satellite observations were the main data sources used in this work. For the estimation of the VAPstart in Paper **I**, FSC daily time series from MODIS (Metsämäki et al. 2012) were applied. The commonly used NDVI and the NDWI were tested as well. For the determination of the VAPend in Paper **II**, time series of soil freeze and thaw states from the SMOS mission were utilised (Rautiainen et al. 2016). In addition, an indicator of the autumnal freeze, based on ERA-Interim reanalysis air temperature data, was calculated (Table 3). Daily time series of the NDWI were employed for the detection of the greening-up of vegetation (Delbart et al. 2005). The data sets are summarized in Table 3. Details on the data processing are given in the respective papers. Here, only some important steps are reported.

Table 2. Ground reference data for the calibration and validation of satellite methods and the papers in which they were employed.

	Phenological event	Definition	Abbreviation	Paper
CO_2 flux measurements	Start of the vegetation active period in evergreen needle-leaved forests.	The day on which the gross photosynthesis index exceeds the 15% threshold of its growing season maximum.	VAPstart	**I, III**[a]
	End of the vegetation active period in evergreen needle-leaved forests.	The day on which the gross photosynthesis index falls below the threshold values 15%, 10%, 5% of its growing season maximum.	$VAPend_{15}$[b] $VAPend_{10}$ $VAPend_5$	**II**
Visual observations of tree phenology	Shoot elongation of Scots pine trees (*Pinus sylvestris L.*).	The beginning of shoot elongation of Scots pine trees (BBCH30, Meier 1997) (Kubin et al. 2007).	May shoot	**I**[c]
	Bud break of birch trees (*Betula pubescens Ehrh.*).	At least 50% of the buds must have broken throughout the tree crown (BBCH07, Meier 1997) (Kubin et al. 2007).	Bud break	**III**

[a] In Papers **I** and **III** the same reference values for the start of the vegetation active period were utilised, however the abbreviations are not consistent. In Paper **I**: the VAPstart is referred to as the growing season start date (GSSD) and in Paper **III** as the start of the vegetation active season in evergreen needle-leaved forests from eddy covariance measurements (ENF_SOS_{EC}).
[b] Subscripts refer to threshold values of gross photosynthesis index.
[c] In Paper **I**, May shoots are referred to as the growth of pine start date (GPSD).

Cloud masking of the MODIS data was carried out with an operational algorithm produced by the Finnish Environment Institute (SYKE) (Metsämäki et al. 2015). An important step for the comparison with ground reference data was the selection of homogenous areas in terms of land cover and elevation around the carbon flux measurement and the phenological sites. This was done to minimise the influence of noise and missing observations in the satellite data. Vegetation indices and FSC observations were averaged for all the pixels of the selected homogenous area. NDVI and NDWI time series were interpolated and smoothed with the adaptive Savitzky-Golay filter (Chen et al. 2004; Jönsson and Eklundh 2004; Savitzky and Golay 1964).

Table 3. Data sets for the detection of the start and end of the vegetation active period in boreal forests, and the papers in which they were employed.

Data set	Product	Spatial grid; resolution	Time periods	Paper
Daily Terra/MODIS –level-1B	Normalised difference vegetation index (NDVI)	Latitude/ longitude WGS-84; 0.0025°× 0.0025°	2001-2010	**I**
	Normalised difference water index (NDWI) (Gao 1996)	Latitude/ longitude WGS-84; 0.005°× 0.005°	2001−2010, 2001−2012, 2011−2017	**I, III, IV**
	Fractional snow cover (FSC) (Metsämäki et al. 2012)	Latitude/ longitude WGS-84; 0.005°× 0.005°	2001−2010, 2011−2017	**I, III**
Daily gridded level 3 brightness temperatures from the Centre Aval de Traitment des Données SMOS (Al Bitar et al. 2017)	Soil freeze and thaw state (Rautiainen et al. 2016)	Equal area Scalable earth (EASE) grid 2.0 (Brodzik et al. 2012); 25 km × 25 km	2010−2016	**II**
ERA-Interim global atmospheric reanalysis air temperature (2 m) (Dee et al. 2011)	First date of autumnal freeze (day of year) defined as the first the day when 10-day average air temperature ≤1°C	0.75 °× 0.75° resampled to EASE grid 2.0; 25 km × 25 km	2010-2016	**II**

For smoothing and gap-filling of FSC time series during the spring snow melt, a sigmoid function was fitted to the time series. The function describes the depletion of the FSC from full snow cover (FSC=1) to complete snowmelt (FSC=0).

$$FSC_f(t; x_1; x_2) = \frac{1}{1+\exp\left(\frac{t-x_1}{x_2}\right)} \tag{1}$$

(Paper **I**)

where t is the time variable (day of year (doy)), x_1 is the inflection point (doy when the FSC reaches 0.5) and x_2 controls the rate of change (doy) (see Figure 3 in Paper **I**). The transition from full snow cover to snow-free ground is usually fast, because an important part of the snow has already melted before bare ground is exposed (Clark et al. 2006).

21

The soil freeze and thaw state was determined from a pixel-based relative frost factor, calculated from the normalised difference of L-Band brightness temperatures at vertical and horizontal polarisations (Rautiainen et al. 2016). The data set gives daily information on the soil freeze and thaw state, which is categorized into three classes: frozen, partially frozen and thawed. The class frozen soil corresponds to a soil frost depth of at least 10 cm over the whole pixel. Partially frozen soil characterises the transition period between the first soil frost occurrences within a pixel until the frozen soil state is observed. The first date of partially frozen soil (doy) and the first date of frozen soil (doy) were defined from the time series.

3.4   Extraction of the start and end of the vegetation active period

3.4.1   Evergreen forests

NDVI, NDWI and FSC time series were compared to the ground references from CO_2 flux measurement sites in Finland to develop methods for the detection of the VAPstart in evergreen forests (Paper **I**). Phenological observations of the May shoot arrival were analysed in comparison to the VAPstart. To determine satellite VAPstart (doy) from FSC_f, a threshold value of 0.99 of FSC was applied to Eq. (1) and the equation was solved for t:

$$\text{Satellite VAPstart} = t = x_1 - \ln(99)\, x_2 \tag{2}$$

(Paper **I**)

The first day of partially frozen soil and frozen soil from the SMOS observations and the first day of autumnal freeze (Table 3) were correlated to the three indicators for the VAPend. A satellite indicator for the VAPend was selected based on highest correspondence with the phenological event and the performance of this indicator was compared to the indicator of the autumnal freeze. The VAPend (doy) was calculated from satellite observations of the date of partially frozen soil (PartialSoilFreezeDate) using a linear regression model:

$$\text{Satellite VAPend} = a\text{PartialSoilFreezeDate} + b \tag{3}$$

(Paper **II**)

with the slope a=0.82 and the offset b=42.8 (Figure 3a in Paper **II**). The VAPend was determined in a similar way from the autumnal freeze indicator (Figure 3b in Paper **II**).

3.4.2 Deciduous forests

The greening-up of vegetation (doy) was determined from a NDWI time series as the last day when NDWI was lower than the minimum annual NDWI, increased by an estimate for the noise level (Delbart et al. 2005):

$$\text{Vegetation greening date } = \arg \max_{t \in [32,200]} f(t) := \{t \mid \text{NDWI}(t) < NDWI_{min} + \varepsilon\} \qquad (4)$$

(Paper **III**)

where $NDWI_{min}$ is the minimum annual NDWI and ε equals 5%. The value of ε was reduced from 20% (Delbart et al. 2005), because of the lower noise level in the averaged and smoothed NDWI time series that were utilised in this work. In Paper **III**, the vegetation greening date was utilised as an indicator of the VAPstart for deciduous forests. This is feasible, because for deciduous trees the VAPstart is closely linked to the development and senescence of leaves (Baldocchi et al. 2005).

3.5 Mapping of the start and end of the vegetation active period

The satellite VAPstart in evergreen and deciduous forests were mapped in Finland based on Eq. 2 and 4, respectively. In addition to the observation periods that were utilised in Papers **I−III** (Table 3), the VAPstart was calculated also until 2017 from the MODIS time series. The major forest type within a MODIS pixel was considered for the mapping of the VAPstart. Thus, only a time series with either evergreen or deciduous forest dominance were averaged to the target grid of the map. Water areas were excluded. The spatial resolution of the target grid varied according to the application. The full 17-years' time series for the VAPstart was calculated at a spatial resolution of 0.05×0.05 degrees.

For the mapping of the VAPend, Eq. (3) was applied to the gridded date of partial soil freeze of pixels in the boreal forest zone in Canada, Finland and surrounding areas. Likewise, the VAPend was calculated from the indicator of the autumnal freeze for the same area.

3.6   Jena scheme for biosphere-atmosphere coupling in Hamburg

Data sets of the satellite VAPstart were utilised in the evaluation of simulated phenology by the biosphere model JSBACH in Paper **III**. This section introduces the model. The JSBACH model (Raddatz et al. 2007; Reick et al. 2013) is a process-based model that calculates the exchanges of carbon, water and energy between the land surface and the atmosphere. The model is part of the Earth System Model by the Max Planck Institute and is a subroutine of its atmospheric component (ECHAM). JSBACH was used in this work to calculate the GPP. The modelling of the carbon cycle is constrained by the leaf area index for which the seasonal cycle is simulated by the phenological model of JSBACH. The details of the phenological model are presented in Paper **III**/Appendix A. The photosynthesis model of JSBACH is based on the biochemical model by Farquhar (1980). Bias-corrected meteorological data from a regional climate model were used to run the model. The VAPstart in deciduous and evergreen forests was determined from the GPP. The applied method was similar to the one used for extracting the VAPstart from the carbon flux measurements (Table 2).

3.7   Modelling of animal phenology

In Paper **IV**, the usability of the vegetation greening date from MODIS satellite observations (section 3.5) for modelling the peak flight periods of herbivorous insects was explored. For this, weekly observations on nocturnal moth phenology of five common species (*Orthosia gothica, Ectropis crepuscularia Operophtera brumata, Cabera exanthemata*, *Dysstroma citrate*) with seasonal differences in their flight activity were obtained from the Finnish national moth monitoring scheme (Leinonen et al. 2016). These observations were related to the vegetation greening date and other variables, such as the temperature-derived growing degree days, latitude and satellite-observed snow melt and the start of the growing season from the fraction of absorbed photosynthetically active radiation, by using linear mixed effect models. The data was randomly divided into model fitting (70%) and model testing (30%) sets. Spatial maps of the peak flight period covering the area of Finland were produced for two species (*Orthosia gothica and Ectropis crepuscularia*) based on single and multivariate models, for which the explanatory variables provided reasonable predictive power in the model testing (Coefficient of determination (R^2) >0.3).

4 Results

4.1 Evergreen forests

In Paper **I**, the analysis of the MODIS time series during the spring revealed that the VAPstart in evergreen forests coincided with the appearance of the first snow-free patches (Figure 5). The satellite VAPstart was estimated from the FSC time series, based on Eq.2, with good accuracy for CO_2 flux measurement sites in Finland (Figure 6a). The satellite indicator explained inter-annual variations well in the VAPstart at all three sites ($R^2 \geq 0.5$). The observed spring-rise in the NDVI values was mainly caused by the melting of snow (Figure 5b). The detection accuracy for the VAPstart from the NDVI was slightly lower compared to the FSC (Figure 11 in Paper **I**). The May shoots of pine trees occurred after complete snow melt.
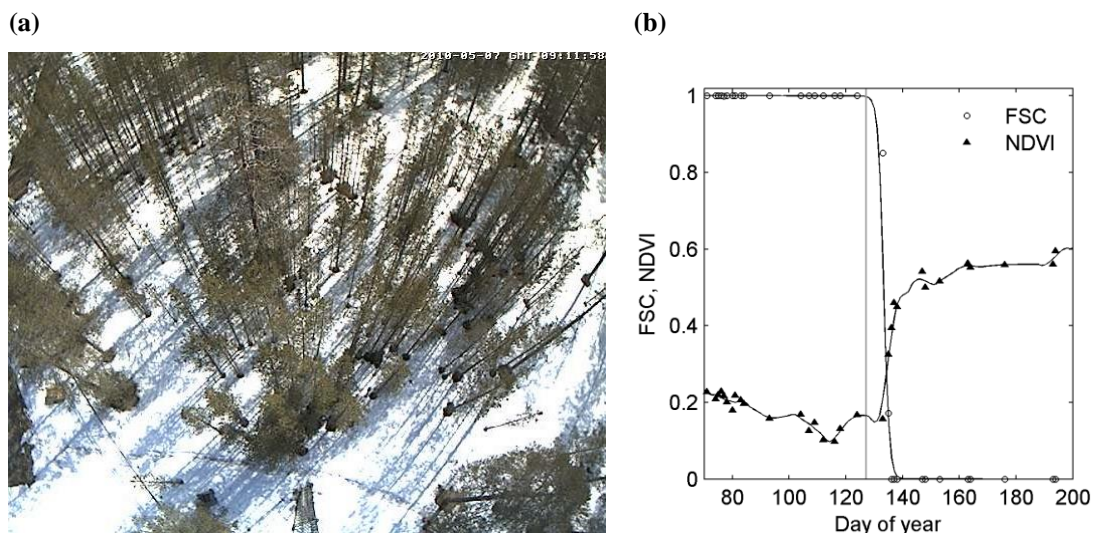
(a) **(b)**

Figure 5. (a) Web camera image taken at Sodankylä on the day of the start of the vegetation active period (07 May 2010). (b) Fractional snow cover (FSC) and the normalised difference vegetation index (NDVI) time-series in spring 2010 for evergreen forests in Sodankylä. The vertical grey line indicates the start of the vegetation active period (from Paper I).

In the comparison of the VAPend against satellite-derived soil freeze data **(**Paper **II)**, the highest correlation was found between the first date of partially frozen soil and the $VAPend_{10}$. The satellite-derived soil freeze data explained the variation in $VAPend_{10}$ well (Figure 6b). On average, the $VAPend_{10}$ occurred about two weeks before partially frozen soil was detected by SMOS. The autumnal freeze indicator of the ERA-Interim air temperature showed a higher correspondence with the $VAPend_{10}$ than the satellite obtained soil freeze data ($R^2 = 0.92$). The higher scatter in the first date of partially frozen soil, relative to the air temperature indicator, may be due to scaling errors caused by the large SMOS footprint. Within the SMOS pixel, soils with finer textures and

higher water contents froze at a slower pace than dry coarse-textured soils with a lower heat capacity (Figure 5 in Paper **II**).

VAPend$_{15}$, VAPend$_{10}$ and VAPend$_5$ at the Finnish and Canadian CO_2 flux measurement sites occurred when the solar elevation at solar noon was already below 30 degrees, thus restricting the possibility for detection with optical instruments at these locations.
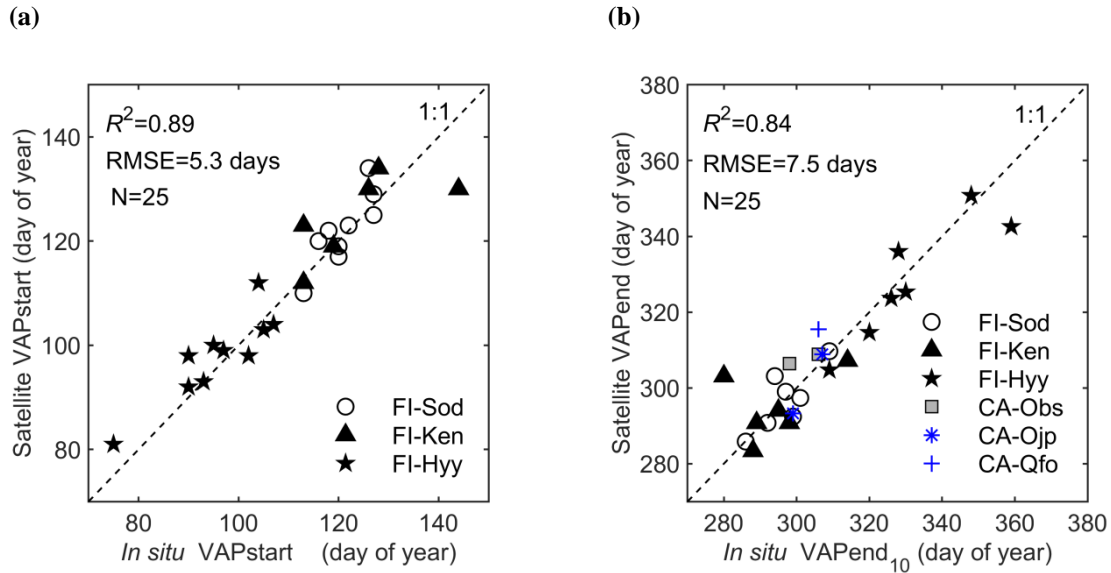
(a)   **(b)**

Figure 6. A scatterplot of the start (VAPstart) (a) and end (b) of the vegetation active period (VAPend$_{10}$) from carbon flux measurements against satellite-derived dates from fractional snow cover (redrawn from Papers I) (a) and soil freeze state (b).

4.2   Deciduous forests

Overall, the NDWI-based greening dates agreed well with the timing of the birch bud break at the phenological sites in Finland. The accuracy was about one week and the bias was lower than one day (Figure 7, Paper **III**). However, there was a considerable scatter in the relationship between the satellite-based greening date and the bud break of birch trees, especially for the southern boreal sites.
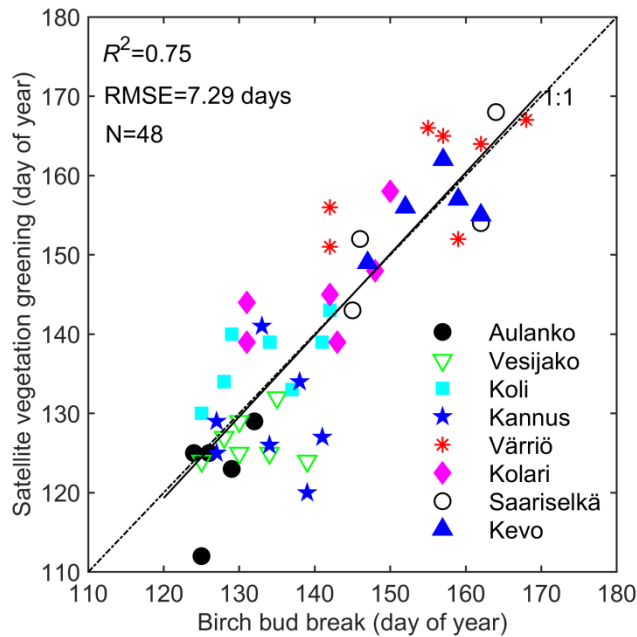
Figure 7. A scatterplot of the satellite-based greening date from the normalised difference water index (NDWI) against the birch bud break observations for the period 2001 to 2008 (adapted from Paper III).

4.3 Start and end of the vegetation active period

The satellite obtained VAPstart in evergreen forests follows the climatic gradient in Finland and advances from the southwest to the northeast (Figure 8). For the period 2001−2017, the VAPstart occurred on average on 4 April in evergreen forests in southern Finland and one month later, on 5 May, in the northern parts of the country. The greening-up of vegetation was delayed by more than a month compared to the VAPstart in evergreen forests. For the same observation period, it occurred in Finland on average on 17 May (doy 137) compared to 13 April (doy 103) for the VAPstart in evergreen forests. The delay time decreased from the southern to the northern boreal zone. The VAPend in evergreen forests was first observed in the north-west of the country and occurred about two months later in the southern coastal areas (Figure 8c). In 2012, the VAPend was observed earlier in parts of southern Finland than in eastern Finland leading to discontinuities in the evolution of the VAPend. This may be due to the weather conditions that year, e.g. early snow fall that prevented the freezing of the soil. The average VAPend for several years showed a more gradual change from middle to southern Finland (Paper II, Figure 6), although some discontinuities remained. A reason for this could be differences in vegetation and soil type distribution that could affect the soil freezing.
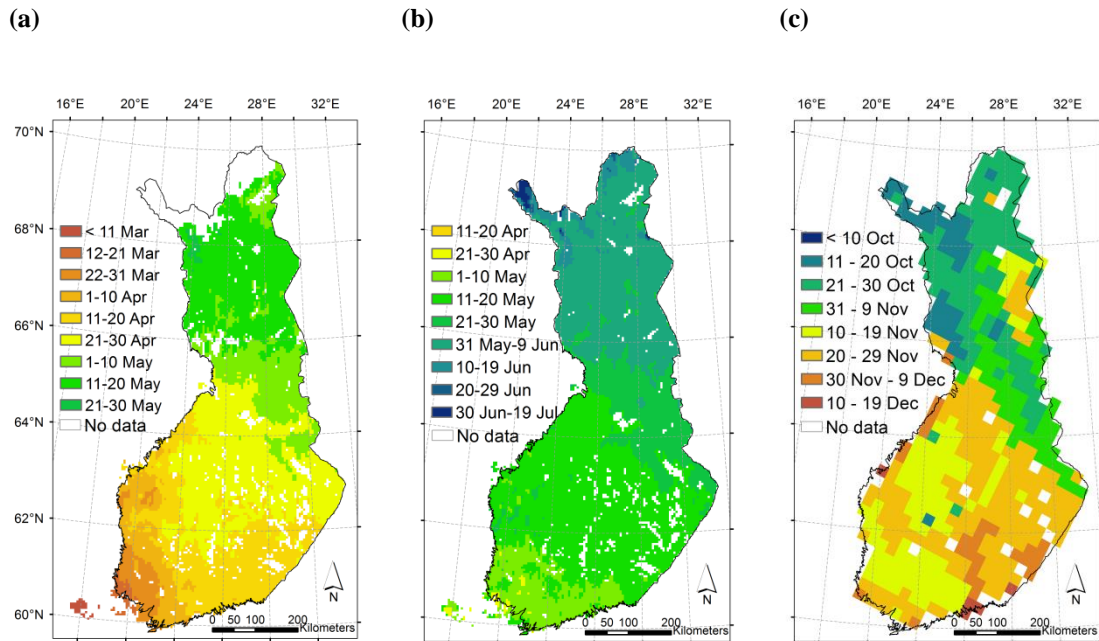
(a)   **(b)**   **(c)**

Figure 8. Maps of the satellite-derived start of the vegetation active period in evergreen forests (a), deciduous vegetation (b), and the end of the vegetation active period in evergreen forests in Finland in 2012.

4.4 Applications

4.4.1 Evaluation of global biosphere model estimates

Maps of the VAPstart were utilised to evaluate model estimates from the global biosphere model JSBACH in Finland (Paper **III**). Multi-year averages of the two independent data sets, and the modelled and satellite VAPstart, showed high spatial agreement for both evergreen and deciduous forests ($R^2 \geq 0.88$, Figure 7 in Paper **III**). The inter-annual variations of the modelled VAPstart were in most cases in agreement with the satellite observations (Figure 9). Nevertheless, the satellite observations helped to discover model deficiencies, such as an overly strong early spring photosynthesis that, consequently, led to an early bias in the modelled date in evergreen forests compared to satellite observations. Instead, the modelled VAPstart in deciduous forests showed a late bias in comparison to the satellite observations. The model biases showed a latitudinal gradient. This increased for evergreen forests and, decreased for deciduous forests, from the southern to the northern boreal zone.
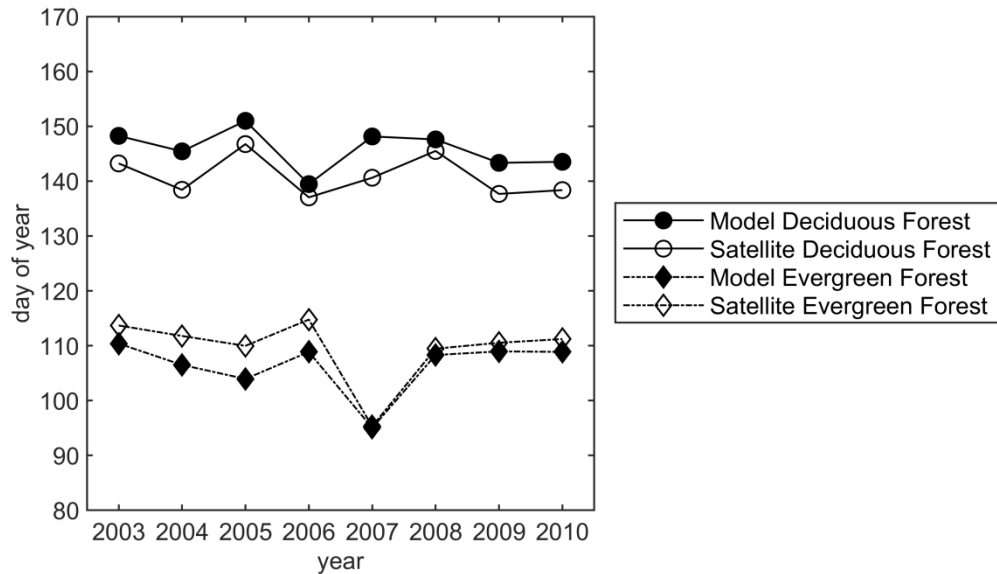
Figure 9. Interannual variations of the start of the vegetation active period in evergreen and deciduous forests in Finland derived from the JSBACH model and from MODIS satellite observations (redrawn from Paper III).

4.4.2 Prediction of the phenology of herbivorous insects using satellite variables

Reasonable predictive power was found for the satellite-derived vegetation greening date in the modelling of the peak flight of early (*Orthosia gothica*) and late spring moth species (*Ectropis crepuscularia*) (R^2>0.3). The snow melt showed the highest predictive power for the early spring species. For the late spring species, the relationship of the peak flight period with growing degree days and the greening-up of the vegetation was equally strong. In contrast to the spring species, latitude was the strongest predictor for the late autumn species (*Operophtera brumata*) and the timing of the peak flight periods for the mid and late summer species (*Cabera exanthemata*, *Dysstroma citrata*) could not be explained with the selected variables. The vegetation greening date was utilised for spatial predictions of the peak flight period for the two spring species based on a multivariate model that included all tested variables (Paper **IV**). For the late spring species, maps based on the multivariate model are presented for an average period of 2001−2013, a phenologically late year (2006) and an early year (2007) (Figure 10). Model predictions based on the vegetation greening date alone, are shown as well for the same average period and selected years in Figure 10. Models based on all variables showed a longer temporal range for the peak flight. According to average predictions for the period 2001-2013 (Figure 10A), the peak flight in the late spring species starts in the beginning of May in south-western Finland and about one month later for the northernmost part of the species range.
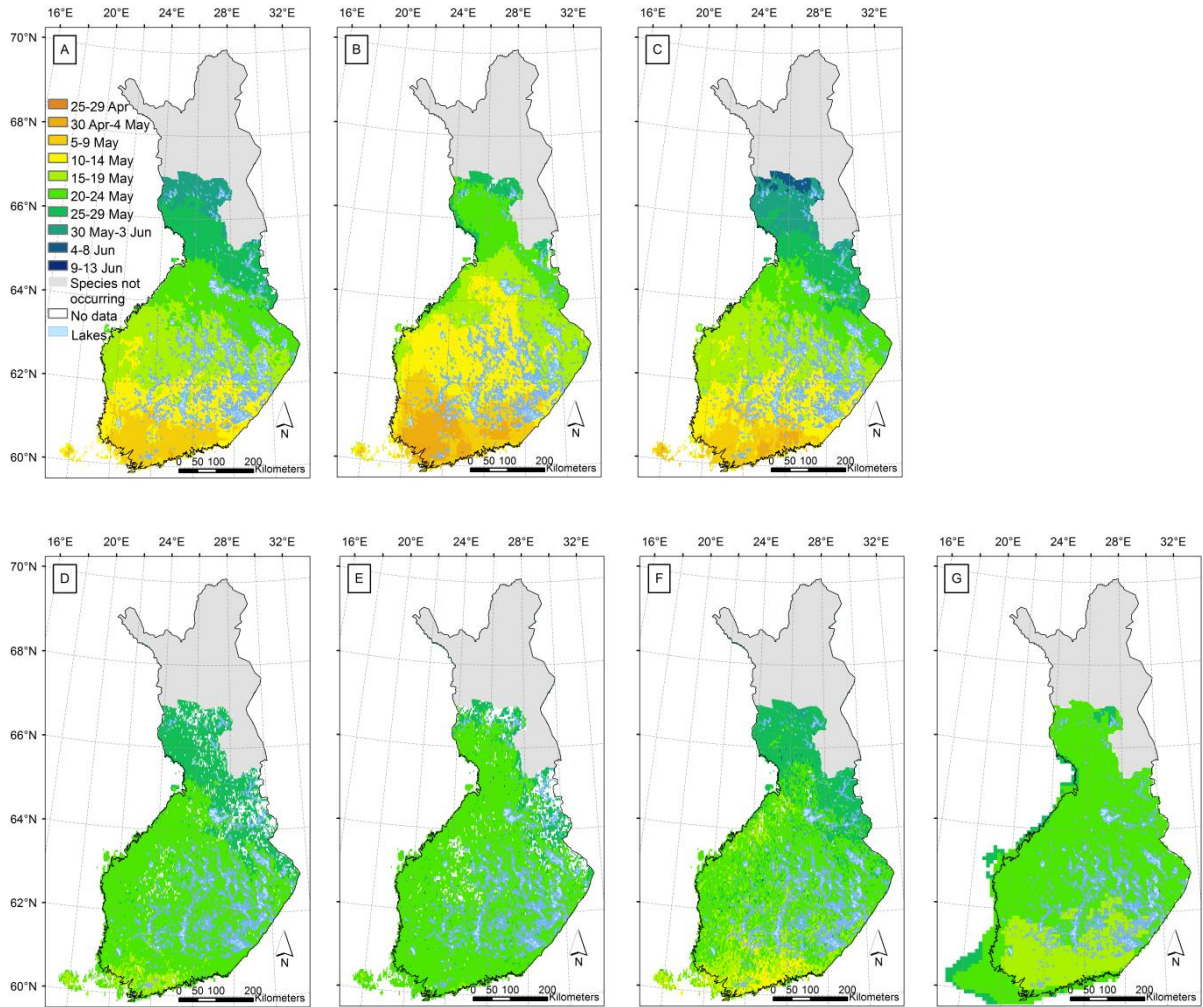
29

Figure 10. Maps of the peak flight periods for *Ectropis crepuscularia*: predictions made on the basis of the total model including the variables: latitude, greening date, weekly accumulated growing degree days and snow melt date for (a) an average period of 2001-2013, (b) a phenologically late year (2006), (c) a phenologically early year (2007); predictions made on the basis of the vegetation greening date for (d) an average period of 2001-2013, (e) a phenologically late year (2006), (f) a phenologically early year (2007); and (g) an average prediction for 2001-2013 based on an alternative variable (weekly accumulating growing degree days). The model formulas are presented in Pöyry et al. (2018), Supplementary Table S2 (data sources: Country borders © ESRI, Lakes © SYKE, Biogeographical provinces ©LUOMUS and SYKE (from Paper IV).

5   Discussion

5.1   Theoretical implications

In this work, satellite observations on snow cover and soil freeze were utilised to derive the start and end dates of photosynthetic activity in boreal evergreen forests. The retrieval of the VAPstart and VAPend is based on the strong relationship that was found between the spring snow melt and VAPstart, and between autumn soil freeze and VAPend, respectively. This is the first time that a proxy indicator from the FSC is proposed for the determination of the VAPstart. The finding is supported by Thum et al. (2009), who suggested that the albedo change during the spring snow melt could serve as an indicator of the photosynthetic recovery of evergreen forests. Very recently, the results of this work were confirmed by Pulliainen et al. (2017) who built a proxy indicator for the VAPstart based on the day of snow clearance from spaceborne microwave radiometer observations covering a period of 35 years. For the detection of the beginning of the snow melt from the FSC time series, a simple method based on a sigmoid function was introduced here to describe the depletion of snow cover during the spring snow melt. In recent work, it has been shown that the sigmoid function fitting to the albedo time series from the AVHRR instrument can be utilised to retrieve the start and end dates of the snow melt in Finland and in the northern hemisphere (Anttila et al. 2018; Manninen et al. 2018), thus, supporting the selection of the method.

In a comparison of the VAPend with the dates of satellite-observed partial soil freeze and soil freeze from microwave L-band observations; it was found that the VAPend can be estimated from the date of partial soil freeze. This is important because optical instruments, which are typically used for the retrieval of the end of the growing season, are not applicable due to the high solar zenith angles during this period in the boreal forest zone. Consequently, the indicator for the VAPend from spaceborne microwave radiometer observations fills an observational gap for the monitoring of the phenology of boreal evergreen forests. The strong link between the freeze and the VAPend is in agreement with results based on temperature observations for Canadian sites by Barr et al. (2009). Only a few other studies have compared satellite-observed landscape freezes with indicators for the VAPend (Barichivich et al. 2013; Kimball et al. 2004). In contrast to the results of this work, those studies reported a low correspondence of satellite-observed landscape freezes with indicators for the VAPend. These differences could be due to the lower sensitivity to the soil freeze and thaw processes of microwave observations in higher frequency bands (Kim et al. 2011; Kimball et al. 2004) and the use of an end of season indicator based on the NDVI (Barichivich et al. 2013).

The developed satellite methods for the VAPstart and VAPend in boreal evergreen forests achieved better agreement with in situ dates from CO_2 flux measurement sites compared to the results from the EVI, such as the MODIS land cover dynamics product (Melaas et al. 2013b) and from the phenological index (Gonsamo and Chen 2016; Gonsamo et al. 2012). The methods allow the mapping of the VAPstart in the two different forest types. Maps of the VAPstart in evergreen forests and deciduous vegetation show a time lag of about one month. This delay between photosynthetic recovery in evergreen and deciduous vegetation in the boreal region agrees with satellite observations of sun-induced chlorophyll fluorescence (Walther et al. 2016). The detection accuracy of the vegetation greening date in deciduous broad-leaved forests of one week was in line with results for deciduous forests in Siberia (Delbart et al. 2005; Delbart et al. 2006) and similar to accuracies reported by Karlsen et al. (2008) for Fennoscandia.

5.2   Practical implications

The produced 17-year time series provides consistent spatial datasets of the VAPstart in evergreen forests and deciduous vegetation in Finland. The maps can be viewed with a web map service and are provided as open access to the public (SYKE Vegetation phenology 2001-2017). The data can be utilised for the monitoring of interannual and decadal changes in the VAPstart and for studying their relationship to changes in climate variables. The information on the vegetation active period is relevant for the calibration of the photosynthesis and phenology components in carbon balance models. Applying them in model calibration could lead to better model descriptions and improved future simulations. The findings from the evaluation of the VAPstart simulations by the JSBACH model with satellite observations (Paper **III**) were adapted into JSBACH model formulations (Holmberg et al. 2018). Satellite VAPstart data can be utilised in the quantification of changes in the carbon balance due to the earlier arrival of spring in a warming climate, as shown by Pulliainen et al. (2017). In addition to carbon balance modelling, the data could be applied in modelling nutrient leaching, for which information on the vegetation growing season is required. Furthermore, the data has applications for monitoring biodiversity and can contribute to the development of EBVs (Skidmore et al. 2015; Vihervaara et al. 2017). The methodologies support the global targets of conserving biodiversity set by the CBD, specifically the strategic goal 'to enhance the benefits to all from biodiversity and ecosystem services' (O'Connor et al. 2015). As shown in Paper **IV**, remote sensing observations of the vegetation greening date are useful for the prediction of the phenology of moth species flying in spring. The utilisation of such data for the prediction of animal phenology is an important application that is relevant also for the management of populations of insect species.

5.3 Reliability and validity

The presented remote sensing methods for the determination of the VAPstart and VAPend rely on correlative relationships between the recovery and cessation of photosynthesis and environmental factors, thus they do not provide direct observations of the start and ending dates of photosynthesis as such. To develop the detection methods, observations from only three eddy covariance sites in evergreen needle-leaved forests in Finland, and for VAPend three additional sites in Canada, were used. Recent investigations by Pulliainen et al. (2017), based on a larger number of sites in the boreal region and on a longer observation period, suggested that the method for the VAPstart is applicable to evergreen needle-leaved forests throughout the boreal zone. Future climate warming and the expected and already observed decrease in snow cover and earlier snow melt in the boreal areas (Metsämäki et al. 2018) may limit the applicability of the method for the VAPstart especially for the southern parts of Fennoscandia. Hence, the detection of the VAPstart from the FSC may fail in winters with low snow depths or sporadic snow events. In that case the direct effect of the low temperature or the combination of low temperature and a high amount of light (Delpierre et al. 2012; Gea-Izquierdo et al. 2010) are more important factors for the restriction of photosynthetic recovery in spring. Although, the results for eddy covariance sites in Finland and Canada indicate a strong relationship between the VAPend and the date of partial soil freeze from SMOS, this needs to be ascertained for additional sites and for a longer period in the boreal forest zone.

In this work, visual phenological observations of the birch bud break for a sample of five trees was compared to satellite-observed greening-up from several MODIS pixels. Heterogeneity in land cover and terrain conditions is one reason for the discrepancies between the ground and satellite data (Badeck et al. 2004, Doktor et al. 2009). For example, variations in the microclimate over an area of several kilometres with elevation differences of less than 50 m are estimated to cause uncertainty of 2.5 days (Badeck et al. 2004). There are also uncertainties related to the phenological observations. At Finnish sites, observations were carried out twice a week and the assumed observer's error is about three days. Variation in the bud break can be quite high in one population ranging from a few days up to four weeks (Rousi et al. 2007). Eddy covariance sites measure the carbon fluxes of an area that extends a couple of hundred meters from the measurement tower and provide information on the VAPstart and VAPend on the ecosystem scale. Although, these observations are better suited for comparison to medium resolution satellite data than phenological observations of single species, the difference in the sampling scale leads to incongruities in comparisons to MODIS data. The discrepancies depend mostly on the homogeneity of the landscape at the flux site and its surroundings. Furthermore, gaps in the time series of the GPI lead to uncertainties in the reference dates. To allow a comparison of MODIS observations with both, eddy covariance and traditional phenological site observations, large

homogenous areas in terms of land cover were selected. Satellite-estimates from single pixels are also more likely to be influenced by noise and missing values. This approach is supported by other studies reporting that the use of large homogenous areas averages out errors and leads to better correlation with in situ observations (Doktor et al. 2009; Zhang et al. 2017).

The precision of the satellite VAPstart is one day; however cloud cover hinders the observations of the land surface with optical instruments. Hence, the quality of the mapped VAPstart is affected by data gaps due to cloud cover. Cloud coverage varies regionally depending on weather patterns and therefore the uncertainties related to cloud coverage are not spatially uniform. Temporal gaps increase the uncertainty when the VAPstart occurs during the cloudy period, and the actual date may have occurred before or after the detected date. Undetected clouds and mixed cloud pixels cause noise in the time series. High quality cloud detection algorithms are, thus, needed to avoid false interpretation of the satellite signal. This is especially challenging during the spring recovery of photosynthesis when there is still snow on the ground. In this work an operational cloud masking algorithm (Metsämäki et al. 2015) that provided good accuracy for the Finnish area also during snow melt was utilised. The microwave L-band observations from SMOS that were used for the determination of the VAPend are not effected by clouds. However, this advantage comes with a loss of spatial detail in comparison to CO_2 flux measurement sites, which causes scaling errors. Although, distributed observation networks are being established at research sites for the calibration and validation of satellite observations (e.g. at the Sodankylä research station (Ikonen et al. 2016), spatial upscaling of site measurements on soil freeze to the satellite pixel remains challenging.

5.4   Recommendations for future research

For the assessment of long-term trends in vegetation phenology, the continuity of time series which are currently based on MODIS observations is very important. MODIS sensors on Terra and Aqua are aging and are expected to be operating until 2020. Further work needs to ensure the continuity of consistent observations for the VAPstart. For this, algorithms need to be transferred to VIIRS or Copernicus Sentinel-3. The Copernicus global land service (https://land.copernicus.eu/) provides the FSC (the snow cover extent) for the northern hemisphere from VIIRS using the algorithm by Metsämäki et al. (2012). An implementation for Sentinel-3 is foreseen. The snow cover extent product could be used as base data set for the determination of the VAPstart in the boreal forest region using the methodology that was developed here. Because of limitations of the detection method based on snow cover in the southern parts of the boreal zone and in the hemi-boreal zone

in Fennoscandia for years with little snow fall (5.3), satellite observations on the soil freeze could possibly complement the methods. This could be analysed in further work.

The SMOS-based VAPend dates need further validation throughout the boreal zone. In this investigation, an autumn freeze indicator based on the ERA-Interim air temperature, showed better agreement with the VAPend than the satellite soil freeze for the CO_2 flux measurement sites. Therefore, satellite observations of the land surface temperature could be investigated as an indicator for the VAPend, in addition to the soil freeze. The land surface temperature is a measure of the 'skin temperature' that could be a useful measure of physiological activity of the top canopy leaves and was applied for the estimation of the GPP (Sims et al. 2008). Compared to the SMOS soil freeze observations, the spatial resolution is higher and corresponds better to the footprint of the carbon flux measurement sites. Further work on the monitoring of the seasonal cycle of photosynthesis in boreal areas may include satellite observations of sun-induced chlorophyll fluorescence (Joiner et al. 2014; Walther et al. 2016). In the investigation of ground observations from CO_2 flux measurement sites in Finland and Canada, it was found that the VAPend occurred when the solar elevation at solar noon was below 30°. Moreover, the large footprint of currently available satellite sensors that are used for the retrieval of sun-induced fluorescence limits comparisons with eddy covariance sites. However, such observations may provide more direct information on the photosynthetic activity of the vegetation from the spring to the early autumn. The fluorescence explorer (FLEX) mission by the European Space Agency will have a new instrument for measuring fluorescence on board, the fluorescence imaging spectrometer (FLORIS). It has a foreseen launch date in 2022. The aim of the mission is to provide global estimates of vegetation fluorescence, activity and stress (Coppo et al. 2017) at a medium spatial resolution (300 m).

The availability of high resolution (5-100 m) satellite time series, e.g. from Copernicus Sentinel-2, give the possibility to produce phenological products at a high spatial resolution (10−20 m) and to address the spatial heterogeneity in phenological development within the coarser resolution satellite pixel to study scaling effects (Zhang et al. 2017). A higher spatial resolution is important for areas and during periods (e.g. in autumn) with high spatial variability in phenological development. Information on fine scales is often required for biodiversity applications, e.g. for the mapping of ecosystem types and conditions. Methodological approaches to estimate spring and autumn seasonal transitions from Landsat data and to combine medium- and high-resolution satellite images (Melaas et al. 2013a; Senf et al. 2017; Zhang et al. 2017) were presented for temperate deciduous broad-leaved forest and agricultural areas but they need to be evaluated in boreal environments with large contributions of evergreen needle-leaved trees to the satellite signal. To bridge the gap between ground and satellite observations, also the use of unmanned

aerial vehicles (UAVs) (Klosterman et al. 2018) would be beneficial. Furthermore, citizen science observations and web camera networks are developing and can provide complementary data sources to traditional phenological observations and could provide useful data for calibration, validation and upscaling to satellite observations (Fritz et al. 2017; Kosmala et al. 2016; Peltoniemi et al. 2018a; Zhang et al. 2018a).

6   Conclusions

This thesis focused on the development of remote sensing methods for the detection of the start and end of the vegetation active period in boreal forests. Based on two case studies, the application of the derived map products was shown for the modelling of the carbon cycle and the prediction of insect phenology. The main conclusions to be drawn from this work are given below, grouped by the objectives.

Development of remote sensing methods for the determination of the start and end of the vegetation active period in evergreen needle-leaved forests in the boreal forest region

1. The time when first snow-free ground appears during the snow melt in spring is strongly linked to the start of photosynthetic activity at boreal evergreen forest sites in Finland.
2. Based on this relationship, the start of the vegetation active period can be estimated from MODIS satellite time series of fractional snow cover. Sigmoid function fitting can be utilised to interpolate the time series and the start of the vegetation active period can be determined from the modelled time series.
3. The time when partially frozen soil is detected from L-band passive microwave radiometer satellite observations has a strong correlative relationship with the end of the vegetation active period at evergreen forest sites in Finland and Canada.
4. The end of the vegetation active period can be determined from the first date of partially frozen soil by using a linear regression model.
5. Although further investigations with more ground data from CO_2 flux measurement sites are recommended, the results suggest that the methods can be utilised to map the spatial distribution of the start and end of the vegetation activity in boreal evergreen forests.

Evaluation of the NDWI-based method for the detection of the greening-up of deciduous broad-leaved forests in Finland

6. The normalised difference water index can be applied for the mapping of the greening-up in Finland.

7. The achieved accuracies in comparison to visual birch bud break observations are in line with previous studies.

Assessment of the performance of a simulated start of the vegetation active period by a large-scale biosphere model in Finland with satellite observations

8. The comparison of simulated dates from the JSBACH model with satellite observations showed that the model captures the spatial and temporal dynamics at the start of the vegetation active period in Finland well.

9. The analysis provided indications to reduce model biases by making adjustments in the photosynthesis and phenological model.

Investigation of the benefit of using satellite-observed vegetation greening-up to predict animal phenology

10. Satellite-observed vegetation greening dates partly explained the timing of the peak flight of spring moths and can be utilised, together with other environmental variables, for spatial predictions of the peak flight period in Finland.

Further work could include the transfer of methods for the start of the vegetation active period to Copernicus Sentinel-3 or VIIRS to ensure continuity of the time series. A transfer of methods for evergreen forests to other areas in the boreal forest zone is possible, however further validation with ground observations from eddy covariance sites is recommended. Copernicus Sentinel-2 data together with web camera observations could be utilised to study the spatial heterogeneity and scaling effects of the phenology of deciduous species, especially in the autumn.

References

Al Bitar, A., Mialon, A., Kerr, Y.H., Cabot, F., Richaume, P., Jacquette, E., Quesney, A., Mahmoodi, A., Tarot, S., Parrens, M., Al-Yaari, A., Pellarin, T., Rodriguez-Fernandez, N., & Wigneron, J.P. (2017). The global SMOS Level 3 daily soil moisture and brightness temperature maps. Earth Syst. Sci. Data, 9, 293-315.

Anttila, K., Manninen, T., Jääskeläinen, E., Riihelä, A., & Lahtinen, P. (2018). The role of climate and land use in the changes in surface albedo prior to snow melt and the timing of melt season of seasonal snow in northern land areas of 40°N–80°N during 1982–2015. Remote Sensing, 10, 1619.

Aurela, M., Tuovinen, J.-P., & Laurila, T. (2001). Net CO_2 exchange of a subarctic mountain birch ecosystem. Theoretical and Applied Climatology, 70, 135-148.

Badeck, F.-W., Bondeau, A., Böttcher, K., Doktor, D., Lucht, W., Schaber, J., & Sitch, S. (2004). Responses of spring phenology to climate change. New Phytologist, 162, 295-309.

Baldocchi, D.D., Black, T.A., Curtis, P.S., Falge, E., Fuentes, J.D., Granier, A., Gu, L., Knohl, A., Pilegaard, K., Schmid, H.P., Valentini, R., Wilson, K., Wofsy, S., Xu, L., & Yamamoto, S. (2005). Predicting the onset of net carbon uptake by deciduous forests with soil temperature and climate data: a synthesis of FLUXNET data. International Journal of Biometeorology, 49, 377-387.

Barichivich, J., Briffa, K.R., Myneni, R.B., Osborn, T.J., Melvin, T.M., Ciais, P., Piao, S.L., & Tucker, C. (2013). Large-scale variations in the vegetation growing season and annual cycle of atmospheric CO_2 at high northern latitudes from 1950 to 2011. Global Change Biology, 19, 3167-3183.

Barr, A., Black, A.T., & McCaughey, H. (2009). Climatic and phenological controls of the carbon and energy balances of three contrasting boreal forest ecosystems in western Canada. In A. Noormets (Ed.), Phenology of ecosystem processes, Applications in global change research (pp. 3-34). Dordrecht: Springer Sciences + Business Media.

Bartsch, A., Kidd, R.A., Wagner, W., & Bartalis, Z. (2007). Temporal and spatial variability of the beginning and end of daily spring freeze/thaw cycles derived from scatterometer data. Remote Sensing of Environment, 106, 360-374.

Bauerle, W.L., Oren, R., Way, D.A., Qian, S.S., Stoy, P.C., Thornton, P.E., Bowden, J.D., Hoffman, F.M., & Reynolds, R.F. (2012). Photoperiodic regulation of the seasonal pattern of photosynthetic capacity and the implications for carbon cycling. Proceedings of the National Academy of Sciences, 109, 8612-8617.

Beck, P.S.A., Atzberger, C., Høgda, K.A., Johansen, B., & Skidmore, A.K. (2006). Improved monitoring of vegetation dynamics at very high latitudes: A new method using MODIS NDVI. Remote Sensing of Environment, 100, 321-334.

Black, T.A., Chen, W.J., Barr, A.G., Arain, M.A., Chen, Z., Nesic, Z., Hogg, E.H., Neumann, H.H., & Yang, P.C. (2000). Increased carbon sequestration by a boreal deciduous forest in years with a warm spring. Geophysical Research Letters, 27, 1271-1274.

Bonan, G.B. (2008). Forests and Climate Change: Forcings, Feedbacks, and the Climate Benefits of Forests. Science, 320, 1444-1449.

Brodzik, M.J., Billingsley, B., Haran, T., Raup, B., & Savoie, M.H. (2012). EASE-Grid 2.0: Incremental but Significant Improvements for Earth-Gridded Data Sets. ISPRS International Journal of Geo-Information, 1, 32.

Buitenwerf, R., Rose, L., & Higgins, S.I. (2015). Three decades of multi-dimensional change in global leaf phenology. Nature Climate Change, 5, 364.

Chen, J., Jönsson, P., Tamura, M., Gu, Z., Matsushita, B., & Eklundh, L. (2004). A simple method for reconstructing a high-quality NDVI time-series data set based on the Savitzky-Golay filter. Remote Sensing of Environment, 91, 332-344.

Chuine, I. (2010). Why does phenology drive species distribution? Philosophical Transactions of the Royal Society B: Biological Sciences, 365, 3149-3160.

Clark, M.P., Slater, A.G., Barrett, A.P., Hay, L.E., McCabe, G.J., Rajagopalan, B., & Leavesley, G.H. (2006). Assimilation of snow covered area information into hydrologic and land-surface models. Advances in Water Resources, 29, 1209-1221.

Cong, N., Piao, S., Chen, A., Wang, X., Lin, X., Chen, S., Han, S., Zhou, G., & Zhang, X. (2012). Spring vegetation green-up date in China inferred from SPOT NDVI data: A multiple model analysis. Agricultural and Forest Meteorology, 165, 104-113.

Coppo, P., Taiti, A., Pettinato, L., Francois, M., Taccola, M., & Drusch, M. (2017). Fluorescence Imaging Spectrometer (FLORIS) for ESA FLEX Mission. Remote Sensing, 9, 649.

Dal Maso, M., Hari, P., & Kulmala, M. (2009). Spring recovery of photosynthesis and atmospheric particle formation. Boreal Environment Research, 14, 711-721.

Dalmonech, D., & Zaehle, S. (2013). Towards a more objective evaluation of modelled land-carbon trends using atmospheric CO_2 and satellite-based vegetation activity observations. Biogeosciences, 10, 4189-4210.

Dee, D.P., Uppala, S.M., Simmons, A.J., Berrisford, P., Poli, P., Kobayashi, S., Andrae, U., Balmaseda, M.A., Balsamo, G., Bauer, P., Bechtold, P., Beljaars, A.C.M., van de Berg, L., Bidlot, J., Bormann, N., Delsol, C., Dragani, R., Fuentes, M., Geer, A.J., Haimberger, L., Healy, S.B., Hersbach, H., Hólm, E.V., Isaksen, L., Kållberg, P., Köhler, M., Matricardi, M., McNally, A.P., Monge-Sanz, B.M., Morcrette, J.J., Park, B.K., Peubey, C., de Rosnay, P., Tavolato, C., Thépaut, J.N., & Vitart, F. (2011). The ERA-Interim reanalysis: configuration and performance of the data assimilation system. Quarterly Journal of the Royal Meteorological Society, 137, 553-597.

Delbart, N., Kergoat, L., Le Toan, T., L'Hermitte, J., & Picard, G. (2005). Determination of phenological dates in boreal regions using normalized difference water index. Remote Sensing of Environment, 97, 26-38.

Delbart, N., Le Toan, T., Kergoat, L., & Fedotova, V. (2006). Remote sensing of spring phenology in boreal regions: A free of snow-effect method using NOAA-AVHRR and SPOT-VGT data (1982-2004). Remote Sensing of Environment, 101, 52-62.

Delbart, N., Picard, G., Le Toan, T., Kergoat, L., Quegan, S., Woodward, I.A.N., Dye, D., & Fedotova, V. (2008). Spring phenology in boreal Eurasia over a nearly century time scale. Global Change Biology, 14, 603-614.

Delpierre, N., Soudani, K., François, C., Le Maire, G., Bernhofer, C., Kutsch, W., Misson, L., Rambal, S., Vesala, T., & Dufrêne, E. (2012). Quantifying the influence of climate and biological drivers on the interannual variability of carbon exchanges in European forests through process-based modelling. Agricultural and Forest Meteorology, 154-155, 99-112.

Derksen, C., Xu, X., Scott Dunbar, R., Colliander, A., Kim, Y., Kimball, J.S., Black, T.A., Euskirchen, E., Langlois, A., Loranty, M.M., Marsh, P., Rautiainen, K., Roy, A., Royer, A., & Stephens, J. (2017). Retrieving landscape freeze/thaw state from Soil Moisture Active Passive (SMAP) radar and radiometer measurements. Remote Sensing of Environment, 194, 48-62.

Doktor, D., Bondeau, A., Koslowski, D., & Badeck, F.-W. (2009). Influence of heterogeneous landscapes on computed green-up dates based on daily AVHRR NDVI observations. Remote Sensing of Environment, 113, 2618-2632.

Falge, E., Aubinet, M., Bakwin, P.S., Baldocchi, D., Berbigier, P., Bernhofer, C., Black, A.T., Ceulemans, R., Davis, K.J., Dolman, A.J., Goldstein, A., Goulden, M.L., Granier, A., Hollinger, D.Y., Jarvis, P.G., Jensen, N.O., Pilegaard, K., Katul, G., Kyaw Tha Paw, P., Law, B.E., Lindroth, A., Loustau, D., Mahli, Y., Monson, R., Moncrieff, P., Moors, E., Munger, J.W., Meyers, T., Oechel, W., Schulze, E.D., Thorgeirsson, H., Tenhunen, J., Valentini, R., Verma, S.B., Vesala, T., & Wofsy, S.C. (2017). FLUXNET Research Network Site Characteristics, Investigators, and Bibliography, 2016, Data set version: 1, Oak Ridge, Tennessee, USA: ORNL DAAC.

Farquhar, G.D., Caemmerer, S., & Berry, J.A. (1980). A biochemical model of photosynthetic CO_2 assimilation in leaves of C3 species. Planta, 149, 78-90.

Fischer, A. (1994). A model for the seasonal variations of vegetation indices in coarse resolution data and its inversion to extract crop parameters. Remote Sensing of Environment, 48, 220-230.

Fitchett, J.M., Grab, S.W., & Thompson, D.I. (2015). Plant phenology and climate change: Progress in methodological approaches and application. Progress in Physical Geography: Earth and Environment, 39, 460-482.

Foster, J.R., Townsend, P.A., & Mladenoff, D.J. (2013). Mapping asynchrony between gypsy moth egg-hatch and forest leaf-out: Putting the phenological window hypothesis in a spatial context. Forest Ecology and Management, 287, 67-76.

Frankenberg, C., O'Dell, C., Berry, J., Guanter, L., Joiner, J., Köhler, P., Pollock, R., & Taylor, T.E. (2014). Prospects for chlorophyll fluorescence remote sensing from the Orbiting Carbon Observatory-2. Remote Sensing of Environment, 147, 1-12.

Friedl, M.A., Henebry, G.M., Reed, B.C., Huete, A., White, M.A., Morisette, J.T., Nemani, R.R., Zhang, X., & Myneni, R. (2006). Land surface phenology. A community white paper requested by NASA. available from

https://cce.nasa.gov/mtg2008_ab_presentations/Phenology_Friedl_whitepaper.pdf (accessed 12.06.2018).

Fritz, S., Fonte, C.C., & See, L. (2017). The Role of Citizen Science in Earth Observation. Remote Sensing, 9 (4), 357.

Ganguly, S., Friedl, M.A., Tan, B., Zhang, X., & Verma, M. (2010). Land surface phenology from MODIS: Characterization of the Collection 5 global land cover dynamics product. Remote Sensing of Environment, 114, 1805-1816.

Gao, B.-C. (1996). NDWI-A normalized difference water index for remote sensing of vegetation liquid water from space. Remote Sensing of Environment, 58, 257-266.

Gea-Izquierdo, G., Mäkelä, A., Margolis, H., Bergeron, Y., Black, T.A., Dunn, A., Hadley, J., Paw U, K.T., Falk, M., Wharton, S., Monson, R., Hollinger, D.Y., Laurila, T., Aurela, M., McCaughey, H., Bourque, C., Vesala, T., & Berninger, F. (2010). Modeling acclimation of photosynthesis to temperature in evergreen conifer forests. New Phytologist, 188, 175-186.

Gonsamo, A., & Chen, J.M. (2016). Circumpolar vegetation dynamics product for global change study. Remote Sensing of Environment, 182, 13-26.

Gonsamo, A., Chen, J.M., Price, D.T., Kurz, W.A., & Wu, C. (2012). Land surface phenology from optical satellite measurement and CO_2 eddy covariance technique. J. Geophys. Res., 117, G03032.

Goward, S.N., Tucker, C.J., & Dye, D.G. (1985). North American vegetation patterns observed with the NOAA-7 advanced very high resolution radiometer. Vegetatio, 64, 3-14.

Gu, L., Post, W.M., Baldocchi, D., Black, A.T., Suyker, A.E., Verma, S.B., Vesala, T., & Wofsy, S. (2009). Characterizing the seasonal dynamics of plant community photosynthesis across a range of vegetation types. In A. Noormets (Ed.), Phenology of ecosystem processes, Applications in global change research (pp. 35-58). Dordrecht: Springer Sciences and Business Media.

Gu, L., Post, W.M., Baldocchi, D., Black, A.T., Verma, S.B., Vesala, T., & Wofsy, S. (2003). Phenology of photosynthesis. In M.D. Schwartz (Ed.), Phenology: An integrative environmental science (pp. 467-485). Dordrecht, The Netherlands.: Kluwer Academic Publisher.

Hall, D.K., Riggs, G.A., & Salomonson, V.V. (1995). Development of methods for mapping global snow cover using moderate resolution imaging spectroradiometer data. Remote Sensing of Environment, 54, 127-140.

Hari, P., Bäck, J., & Nikinmaa, E. (2009). Process responses to climate change. In P. Hari, & L. Kulmala (Eds.), Boreal forest and climate change (pp. 494-495): Springer Science + Business Media B.V.

Härmä, P., Teiniranta, R., Törmä, M., Repo, R., Järvenpää, E., & Kallio, E. (2005). CLC2000 Finland: Final Report. Finnish Environment Institute, Geoinformatics and Land Use Division.

Hmimina, G., Dufrêne, E., Pontailler, J.Y., Delpierre, N., Aubinet, M., Caquet, B., de Grandcourt, A., Burban, B., Flechard, C., Granier, A., Gross, P., Heinesch, B., Longdoz, B., Moureaux, C., Ourcival, J.M., Rambal, S., Saint André, L., & Soudani, K. (2013). Evaluation of the potential of MODIS satellite data to predict vegetation phenology in different biomes: An investigation using ground-based NDVI measurements. Remote Sensing of Environment, 132, 145-158.

Holmberg, M., Aalto, T., Akujärvi, A., Arslan, A.N., Bergström, I., Böttcher, K., Lahtinen, I., Mäkelä, A., Markkanen, T., Minunno, F., Peltoniemi, M., Rankinen, K., Vihervaara, P., & Forsius, M. (2019). Ecosystem services related to the carbon cycling - modelling present and future impacts in boreal forests. Frontiers in Plant Sciences, 10, 343.

Hölttä, T., Lintunen, A., Chan, T., Mäkelä, A., & Nikinmaa, E. (2017). A steady-state stomatal model of balanced leaf gas exchange, hydraulics and maximal source–sink flux. Tree Physiology, 37, 851-868.

Huete, A., Didan, K., Miura, T., Rodriguez, E.P., Gao, X., & Ferreira, L.G. (2002). Overview of the radiometric and biophysical performance of the MODIS vegetation indices. Remote Sensing of Environment, 83, 195-213.

Hufkens, K., Friedl, M., Sonnentag, O., Braswell, B.H., Milliman, T., & Richardson, A.D. (2012). Linking near-surface and satellite remote sensing measurements of deciduous broadleaf forest phenology. Remote Sensing of Environment, 117, 307-321.

Ikonen, J., Vehviläinen, J., Rautiainen, K., Smolander, T., Lemmetyinen, J., Bircher, S., & Pulliainen, J. (2016). The Sodankylä in situ soil moisture observation network: an example application of ESA CCI soil moisture product evaluation. Geosci. Instrum. Method. Data Syst., 5, 95-108.

IPCC (2013). Climate change 2013: The physical science basis. Contribution of Working Group I to the fifth assessment report of the intergovernmental panel on climate change. United Kingdom and New York, NY, USA.

Ivits, E., Cherlet, M., Tóth, G., Sommer, S., Mehl, W., Vogt, J., & Micale, F. (2012). Combining satellite derived phenology with climate data for climate change impact assessment. Global and Planetary Change, 88-89, 85-97.

Jackson, R.D., & Huete, A.R. (1991). Interpreting vegetation indices. Preventive Veterinary Medicine, 11, 185-200.

Jarvis, P., & Linder, S. (2000). Constraints to growth of boreal forests. Nature, 405, 904.

Jeganathan, C., Dash, J., & Atkinson, P.M. (2014). Remotely sensed trends in the phenology of northern high latitude terrestrial vegetation, controlling for land cover change and vegetation type. Remote Sensing of Environment, 143, 154-170.

Jeong, S.-J., Medvigy, D., Shevliakova, E., & Malyshev, S. (2012). Uncertainties in terrestrial carbon budgets related to spring phenology. Journal of Geophysical Research: Biogeosciences, 117, G01030.

Jepsen, J.U., Hagen, S.B., Høgda, K.A., Ims, R.A., Karlsen, S.R., Tømmervik, H., & Yoccoz, N.G. (2009). Monitoring the spatio-temporal dynamics of geometrid moth outbreaks in birch forest using MODIS-NDVI data. Remote Sensing of Environment, 113, 1939-1947.

Jin, H., & Eklundh, L. (2014). A physically based vegetation index for improved monitoring of plant phenology. Remote Sensing of Environment, 152, 512-525.

Joiner, J., Yoshida, Y., Vasilkov, A.P., Schaefer, K., Jung, M., Guanter, L., Zhang, Y., Garrity, S., Middleton, E.M., Huemmrich, K.F., Gu, L., & Belelli Marchesini, L. (2014). The seasonal cycle of satellite chlorophyll fluorescence observations and its relationship to vegetation phenology and ecosystem atmosphere carbon exchange. Remote Sensing of Environment, 152, 375-391.

Jönsson, A.M., Eklundh, L., Hellström, M., Bärring, L., & Jönsson, P. (2010). Annual changes in MODIS vegetation indices of Swedish coniferous forests in relation to snow dynamics and tree phenology. Remote Sensing of Environment, 114, 2719-2730.

Jönsson, P., & Eklundh, L. (2004). TIMESAT-a program for analyzing time-series of satellite sensor data. Computers & Geosciences, 30, 833-845.

Justice, C.O., Townshend, J.R.G., Holben, B.N., & Tucker, C.J. (1985). Analysis of the phenology of global vegetation using meteorological satellite data. International Journal of Remote Sensing, 6, 1271-1318.

Karlsen, S.R., Elvebakk, A., Høgda, K.A., & Johansen, B. (2006). Satellite-based mapping of the growing season and bioclimatic zones in Fennoscandia. Global Ecology and Biogeography, 15, 416-430.

Karlsen, S.R., Tolvanen, A., Kubin, E., Poikolainen, J., Høgda, K.A., Johansen, B., Danks, F.S., Aspholm, P., Wielgolaski, F.E., & Makarova, O. (2008). MODIS-NDVI-based mapping of the length of the growing season in northern Fennoscandia. International Journal of Applied Earth Observation and Geoinformation, 10, 253-266.

Kim, Y., Kimball, J.S., McDonald, K.C., & Glassy, J. (2011). Developing a global data record of daily landscape freeze/thaw status using satellite passive microwave remote sensing. IEEE Transactions on Geoscience and Remote Sensing, 49, 949-960.

Kimball, J.S., McDonald, K.C., Running, S.W., & Frolking, S.E. (2004). Satellite radar remote sensing of seasonal growing seasons for boreal and subalpine evergreen forests. Remote Sensing of Environment, 90, 243-258.

Klosterman, S., Melaas, E., Wang, J.A., Martinez, A., Frederick, S., O'Keefe, J., Orwig, D.A., Wang, Z.S., Sun, Q.S., Schaaf, C., Friedl, M., & Richardson, A.D. (2018). Fine-scale perspectives on landscape phenology from unmanned aerial vehicle (UAV) photography. Agricultural and Forest Meteorology, 248, 397-407.

Klosterman, S.T., Hufkens, K., Gray, J.M., Melaas, E., Sonnentag, O., Lavine, I., Mitchell, L., Norman, R., Friedl, M.A., & Richardson, A.D. (2014). Evaluating remote sensing of deciduous forest phenology at multiple spatial scales using PhenoCam imagery. Biogeosciences, 11, 4305-4320.

Körner, C., & Basler, D. (2010). Phenology under global warming. Science, 327, 1461-1462.

Kosmala, M., Crall, A., Cheng, R., Hufkens, K., Henderson, S., & Richardson, A.D. (2016). Season Spotter: Using Citizen Science to Validate and Scale Plant Phenology from Near-Surface Remote Sensing. Remote Sensing, 8 (9), 726.

Kubin, E., Kotilainen, E., Poikolainen, J., Hokkanen, T., Nevalainen, S., Pouttu, A., Karhu, J., & Pasanen, J. (2007). Fenologisen havaintoverkon seurantaohjeet (p. 44): Finnish Forest Research Institute.

Kuusisto, E. (1984). Snow accumulation and snowmelt in Finland. Publications of the Water Research Institute (p. 149). Helsinki, Finland: National Board of Waters.

Leinonen, R., Pöyry, J., Söderman, G., & Tuominen-Roto, L. (2016). Suomen yöperhoseseuranta (Nocturna) 1993-2012 [The Finnish moth monitoring scheme (Nocturna) 1993-2012]. Reports of the Finnish Environment Institute (p. 71): Finnish Environment Institute.

Leyequien, E., Verrelst, J., Slot, M., Schaepman-Strub, G., Heitkönig, I.M.A., & Skidmore, A. (2007). Capturing the fugitive: Applying remote sensing to terrestrial animal distribution and diversity. International Journal of Applied Earth Observation and Geoinformation, 9, 1-20.

Liang, L.A., Schwartz, M.D., & Fei, S.L. (2011). Validating satellite phenology through intensive ground observation and landscape scaling in a mixed seasonal forest. Remote Sensing of Environment, 115, 143-157.

Lieth, H. (1974). Phenology and seasonality modelling. Berlin: Springer Verlag.

Linkosalo, T., Häkkinen, R., Terhivuo, J., Tuomenvirta, H., & Hari, P. (2009). The time series of flowering and leaf bud burst of boreal trees (1846–2005) support the direct temperature observations of climatic warming. Agricultural and Forest Meteorology, 149, 453-461.

Luo, Y.Q., Randerson, J.T., Abramowitz, G., Bacour, C., Blyth, E., Carvalhais, N., Ciais, P., Dalmonech, D., Fisher, J.B., Fisher, R., Friedlingstein, P., Hibbard, K., Hoffman, F., Huntzinger, D., Jones, C.D., Koven, C., Lawrence, D., Li, D.J., Mahecha, M., Niu, S.L., Norby, R., Piao, S.L., Qi, X., Peylin, P., Prentice, I.C., Riley, W., Reichstein, M., Schwalm, C., Wang, Y.P., Xia, J.Y., Zaehle, S., & Zhou, X.H. (2012). A framework for benchmarking land models. Biogeosciences, 9, 3857-3874.

Mahowald, N., Lo, F., Zheng, Y., Harrison, L., Funk, C., & Lombardozzi, D. (2015). Leaf Area Index in Earth System Models: evaluation and projections. Earth Syst. Dynam. Discuss., 6, 761-818.

Manninen, T., Aalto, T., Markkanen, T., Peltoniemi, M., Böttcher, K., Metsämäki, S., Anttila, K., Pirinen, P., & Arslan, A.N. (2019). Monitoring changes in forestry and seasonal snow using surface albedo during 1982–2016 as an indicator. Biogeosciences Discussion, 16, 223-240.

Meier, U. (Ed.) (1997). BBCH-Monograph. Growth stages of mono- and dicotyledonous plants. Berlin: Blackwell.

Melaas, E.K., Friedl, M.A., & Zhu, Z. (2013a). Detecting interannual variation in deciduous broadleaf forest phenology using Landsat TM/ETM plus data. Remote Sensing of Environment, 132, 176-185.

Melaas, E.K., Richardson, A.D., Friedl, M.A., Dragoni, D., Gough, C.M., Herbst, M., Montagnani, L., & Moors, E. (2013b). Using FLUXNET data to improve models of springtime vegetation activity onset in forest ecosystems. Agricultural and Forest Meteorology, 171–172, 46-56.

Menzel, A., & Fabian, P. (1999). Growing season extended in Europe. Nature, 397, 659-659.

Menzel, A., Sparks, T.H., Estrella, N., Koch, E., Aasa, A., Ahas, R., Alm-Kubler, K., Bissolli, P., Braslavska, O., Briede, A., Chmielewski, F.M., Crepinsek, Z., Curnel, Y., Dahl, A., Defila, C., Donnelly, A., Filella, Y., Jatcza, K., Mage, F., Mestre, A., Nordli, O., Penuelas, J., Pirinen, P., Remisova, V., Scheifinger, H., Striz, M., Susnik, A., Van Vliet, A.J.H., Wielgolaski, F.E., Zach, S., & Zust, A. (2006). European phenological response to climate change matches the warming pattern. Global Change Biology, 12, 1969-1976.

Metsämäki, S., Böttcher, K., Pulliainen, J., Luojus, K., Cohen, J., Takala, M., Mattila, O.-P., Schwaizer, G., Derksen, C., & Koponen, S. (2018). The accuracy of snow melt-off day derived from optical and microwave radiometer data — A study for Europe. Remote Sensing of Environment, 211, 1-12.

Metsämäki, S., Mattila, O.-P., Pulliainen, J., Niemi, K., Luojus, K., & Böttcher, K. (2012). An optical reflectance model-based method for fractional snow cover mapping applicable to continental scale. Remote Sensing of Environment, 123, 508-521.

Metsämäki, S., Pulliainen, J., Salminen, M., Luojus, K., Wiesmann, A., Solberg, R., Böttcher, K., Hiltunen, M., & Ripper, E. (2015). Introduction to GlobSnow Snow Extent products with considerations for accuracy assessment. Remote Sensing of Environment, 156, 96-108.

Monson, R., Sparks, J., Rosenstiel, T., Scott-Denton, L., Huxman, T., Harley, P., Turnipseed, A., Burns, S., Backlund, B., & Hu, J. (2005). Climatic influences on net ecosystem CO_2 exchange during the transition from wintertime carbon source to springtime carbon sink in a high-elevation, subalpine forest. Oecologia, 146, 130-147.

Moulin, S., Kergoat, L., Viovy, N., & Dedieu, G. (1997). Global-scale assessment of vegetation phenology using NOAA/AVHRR satellite measurements. Journal of Climate, 10, 1154-1155.

O'Connor, B., Secades, C., Penner, J., Sonnenschein, R., Skidmore, A., Burgess, N.D., & Hutton, J.M. (2015). Earth observation as a tool for tracking progress towards the Aichi Biodiversity Targets. Remote Sensing in Ecology and Conservation, 1, 19-28.

Olsson, P.-O., Lindström, J., & Eklundh, L. (2016). Near real-time monitoring of insect induced defoliation in subalpine birch forests with MODIS derived NDVI. Remote Sensing of Environment, 181, 42-53.

Öquist, G., & Huner, N.P.A. (2003). Photosynthesis of overwintering evergreen plants. Annual Reviews of Plant Biology, 54, 329-355.

Pan, Y.D., Birdsey, R.A., Fang, J.Y., Houghton, R., Kauppi, P.E., Kurz, W.A., Phillips, O.L., Shvidenko, A., Lewis, S.L., Canadell, J.G., Ciais, P., Jackson, R.B., Pacala, S.W., McGuire, A.D., Piao, S.L., Rautiainen, A., Sitch, S., & Hayes, D. (2011). A large and persistent carbon sink in the world's forests. Science, 333, 988-993.

Pecl, G.T., Araújo, M.B., Bell, J.D., Blanchard, J., Bonebrake, T.C., Chen, I.-C., Clark, T.D., Colwell, R.K., Danielsen, F., Evengård, B., Falconi, L., Ferrier, S., Frusher, S., Garcia, R.A., Griffis, R.B., Hobday, A.J., Janion-Scheepers, C., Jarzyna, M.A., Jennings, S., Lenoir, J., Linnetved, H.I., Martin, V.Y., McCormack, P.C., McDonald, J., Mitchell, N.J., Mustonen, T., Pandolfi, J.M., Pettorelli, N., Popova, E., Robinson, S.A., Scheffers, B.R., Shaw, J.D., Sorte, C.J.B., Strugnell, J.M., Sunday, J.M., Tuanmu, M.-N., Vergés, A., Villanueva, C., Wernberg, T., Wapstra, E., & Williams, S.E. (2017). Biodiversity redistribution under climate change: Impacts on ecosystems and human well-being. Science, 355, eaai9214.

Peltoniemi, M., Aurela, M., Böttcher, K., Kolari, P., Loehr, J., Hokkanen, T., Karhu, J., Linkosalmi, M., Tanis, C.M., Metsämäki, S., Tuovinen, J.-P., Vesala, T., & Arslan, A.N. (2018a). Networked web-cameras monitor congruent seasonal development of birches with phenological field observations. Agricultural and Forest Meteorology, 249, 335-347.

Peltoniemi, M., Aurela, M., Böttcher, K., Kolari, P., Loehr, J., Karhu, J., Linkosalmi, M., Tanis, C.M., Tuovinen, J.P., & Arslan, A.N. (2018b). Webcam network and image database for studies of phenological changes of vegetation and snow cover in Finland, image time series from 2014 to 2016. Earth Syst. Sci. Data, 10, 173-184.

Peñuelas, J., Rutishauser, T., & Filella, I. (2009). Phenology Feedbacks on Climate Change. Science, 324, 887-888.

Pereira, H.M., Ferrier, S., Walters, M., Geller, G.N., Jongman, R.H.G., Scholes, R.J., Bruford, M.W., Brummitt, N., Butchart, S.H.M., Cardoso, A.C., Coops, N.C., Dulloo, E., Faith, D.P., Freyhof, J., Gregory, R.D., Heip, C., Hoeft, R., Hurtt, G., Jetz, W., Karp, D.S., McGeoch, M.A., Obura, D., Onoda, Y., Pettorelli, N., Reyers, B., Sayre, R., Scharlemann, J.P.W., Stuart, S.N., Turak, E., Walpole, M., & Wegmann, M. (2013). Essential Biodiversity Variables. Science, 339, 277-278.

Pettorelli, N., Laurance, W.F., O'Brien, T.G., Wegmann, M., Nagendra, H., & Turner, W. (2014). Satellite remote sensing for applied ecologists: opportunities and challenges. Journal of Applied Ecology, 51, 839-848.

Picard, G., Quegan, S., Delbart, N., Lomas, M.R., Le Toan, T., & Woodward, F.I. (2005). Bud-burst modelling in Siberia and its impact on quantifying the carbon budget. Global Change Biology, 11, 2164-2176.

Pirinen, P., Simola, H., Aalto, J., Kaukoranta, J.-P., Karlsson, P., & Ruuhela, R. (2012). TILASTOJA SUOMEN ILMASTOSTA 1981-2010 (Climatological statistics of Finland 1981-2010). Reports (p. 96). Helsinki, Finland: Finnish Meteorological Insitute.

Potter, C., Tan, P.N., Steinbach, M., Klooster, S., Kumar, V., Myneni, R., & Genovese, V. (2003). Major disturbance events in terrestrial ecosystems detected using global satellite data sets. Global Change Biology, 9, 1005-1021.

Pöyry, J., Böttcher, K., Fronzek, S., Gobron, N., Leinonen, R., Metsämäki, S., & Virkkala, R. (2018). Predictive power of remote sensing versus temperature-derived variables in modelling phenology of herbivorous insects. Remote Sensing in Ecology and Conservation, 4, 113-126.

Pöyry, J., Luoto, M., Heikkinen, R.K., Kuussaari, M., & Saarinen, K. (2009). Species traits explain recent range shifts of Finnish butterflies. Global Change Biology, 15, 732-743.

Pudas, E., Leppälä, M., Tolvanen, A., Poikolainen, J., Venäläinen, A., & Kubin, E. (2008). Trends in phenology of Betula pubescens across the boreal zone in Finland. International Journal of Biometeorology, 52, 251-259.

Pulliainen, J., Aurela, M., Laurila, T., Aalto, T., Takala, M., Salminen, M., Kulmala, M., Barr, A., Heimann, M., Lindroth, A., Laaksonen, A., Derksen, C., Mäkelä, A., Markkanen, T., Lemmetyinen, J., Susiluoto, J., Dengel, S., Mammarella, I., Tuovinen, J.-P., & Vesala, T. (2017). Early snowmelt significantly enhances boreal springtime carbon uptake. Proceedings of the National Academy of Sciences of the United States of America, 114, 11081-11086.

Pureswaran, D.S., De Grandpré, L., Paré, D., Taylor, A., Barrette, M., Morin, H., Régnière, J., & Kneeshaw, D.D. (2015). Climate-induced changes in host tree–insect phenology may drive ecological state-shift in boreal forests. Ecology, 96, 1480-1491

Raddatz, T.J., Reick, C.H., Knorr, W., Kattge, J., Roeckner, E., Schnur, R., Schnitzler, K.G., Wetzel, P., & Jungclaus, J. (2007). Will the tropical land biosphere dominate the climate–carbon cycle feedback during the twenty-first century? Climate Dynamics, 29, 565-574.

Räisänen, J., & Tuomenvirta, H. (2009). Interactions between boreal forests and climate change. In P. Hari, & L. Kulmala (Eds.), Boreal forest and climate change (pp. 479-493). Springer Science+Business Media B.V..

Rautiainen, K., Parkkinen, T., Lemmetyinen, J., Schwank, M., Wiesmann, A., Ikonen, J., Derksen, C., Davydov, S., Davydov, A., Boike, J., Langer, M., Drusch, M.T., & Pulliainen, J. (2016). SMOS prototype algorithm for detecting autumn soil freezing. Remote Sensing of Environment, SMOS special issue, 180, 346-360

Reed, B.C., Brown, J.F., Vanderzee, D., Loveland, T.R., Merchant, J.W., & Ohlen, D.O. (1994). Measuring phenological variability from satellite imagery. Journal of Vegetation Sciences, 5, 703-714.

Reed, B.C., Schwartz, M.D., & Xiao, X. (2009). Remote sensing phenology. In A. Noormets (Ed.), Phenology of ecosystem processes Applications in global change research (pp. 231-246). Dordrecht: Springer.

Reick, C.H., Raddatz, T., Brovkin, V., & Gayler, V. (2013). Representation of natural and anthropogenic land cover change in MPI-ESM. Journal of Advances in Modeling Earth Systems, 5, 459-482.

Richardson, A.D., Anderson, R.S., Arain, M.A., Barr, A.G., Bohrer, G., Chen, G., Chen, J.M., Ciais, P., Davis, K.J., Desai, A.R., Dietze, M.C., Dragoni, D., Garrity, S.R., Gough, C.M., Grant, R., Hollinger, D.Y., Margolis, H.A., McCaughey, H., Migliavacca, M., Monson, R.K., Munger, J.W., Poulter, B., Raczka, B.M., Ricciuto, D.M., Sahoo, A.K., Schaefer, K., Tian, H., Vargas, R., Verbeeck, H., Xiao, J., & Xue, Y. (2012). Terrestrial biosphere models need better representation of vegetation phenology: results from the North American Carbon Program Site Synthesis. Global Change Biology, 18, 566-584.

Richardson, A.D., Black, T.A., Ciais, P., Delbart, N., Friedl, M.A., Gobron, N., Hollinger, D.Y., Kutsch, W.L., Longdoz, B., Luyssaert, S., Migliavacca, M., Montagnani, L., Munger, J.W., Moors, E., Piao, S., Rebmann, C., Reichstein, M., Saigusa, N., Tomelleri, E., Vargas, R., & Varlagin, A. (2010). Influence of spring and autumn phenological transitions on forest ecosystem productivity. Philos Trans R Soc Lond B Biol Sci, 365, 3227-3246.

Richardson, A.D., Hollinger, D.Y., Dail, D.B., Lee, J.T., Munger, J.W., & O'Keefe, J. (2009). Influence of spring phenology on seasonal and annual carbon balance in two contrasting New England forests. Tree Physiology, 29, 321-331.

Richardson, A.D., Hufkens, K., Milliman, T., Aubrecht, D.M., Chen, M., Gray, J.M., Johnston, M.R., Keenan, T.F., Klosterman, S.T., Kosmala, M., Melaas, E.K., Friedl, M.A., & Frolking, S. (2018). Tracking vegetation phenology across diverse North American biomes using PhenoCam imagery. Scientific Data, 5, 180028.

Richardson, A.D., Jenkins, J.P., Braswell, B.H., Hollinger, D.Y., Ollinger, S.V., & Smith, M.-L. (2007). Use of digital webcam images to track spring green-up in a deciduous broadleaf forest. Oecologia, 152, 323-334.

Richardson, A.D., Keenan, T.F., Migliavacca, M., Ryu, Y., Sonnentag, O., & Toomey, M. (2013). Climate change, phenology, and phenological control of vegetation feedbacks to the climate system. Agricultural and Forest Meteorology, 169, 156-173.

Rousi, M., & Heinonen, J. (2007). Temperature sum accumulation effects on within-population variation and long-term trends in date of bud burst of European white birch (Betula pendula). Tree Physiology, 27, 1019-1025.

Roy, A., Royer, A., Derksen, C., Brucker, L., Langlois, A., Mialon, A., & Kerr, Y.H. (2015). Evaluation of Spaceborne L-Band Radiometer Measurements for Terrestrial Freeze/Thaw Retrievals in Canada. IEEE Journal of Selected Topics in Applied Earth Observations and Remote Sensing, 8, 4442-4459.

Ruckstuhl, K.E., Johnson, E.A., & Miyanishi, K. (2008). Introduction. The boreal forest and global change. Philosophical Transactions of the Royal Society B: Biological Sciences, 363, 2245-2249.

Savitzky, A., & Golay, M.J.E. (1964). Smoothing and differentiation of data by simplified least squares procedures. Analytical Chemistry, 36, 1627-1639.

Schultz, J. (1995). Die Ökozonen der Erde. (2 nd. ed.). Stuttgart: Ulmer.

Schwartz, M.D. (1998). Green-wave phenology. Nature, 394, 839-840.

Secades, C., O'Connor, B., Brown, C., & Walpole, M. (2014). Earth observation for biodiversity monitoring: A review of current approaches and future opportunities for tracking progress towards the Aichi biodiversity targets. e-book CBD Technical Series, Vol.72, Secretariat of the Convention on Biological Diversity, Montreal, Canada.

Senf, C., Pflugmacher, D., Heurich, M., & Krueger, T. (2017). A Bayesian hierarchical model for estimating spatial and temporal variation in vegetation phenology from Landsat time series. Remote Sensing of Environment, 194, 155-160.

Sevanto, S., Suni, T., Pumpanen, J., Grönholm, T., Kolari, P., Nikinmaa, E., Hari, P., & Vesala, T. (2006). Wintertime photosynthesis and water uptake in a boreal forest. Tree Physiology, 26, 749-757.

Shutova, E., Wielgolaski, F.E., Karlsen, S.R., Makarova, O., Berlina, N., Filimonova, T., Haraldsson, E., Aspholm, P.E., Flø, L., & Høgda, K.A. (2006). Growing seasons of Nordic mountain birch in northernmost Europe as indicated by long-term field studies and analyses of satellite images. International Journal of Biometeorology, 51, 155-166.

Sims, D.A., Rahman, A.F., Cordova, V.D., El-Masri, B.Z., Baldocchi, D.D., Bolstad, P.V., Flanagan, L.B., Goldstein, A.H., Hollinger, D.Y., Misson, L., Monson, R.K., Oechel, W.C., Schmid, H.P., Wofsy, S.C., & Xu, L. (2008). A new model of gross primary productivity for North American ecosystems based solely on the enhanced vegetation index and land surface temperature from MODIS. Remote Sensing of Environment, 112, 1633-1646.

Skidmore, A.K., Pettorelli, N., Coops, N.C., Geller, G.N., Hansen, M., Lucas, R., Mücher, C.A., O'Connor, B., Paganini, M., Pereira, H.M., Schaepman, M., Turner, W., Wang, T., & Wegmann, M. (2015). Agree on biodiversity metrics to track from space. Nature, 523, 403-405.

Smith, N.V., Saatchi, S.S., & Randerson, J.T. (2004). Trends in high northern latitude soil freeze and thaw cycles from 1988 to 2002. Journal of Geophysical Research: Atmospheres, 109, D12101.

Sonnentag, O., Hufkens, K., Teshera-Sterne, C., Young, A.M., Friedl, M., Braswell, B.H., Milliman, T., O'Keefe, J., & Richardson, A.D. (2012). Digital repeat photography for phenological research in forest ecosystems. Agricultural and Forest Meteorology, 152, 159-177.

Soudani, K., le Maire, G., Dufrêne, E., François, C., Delpierre, N., Ulrich, E., & Cecchini, S. (2008). Evaluation of the onset of green-up in temperate deciduous broadleaf forests derived from Moderate Resolution Imaging Spectroradiometer (MODIS) data. Remote Sensing of Environment, 112, 2643-2655.

Spruce, J.P., Sader, S., Ryan, R.E., Smoot, J., Kuper, P., Ross, K., Prados, D., Russell, J., Gasser, G., McKellip, R., & Hargrove, W. (2011). Assessment of MODIS NDVI time series data products for detecting forest defoliation by gypsy moth outbreaks. Remote Sensing of Environment, 115, 427-437.

Stenberg, P., Rautiainen, M., Manninen, T., Voipio, P., & Smolander, S. (2004). Reduced simple ratio better than NDVI for estimating LAI in Finnish pine and spruce stands. Silva Fennica, 38, 3-14.

Suni, T., Berninger, F., Markkanen, T., Keronen, P., Rannik, Ü., & Vesala, T. (2003a). Interannual variability and timing of growing-season CO_2 exchange in a boreal forest. Journal of Geophysical Research: Atmospheres, 108 (D9), 4265.

Suni, T., Berninger, F., Vesala, T., Markkanen, T., Hari, P., Mäkelä, A., Ilvesniemi, H., Hänninen, H., Nikinmaa, E., Huttula, T., Laurila, T., Aurela, M., Grelle, A., Lindroth, A., Arneth, A., Shibistova, O., & Lloyd, J. (2003b). Air temperature triggers the recovery of evergreen boreal forest photosynthesis in spring. Global Change Biology, 9, 1410-1426.

SYKE Vegetation phenology 2001-2017. Maps of the start of the vegetation active period in Finland, updated 27.09.2018. Available from http://syke.maps.arcgis.com/apps/webappviewer/index.html?id=a446e987496b4d8794b307e882da718a (accessed 05.10.2018).

Thum, T., Aalto, T., Laurila, T., Aurela, M., Hatakka, J., Lindroth, A., & Vesala, T. (2009). Spring initiation and autumn cessation of boreal coniferous forest CO_2 exchange assessed by meteorological and biological variables. Tellus B, 61, 701-717.

Vesala, T., Launiainen, S., Kolari, P., Pumpanen, J., Sevanto, S., Hari, P., Nikinmaa, E., Kaski, P., Mannila, H., Ukkonen, E., Piao, S.L., & Ciais, P. (2010). Autumn temperature and carbon balance of a boreal Scots pine forest in Southern Finland. Biogeosciences, 7, 163-176.

Vihervaara, P., Auvinen, A.-P., Mononen, L., Törmä, M., Ahlroth, P., Anttila, S., Böttcher, K., Forsius, M., Heino, J., Heliölä, J., Koskelainen, M., Kuussaari, M., Meissner, K., Ojala, O., Tuominen, S., Viitasalo, M., & Virkkala, R. (2017). How Essential Biodiversity Variables and remote sensing can help national biodiversity monitoring. Global Ecology and Conservation, 10, 43-59.

Vogg, G., Heim, R., Hansen, J., Schäfer, C., & Beck, E. (1998). Frost hardening and photosynthetic performance of Scots pine (Pinus sylvestris L.) needles. I. Seasonal changes in the photosynthetic apparatus and its function. Planta, 204, 193-200.

Walther, S., Voigt, M., Thum, T., Gonsamo, A., Zhang, Y., Köhler, P., Jung, M., Varlagin, A., & Guanter, L. (2016). Satellite chlorophyll fluorescence measurements reveal large-scale decoupling of photosynthesis and greenness dynamics in boreal evergreen forests. Global Change Biology, 22, 2979-2996.

White, M.A., & Nemani, R.R. (2006). Real-time monitoring and short-term forecasting of land surface phenology. Remote Sensing of Environment, 104, 43-49.

White, M.A., Thornton, P.E., & Running, S.W. (1997). A Continental Phenology Model for Monitoring Vegetation Responses to Interannual Climatic Variability. Global Biogeochem. Cycles, 11, 217-234.

Yang, X., Mustard, J.F., Tang, J., & Xu, H. (2012). Regional-scale phenology modeling based on meteorological records and remote sensing observations. Journal of Geophysical Research: Biogeosciences, 117, G0302.

Zhang, X., Friedl, M.A., & Schaaf, C.B. (2006). Global vegetation phenology from Moderate Resolution Imaging Spectroradiometer (MODIS): Evaluation of global patterns and comparison with in situ measurements. Journal of Geophysical Research: Biogeosciences, 111, G04017.

Zhang, X., Jayavelu, S., Liu, L., Friedl, M.A., Henebry, G.M., Liu, Y., Schaaf, C.B., Richardson, A.D., & Gray, J. (2018a). Evaluation of land surface phenology from VIIRS data using time series of PhenoCam imagery. Agricultural and Forest Meteorology, 256-257, 137-149.

Zhang, X., Liu, L., Liu, Y., Jayavelu, S., Wang, J., Moon, M., Henebry, G.M., Friedl, M.A., & Schaaf, C.B. (2018b). Generation and evaluation of the VIIRS land surface phenology product. Remote Sensing of Environment, 216, 212-229

Zhang, X., Wang, J., Gao, F., Liu, Y., Schaaf, C., Friedl, M., Yu, Y., Jayavelu, S., Gray, J., Liu, L., Yan, D., & Henebry, G.M. (2017). Exploration of scaling effects on coarse resolution land surface phenology. Remote Sensing of Environment, 190, 318-330.

MODIS time-series-derived indicators for the beginning of the growing season in boreal coniferous forest — A comparison with CO_2 flux measurements and phenological observations in Finland

Kristin Böttcher [a,*], Mika Aurela [b], Mikko Kervinen [a], Tiina Markkanen [b], Olli-Pekka Mattila [a], Pasi Kolari [c], Sari Metsämäki [a], Tuula Aalto [b], Ali Nadir Arslan [b], Jouni Pulliainen [b]

[a] *Finnish Environment Institute, Geoinformatics Division, FI-00251 Helsinki, Finland*
[b] *Finnish Meteorological Institute, FI-00560 Helsinki, Finland*
[c] *University of Helsinki, Forest Sciences, FI-00014 University of Helsinki, Finland*

ABSTRACT

Spring phenological events are important for the assessment of the carbon budget in forest ecosystems. In large parts of the boreal zone the evergreen conifers are dominant, but most available satellite-based methods for the detection of the start of the growing season have focussed on the greening-up of deciduous species. We investigated the possibility of determining spring phenological events of boreal evergreen coniferous forest from Moderate Resolution Imaging Spectroradiometer (MODIS) time-series based on test sites in Finland. The beginning of the photosynthetically active period, determined from the CO_2 fluxes measured with the eddy covariance (EC) method, was used as a primary reference for the onset of the growing season (growing season start date, GSSD). Furthermore, phenological observations of pine trees, such as the beginning of shoot elongation (growth of pine start date, GPSD) were included in the comparison. The corresponding indicators were derived from MODIS data and compared with *in situ* phenological observations. This was carried out using cloud-filtered daily MODIS time-series of Normalized Difference Vegetation Index (NDVI), Normalized Difference Water Index (NDWI) and Fractional Snow Cover (FSC) from homogenous areas around *in situ* sites (3 EC sites and 4 phenological sites in Finland). GSSD in coniferous forest showed correspondence with the time during snowmelt when the ground starts to be exposed, which was indicated by a decrease in FSC and the spring-rise in NDVI time-series. GPSD occurred in general after complete snow melt. Satellite-derived GSSD from NDVI ($GSSD_{NDVI}$) and FSC ($GSSD_{FSC}$) showed good correspondence with *in situ* observations for both NDVI and FSC ($R^2 > 0.8$, RMSE < 7 days) including observations from two CO_2 flux measurement sites in Northern Finland and one in Southern Finland. The highest site-wise correlations were obtained for the satellite indicator $GSSD_{FSC}$. Finally, the national-scale mapping of GSSD was demonstrated based on the satellite-derived indicator $GSSD_{FSC}$.

© 2013 Elsevier Inc. All rights reserved.

1. Introduction

Spring phenology is one important factor influencing the carbon balance of boreal forest ecosystems (Richardson et al., 2009, 2010) and therefore accurate information related to spring phenology is needed for studies of the carbon budget of this region. The recovery of photosynthetic activity (referred here as growing season start date, GSSD) in an ecosystem can be determined from *in situ* eddy covariance (EC) measurements of the CO_2 fluxes at local sites (e.g. Suni et al., 2003). These point-wise measurements need to be generalised to larger areas and satellite observations could be one possibility to achieve that.

Time-series of vegetation indices, such as the Normalized Difference Vegetation Index (NDVI), are widely used for monitoring of vegetation phenology (Badeck et al., 2004; Reed et al., 1994; White, Thornton, & Running, 1997). The NDVI eliminates dependence on sun–target–sensor geometry to a certain extent, but due to differences in the anisotropic behaviour of canopies in red and near-infrared reflectance, NDVI is slightly geometry-dependent (Gutman, 1991). The sensitivity of NDVI to sun zenith angle (SZA) is low (Huemmrich, Black, Jarvis, McCaughey, & Hall, 1999) and depends on the leaf area of the canopy and reflectivity of the ground. The influence of SZA decreases with increasing canopy leaf area and darker ground (Kaufmann et al., 2000). The contrast between red and near-infrared reflectance is reduced by atmospheric effects, which usually lead to lower NDVI (Gutman, 1991). According to theoretical analysis by Sellers (1985), NDVI can be directly related to photosynthesis in non-water-limited environments; correlations between NDVI and gross primary production (GPP) (Wang et al., 2004) and modelled photosynthetic capacity in boreal forests (Gea-Izquierdo et al., 2010) were reported. For the extraction of phenological key-stages of vegetation from NDVI time-series, such as

---

onset of greenness, good correspondence has been obtained between satellite-derived budburst day and field observations for deciduous trees in the temperate region (Badeck et al., 2004; Duchemin, Goubier, & Courrier, 1999; Maignan, Bréon, Bacour, Demarty, & Poirson, 2008; Soudani et al., 2008).

However, in the boreal region greening-up and snow melt cannot be well distinguished in NDVI time-series (Delbart, Kergoat, Le Toan, L'Hermitte, & Picard, 2005; Jönsson, Eklundh, Hellström, Bärring, & Jönsson, 2010; Moulin, Kergoat, Viovy, & Dedieu, 1997; White et al., 2009), because the NDVI already shows a steep increase when snow melts, due to a strong decrease in reflectance. Therefore adapted methods were developed to determine the greening-up in this region (Beck, Atzberger, Høgda, Johansen, & Skidmore, 2006; Delbart et al., 2005; Karlsen et al., 2008). In order to avoid the influence of snow cover on the retrieval of the greening-up, Delbart et al. (2005) developed a method based on the Normalized Difference Vegetation Index (NDWI). NDWI was initially applied for the monitoring of vegetation liquid water content from space using radiances at wavelengths 860 nm and 1240 nm (Gao, 1996). Both wavelengths are located in the reflectance plateau of vegetation canopies and therefore sense similar depth through vegetation canopies, in contrast to NDVI for which the red channel is located in the strong chlorophyll absorption region. NDWI is less sensitive to atmospheric scattering than NDVI (Gao, 1996). It decreases during snowmelt and increases when vegetation is greening up, thus allowing a free-of snow effect determination of greening-up in the boreal region (Delbart et al., 2005).

In contrast to deciduous trees, seasonal changes in evergreen conifers are not easily observed. Photosynthesis is inhibited during winter, but close-to-full photosynthetic capacity can be reached only after a few days with optimal environmental conditions (Sevanto et al., 2006). Photosynthetic recovery is mainly driven by air temperature (Suni et al., 2003), independent from changes in canopy structure (Richardson et al., 2009), includes multiple steps and is reversible (Monson et al., 2005). While air temperature was found to be the main factor for the onset of photosynthesis, soil temperature is an important limiting factor for full photosynthetic recovery in late spring after the end of the snow melt (Bergh & Linder, 1999; Wu, Jansson, & Kolari, 2012).

Differences in the beginning of the growing season between evergreen coniferous forests and other vegetation species, such as deciduous broadleaved forest, were mostly overlooked in mapping of this event from satellite-derived time-series, and the same methodology (using in general bud burst observation of deciduous trees as reference) was applied for different land cover classes and regions, for example in the MODIS phenology product (Ganguly, Friedl, Tan, Zhang, & Verma, 2010). Comparisons between springtime source-sink transition indicators derived from CO_2 flux measurements and satellite-derived phenological indicators across deciduous broadleaved and evergreen coniferous forest sites showed correlations for both ecosystems, but the flux-derived date in evergreen coniferous forests preceded the satellite-derived indicator by several weeks (Melaas et al., 2013; Richardson et al., 2010).

The satellite-derived greening-up in evergreen coniferous forest may correspond to the start of needle growth (Beck et al., 2007), but satellite-retrievals were usually not verified with phenological observations of evergreen conifers (Gonsamo, Chen, Price, Kurz, & Wu, 2012). Only a few studies compared spring phenological events in evergreen coniferous forest with satellite-derived time series (Gonsamo et al., 2012; Jönsson et al., 2010; Thum et al., 2009). The timing of budburst of evergreen conifers in Swedish forest could not be derived with absolute nor relative threshold values of vegetation indices, due to the influence of snow cover and the small and slow changes of needle biomass (Jönsson et al., 2010). Thum et al. (2009) found that the beginning of snow melt, determined from Moderate Resolution Imaging Spectrometer (MODIS) surface albedo observations, appeared to be a good estimator for the beginning of the active period of coniferous forest as observed from EC measurements.

The aim of this work was therefore to evaluate the possibility to use satellite-derived proxy indicators for the determination of GSSD in evergreen coniferous forest in the boreal region. A special interest of this paper was to investigate the feasibility of using the Earth observation-based Fractional Snow Cover (FSC) product as indicator for GSSD. The applied FSC estimates are derived with the reflectance model-based snow monitoring method SCA*mod* (Metsämäki, Anttila, Huttunen, & Vepsäläinen, 2005) of the Finnish Environment Institute (SYKE), developed for boreal forest and the tundra belt. It has been shown to provide reliable estimates of the fractional snow cover for forested areas; validation against ground truth data from distributed snow surveys in Finland showed a root mean squared error (RMSE) of 0.11 FSC and higher retrieval accuracies for boreal forests than e.g. the MODIS fractional snow cover product by NASA/Goddard Space Flight Center (Hall & Riggs, 2007; Riggs, Hall, & Salomonson, 2006) were demonstrated (Metsämäki et al., 2012). Hence, MODIS-derived time-series of FSC, as well as commonly used vegetation indices such as NDVI and NDWI, were compared with *in situ* dates of GSSD from three EC sites in order to develop a method for the detection of GSSD from satellite-derived time-series. In order to allow comparisons with other studies

Table 1
Characteristics of *in situ* sites.

Site	Observation/ organisation	Geographic coordinates	Altitude above sea (m)	Forest type	Phytogeographical zone[1]	Mean annual air temperature (°C) and precipitation (mm)[2]	Observation period
Äkäslompolo	Phenology/METLA	67° 35′ N 24° 12′ E	340	Scots pine	Northern boreal	−1.4[a] 484	2001–2006
Hyytiälä	CO_2 flux/ University of Helsinki	61° 51′ N 24° 17′ E	170	Scots pine/ Norway spruce	Southern boreal	3.5[b] 601	2001–2010
Kenttärova	CO_2 flux/FMI	67° 59′ N 24° 15′ E	347	Norway spruce	Northern boreal	−1.8[c] 501	2003–2010
Paljakka	Phenology/METLA	64° 40′ N 28° 03′ E	295	Scots pine	Middle boreal	1.7[d] 532	2001–2010
Parkano	Phenology/METLA	62° 01′ N 23° 03′ E	115	Scots pine	Southern boreal	2.7[e] 632	2001–2008, 2010
Saariselkä	Phenology/METLA	68° 24′ N 27° 23′ E	300	Scots pine	Northern boreal	−0.8[f] 435	2001–2006
Sodankylä	CO_2 flux/FMI	67° 21′ N 26° 38′ E	179	Scots pine	Northern boreal	−0.8 507	2001–2010

METLA, Finnish Forest Research Institute. FMI, Finnish Meteorological Institute.
[1] Definition of phytogeographical zones according to Ahti, Hämet-Ahti, and Jalas (1968).
[2] Long term records of air temperature and precipitation are for the period from 1971 to 2000 from stations: [a]Muonio Alamuonio, [b]Jämsä, [c]Kittilä Pulju, [d]Kajaani airport, [e]Ähtäri Myllymäki, [f]Inari/Ivalo airport (Drebs, Nordlund, Karlsson, Helminen, & Rissanen, 2002).
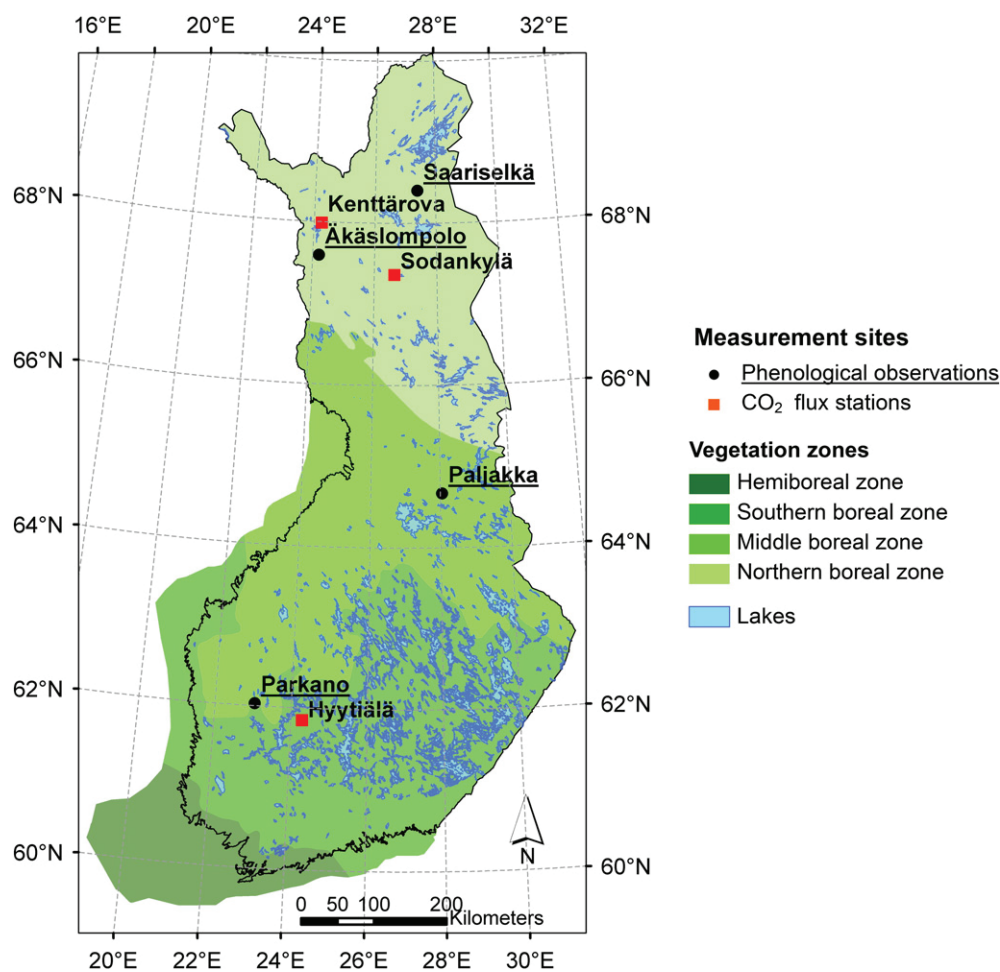
Fig. 1. Location of measurement sites and main phytogeographical zones (Ahti et al., 1968) in Finland.

aiming at the greening-up of the vegetation, phenological observations of beginning of growth of pine trees were also compared at four phenological sites. Satellite-derived GSSDs were evaluated against *in situ* measurements at three sites and the mapping of GSSD was demonstrated in Finland.

2. Data set and methods

2.1. Measurement sites

The measurement sites are located in coniferous forests in Finland, including three CO_2 flux sites and four phenology observation sites (Table 1 and Fig. 1), and stretch from the Southern boreal to the Northern boreal phytogeographical zone. The dominant tree species for all sites is Scots pine (*Pinus sylvestris*), except for Kenttärova with dominance of Norway spruce (*Picea abies*). All sites are located on mineral soils. The snow covered period extends typically from November to May in Northern and from December to April in Southern Finland, covering 6 and 4 months at northern and southern sites, respectively (Kuusisto, 1984).

2.2. CO₂ flux measurements

The *in situ* fluxes of CO_2 were measured by the micrometeorological eddy covariance method, which gives us direct measurements of CO_2 fluxes averaged on an ecosystem scale. In the EC method, the vertical CO_2 flux is obtained as the covariance of the high frequency (10 Hz) observations of vertical wind speed and the CO_2 concentration (Baldocchi, 2003). The eddy covariance measurement systems at Sodankylä and Kenttärova included a USA-1 (METEK GmbH, Elmshorn, Germany) three-axis sonic anemometer/thermometer and a closed-path LI-7000 (Li-Cor., Inc., Lincoln, NE, USA) CO_2/H_2O gas analyzer. In Hyytiälä a Solent 1012R3 anemometer (Gill Instruments Ltd., Lymington, UK) with closed-path LI-6262 analyser (Li-Cor Inc., Lincoln, NE, USA) was used. The measurements were performed 5 to 10 m above the mean forest height. The EC fluxes were calculated as half-hourly averages, taking into account the appropriate corrections. The measurement systems and the post-processing procedures are presented in more detail by Aurela (2005) and Aurela et al. (2009) for Sodankylä and Kenttärova, and by Rannik, Keronen, Hari, and Vesala (2004) and Mammarella et al. (2009) for Hyytiälä. Details on meteorological measurements in Hyytiälä can be found in Vesala et al. (2005). Additional meteorological measurements at each site include precipitation, air temperature at different heights (here we used temperature at 18 m height for Sodankylä and Kenttärova and at 8 m height for Hyytiälä) and soil temperature and volumetric soil liquid water content (SWC) at different depths.

2.3. Determination of GSSD from CO₂ flux measurements

The growing season start date was determined for Sodankylä (2001–2010), Hyytiälä (2001–2010) and Kenttärova (2003–2010) from the continuous CO_2 flux measurement data. GSSD could not be calculated for site Kenttärova for year 2004 due to data gaps. The GSSD is here defined as the day on which the CO_2 uptake exceeds permanently the 15% level of the growing season maximum (Fig. 2). In practice, the GSSD was obtained from the annual cycle of gross photosynthesis index (PI, Aurela, Tuovinen, & Laurila, 2001), which indicates the apparent photosynthetical activity on a daily scale. It is calculated as a
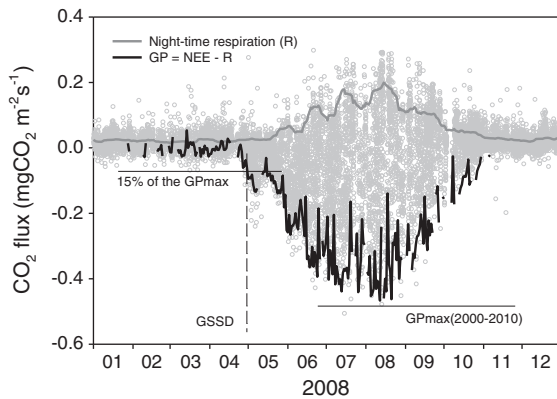
Fig. 2. Determination of GSSD from eddy covariance data (grey circles) at Sodankylä. A common maximum of gross photosynthesis (GPmax) for the whole measurement period (2001–2010) was obtained as the 90th percentile of the daily GP values representing the month of the highest uptake of each year. Daily GP was obtained as a difference of daytime NEE (net ecosystem CO2 exchange) and night-time respiration. The GSSD for different years was then obtained as the date when daily GP exceeds 15% of this common GPmax.

difference of the daily averages of daytime (Photosynthetic Photon Flux Density (PPFD) $> 600 \, \mu mol \, m^{-2} \, s^{-1}$) Net Ecosystem Exchange of CO_2 (NEE) and night-time (PPFD $< 20 \, \mu mol \, m^{-2} \, s^{-1}$) respiration and is scaled with the growing season maximum. The obtained index is not actual gross photosynthesis (GP), as the night-time respiration differs from the daytime respiration, but as it is used as a relative measure it provides a reasonable estimate. The growing season maximum is the 90th percentile of the daily GP indexes during the month of highest uptake for the multi-year measurement period. The method used for the determination of GSSD differs from the method used for the same sites by Suni et al. (2003) and Thum et al. (2009). They used instantaneous (30-min) NEE values as compared to daily averages of GP utilized here. However, the progress in photosynthetic activity is typically very fast in these boreal sites, indicating that results are not particularly sensitive to such differences in the method.

2.4. Phenological observations

Phenological observations on pine trees at four sites: Parkano, Paljakka, Äkäslompolo and Saariselkä (Table 1 and Fig. 1), for the years 2001–2010 were obtained from the Finnish Forest Research Institute (METLA). The phenophase (BBCH codes in brackets (Meier, 1997)) beginning of shoot elongation (May shoot, BBCH30) of Scots pine was used in this study. Hereafter, beginning of shoot elongation is referred to as growth of pine start date (GPSD). Phenological observations were carried out twice a week in advanced thinning stands growing on medium fertile

soil. The microclimate at the site must be representative of the local climatic conditions. The monitored trees (5 trees) are of local provenance and preferably naturally regenerated. In order to allow accurate observation of shoot elongation, small sized trees in well-illuminated plots were selected. Since 2007 the same trees have been monitored every year, but before that the trees may have changed from year to year. Further details on observations are given in Kubin et al. (2007).

2.5. Snow observations

Daily observations of snow depth and snow coverage for each site were obtained from the nearest weather station, operated by the Finnish Meteorological Institute (FMI). Snow coverage is estimated visually at each station in coarse classes (e-codes) following the definitions by the World Meteorological Organization.

2.6. MODIS data and processing

MODIS-derived FSC and vegetation indices (NDVI and NDWI) were investigated for the use as proxy indicators for GSSD and GPSD. Daily Terra/MODIS Level-1B data (1 km, 500 m and 250 m products) were collected from NASA's Level 1 Land and Atmosphere Archive and Distribution System (LAADS) and/or from the receiving station of FMI in Sodankylä for the period from February to October 2001–2010. Raw instrument data were calibrated to top-of-atmosphere reflectances including sun angle cosine correction. Observations with solar zenith angles greater than 70° and sensor zenith angles greater than 60° were excluded. Calibrated data were projected to geographic latitude/longitude projection (datum WGS-84). Normalized Difference Vegetation Index (NDVI) was computed at 0.0025° resolution with Eq. (1)

$$NDVI = \frac{R_{NIR} - R_{RED}}{R_{NIR} + R_{RED}} \tag{1}$$

where R_{NIR} and R_{RED} refer to near-infrared and red reflectance in MODIS band 2 (841–876 nm) and 1 (620–670 nm), respectively.

In addition to NDVI, the NDWI was computed at 0.005° resolution using Eq. (2)

$$NDWI = \frac{R_{NIR} - R_{MIR}}{R_{NIR} + R_{MIR}} \tag{2}$$

where R_{MIR} refers to middle infrared reflectance in MODIS band 6 (1628–1652 nm).

FSC (0–1) was derived at a pixel size of $0.005 \times 0.005°$ using the SCAmod algorithm. The method uses at-satellite observed single-band reflectance and pixel-wise average forest transmissivity for the provision of FSC. With MODIS, band 4 (545–565 nm) reflectance is applied. Clouds were masked in satellite-derived indices using SYKE's operational cloud

Table 2
Characteristics of selected areas from MODIS satellite data.

Site	Number of NDVI pixels[1]	Number of FSC/NDWI pixels[2]	Coniferous forest fraction[3] (%)	Altitude (SD) (m) a.s.l.[4]	Crown cover mean (SD) (%)[5]
Äkäslompolo	55	16	95	329 (23.5)	34 (10.7)
Hyytiälä	175	23	100	170 (3.6)	36 (14.5)
Kenttärova	19	8	95	325 (17.4)	29 (6.4)
Paljakka	65	17	100	292 (29.0)	50 (8.1)
Parkano	11	8	90	144 (6.6)	53 (10.3)
Saariselkä	69	21	90	311 (12.1)	32 (2.8)
Sodankylä	27	9	100	213 (11.5)	27 (9.5)

SD, standard deviation.

[1] Resolution of Normalized Difference Vegetation Index (NDVI) pixels is 0.0025°.

[2] Resolution of Fractional Snow Cover (FSC) and Normalized Difference Water Index (NDWI) pixels is 0.005°.

[3] Fraction of coniferous forest was determined based on CORINE Land Cover 2000 for Finland (Härmä et al., 2005).

[4] Altitude is derived from digital elevation model provided by the National Land Survey of Finland with a grid size of 25×25 m and a height precision of 2 m.

[5] Crown cover is determined for NDVI pixels and was calculated from field sample plots measured in National Forest Inventory of Finland and Image2006 satellite data (IRS LISS and SPOT XS data) at the resolution of 25 m using the k-nearest neighbour (k-NN) classification method (Haakana et al., 2008).

masking algorithm. Observations from two satellite swaths in one day were combined to daily composites using the maximum of the observed vegetation index (Holben, 1986) and the mean value of daily FSC observations.

2.7. Selection of homogenous areas for comparison with in situ observations

For comparison of *in situ* measurements (GSSD and GPSD) with satellite-derived time-series, we selected seven quasi homogenous areas covered with coniferous forest in the vicinity of *in situ* sites (Fig. 1), and that have the same environmental conditions as prevalent at the respective *in situ* site (Table 2). We aimed at large areas in order to minimize the influence of noise and missing observations in satellite data. Thus, the size of the area observed by the satellite sensor varied by site. Selection of areas was based on: (i) fractional cover with coniferous forest (≥90%), determined from CORINE (Coordinated Information on the European Environment) Land Cover 2000 for Finland (CLC 2000, Härmä et al. (2005)) and (ii) altitude. Altitude difference between *in situ* sites and selected MODIS pixels was limited to 50 m and was determined from a digital elevation model for Finland, provided by the National Land Survey of Finland with a pixel size of 25 × 25 m and a height precision of 2 m. In some cases the location of the area was shifted away from the *in situ* site (maximal distance of 10 km), because of inhomogeneity in land cover or close distance to water bodies of the pixel covering the site. MODIS pixels with fractional water coverage were excluded. Crown coverage was in general higher for southern sites than for northern sites, and altitude was higher for northern than for southern sites (Table 2).

2.8. MODIS time-series processing

Vegetation index (NDVI and NDWI) and FSC observations were averaged for all pixels of the seven selected areas (see Table 2). Missing observations in NDVI time-series until mid-February were filled with the NDVI value for full snow cover. Full snow cover NDVI was determined for each pixel based on several observations at the beginning of March 2010. Gaps in daily observations due to cloud cover were filled using linear interpolation and interpolated profiles were smoothed afterwards using the adaptive Savitzky–Golay filter (Chen et al., 2004; Savitzky & Golay, 1964), implemented in TimeSat software, version 2.3 (Jönsson & Eklundh, 2004), with a window size of five days. Linear interpolation was applied to NDWI time-series.

The general shape of snow depletion curves (changes of FSC during the melt season) for an area can be described by an exponential function
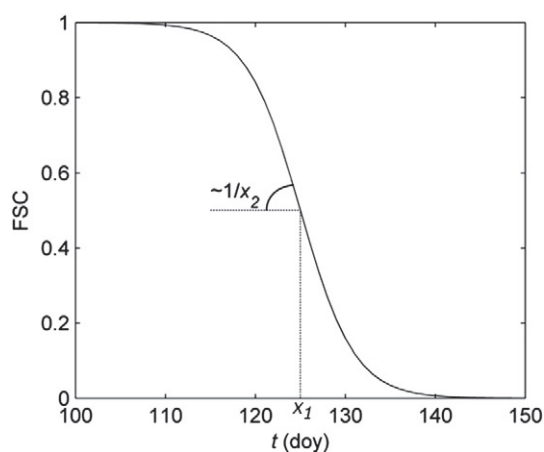

Fig. 3. Example of the sigmoid function (Eq. 3) used to model the FSC time-series during the melting period. It is defined by the inflection point (x_1) and the rate of decrease of FSC at x_1, controlled by x_2.

(Hall & Martinec, 1985) or by fitted splines (Lee, Klein, & Over, 2005). Here, a simple sigmoid function (3) was used to describe the depletion of FSC in spring from full snow cover (FSC = 1) to complete snowmelt (FSC = 0).

$$FSC_f(t; x_1; x_2) = \frac{1}{1 + \exp\left(\frac{t - x_1}{x_2}\right)} \tag{3}$$

where t is the time variable (day), x_1 is the inflection point (day when FSC reaches 0.5) and x_2 controls the rate of change (day) (Fig. 3). The transition from full snow cover to 0% snow cover occurs usually very fast, because an important part of snowmelt occurs before bare ground is exposed (Clark et al., 2006). From visual inspection of satellite-derived time-series of FSC at different locations in Finland, it was found that this simple sigmoid function described well the mean behaviour of snow melt in an area.

Fitting of function (3) to FSC time-series was done in two steps by minimizing the sum of squares of differences between Eq. (3) and measured FSC using the Nelder–Mead Simplex algorithm. Firstly, all observations within the period from February to July were used and initial parameter values were set to $x_1 = 129$ and $x_2 = 1$. Secondly, the time interval for fitting was limited to the melting period and parameters x_1 and x_2 obtained from the first fitting run were used as initial parameters for the second fitting. Using this approach, gaps due to cloud cover can be filled, and noise due to varying viewing and illumination conditions, atmospheric influence, residual clouds or stripes can be smoothed. However, intermittent new snow fall during the ablation period is not captured with this function.

2.9. Extraction of GSSD and GPSD from MODIS satellite indices

We determined GSSD from time-series of NDVI and FSC_f. GSSD was extracted from NDVI at the time when NDVI's spring-rise began (see Section 3.1). The minimum NDVI during the period from 1st of February to 19th of July was determined from smoothed NDVI profiles and an estimate of the noise level (ε) of the time-series data was defined. Secondly, the condition in Eq. (4a) was applied and the last day fulfilling the condition was determined as GSSD from NDVI:

$$GSSD_{NDVI} = \arg\max_{t \in [32,200]} f(t) := \{t | NDVI(t) < NDVI_{min} + \varepsilon\} \tag{4a}$$

with t referring to day of the year (doy), $NDVI_{min}$ is minimum of NDVI from 1st of February (doy 32) to 19th of July (doy 200) and ε equals 10% of the NDVI amplitude, defined as difference of the maximum NDVI and $NDVI_{min}$ for each year. For the determination of GSSD from FSC_f (hereafter denoted as $GSSD_{FSC}$) a threshold value of 0.99 FSC was applied to Eq. (3), giving the $GSSD_{FSC}$ as follows:

$$GSSD_{FSC} = x_1 - \ln(99)x_2. \tag{4b}$$

Due to long periods with cloud cover in spring, $GSSD_{FSC}$ and $GSSD_{NDVI}$ could not be obtained for year 2002 in Sodankylä and Kenttärova and for year 2009 in Hyytiälä. Additionally, FSC data was not sufficient for the retrieval of $GSSD_{FSC}$ for year 2005 in Kenttärova.

For the extraction of GPSD a similar criterion as proposed by Delbart et al. (2005) for determination of the greening-up in the boreal region was used. According to visual comparison of GPSD and NDWI time-series for phenological sites in this study, GPSD occurred earlier than the greening-up (see Section 3.1). GPSD from NDWI was defined as follows:

$$GPSD_{NDWI} = \arg\min_{t \in [32,200]} f(t) := \{t | NDWI(t) < NDWI_{min} + \varepsilon\} \tag{5}$$

with $NDWI_{min}$ referring to the minimum NDWI and ε equals 20% of NDWI's spring amplitude. The first observation fulfilling the condition

Table 3
Statistical equations used in the evaluation of satellite estimates.

Statistics	Equation
Root mean squared error	$RMSE = \sqrt{\sum_{i=1}^{N} (y_i - \hat{y}_i)^2 / N}$
Bias	$B = \sum_{i=1}^{N} (\hat{y}_i - y_i) / N$
Coefficient of determination	$R^2 = \dfrac{\sum_{i=1}^{N} (\hat{y}_i - \bar{y})^2}{\sum_{i=1}^{N} (y_i - \bar{y})^2}$

y_i is the *in situ* observation and $\hat{y}_i$ is the satellite estimate, $\bar{y}$ is the arithmetic average of y values, and N is the number of observations.

was retained as $GPSD_{NDWI}$. GPSD was determined for the four phenological sites for years with phenological observations (Table 1). Due to long periods with missing data, GPSD was not retrieved for year 2005 in Äkäslompolo and year 2001 in Saariselkä.

Satellite-derived phenological events were evaluated by comparing estimated and *in situ* dates for GSSD and GPSD for all site-years and separately by site. The applied statistical measures were RMSE, the coefficient of determination (R^2) and the bias (B). The equations for statistical measures are presented in Table 3.

3. Results

3.1. Comparison of satellite-derived time-series and in situ observations

Temporal profiles of FSC, NDVI and NDWI in spring 2006 at Sodankylä are shown in Fig. 4. FSC decreased below 1 shortly after the GSSD on 26.04.2006 and when NDVI had a minimum before its spring-rise. NDWI decreased after GSSD. A web-camera image (Fig. 5a) taken from above the canopy at the Nordkalotten Satellite Evaluation co-operation Network (NorSEN) mast (Sukuvaara et al., 2007) in Sodankylä, illustrated that snow had melted around tree trunks at time of GSSD (07.05.2010) and FSC decreased about this time (Fig. 5b). Similar behaviour of GSSD in relation to satellite-indices, as described above, was observed for the southern boreal site Hyytiälä (Fig. 6) and the spruce dominated northern site Kenttärova (not shown); GSSD occurred during snow melt, when depletion of FSC started and NDVI began its spring-rise. GPSD occurred after snowmelt, indicated by an NDWI minimum (Delbart et al., 2005) and a FSC of 0 (Figs. 7 and 8).

Time-series of air and soil temperature, snow depth and SWC in spring together with the time of GSSD are shown in Figs. 9 and 10 for Sodankylä (year 2006) and Hyytiälä (year 2004), respectively. In Sodankylä, air temperature was for several days continuously above 0 °C and soil temperature stayed at 0 °C before GSSD (Fig. 9b). Snow depth was 34 cm and SWC reached 10% (Fig. 9a). In Hyytiälä, air temperatures rose above 0 °C before GSSD and a constant soil temperature of 0 °C was observed during the time period before GSSD (Fig. 10b). Soil temperature increased shortly after that date. SWC was above 20% for the whole period (Fig. 10a).

Meteorological and soil characteristics at time of GSSD were compared between one northern boreal site, Sodankylä, and the southern boreal site Hyytiälä (Table 4). Mean snow depth was higher at Sodankylä (40 cm) than in Hyytiälä (23 cm). Highest snow depth of 65 cm at time of GSSD was found in Sodankylä in year 2005, which was characterized by an intermittent frost period and new snowfall during the snow depletion period. E-code observations at both sites showed similar characteristics related to snow patchiness; the most dominant e-code was 7 (Wet or refrozen snow covering 100% terrain, 11/16 observation years) followed by e-code 6 (Wet or re-frozen snow covering over 50%, but less than 100%, 4/16 observation years). First snow-free spots appear usually early during snow melt at the bases of trees or large rocks (Kuusisto, 1984). These first snow free

spots are not depicted by e-code observation at the weather station. Measurements of SWC at sites Hyytiälä and Sodankylä indicated an influx of snow melt water into the soil at time of GSSD (Figs. 9a, 10a and Table 3), increasing the soil temperature and the water availability to trees. Air temperature for both sites was always above 0 °C at time of GSSD, and soil temperature for the upper soil layer ranged between −0.52 and 0.25 °C in Sodankylä (5 cm depth), and 0.07 and 0.77 °C (A-horizon) in Hyytiälä (Table 4). The upper soil layer was usually not completely frozen during the period from February to GSSD in Hyytiälä, but in Sodankylä negative soil temperatures were commonly observed until the influx of snow melt water. The 5-day moving average of air temperature ($T5_{air}$, Table 4), which had previously been used for the prediction of GSSD by Thum et al. (2009), showed differences in $T5_{air}$ at time of GSSD: the average $T5_{air}$ as well as its range was higher for Sodankylä (4.2 °C, 9 °C) than for Hyytiälä (3.6 °C, 5 °C).

3.2. GSSD based on MODIS time-series

Comparisons between satellite-derived GSSD ($GSSD_{NDVI}$ and $GSSD_{FSC}$) and *in situ* dates from three boreal coniferous sites covering observation years 2001 to 2010 are shown in Figs. 11 and 12. Both indices depicted well the growing season start date with a slightly lower RMSE of 5.3 days for $GSSD_{FSC}$ compared to 6.3 days for $GSSD_{NDVI}$. The range of GSSD from the southern to northern sites was captured with the indicators $GSSD_{NDVI}$ and $GSSD_{FSC}$, but data points were grouped for the northern and southern sites, especially for $GSSD_{NDVI}$, implying that inter-annual differences at a specific site are less well captured by $GSSD_{NDVI}$. The satellite-indicators detected on average the growing season start 1–2 days later than *in situ* observations (Table 5). High R^2 (>0.8) values resulted also from the large range between northern and southern sites in time of GSSD and we examined therefore also site-wise correspondence (Table 5). Correlations between $GSSD_{NDVI}$ and *in situ* dates were significant only for site Hyytiälä, whereas significant site-wise correlations between $GSSD_{FSC}$ and *in situ* dates were obtained for sites Sodankylä and Hyytiälä (R^2 > 0.7), as well as a higher R^2 for site Kenttärova. Note that for the Kenttärova site only 6 years were available for comparison. The combination of observations for the two northern boreal sites led to an R^2 of 0.53 for $GSSD_{FSC}$. The lower R^2 for northern sites is mainly due to larger errors for the Kenttärova site with dominance of spruce. Latest GSSD according to flux measurements was observed in Kenttärova on 23rd of May 2008. Both satellite-indices suggested a start of season too early in that year with 14 days and 9 days differences for $GSSD_{FSC}$ and $GSSD_{NDVI}$, respectively. This was also the largest error obtained for $GSSD_{FSC}$. Actual recovery lagged snow melt in that year (zero cm snow depth on 19th of May 2008), which might be due to a cold spell, as observed by air temperature observations in Kenttärova. Largest error for $GSSD_{NDVI}$ of 16 days in year 2003 was as well found for this site.

3.3. GPSD based on MODIS time-series

Results for the determination of $GPSD_{NDWI}$ for four phenological sites according to Eq. (5) are shown in Table 6 and Fig. 13. Satellite-derived $GPSD_{NDWI}$ for 29 site-years accounted only for 54% of the variation *in situ* observations and data point were dispersed and grouped by site (Fig. 13). Site-wise correlations were not significant and R^2 remained below 0.5 for three out of four sites (Table 6), hence inter-annual variability at site-level cannot be captured. Mean GPSD for each phenological site could nevertheless be depicted by NDWI time-series with B ranging from −2 to 3 days for different sites (Table 6). We observed differences in B between sites from southern and central Finland (Parkano, Paljakka), and northern sites (Äkäslompolo, Saariselkä), with an early B (2–3 days) for the first two stations and a late B (2–3 days) for the latter.
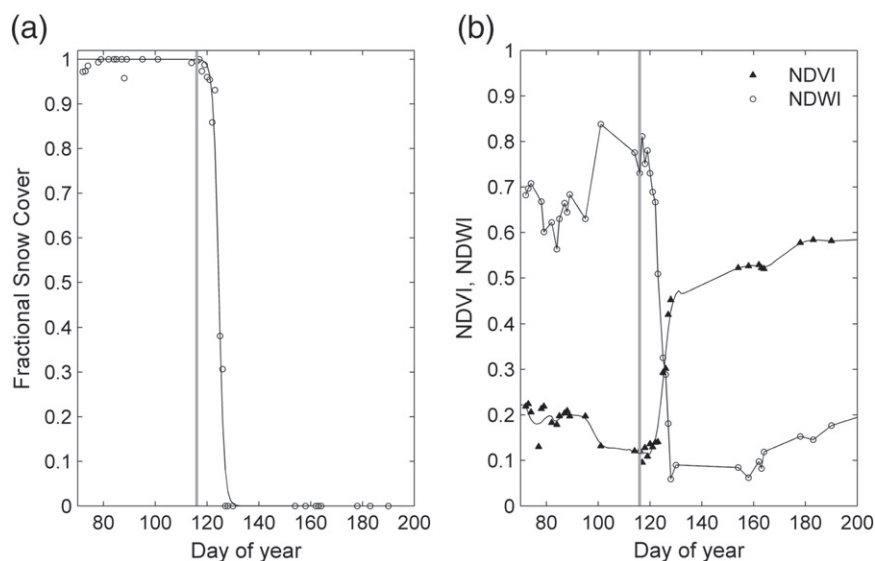
Fig. 4. Satellite-derived time-series of vegetation indices and snow cover at Sodankylä during the period from mid-March to July 2006: (a) Fractional Snow Cover, FSC$_f$; (b) NDVI and NDWI. The vertical grey line indicates GSSD on 26.04.2006.

3.4. Demonstration of the mapping of GSSD for Finland

The results described in previous sections suggest that the MODIS-derived estimate of FSC can be used as proxy for the spatial mapping of GSSD (Fig. 12). This is shown in Fig. 14 by applying Eq. (4b) to time-series of FSC$_f$. In order to reduce noise and gaps due to cloud cover in FSC time-series, daily observations from pixels with at least 70% coniferous forest coverage were aggregated to a grid size of 0.1 × 0.1°. The aggregation of time-series to a coarser grid was found useful for the mapping of the autumn colouring from MODIS time-series (Rauste et al., 2007). Furthermore, maps are intended for comparison with the spatial distribution of modelled GSSD by a land surface scheme forced with regional

meteorological data, which are typically calculated at a coarser grid size than MODIS satellite observations. Daily FSC observations were averaged for each grid cell after removing outliers based on the criterion of two standard deviations. Function (3) was fitted to average FSC time-series of each grid cell and GSSD$_{FSC}$ was extracted from the fitted profile based on Eq. (4b). The delay of spring photosynthetic recovery in coniferous forest in Finland from Southwest to Northeast is illustrated in Fig. 14. This is in correspondence with the climatic gradient. The map for year 2007 showed an earlier GSSD for most areas in Finland compared to year 2004. Thermal spring in 2007 began about one month earlier than average in Finland; mean temperatures in March 2007 were higher than normal (Finnish Meteorological Institute, 2012).
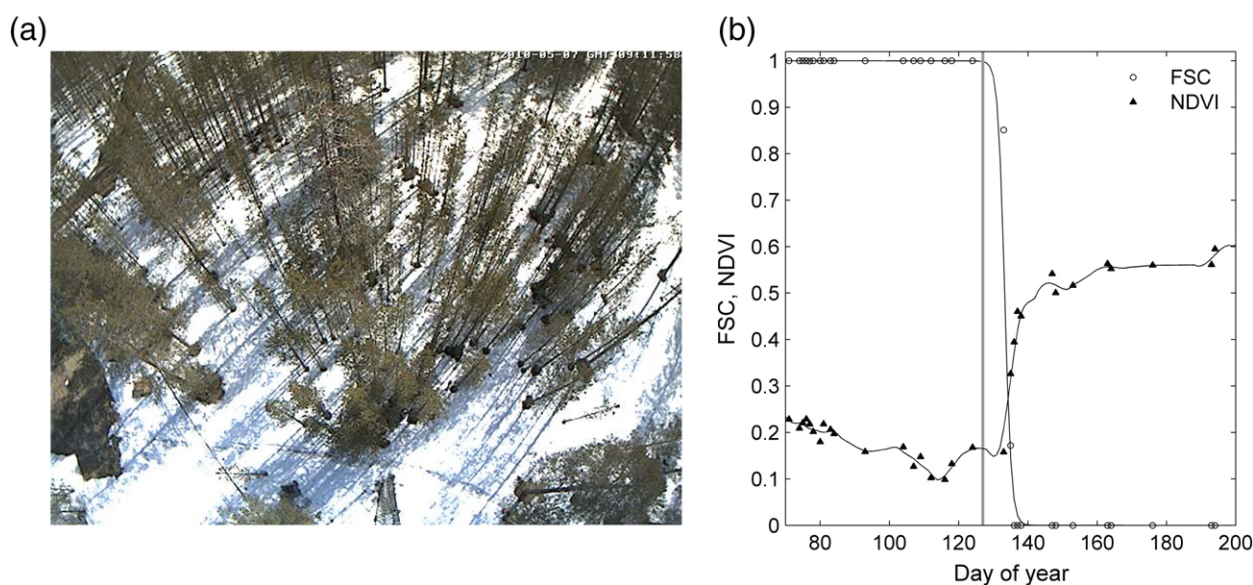

Fig. 5. (a) Web-camera photograph taken from the NorSEN mast (30 m height) in Sodankylä on GSSD (07.05.2010). (b) FSC and NDVI time-series in Sodankylä in spring 2010. The vertical grey line indicates GSSD.
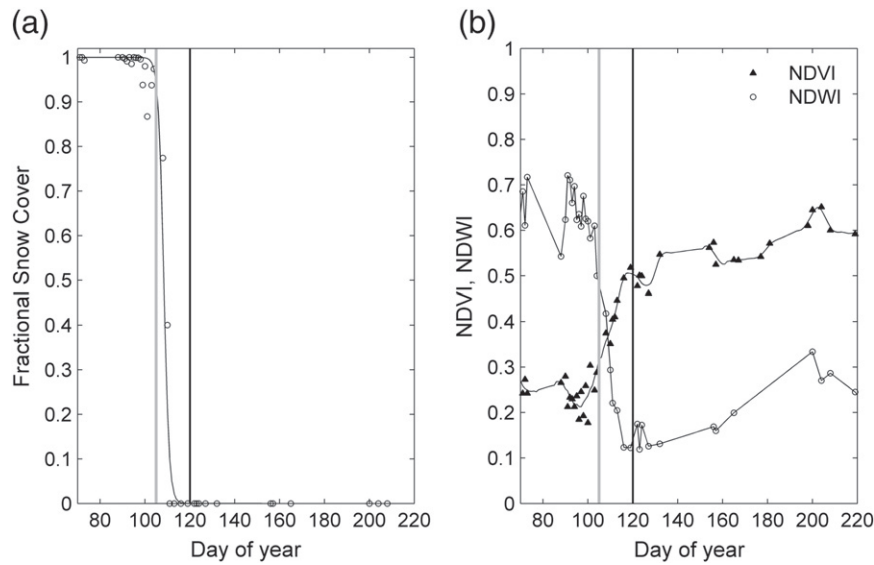
Fig. 6. Satellite-derived time-series of vegetation indices and snow evolution at Hyytiälä from mid-March–August in 2004: (a) Fractional Snow Cover, FSC$_f$ and (b) NDVI and NDWI. The grey vertical line indicates GSSD (14.04.2004) and the black vertical line GPSD (Parkano, 29.04.2004).

4. Discussion

4.1. Snow melt as indicator for photosynthetic recovery

We found correspondence of the time of photosynthetic recovery in boreal evergreen conifers with the time during snowmelt when ground starts to be exposed as observed by satellite-derived indices. Our findings are supported by the results by Thum et al. (2009), who reported that the beginning of growing season in boreal conifers corresponded well with the decrease of MODIS/Terra + Aqua albedo observations. Furthermore, Kimball, McDonald, Running, and Frolking (2004) found good correspondence between timing of seasonal snow melt observed by radar backscatter measurements and growing season initiation (start of xylem sap flow), as well as with ecosystem process model simulations for boreal, maritime and subalpine sites in Northern America.

Photosynthetic recovery in boreal conifers is mainly controlled by increasing air temperature (Mäkelä et al., 2004; Suni et al., 2003), which also controls the snow melt. The response to air temperature seems to be slower in colder northern sites than southern boreal sites (Gea-Izquierdo et al., 2010; Suni et al., 2003; Thum et al., 2009),

which may be attributed to deeper frozen soils in northern sites than in southern sites and a longer time lag between the rise in air and soil temperatures. Also in this study, T5$_{air}$ at time of GSSD was higher for the northern site Sodankylä than at the Hyytiälä site; northern sites Kenttärova and Sodankylä are characterized by a larger snow pack and lower soil temperatures in winter (Figs. 9 and 10) than the Hyytiälä site. Besides favourable air temperature, the isothermality of the snow pack is a pre-requisite for full springtime recovery of photosynthetic uptake, permitting continuous daytime percolation of melted snow water through the vertical snow profile and availability of snow melt water to trees (Kimball et al., 2004; Monson et al., 2005). The GSSD, determined here at a fixed rate of growing season GPP, occurred when a high amount of snow had already melted and melt water percolated into the soil as indicated by relatively high levels of soil water content (Table 4 and Figs. 9a, 10a).

4.2. Detection of GSSD from MODIS time-series

The depletion of snow cover in spring was used as indicator for the extraction of GSSD from daily time-series of FSC and NDVI for
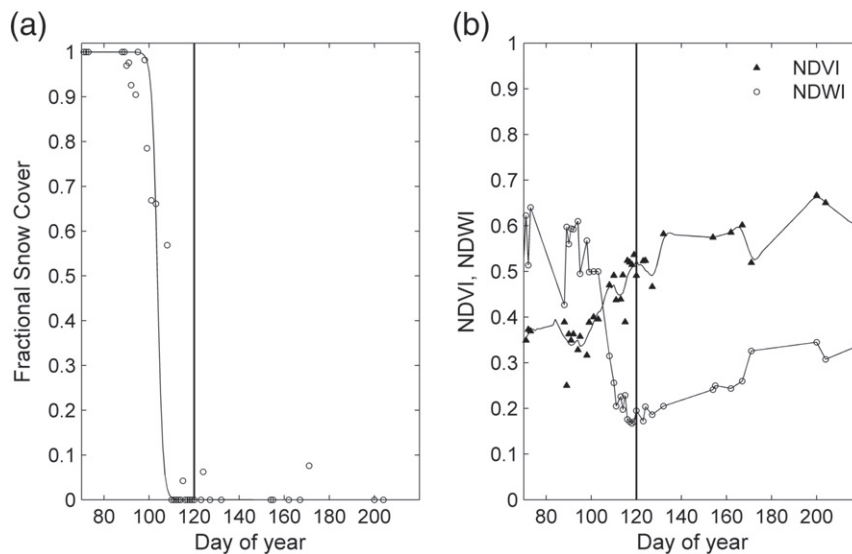

Fig. 7. Satellite-derived time-series of vegetation indices and snow evolution at Parkano from mid-March–August in 2004: (a) Fractional Snow Cover, FSC$_f$ and (b) NDVI and NDWI. The black vertical line indicates GPSD (29.04.2004).
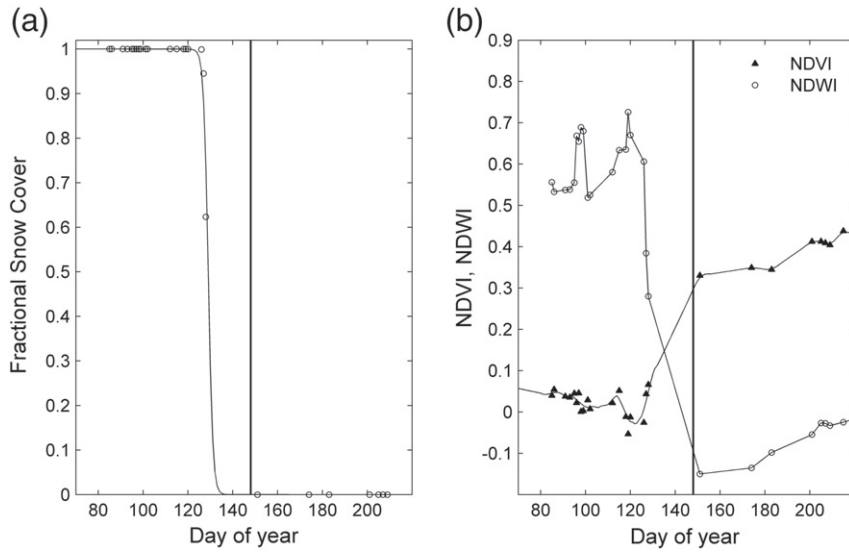
Fig. 8. Satellite-derived time-series of vegetation indices and snow evolution at Saariselkä from mid-March–August in 2004: (a) Fractional Snow Cover, FSC$_f$ and (b) NDVI and NDWI. The black vertical line indicates GPSD (27.05.2004).

three boreal evergreen coniferous sites in Finland (Figs. 4a and 6a). GSSD$_{FSC}$ was better suited for the detection of GSSD than GSSD$_{NDVI}$ (Table 5, Figs. 11, 12). FSC time-series used in this study were derived with the SCA*mod* method, which provides low omission errors for full snow cover as well as for low snow fractions (Metsämäki et al., 2012), which is an advantage for the detection of timing of melting onset and snow clearance. Furthermore, the method compensates for the effect of different crown coverage of the forest

sites (Table 2) by using forest transmissivity in the retrieval of FSC (Metsämäki et al., 2005). In contrast, the NDVI winter level is dependent on crown coverage, e.g. showing higher NDVI values for southern boreal sites (Figs. 6b, 7b) than for the northern sites (Figs. 4b and 8b). This was accounted for by using a relative NDVI threshold for the detection of GSSD, which is similar to approaches for the greening-up of temperate deciduous forests (Badeck et al., 2004; White et al., 1997).
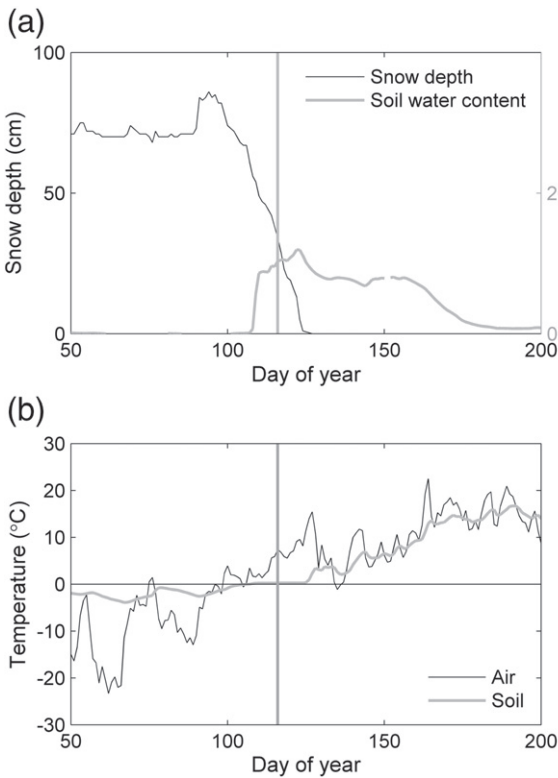

Fig. 9. Time-series of meteorological and soil parameters at Sodankylä for the period from mid-February to July 2006: (a) Snow depth (cm) and volumetric SWC (%) and (b) daily air and soil temperature (°C). The vertical grey line indicates GSSD on 26.04.2006. Soil water content and soil temperature were measured at 5 cm depth.
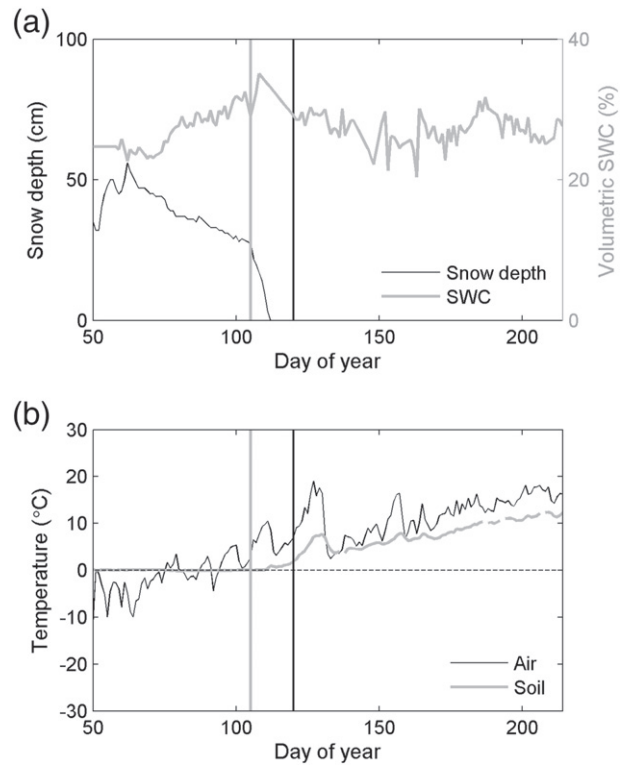
Fig. 10. Time-series of mean daily meteorological and soil parameters at Hyytiälä for the period from mid-February to August 2004: (a) Snow depth (cm) and volumetric SWC (%) and (b) air and soil temperature (°C). The vertical grey line indicates GSSD on 14.04.2004 and the black vertical line GPSD (Parkano, 29.04.2004). Soil water content and soil temperature were measured for soil A-horizon (0–10 cm depth).

Table 4

Growing season start dates (GSSD) together with meteorological and soil characteristics on GSSD at CO_2 flux measurement stations in Sodankylä and Hyytiälä.

Site	Year	GSSD (doy)	Snow depth (cm)	e-code	SWC (%)	T5$_{air}$ (°C)	T$_{soil}$ (°C)
Hyytiälä	2001	95	25	7	32	4.33	0.17
	2002	102	20	6	36	6.22	0.77
	2003	107	15	5	29	5.14	0.35
	2004	105	27	6	29	3.51	0.07
	2005	93	19	*	30	5.13	0.10
	2006	104	33	7	24	2.69	0.17
	2007	75	14	7	29	1.46	0.16
	2008	90	34	7	32	4.12	0.64
	2009	97	*	7	30	1.11	0.15
	2010	90	*	7	19	2.75	0.25
Sodankylä	2001	118	34	7	*	4.39	−0.29
	2002	114	43	7	*	6.63	−0.52
	2003	127	20	6	*	2.63	−0.27
	2004	120	37	6	*	5.07	0.01
	2005	126	65	7	*	0.04	0.04
	2006	116	34	7	10	6.32	0.23
	2007	113	44	7	25	0.24	0.06
	2008	122	43	*	*	9.43	0.22
	2009	120	*	*	11	5.01	0.24
	2010	127	*	*	22	1.76	0.25

SWC, volumetric soil water content. T5$_{air}$, 5 day moving average of daily air temperature. T$_{soil}$, daily soil temperature measured at 5 cm depth in Sodankylä and for the A-horizon (0–10 cm depth) in Hyytiälä.

Snow depth and e-codes for Hyytiälä and Sodankylä were obtained from meteorological stations Juupajoki Hyytiälä and Sodankylä Arctic Research Centre of FMI, respectively. An asterisk (*) denotes missing observations. Description for e-code values: 5, Snow covering over 0%, but less than 50% of the terrain; 6, Wet or re-frozen snow covering over 50%, but less than 100% of the terrain; 7, Wet or re-frozen snow covering 100% of the terrain.

We used large homogenous areas near *in situ* sites for the retrieval of satellite-indicators. Better correlations were obtained for comparisons between satellite-derived and ground observation of phenology for homogenous vegetation covers, and it was suggested that land cover heterogeneity is a main error source (Doktor, Bondeau, Koslowski, & Badeck, 2009; Maignan et al., 2008). In addition, due to the mismatch between the spatial scales of satellite and field observations (Liang, Schwartz, & Fei, 2011) and the averaging out of errors in coarser measurements, higher spatial representation (coarser resolution) of satellite estimates led to better correlations with seasonal transitions derived from EC measurements (Garrity et al., 2011). Satellite-estimates from single pixels are more likely to be influenced by noise and missing values. Reducing the size of the area for the retrieval of GSSD$_{FSC}$ for the Hyytiälä site from 23 to 9 pixels ($0.005 \times 0.005°$ resolution) decreased accuracy slightly, with lower R^2 (0.71) and higher B (2.9 days). Missing data is especially

relevant for northern latitudes with long periods of cloud cover and a fast development of vegetation in spring (Beck et al., 2006). A daily coverage of satellite observations is beneficial in capturing the timing of snow cover decrease, as snowmelt proceeds very fast after the peak of melting; the period corresponding to partial snow cover in forest lasts in northern, central and southern Finland about 15 days in average (Kuusisto, 1984). However, even with daily observations and large areas, data gaps in cloud-free MODIS observations for the spring period in some years were too long for the retrieval of satellite-proxy indicators (e.g. time period in Sodankylä with missing observations was more than a month in 2002).

Most available methods for the retrieval of the beginning of the growing season in the boreal zone from optical satellite observations aimed at the detection of the greening-up of deciduous vegetation with reference to the bud burst of deciduous trees (Delbart, Le
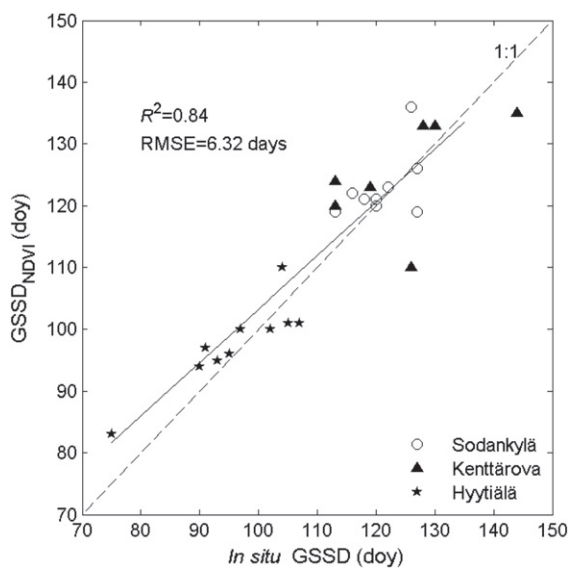

Fig. 11. Comparison of *in situ* measurements of GSSD with estimates derived from time-series of NDVI (GSSD$_{NDVI}$). Doy is day of year. Black line shows linear regression line between *in situ* data and GSSD$_{NDVI}$.
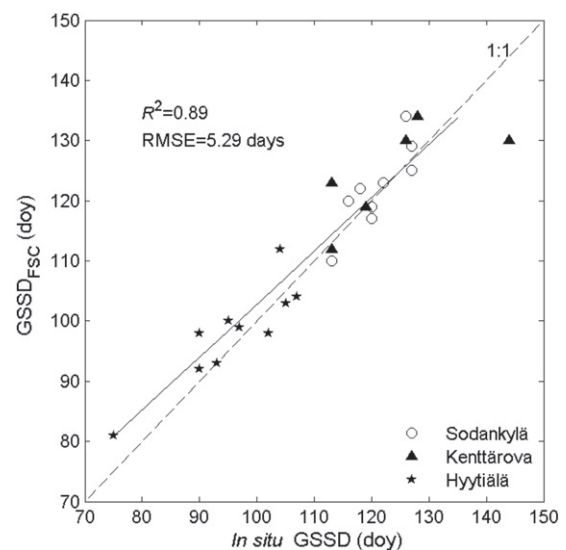

Fig. 12. Comparison of *in situ* measurements of GSSD with estimates derived from time-series of Fractional Snow Cover (GSSD$_{FSC}$). Doy is day of year. Black line shows linear regression line between *in situ* data and GSSD$_{FSC}$.

Table 5

Growing season start date (GSSD) as measured by NDVI and FSC and as defined from CO_2 flux measurement sites.

Site	In situ	Estimate from NDVI				Estimate from FSC			
	Mean GSSD (doy)	# y	Mean GSSD$_{NDVI}$ (doy)	R^2	B (day)	# y	Mean GSSD$_{FSC}$ (doy)	R^2	B (day)
Hyytiälä	96	10	98	0.80**	2	10	98	0.79**	2
Kenttärova	124	7	125	0.30	1	6	125	0.50	1
Sodankylä	121	9	123	0.25	2	9	122	0.73**	1
All sites	112	26	114	0.84**	2	25	113	0.89**	1

#y, number of years when both *in situ* data and satellite observations were available for comparison. GSSD, growing season start date from CO_2 flux measurements. Doy, day of year. GSSD$_{NDVI}$, growing season start date from NDVI. GSSD$_{FSC}$, growing season start date from Fractional Snow Cover. R^2, coefficient of determination, * significant at 5% level, ** significant at 1% level. B is bias.

Toan, Kergoat, & Fedotova, 2006; Delbart et al., 2005, 2008; Karlsen, Elvebakk, Høgda, & Johansen, 2006; Karlsen et al., 2007, 2008; Shutova et al., 2006). Therefore, these results are not directly comparable to our results. Recently, Gonsamo et al. (2012) developed a new phenological index (PI) combining the advantages of NDVI and Normalized Difference Infrared Index (NDII), similar to NDWI. The results based on PI for boreal coniferous sites in Canada, with a similar range of start of season dates as in this study, showed low correlation and an RMSE of 17.2 days. Estimates of growing season initiation from radar observations occurred up to 10 days earlier than site measurements of growing season initiations (onset of xylem sap flow) for two years of observations across 10 evergreen forest study sites in Northern America (Kimball et al., 2004). The observed RMSE from radar estimates was with 9.9 days (Kimball et al., 2004) and 8.7 days (Bartsch, Kidd, Wagner, & Bartalis, 2007) higher than for GSSD$_{FSC}$ as well as GSSD$_{NDVI}$ (Figs. 11 and 12).

Since air temperature is commonly used as predictor for GSSD, we compared our results also with air-temperature derived estimates of GSSD. Good accuracy was achieved for northern latitudes when optimizing temperature threshold values for a specific site. Suni et al. (2003) found good agreement between the commencement day of photosynthesis (*P*, defined here from NEE) and the day when the threshold values of T5$_{air}$ (3.3 °C and 6.5 °C for Hyytiälä and Sodankylä, respectively) was exceeded. Temperature-derived *P* deviated from observations in the range of 0–2 and 2–3 days for Hyytiälä and Sodankylä, respectively. However, applying a common threshold to five different sites in the boreal region led to a prediction error of 8.6 days, compared to 5.3 days for GSSD$_{FSC}$ in this study (Fig. 12), and systematically later observed *P* for the northern sites and *vice versa* for the warmer Hyytiälä site. The bias of GSSD$_{FSC}$ was low for all three sites in Finland, showing only a one day larger *B* for Hyytiälä than for the northern sites (Table 5). In a study including more site-years, but applying the same method as Suni et al. (2003) for the determination of *P*, prediction error for T5$_{air}$ ranged between 1–5 and 2–22 days for Hyytiälä and Sodankylä, respectively (Thum et al., 2009). Prediction of *P* from T5$_{air}$ in Hyytiälä preceded observed *P* always. RMSE for site-specific thresholds of T5$_{air}$ for 11 sites-years from Hyytiälä, Sodankylä and Kenttärova was 7.3 days.

4.3. Detection of GPSD from MODIS time-series

We derived GPSD from daily NDWI time-series for four sites with dominance of pine trees (Fig. 13). The method applied here does not actually detect the beginning of shoot growth, but GPSD is related to the end of snow melt as described by the decrease of NDWI. Mean GPSD$_{NDWI}$ occurred before the greening-up of deciduous species determined by the method of Delbart et al. (2005). Early bias in GPSD$_{NDWI}$ for northern sites (Äkäslompolo and Saariselkä) (Table 6) suggested an overlap of snowmelt and beginning of shoot growth as also reported by Gonsamo et al. (2012). Changes in NDVI as well as NDWI time-series after the end of snow melt were very small (Figs. 7 and 8), which corresponds to observations by Jönsson et al. (2010). Vegetation indices specifically developed for the tracking of seasonal change in leaf area index of evergreen coniferous forest (e.g. Stenberg, Rautiainen, Manninen, Voipio, & Smolander, 2004) might be better suited for the determination of GPSD and should be considered in further studies.

4.4. Mapping of GSSD in Finland

Satellite-derived maps for the start of the growing season (defined as greening-up) in Fennoscandia were presented by Beck et al. (2006)
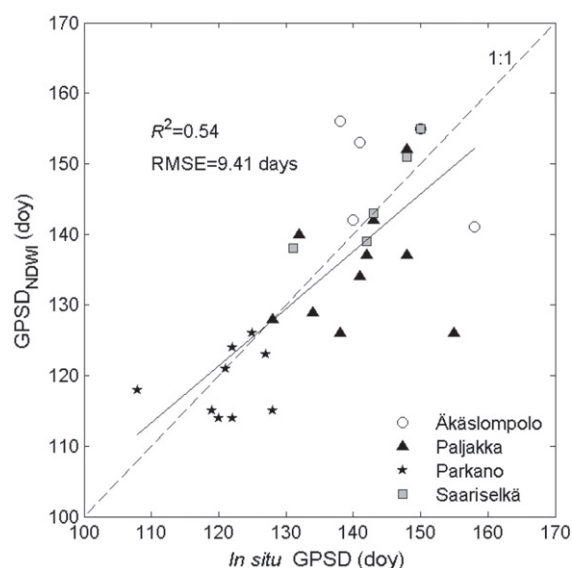
Table 6

Growth of pine start date (GPSD) as measured by NDWI and as observed at phenological sites.

Site	# y	Mean GPSD (doy)	Mean GPSD$_{NDWI}$ (doy)	R^2	B (day)
Äkäslompolo	5	145	149	0.18	3
Paljakka	10	139	136	0.05	−3
Parkano	9	121	119	0.05	−2
Saariselkä	5	143	145	0.74	2
All sites	29	136	134	0.54**	−2

#y, number of years when both *in situ* and satellite data were available for comparison. GPSD, growth of pine start date from phenological observation. Doy, day of year. GPSD$_{NDWI}$, growth of pine start date from Normalized Difference Water Index. R^2, coefficient of determination, ** significant at 1% level. B is bias.

Fig. 13. Comparison of *in situ* measurements of GPSD with estimates derived from time-series of NDWI (GPSD$_{NDWI}$). Doy is day of year. Black line shows linear regression line between *in situ* data and GPSD$_{NDWI}$.
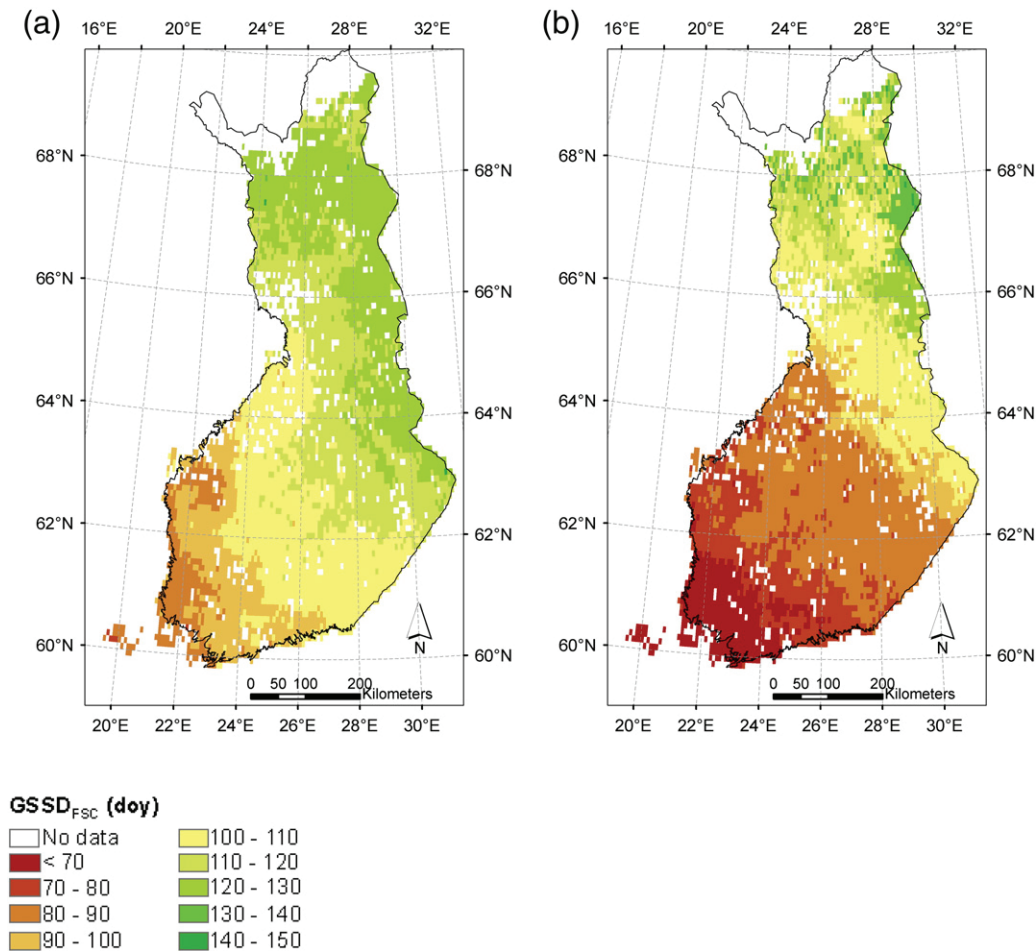
GSSD$_{FSC}$ (doy)

☐ No data	☐ 100 - 110
■ < 70	☐ 110 - 120
■ 70 - 80	■ 120 - 130
■ 80 - 90	■ 130 - 140
☐ 90 - 100	■ 140 - 150

Fig. 14. Maps of satellite-derived growing season start date from Fractional Snow Cover (GSSD$_{FSC}$) for years (a) 2004 and (b) 2007 in evergreen coniferous forest in Finland.

and Karlsen et al. (2007). Here, we targeted at the detection of recovery of photosynthetic activity in evergreen coniferous forest, thus results are not comparable in their timing. The greening-up in Southern Finland occurred on average (years 1982–2002) between 1 and 15 May in the results of Karlsen et al. (2007). In this study, GSSD$_{FSC}$ was observed as early as mid-March to mid-April (Fig. 14). However, the spatial patterns were in general consistent between greening-up and GSSD as well as with modelled bud-burst of birch (Bennie, Kubin, Wiltshire, Huntley, & Baxter, 2010) and followed the climatic gradient. GSSD maps suggested a very early start of the growing season in the south-western coastal areas (Fig. 14; hemiboreal zone, Fig. 1) in Finland. The applicability of the method for mapping of GSSD based on FSC to the hemiboreal zone and also to the southern part of the boreal zone may fail in winters with very low snow depth, when the direct effect of low temperature or the combination of low temperature and high light (Delpierre et al., 2012; Gea-Izquierdo et al., 2010) are more important for the restriction of photosynthetic recovery in spring. In contrast to other studies, we separated the coniferous forest from other land cover classes for the mapping of GSSD and considered only MODIS pixels with dominant coniferous fraction. Although, maps were presented at coarse resolution (0.1 × 0.1°), this approach has the advantage that different methods can be applied for areas with different vegetation cover, thus allowing comparisons with GSSD calculated by a land surface scheme for different plant functional types.

5. Conclusion

In this study, MODIS-derived time-series of NDVI, NDWI and FSC were compared with *in situ* measurements of the start of growing

season determined from CO_2 flux measurements and with phenological observations of the beginning of pine growth at four sites in Finland in order to find suitable satellite indicators for these events. The time during snow melt when ground starts to be exposed corresponded well with GSSD ($R^2 > 0.8$, RMSE <7 days) at three flux measurement sites in boreal evergreen coniferous forest. The satellite-indicator can be derived from both NDVI and FSC time-series, but with higher accuracy from FSC time-series. This is important for the mapping of the beginning of the growing season in the boreal region, as current optical satellite-based methods (e.g. Delbart et al., 2008; Karlsen et al., 2008) rely mainly on validation with observations of bud burst of deciduous trees, which lag behind the beginning of photosynthetic recovery in coniferous trees. The satellite-derived indicator GSSD$_{FSC}$ did not show systematic differences between northern and the southern sites and estimation errors seem to be lower compared to air temperature derived indicators when using common thresholds for sites in different zones of the boreal region. Furthermore, the mapping of GSSD$_{FSC}$ was demonstrated in this paper. In contrast, the satellite-derived indicator GPSD$_{NDWI}$ showed only low correlation with phenological observations of pine growth and cannot be applied for the mapping of this event. The calibration of satellite indicators to GSSD from CO_2 flux measurements opens the possibility to evaluate the spatial distribution of land-surface model-derived beginning of growing season against satellite observations.

References

Ahti, T., Hämet-Ahti, L., & Jalas, J. (1968). Vegetation zones and their sections on north-western Europe. Annales Botanica Fennica, 5, 169–211.

Aurela, M. (2005). Carbon dioxide exchange in subarctic ecosystems measured by a micrometeorological technique. (PhD thesis). Helsinki, Finland: Finnish Meteorological Institute.

Aurela, M., Lohila, A., Tuovinen, J. -P., Hatakka, J., Riutta, T., & Laurila, T. (2009). Carbon-dioxide exchange on a northern boreal fen. Boreal Environmental Research, 14, 699–710.

Aurela, M., Tuovinen, J. -P., & Laurila, T. (2001). Net CO_2 exchange of a subarctic mountain birch ecosystem. Theoretical and Applied Climatology, 70, 135–148.

Badeck, F. -W., Bondeau, A., Böttcher, K., Doktor, D., Lucht, W., Schaber, J., & Sitch, S. (2004). Responses of spring phenology to climate change. New Phytologist, 162, 295–309.

Baldocchi, D.D. (2003). Assessing the eddy covariance technique for evaluating carbon dioxide exchange rates of ecosystems: Past, present and future. Global Change Biology, 9, 479–492.

Bartsch, A., Kidd, R. A., Wagner, W., & Bartalis, Z. (2007). Temporal and spatial variability of the beginning and end of daily spring freeze/thaw cycles derived from scatterometer data. Remote Sensing of Environment, 106, 360–374.

Beck, P.S. A., Atzberger, C., Høgda, K. A., Johansen, B., & Skidmore, A. K. (2006). Improved monitoring of vegetation dynamics at very high latitudes: A new method using MODIS NDVI. Remote Sensing of Environment, 100, 321–334.

Beck, P.S. A., Jönsson, P., Høgda, K. -A, Karlsen, S. R., Eklundh, L., & Skidmore, A. K. (2007). A ground-validated NDVI dataset for monitoring vegetation dynamics and mapping phenology in Fennoscandia and the Kola peninsula. International Journal of Remote Sensing, 28, 4311–4330.

Bennie, J., Kubin, E., Wiltshire, A., Huntley, B., & Baxter, R. (2010). Predicting spatial and temporal patterns of bud-burst and spring frost risk in north-west Europe: The implications of local adaptation to climate. Global Change Biology, 16, 1503–1514.

Bergh, J., & Linder, S. (1999). Effects of soil warming during spring on photosynthetic recovery in boreal Norway spruce stands. Global Change Biology, 5, 245–253.

Chen, J., Jönsson, P., Tamura, M., Gu, Z., Matsushita, B., & Eklundh, L. (2004). A simple method for reconstructing a high-quality NDVI time-series data set based on the Savitzky–Golay filter. Remote Sensing of Environment, 91, 332–344.

Clark, M. P., Slater, A. G., Barrett, A. P., Hay, L. E., McCabe, G. J., Rajagopalan, B., & Leavesley, G. H. (2006). Assimilation of snow covered area information into hydrologic and land-surface models. Advances in Water Resources, 29, 1209–1221.

Delbart, N., Kergoat, L., Le Toan, T., L'Hermitte, J., & Picard, G. (2005). Determination of phenological dates in boreal regions using normalized difference water index. Remote Sensing of Environment, 97, 26–38.

Delbart, N., Le Toan, T., Kergoat, L., & Fedotova, V. (2006). Remote sensing of spring phenology in boreal regions: A free of snow-effect method using NOAA-AVHRR and SPOT-VGT data (1982–2004). Remote Sensing of Environment, 101, 52–62.

Delbart, N., Picard, G., Le Toan, T., Kergoat, L., Quegan, S., Woodward, I. A. N., Dye, D., & Fedotova, V. (2008). Spring phenology in boreal Eurasia over a nearly century time scale. Global Change Biology, 14, 603–614.

Delpierre, N., Soudani, K., François, C., Le Maire, G., Bernhofer, C., Kutsch, W., Misson, L., Rambal, S., Vesala, T., & Dufrêne, E. (2012). Quantifying the influence of climate and biological drivers on the interannual variability of carbon exchanges in European forests through process-based modelling. Agricultural and Forest Meteorology, 154–155, 99–112.

Doktor, D., Bondeau, A., Koslowski, D., & Badeck, F. -W. (2009). Influence of heterogeneous landscapes on computed green-up dates based on daily AVHRR NDVI observations. Remote Sensing of Environment, 113, 2618–2632.

Drebs, A., Nordlund, A., Karlsson, P., Helminen, J., & Rissanen, P. (2002). Climatological statistics of Finland 1971–2000. Helsinki: Finnish Meteorological Institute.

Duchemin, B., Goubier, J., & Courrier, G. (1999). Monitoring phenological key stages and cycle duration of temperate deciduous forest ecosystems with NOAA/AVHRR data. Remote Sensing of Environment, 67, 68–82.

Finnish Meteorological Institute (2012). Weather in recent years. http://en.ilmatieteenlaitos.fi/weather-in-recent-years (Accessed on 07/05/2012)

Ganguly, S., Friedl, M.A., Tan, B., Zhang, X., & Verma, M. (2010). Land surface phenology from MODIS: Characterization of the Collection 5 global land cover dynamics product. Remote Sensing of Environment, 114, 1805–1816.

Gao, B. -C. (1996). NDWI—A normalized difference water index for remote sensing of vegetation liquid water from space. Remote Sensing of Environment, 58, 257–266.

Garrity, S. R., Bohrer, G., Maurer, K. D., Mueller, K. L., Vogel, C. S., & Curtis, P.S. (2011). A comparison of multiple phenology data sources for estimating seasonal transitions in deciduous forest carbon exchange. Agricultural and Forest Meteorology, 151, 1741–1752.

Gea-Izquierdo, G., Mäkelä, A., Margolis, H., Bergeron, Y., Black, T. A., Dunn, A., Hadley, J., Paw U, K. T., Falk, M., Wharton, S., Monson, R., Hollinger, D. Y., Laurila, T., Aurela, M., McCaughey, H., Bourque, C., Vesala, T., & Berninger, F. (2010). Modeling acclimation of photosynthesis to temperature in evergreen conifer forests. New Phytologist, 188, 175–186.

Gonsamo, A., Chen, J. M., Price, D. T., Kurz, W. A., & Wu, C. (2012). Land surface phenology from optical satellite measurement and CO_2 eddy covariance technique. Journal of Geophysical Research, 117, G03032.

Gutman, G. G. (1991). Vegetation indices from AHVRR: An update and future prospects. Remote Sensing of Environment, 35, 121–136.

Haakana, M., Hatunen, S., Härmä, P., Kallio, M., Katila, M., Kiiski, T., Mäkisara, K., Peräsaari, J., Piepponen, H., Repo, R., Teiniranta, R., Tomppo, E., & Törmä, M. (2008). Finnish CORINE 2006-project: determining changes in land cover in Finland between 2000 and 2006. SPIE Europe Remote Sensing Congress. Cardiff, Wales, United Kingdom.

Hall, D. K., & Martinec, J. (1985). Remote sensing of ice and snow. London: Chapman and Hall.

Hall, D. K., & Riggs, G. A. (2007). Accuracy assessment of the MODIS snow products. Hydrological Processes, 21, 1534–1547.

Härmä, P., Teiniranta, R., Törmä, M., Repo, R., Järvenpää, E., & Kallio, E. (2005). CLC2000 Finland: final report. Finnish Environment Institute, Geoinformatics and Land Use Division.

Holben, B. (1986). Characteristics of maximum-value composite images from temporal AVHRR data. International Journal of Remote Sensing, 7, 1417–1434.

Huemmrich, K. F., Black, T. A., Jarvis, P. G., McCaughey, J. H., & Hall, F. G. (1999). High temporal resolution NDVI phenology from micrometeorological radiation sensors. Journal of Geophysical Research: Atmospheres, 104, 27935–27944.

Jönsson, P., & Eklundh, L. (2004). TIMESAT-a program for analyzing time-series of satellite sensor data. Computers & Geosciences, 30, 833–845.

Jönsson, A.M., Eklundh, L., Hellström, M., Bärring, L., & Jönsson, P. (2010). Annual changes in MODIS vegetation indices of Swedish coniferous forests in relation to snow dynamics and tree phenology. Remote Sensing of Environment, 114, 2719–2730.

Karlsen, S. R., Elvebakk, A., Høgda, K. A., & Johansen, B. (2006). Satellite-based mapping of the growing season and bioclimatic zones in Fennoscandia. Global Ecology and Biogeography, 15, 416–430.

Karlsen, S., Solheim, I., Beck, P., Høgda, K., Wielgolaski, F., & Tømmervik, H. (2007). Variability of the start of the growing season in Fennoscandia, 1982–2002. International Journal of Biometeorology, 51, 513–524.

Karlsen, S. R., Tolvanen, A., Kubin, E., Poikolainen, J., Høgda, K. A., Johansen, B., Danks, F. S., Aspholm, P., Wielgolaski, F. E., & Makarova, O. (2008). MODIS-NDVI-based mapping of the length of the growing season in northern Fennoscandia. International Journal of Applied Earth Observation and Geoinformation, 10, 253–266.

Kaufmann, R. K., Zhou, L., Knyazikhin, Y., Shabanov, N. V., Myneni, R. B., & Tucker, C. J. (2000). Effect of orbital drift and sensor changes on the time series of AVHRR Vegetation Index Data. IEEE Transactions on Geoscience and Remote Sensing, 38, 2584–2597.

Kimball, J. S., McDonald, K. C., Running, S. W., & Frolking, S. E. (2004). Satellite radar remote sensing of seasonal growing seasons for boreal and subalpine evergreen forests. Remote Sensing of Environment, 90, 243–258.

Kubin, E., Kotilainen, E., Poikolainen, J., Hokkanen, T., Nevalainen, S., Pouttu, A., Karhu, J., & Pasanen, J. (2007). Fenologisen havaintoverkon seurantaohjeet. Finnish Forest Research Institute.

Kuusisto, E. (1984). Snow accumulation and snowmelt in Finland. Helsinki, Finland: National Board of Waters.

Lee, S., Klein, A. G., & Over, T. M. (2005). A comparison of MODIS and NOHRSC snow-cover products for simulating streamflow using the Snowmelt Runoff Model. Hydrological Processes, 19, 2951–2972.

Liang, L., Schwartz, M.D., & Fei, S. (2011). Validating satellite phenology through intensive ground observation and landscape scaling in a mixed seasonal forest. Remote Sensing of Environment, 115, 143–157.

Maignan, F., Bréon, F. M., Bacour, C., Demarty, J., & Poirson, A. (2008). Interannual vegetation phenology estimates from global AVHRR measurements: Comparison with in situ data and applications. Remote Sensing of Environment, 112, 496–505.

Mäkelä, A., Hari, P., Berninger, F., Hänninen, H., & Nikinmaa, E. (2004). Acclimation of photosynthetic capacity in Scots pine to the annual cycle of temperature. Tree Physiology, 24, 369–376.

Mammarella, I., Launiainen, S., Grönholm, T., Keronen, P., Pumpanen, J., Rannik, Ü., & Vesala, T. (2009). Relative humidity effect on the high frequency attenuation of water vapour flux measured by a closed path eddy covariance system. Journal of Atmospheric and Oceanic Technology, 26, 1856–1866.

Meier, U. (Ed.). (1997). BBCH-Monograph. Growth stages of mono- and dicotyledonous plants. Berlin: Blackwell.

Melaas, E. K., Richardson, A.D., Friedl, M.A., Dragoni, D., Gough, C. M., Herbst, M., Montagnani, L., & Moors, E. (2013). Using FLUXNET data to improve models of springtime vegetation activity onset in forest ecosystems. Agricultural and Forest Meteorology, 171–172, 46–56.

Metsämäki, S. J., Anttila, S. T., Huttunen, M. J., & Vepsäläinen, J. M. (2005). A feasible method for fractional snow cover mapping in boreal zone based on a reflectance model. Remote Sensing of Environment, 95, 77–95.

Metsämäki, S., Mattila, O. -P., Pulliainen, J., Niemi, K., Luojus, K., & Böttcher, K. (2012). An optical reflectance model-based method for fractional snow cover mapping applicable to continental scale. Remote Sensing of Environment, 123, 508–521.

Monson, R., Sparks, J., Rosenstiel, T., Scott-Denton, L., Huxman, T., Harley, P., Turnipseed, A., Burns, S., Backlund, B., & Hu, J. (2005). Climatic influences on net ecosystem CO_2 exchange during the transition from wintertime carbon source to springtime carbon sink in a high-elevation, subalpine forest. Oecologia, 146, 130–147.

Moulin, S., Kergoat, L., Viovy, N., & Dedieu, G. (1997). Global-scale assessment of vegetation phenology using NOAA/AVHRR satellite measurements. *Journal of Climate, 10*, 1154–1155.

Rannik, Ü., Keronen, P., Hari, P., & Vesala, T. (2004). Estimation of forest atmosphere CO_2 exchange by eddy covariance and profile techniques. *Agricultural and Forest Meteorology, 126*, 141–155.

Rauste, Y., Astola, H., Häme, T., Berglund, R., Sirro, L., Veijonen, T., Veikkanen, B., Kubin, E., & Aulamo, O. (2007). Automatic monitoring of autumn colours using MODIS data. *IEEE International Geoscience and Remote Sensing Symposium, IGARSS 2007. Barcelona, Spain* (pp. 1295–1298).

Reed, B. C., Brown, J. F., Vanderzee, D., Loveland, T. R., Merchant, J. W., & Ohlen, D. O. (1994). Measuring phenological variabilty from satellite imagery. *Journal of Vegetation Sciences, 5*, 703–714.

Richardson, A.D., Andy Black, T., Ciais, P., Delbart, N., Friedl, M.A., Gobron, N., Hollinger, D. Y., Kutsch, W. L., Longdoz, B., Luyssaert, S., Migliavacca, M., Montagnani, L., William Munger, J., Moors, E., Piao, S., Rebmann, C., Reichstein, M., Saigusa, N., Tomelleri, E., Vargas, R., & Varlagin, A. (2010). Influence of spring and autumn phenological transitions on forest ecosystem productivity. *Philosophical Transactions of the Royal Society B: Biological Sciences, 365*, 3227–3246.

Richardson, A.D., Hollinger, D. Y., Dail, D. B., Lee, J. T., Munger, J. W., & O'keefe, J. (2009). Influence of spring phenology on seasonal and annual carbon balance in two contrasting New England forests. *Tree Physiology, 29*, 321–331.

Riggs, G. A., Hall, D. K., & Salomonson, V. V. (2006). *MODIS snow products user guide to collection 5.* Boulder, CO, USA: National Snow & Ice Data Centre.

Savitzky, A., & Golay, M. J. E. (1964). Smoothing and differentiation of data by simplified least squares procedures. *Analytical Chemistry, 36*, 1627–1639.

Sellers, P. J. (1985). Canopy reflectance, photosynthesis and transpiration. *International Journal of Remote Sensing, 6*, 1335–1372.

Sevanto, S., Suni, T., Pumpanen, J., Grönholm, T., Kolari, P., Nikinmaa, E., Hari, P., & Vesala, T. (2006). Wintertime photosynthesis and water uptake in a boreal forest. *Tree Physiology, 26*, 749–757.

Shutova, E., Wielgolaski, F., Karlsen, S., Makarova, O., Berlina, N., Filimonova, T., Haraldsson, E., Aspholm, P., Flø, L., & Høgda, K. (2006). Growing seasons of Nordic mountain birch in northernmost Europe as indicated by long-term field studies and analyses of satellite images. *International Journal of Biometeorology, 51*, 155–166.

Soudani, K., le Maire, G., Dufrêne, E., François, C., Delpierre, N., Ulrich, E., & Cecchini, S. (2008). Evaluation of the onset of green-up in temperate deciduous broadleaf forests derived from Moderate Resolution Imaging Spectroradiometer (MODIS) data. *Remote Sensing of Environment, 112*, 2643–2655.

Stenberg, P., Rautiainen, M., Manninen, T., Voipio, P., & Smolander, S. (2004). Reduced simple ratio better than NDVI for estimating LAI in Finnish pine and spruce stands. *Silva Fennica, 38*, 3–14.

Sukuvaara, T., Pulliainen, J., Kyrö, E., Suokanerva, H., Heikkinen, P., & Suomalainen, J. (2007). Reflectance spectroradiometer measurement system in 30 meter mast for validating satellite images. *IEEE 2007 International Geoscience and Remote Sensing Symposium (IGARSS), Sensing and understanding our planet. Barcelona, Spain* (pp. 1524–1528).

Suni, T., Berninger, F., Vesala, T., Markkanen, T., Hari, P., Mäkelä, A., Ilvesniemi, H., Hänninen, H., Nikinmaa, E., Huttula, T., Laurila, T., Aurela, M., Grelle, A., Lindroth, A., Arneth, A., Shibistova, O., & Lloyd, J. (2003). Air temperature triggers the recovery of evergreen boreal forest photosynthesis in spring. *Global Change Biology, 9*, 1410–1426.

Thum, T., Aalto, T., Laurila, T., Aurela, M., Hatakka, J., Lindroth, A., & Vesala, T. (2009). Spring initiation and autumn cessation of boreal coniferous forest CO_2 exchange assessed by meteorological and biological variables. *Tellus B, 61*, 701–717.

Vesala, T., Suni, T., Rannik, Ü., Keronen, P., Markkanen, T., Sevanto, S., Grönholm, T., Smolander, S., Kulmala, M., Ilvesniemi, H., Ojansuu, R., Uotila, A., Levula, J., Mäkelä, A., Pumpanen, J., Kolari, P., Kulmala, L., Altimir, N., Berninger, F., Nikinmaa, E., & Hari, P. (2005). Effect of thinning on surface fluxes in a boreal forest. *Global Biogeochemical Cycles, 19*, GB2001.

Wang, Q., Tenhunen, J., Dinh, N. Q., Reichstein, M., Vesala, T., & Keronen, P. (2004). Similarities in ground- and satellite-based NDVI time series and their relationship to physiological activity of a Scots pine forest in Finland. *Remote Sensing of Environment, 93*, 225–237.

White, M.A., De Beurs, K. M., Didan, K., Inouye, D. W., Richardson, A.D., Jensen, O. P., O'Keefe, J., Zhang, G., Nemani, R. R., Van Leeuwen, W. J.D., Brown, J. F., De Wit, A., Schaepman, M., Lin, X., Dettinger, M., Bailey, A. S., Kimball, J., Schwartz, M.D., Baldocchi, D.D., Lee, J. T., & Lauenroth, W. K. (2009). Intercomparison, interpretation, and assessment of spring phenology in North America estimated from remote sensing for 1982–2006. *Global Change Biology, 15*, 2335–2359.

White, M.A., Thornton, P. E., & Running, S. W. (1997). A Continental Phenology Model for Monitoring Vegetation Responses to Interannual Climatic Variability. *Global Biogeochemical Cycles, 11*, 217–234.

Wu, S. H., Jansson, P. -E., & Kolari, P. (2012). The role of air and soil temperature in the seasonality of photosynthesis and transpiration in a boreal Scots pine ecosystem. *Agricultural and Forest Meteorology, 156*, 85–103.

II

DGPF

CrossMark

ORIGINAL ARTICLE

Proxy Indicators for Mapping the End of the Vegetation Active Period in Boreal Forests Inferred from Satellite-Observed Soil Freeze and ERA-Interim Reanalysis Air Temperature

Kristin Böttcher[1] · Kimmo Rautiainen[2] · Mika Aurela[2] · Pasi Kolari[3] · Annikki Mäkelä[4] · Ali N. Arslan[2] · T. Andrew Black[5] · Sampsa Koponen[1]

Abstract

Triggered by decreases in photoperiod and temperature, evergreen needle-leaved trees in the boreal region downregulate photosynthetic activity and enter dormancy in autumn. Accompanying changes in canopy structure and chlorophyll content are small and precede the cessation of photosynthetic activity. Low solar elevation and cloud cover during this period pose additional challenges for the use of optical satellite instruments. Alternatively, environmental variables that correlate with photosynthesis, such as soil freeze, can be detected from satellite microwave observations independent of weather and illumination conditions. We tested for the first time the usability of satellite-observed soil freeze from the Soil Moisture and Ocean Salinity (SMOS) instrument as a proxy indicator for the end of vegetation active period (VAPend) at six eddy covariance sites in Finland and Canada. The time when soil freeze commenced over the large SMOS pixel can be employed to estimate VAPend ($R^2 = 0.84$, RMSE = 7.5 days), defined as the time when the photosynthetic capacity of the forest drops below 10% of the growing season maximum. In comparison to satellite-based soil freeze timing, an air temperature-based proxy from ERA-Interim reanalysis data showed better performance ($R^2 = 0.92$, RMSE = 5.2 days). VAPend was mapped in the boreal forest zone in Finland and Canada from both indicators based on linear regression models.

✉ Kristin Böttcher
kristin.bottcher@environment.fi

Kimmo Rautiainen
kimmo.rautiainen@fmi.fi

Mika Aurela
mika.aurela@fmi.fi

Pasi Kolari
pasi.kolari@helsinki.fi

Annikki Mäkelä
annikki.makela@helsinki.fi

Ali N. Arslan
ali.nadir.arslan@fmi.fi

T. Andrew Black
andrew.black@ubc.ca

Sampsa Koponen
sampsa.koponen@environment.fi

[1] Finnish Environment Institute, Geoinformatics Research, 00790 Helsinki, Finland

[2] Finnish Meteorological Institute, 00560 Helsinki, Finland

[3] Institute for Atmospheric and Earth System Research/Physics, University of Helsinki, 00014 Helsinki, Finland

[4] Department of Forest Sciences, University of Helsinki, 00014 Helsinki, Finland

[5] Faculty of Land and Food Systems, University of British Columbia, Vancouver, Canada

 Springer

Zusammenfassung

Die Ableitung des Zeitpunktes des Endes der photosynthetisch aktiven Periode borealer Wälder aus Satellitendaten zum Bodenfrost und ERA-Interim Temperaturdaten. Im Herbst regeln immergrüne Nadelbäume in der borealen Zone ihre photosynthetische Aktivität herab und gehen in einen Ruhezustand über. Dieser Prozess wird durch eine Verringerung der Photoperiode und der Temperatur ausgelöst. Veränderungen in der Kronenstruktur und des Chlorophyllgehaltes, die diesen Prozess begleiten, sind kaum sichtbar und treten bereits vor der Einstellung der Photosynthese auf. In diesem Zeitraum erschweren darüber hinaus der tiefe Sonnenstand und häufige Bewölkung die Anwendung von optischen Satellitendaten. Als Alternative können Umweltfaktoren, die die Photosynthese beeinflussen, wie z.B. der Bodenfrost, unabhängig von Wetterbedingungen mittels Mikrowellen-Fernerkundung erfasst werden. Anhand von sechs Beobachtungsstandorten in Finnland und Kanada wurde daher in dieser Arbeit untersucht, ob Satellitendaten zum Bodenfrost zur Bestimmung des Zeitpunktes des Endes der aktiven Vegetationsperiode (VAPend) immergrüner borealer Nadelwälder geeignet sind. VAPend wurde an den Beobachtungsstandorten aus Messungen des Kohlenstoffflusses mit der Eddy-Kovarianz-Methode bestimmt. Erstmals wurden für die Analyse des Zusammenhangs von Bodenfrost und VAPend Satellitendaten der Soil Moisture and Ocean Salinity (SMOS) Mission eingesetzt. Zum Vergleich wurde der Beginn des Luftfrosts aus ERA-Interim Reanalyse Daten abgeleitet. Die Untersuchung ergab einen engen Zusammenhang des Zeitpunktes des Beginns der Frostperiode mit VAPend, wobei der erste Luftfrosttag eine höhere Korrelation mit VAPend zeigte ($R^2 = 0{,}92$, RMSE = 5,2 Tage) als der erste SMOS-basierte Bodenfrosttag ($R^2 = 0{,}84$, RMSE = 7,5 Tage). VAPend wurde mit Hilfe linearer Regressionsmodelle aus dem ersten Luft- und Bodenfrosttag abgeleitet und in der borealen Zone in Finnland und Kanada dargestellt.

1 Introduction

Ecosystem processes related to carbon, water and nutrient cycling are directly linked to vegetation phenology. Climate change is affecting the timing of phenological events, and vegetation phenology has, therefore, been proposed as an indicator for long-term biological impacts of climate change on terrestrial ecosystems (Schwartz 1998; Menzel and Fabian 1999; Richardson et al. 2013). Lengthening of the growing season is expected as the consequence of increasing temperatures caused by climate change (Fronzek et al. 2012; Laapas et al. 2012). An earlier start of the growing season in the boreal forest increases carbon sequestration (Black et al. 2000; Pulliainen et al. 2017). Warmer autumns resulted in a greater increase in respiration compared to gains in photosynthesis (Piao et al. 2008; Vesala et al. 2010). Still, the impacts of predicted warming with rising temperatures in autumn and the foreseen lowered temperature seasonality (Xu et al. 2013) are uncertain and photoperiod may constrain potential future lengthening of the growing season in autumn (Mäkelä et al. 2006). Despite the importance of autumn phenology for the variability of productivity, it has received less consideration than spring phenology (Wu et al. 2012; Gonsamo and Chen 2016).

Trends in autumn phenological events, such as leaf colouring, were analysed from in situ observations of deciduous species and from satellite-observed phenology based on vegetation indices. Results vary regionally depending on the considered time period. Satellite observations show delayed leaf senescence in the boreal forest in Eurasia, parts of Fennoscan-dia and in Northern America for the period 1982–2008 (Jeong et al. 2011). A later end of the growing season was observed in southern Fennoscandia for the period 1982–2006 (Karlsen et al. 2009). Instead, from ground observations of leaf colouring of birch in Finland, no significant changes were found for the period 1997–2006 (Pudas et al. 2008). Autumn Normalized Difference Vegetation Index (NDVI) increased during the period 1982–2006 in large parts of Eurasia (Piao et al. 2011). However, trends in autumn senescence from the Phenological Index were not significant for most parts of the boreal region for the period 1999–2013 (Gonsamo and Chen 2016).

To protect their photosynthetic apparatus against frost damage during winter, coniferous trees in the boreal zone develop frost hardiness and enter dormancy. The decrease in photosynthetic capacity and the cessation of growth are triggered by shortening of the photoperiod and decreasing temperature (Vogg et al. 1998; Öquist and Huner 2003; Suni et al. 2003; Sevanto et al. 2006; Vesala et al. 2010; Bauerle et al. 2012). The oldest leaves of evergreen needle-leaved trees are shed in autumn with the lifespan and turnover rates depending on the tree species. The lifespan increases and turnover rates decrease from south to north in the boreal evergreen forests (Reich et al. 2014). After the oldest foliage drops, evergreen needle-leaved trees continue to photosynthesize until the occurrence of severe frosts (Vogg et al. 1998; Suni et al. 2003; Wu et al. 2012). The development of frost hardiness leads to a loss of chlorophyll and an increasing capacity to transform absorbed light into heat (Öquist and Huner 2003). The process of downregulation of photosyn-

thesis in autumn can be divided into two stages. First, an initial decline is observed as a response to low temperatures. During this stage, photosynthesis recovers fast when conditions become favourable. Second, a more persistent stage of dormancy is reached with harsher winter conditions and photosynthesis recovers more slowly even when conditions become favourable (Kolari et al. 2014). We refer to the latter stage as the end of the vegetation active period (VAPend), where the vegetation active period (VAP) is defined as the period of the year when vegetation is assimilating carbon through photosynthesis.

Satellite methods that track changes in the leaf area index (Jin and Eklundh 2014), the pigment content (Gamon et al. 2016; Ulsig et al. 2017), and the end of the growing season (Gonsamo and Chen 2016) in boreal evergreen needle-leaved forest from vegetation indices were developed, but the detection of VAPend from satellite observations remains challenging. Observations with optical instruments are hindered by frequent cloud cover and low solar elevation in autumn at high latitudes. Recently, the re-emission of excess energy, not used in the photosynthetic process, has been observed as sun-induced chlorophyll fluorescence (SIF) from space (Joiner et al. 2014; Walther et al. 2016). Satellite retrievals of surface fluorescence were found to be less affected by atmospheric scattering than those of surface reflectance (Frankenberg et al. 2012; Frankenberg et al. 2014; Köhler et al. 2015); however, at low solar elevation, the noise in the SIF signal increases and is possibly biased by rotational-Raman scattering (Joiner et al. 2014). Moreover, currently available satellite measurements of chlorophyll fluorescence have a large footprint which complicates comparison with CO_2 flux measurements (Joiner et al. 2014).

Therefore, the development of robust satellite indicators for VAPend in boreal evergreen needle-leaved forest is still lacking. In addition to observations of changes in canopy structure, chlorophyll content and, more directly, chlorophyll fluorescence, environmental variables that correlate with photosynthesis, such as temperature, soil freeze (Jarvis and Linder 2000; Barr et al. 2009; Barichivich et al. 2013), snow cover, and incoming radiation could help to track autumn seasonal changes in boreal forests from space. In this work, we will focus on satellite indicators of soil freeze.

Despite the fact that soil freeze is not a primary cause for the start of photosynthetic downregulation in autumn, we hypothesize that it can be used as a proxy indicator for VAPend in evergreen boreal trees. Photosynthesis is always associated with water loss due to transpiration that needs either be balanced by soil water uptake or change in stem water storage (Sevanto et al. 2006). As soil freeze will block the water transport from the soil to trees, it may be more directly related to photosynthesis (Hölttä et al. 2017), even though photosynthesis has been observed when the soil and

tree stem were partially frozen in boreal coniferous forest (Suni et al. 2003; Sevanto et al. 2006).

Soil freeze can be detected from active and passive microwave observations (Kimball et al. 2004; Smith et al. 2004; Bartsch et al. 2007; Kim et al. 2011; Kim et al. 2012; Roy et al. 2015; Rautiainen et al. 2016; Derksen et al. 2017) with the advantage of independence from weather conditions and low solar elevation during autumn and winter in the high latitudes. New observations of the soil freeze state from L-band (1–2 GHz) active radar and passive microwave radiometers (Roy et al. 2015; Rautiainen et al. 2016; Derksen et al. 2017) bring the advantage of higher emission depth and lower sensitivity to vegetation and snow cover compared to observations from higher frequencies (Kimball et al. 2004; Kim et al. 2011) that have been used earlier to derive information on soil freeze (Rautiainen et al. 2012; Roy et al. 2015).

The objective of this study was to investigate the possibility of applying satellite-observed soil freeze as a proxy indicator for VAPend in boreal evergreen needle-leaved forests. For this, we utilized observations of soil freeze state detected from L-Band passive microwave observations from the European Space Agency's Soil Moisture and Ocean Salinity (SMOS) mission (Rautiainen et al. 2016). In addition to satellite-derived soil freeze, we also included an autumnal freeze indicator from ERA-Interim reanalysis air temperature data in our analysis. We described the late stages of photosynthetic downregulation with three dates for VAPend (see Sect. 2.4) that were determined from CO_2 flux measurements for six sites in the boreal forest zone in Finland and Canada. The relationship between VAPend and indicators for air and soil freeze was analysed, and based on that, proxy indicators for mapping of VAPend at continental to global scales were developed.

2 Materials and Methods

2.1 Measurement Sites

We selected six CO_2 flux measurement sites in evergreen needle-leaved boreal forest. Three sites are located in Finland and three sites in Canada (Fig. 1, Table 1). The Canadian sites (CA-Obs, CA-Ojp and CA-Qfo), and one Finnish site (Hyytiälä, FI-Hyy) belong to the southern boreal phytogeographical zone, whereas two Finnish sites, Kenttärova (FI-Ken) and Sodankylä (FI-Sod), belong to the northern boreal zone. All Finnish sites are located further north (62–68°N) than the Canadian sites (50–54°N). The solar elevation at solar noon decreases below 30° at the end of October at CA-Qfo but at the beginning of September at FI-Ken. The dominant tree and understory species vary by site.

CA-Obs and CA-Ojp are located at the southern edge of the boreal forest about 100 km north-east of Prince Albert in

Fig. 1 Location of CO_2 flux measurement sites in the boreal forest zone in Canada (**a**), and Finland (**b**)
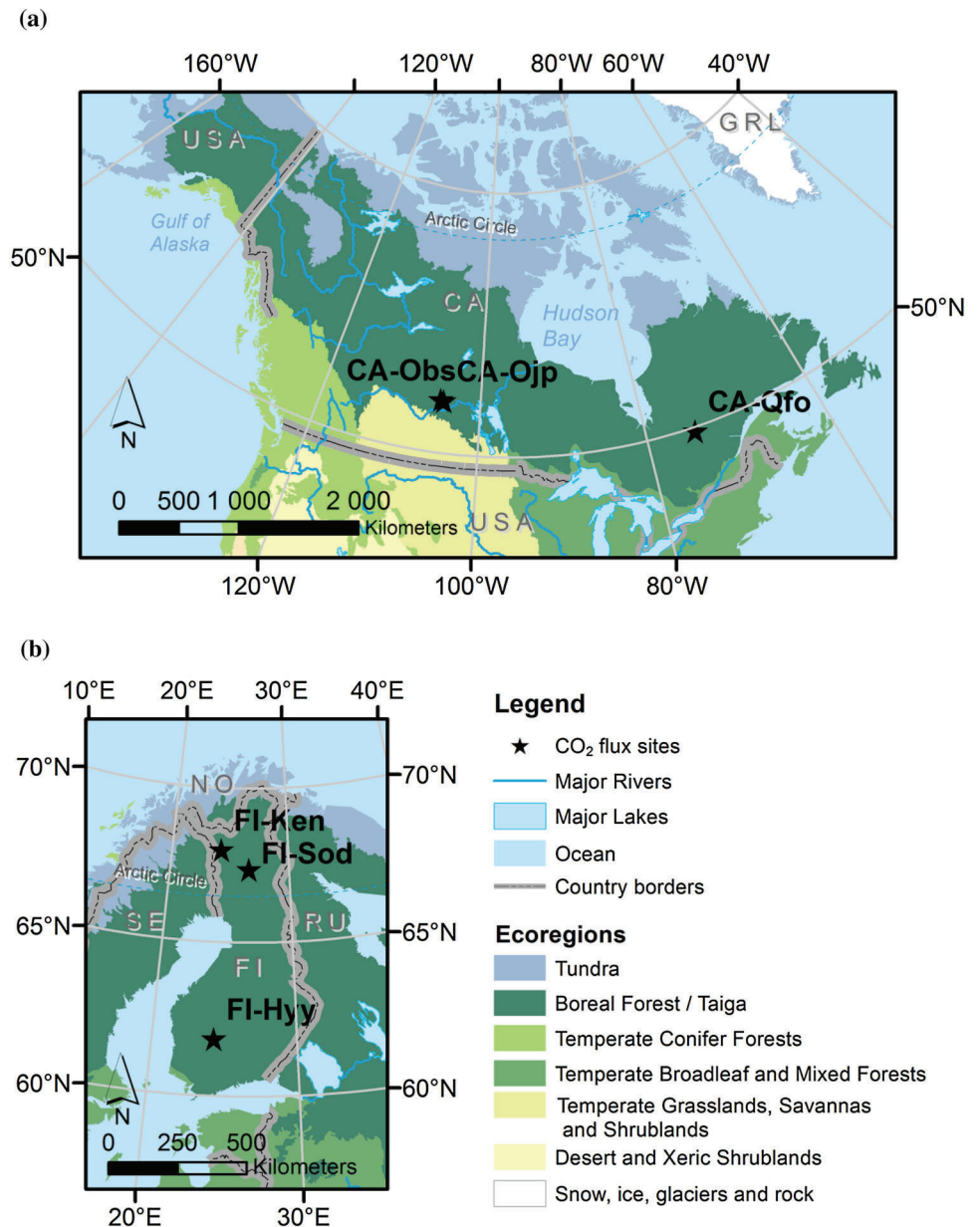
Data sources:
World Map (ArcWorld Supplement, ESRI Data & Maps, 2008), Global Ecoregions, Major Habitat Types, Biogeographical Realms and The Nature Conservancy Terrestrial Assessment Units as of December 14, 2009 (The Nature Conservancy).
Projection:
Canada: Lambert conformal conic; Finland: EUREF FIN/ ETRS-TM35FIN

central Saskatchewan, Canada. The distance between the two sites is approximately 30 km. Both sites are characterized by old growth forests that regenerated after fire events in 1879 and 1929 at CA-Obs and CA-Ojp, respectively (Kljun et al. 2006). CA-Obs is dominated by black spruce (*Picea mariana* Mill. BSP) with sparsely distributed tamarack (*Larix laricina* Du Roi) and jack pine (*Pinus banksiana* Lamb), and the ground cover consists of mosses (sphagnum and feather mosses) and sparse understory. Further site characteristics

are given in Kljun et al. (2006), Bergeron et al. (2007) and Krishnan et al. (2008). CA-Ojp is a homogenous jack pine forest with a uniform age structure (Griffis et al. 2003; Kljun et al. 2006). The understory is dominated by lichen and green alder (*Alnuscrispa* Ait.). Due to its location in a topographic depression, CA-Obs is poorly drained and has a high water table. Soil at CA-Ojp is coarse textured and well drained (Kljun et al. 2006).

Table 1 Characteristics of *CO₂ flux measurement* sites

Site	FI-Hyy	FI-Ken	FI-Sod	CA-Obs	CA-Ojp	CA-Qfo
Name	Hyytiälä	Kenttärova	Sodankylä	Saskatchewan, southern old black spruce	Saskatchewan, old jack pine	Quebec, eastern old black spruce
Country	Finland	Finland	Finland	Canada	Canada	Canada
Latitude (decimal degrees)	61.85N	67.99N	67.36N	53.99N	53.92N	49.69N
Longitude (decimal degrees)	24.29E	24.24E	26.64E	105.12W	104.69W	74.34W
Altitude above sea level (m)	170	347	179	629	579	382
Forest type	Scots pine/ Norway spruce	Norway spruce	Scots pine	Mature black spruce	Mature jack pine	Mature black spruce
Mean annual air temperature (°C) and precipitation (mm)	3.5[a] 711	− 1.8[b] 501	− 0.8[c] 507	0.4[d] 467	0.4[d] 467	− 0.0[e] 961
Data availability	2001–2016	2003–2015	2001–2016	2001–2011	2001–2011	2003–2010

Long-term records of air temperature and precipitation are for the period
[a] 1981–2010 in Hyytiälä
[b] 1971–2000 from station Kittilä Pulju
[c] 1971–2000 from station Sodankylä (Drebs et al. 2002)
Long-term averages of air temperature and precipitation for the period
[d] 1971–2000 at station Waskesiu Lake
[e] 1971–2000 at station Chapais 2 (www.climate.weatheroffice.gc.ca. Accessed 17 Oct 2018)

CA-Qfo, located 30 km south of Chibougamau (Quebec), is dominated by black spruce and the forest floor consists mainly of feather mosses, sphagnum and lichen. The forest stand covers the tower flux footprint, except in the south-east direction where a peatland is situated. Further details of the site are given in Bergeron et al. (2007) and Coursolle et al. (2012).

FI-Hyy in southern Finland belongs to the SMEAR II station (Station for Measuring Ecosystem-Atmosphere Relations) of the University of Helsinki. The stand is dominated by Scots pine (*Pinus sylvestris* L.) sown in 1962 with some naturally regenerated Norway spruce (*Picea abies*) and scattered deciduous trees. It is a typically managed forest (Vesala et al. 2010). The forest floor is composed of dwarf shrubs and mosses (Kulmala et al. 2008).

Sites FI-Ken and FI-Sod are located above the Arctic Circle in Finnish Lapland. The Scots pine forest in FI-Sod is naturally regenerated and is representative of pine-dominated forested areas in central Lapland (Thum et al. 2009). The site belongs to the Arctic Research Centre of the Finnish Meteorological Institute. FI-Ken, a homogenous Norway spruce (*Picea abies* [L.] H. Karst.) forest, is situated in the Pallas-Yllästunturi National Park (Aurela et al. 2015).

According to the GlobCover map (Arino et al. 2012), open (15–40%) needle-leaved deciduous or evergreen forests is the dominant land cover type for the surrounding areas of all CO₂ flux measurement sites corresponding to the area covered by the SMOS pixels. The coverage differs by site showing the highest proportions for CA-Ojp (84%) and lowest for CA-Qfo (42%) (Online Resource Table S1). The second highest contributions come from closed to open (> 15%) mixed broadleaved and needle-leaved forest for FI-Sod and FI-Hyy. For CA-Obs and CA-Qfo, the proportion of open water bodies within the SMOS pixel is relatively high (14% and 24%, respectively).

2.2 CO₂ Flux Measurements

The in situ fluxes of CO_2 were measured by the micrometeorological eddy covariance method which provides direct measurements of CO_2 exchange between atmosphere and biosphere averaged on an ecosystem scale. In the eddy covariance method, the vertical CO_2 flux is obtained as the covariance of the high-frequency (10 Hz) observations of vertical wind speed and the CO_2 concentration (Baldocchi 2003). The measurements were made 5–10 m above the mean forest height.

The eddy covariance measurement systems at FI-Sod and FI-Ken included a USA-1 three-dimensional sonic anemometer/thermometer (3D SAT) (METEK GmbH, Elmshorn, Germany) and a closed-path LI-7000 CO_2/H_2O infrared gas analyser (IRGA) (LI-COR, Inc., Lincoln, NE,

USA). At FI-Hyy, a Solent 1012R3 3D SAT (Gill Instruments Ltd., Lymington, UK) with a closed-path LI-6262 IRGA (LI-COR Inc.) was used. All three Canadian sites used LI-7000 IRGAs together with a Solent 1012R3 3D SAT at CA-Obs, and CSAT3 3D SATs (Campbell Scientific Inc. (CSI) Logan, UT, USA) at CA-Ojp and CA-Qfo.

The eddy covariance fluxes were calculated as half-hourly averages taking into account the appropriate corrections following Aubinet et al. (2012). The measurement systems and the post-processing procedures have been presented in more detail for FI-Hyy by Kolari et al. (2004), Vesala et al. (2005) and Mammarella et al. (2009), for FI-Sod and FI-Ken by Aurela et al. (2009) and Aurela et al. (2015), for CA-Obs and CA-Ojp by Barr et al. (2004), and for CA-Qfo by Bergeron et al. 2007. The AmeriFlux Base data products (version 1-1) were used for the Canadian sites (Black 1999a, b; Margolis 2003).

2.3 Soil Temperature Measurements at Sodankylä

To compare satellite-based soil freeze with in situ observations, we utilized measurements from 8 measurement sites of the automatic network of in situ soil moisture and soil temperature observations at the Arctic Research Centre at Sodankylä (Ikonen et al. 2016). The sites cover typical soil types and land cover classes in the area and allow better representation of soil freeze conditions for the large areas covered by the SMOS footprint compared to the local data at the CO_2 flux sites. Sites are located in 170 m to 23 km distance to FI-Sod. At each soil measurement site, the vertical profile of soil properties (dielectric constant, electric conductivity and soil temperature) is measured at different depths with 5TE (Decagon Devices Inc., Pullman, WA, USA) or CS655 (Campbell Scientific Inc., Logan, UT, USA) soil moisture sensors. Two additional sensors are located 10 m away from each vertical profile in opposing directions and measure at 10 and 5 cm depths. Further details of the measurement setup are described in Ikonen et al. (2016). In this study, we utilized daily average soil temperature observations at the 5 cm depth for the period 2011–2016. Measurements from the available sensors were averaged for each site. To account for inaccuracy in the temperature measurements (± 1 °C for 5TE and ± 0.5 °C for CS655) and dependence of the freezing point on soil water content (Kozlowski 2004, 2016), we defined the freezing point for each site individually during the melting period in spring as the temperature of the temporary plateau that is observed until all ice has melted. The first date when soil temperature dropped below the freezing point and the first date of the period with continuous soil freeze were determined. The number of available sites for each year ranged from 5 to 8.

2.4 Indicators of the End of the Vegetation Active Period

VAPend was determined for the 6 CO_2 flux measurement sites (Table 1) from the continuous CO_2 flux data measured by the micrometeorological eddy covariance method. The downregulation of photosynthesis in autumn is a gradual process and it is difficult to calculate definite dates for VAPend from CO_2 flux measurements. Different approaches, based on curve-fitting and absolute or relative threshold values, were utilized to describe the seasonal cycle of photosynthesis of plant communities from time series of net or gross ecosystem photosynthesis (e.g. Gu et al. 2009; Thum et al. 2009; Richardson et al. 2010). Here, the day on which the CO_2 uptake falls below a selected threshold level is defined as VAPend (Fig. 2). This is similar to the method for the extraction of the start of VAP in Böttcher et al. (2014) and Pulliainen et al. (2017). In practice, the dates were obtained from the annual cycle of the gross photosynthesis index (GPI), which indicates the photosynthetic capacity of the ecosystem on a daily time scale. It was calculated as a difference between daily averages of nighttime (photosynthetic photon flux density (PPFD) < 20 μmol m^{-2} s^{-1}) and daytime (PPFD > 600 μmol m^{-2} s^{-1}) 30-min CO_2 flux values (i.e. GPI $= F_{CO2night} - F_{CO2day}$).

The obtained GPI value does not strictly represent gross ecosystem photosynthesis since the nighttime respiration differs from the daytime respiration, but it provides a reasonable estimate when used as a relative measure. We tested three different GPI threshold (GPIth) values: 5%, 10% and 15% of the growing season maximum, which is the 90th percentile of the daily GPI values during the month of the highest uptake for
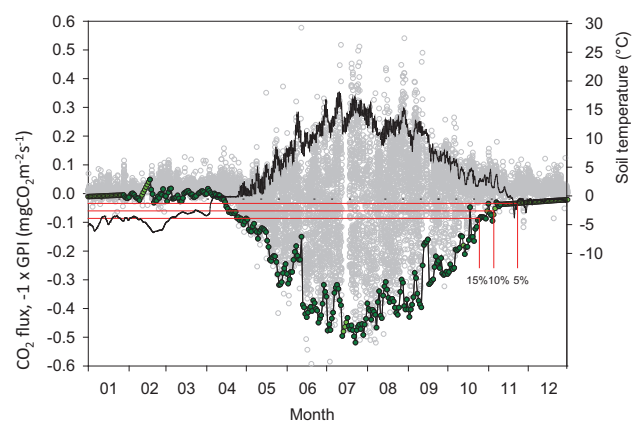

Fig. 2 Determination of end of vegetation active period, VAPend, from half-hourly eddy covariance CO_2 fluxes (grey circles) at Sodankylä in 2011. Red lines indicate the thresholds levels of 15%, 10% and 5% of the growing season maximum gross photosynthesis index (GPI). GPI is shown as green circles and interpolated values of GPI are highlighted in light green. Soil temperature is the solid black line

Table 2 Mean (± 1 standard deviation) end of the vegetation active period (VAPend) dates (day of year) from CO_2 flux measurements. Subscripts refer to the threshold value of the gross photosynthesis index (GPI) that was used to determine VAPend

Site	Year	VAPend$_5$	VAPend$_{10}$	VAPend$_{15}$
FI-Hyy	2001–2016	342 ± 18	323 ± 19	312 ± 15
FI-Ken	2003–2015	302 ± 9	295 ± 11	291 ± 8
FI-Sod	2001–2016	307 ± 21	298 ± 12	294 ± 7
CA-Obs	2001–2011	305 ± 10	298 ± 8	295 ± 7
CA-Ojp	2001–2011	308 ± 9	298 ± 8	297 ± 7
CA-Qfo	2003–2010	310 ± 13	306 ± 10	302 ± 9

the multi-year measurement period. Different threshold values were included because we do not have prior knowledge as to which one would be most useful indicator for VAPend. As an additional condition, the GPI has to stay below the GPIth for three consecutive days, and the number of following days with GPI>GPIth may not exceed the number of days with GPI<GPIth. The GPI time series was linearly gap-filled in order to estimate VAPend. The length of the gap and the timing of VAPend within the gap are recorded and taken into account when estimating the uncertainties of the data. To obtain information about multi-year mean and interannual variability of VAPend for each site, we calculated the dates of VAPend based on the three threshold (VAPend$_{th}$) values for all available observation years (see Table 2).

2.5 ERA-Interim Air Temperature Data

ERA-Interim global atmospheric reanalysis air temperature (2 m) data produced by the European Centre for Medium-Range Weather Forecasts (ECMWF) (Dee et al. 2011) was utilized to derive an indicator on autumn freeze. ERA-Interim reanalysis data are not direct observations. The data set is produced with a forecast model that includes coupled components of the atmosphere, land surface and the ocean waves. Available observational data sets from satellites and conventional observing systems are assimilated into the forecast model to constrain the state of the atmosphere and the Earth surface. Interpolated temperature observations from the synoptic station network over land are combined with the latest state of the atmosphere from the forecast model and utilized to update temperature estimates of the land surface model, thus indirectly influencing the background forecast model (Dee et al. 2011). The accuracy of ERA-Interim surface temperature is higher for areas with a dense station network (Simmons et al. 2010). The air temperature data set in the original spatial resolution of $0.75° \times 0.75°$ was resampled to the Equal Area Scalable Earth (EASE) grid 2.0 (Brodzik et al. 2012) corresponding to the SMOS soil state data. We calculated the 10-day

moving average air temperature (T_{10}) and defined the first date of autumnal freeze as the day when $T_{10} \leq -1$ °C. This threshold corresponds to a considerable reduction of ecosystem carbon uptake in boreal coniferous forest according to Hollinger et al. (1999).

2.6 Soil Freeze from Microwave Observations

Soil freeze/thaw state was determined from SMOS satellite data using the method by Rautiainen et al. (2016). We used global SMOS daily gridded level 3 brightness temperature from the Centre Aval de Traitement des Données SMOS (CATDS) (Al Bitar et al. 2017) as input data. The soil freeze/thaw detection algorithm is based on variations in soil permittivity that occur during soil freeze and thaw (permittivity of liquid water ~ 80 and of ice ~ 3 in L-Band) (Mätzler et al. 2006). This change in permittivity leads to higher L-Band brightness temperature of frozen soil compared to thawed moist soil. The algorithm uses a pixel-based relative frost factor calculated from the normalized ratio of brightness temperatures at vertical and horizontal polarizations which is compared against pixel-based thaw and freeze references to determine the soil freeze and thaw state. To reduce noise and the effect of short-term variations on the frost factor, a moving average with a window size of 20 days was applied. Ancillary information on air temperature from the ERA-Interim reanalysis data (see Sect. 2.5) is used to remove false summer freeze and winter thaw detections. Further details of the method are described in Rautiainen et al. (2016). The data set gives daily information on global soil freeze and thaw state in Northern Hemisphere at a spatial resolution of 25 km × 25 km in the EASE grid 2.0 for the period 2010–2016. The soil state is categorized into three classes: frozen, partially frozen and thawed. The SMOS instrument retrieves information from the top-soil layer (down to depths of 10–20 cm, depending on soil type and vegetation). Thus, the frozen soil state can be understood as a soil frost depth of at least 10 cm over the whole pixel. The class partially frozen corresponds to the transition period between first soil frost occurrences to completely frozen soil within one pixel. The soil data set

was compared with (1) global atmospheric reanalysis (ERA-Interim) soil temperature data and (2) local, point scale in situ measurements of soil temperature and the volumetric liquid water content (Rautiainen et al. 2016). For comparison with global (1) and local (2) data, the unbiased root mean square error was 20 and 17 days, respectively. The SMOS product indicates systematically later (about 2 weeks) first soil freeze than that using the ERA-Interim Level 2 soil temperature (7–28 cm layer) data set. The bias was smaller for the comparison with in situ data sets (7 days for soil temperature and 1 day for volumetric liquid moisture content), but the correlations were moderate which is probably due to the fact that in situ observations do not represent soil state within the large SMOS pixel adequately (Rautiainen et al. 2016).

Time series of freeze and thaw state were extracted for the six CO_2 flux sites in Finland and Canada using the ascending (6 am) and descending SMOS orbits (6 pm), respectively. Different orbits were used to avoid signal contamination from man-made radio frequency interference (Soldo et al. 2015). We extracted the first day of partially frozen and frozen soil from time series of the soil freeze and thaw state for the comparison with VAPend. For years with a sudden freeze of the soil, when partially frozen soil was not observed, the first date of partially frozen soil was set to the first date of soil freeze.

2.7 Proxy Indicators for Mapping the End of the Vegetation Active Period

We analysed the correspondence of the $VAPend_{th}$ dates with the satellite-derived first date of partially frozen soil, the first date of frozen soil, and the first date of autumnal freeze based on air temperature. The analysis was limited to the period 2010–2016 for which SMOS observations were available. The following observation years were used: FI-Sod and FI-Hyy 2010–2016, FI-Ken 2010–2015, CA-Obs and CA-Ojp 2010–2011 and CA-Qfo 2010. To assess the relationship between the freeze indicators and $VAPend_{th}$, the coefficient of determination (R^2), the root mean square error (RMSE) and the bias were calculated. We selected the satellite soil freeze indicator and the $VAPend_{th}$ date which showed the highest correspondence to define a proxy indicator for VAPend based on linear regression. The performance of the proxy indicator from satellite soil freeze was compared with the air temperature-based indicator.

To produce spatial maps of VAPend for the average period 2010–2016, we applied the respective linear regression equations to the gridded soil freeze and air freeze indicator data set covering the boreal vegetation zone in Canada, Finland and surrounding areas. Areas outside the boreal forest zone (see Fig. 1) were masked out.

3 Results

3.1 End of Vegetation Active Period at Measurement Sites

We utilized three dates for VAPend based on threshold values 15%, 10% and 5% of the maximum GPI (Fig. 2) to describe stages of the gradual change in photosynthetic downregulation in boreal evergreen needle-leaved forest (Sect. 2.4). Among all six sites, FI-Hyy in the southern boreal zone showed the latest VAPend dates and the highest interannual variability in the observed dates (Table 2). For the average period 2001–2016, $VAPend_{15}$ to $VAPend_5$ at FI-Hyy were observed on 7 November, 18 November and 7 December, respectively. The earliest dates of VAPend were found for the northernmost and coldest site FI-Ken. On average, $VAPend_{15}$ occurred on 17 October, 20 days earlier than in FI-Hyy. The time difference between FI-Hyy and FI-Ken increased to 40 days for the transition date $VAPend_5$ which was observed on 28 October in FI-Ken. The differences in multi-year mean VAPend dates between FI-Ken and the Canadian sites and FI-Sod were rather small (≤ 11 d). For the two neighbouring Canadian sites, CA-Obs and CA-Ojp, with different tree and soil types, the mean $VAPend_{10}$ transition date for the period 2001–2011 occurred on 28 October. Average $VAPend_5$ and $VAPend_{15}$ were observed within 3 days at the two sites.

3.2 Comparison of the End of the Vegetation Active Period with Autumnal Freeze and Satellite-Derived Soil Freeze

The VAPend dates were significantly correlated with the satellite-derived first date of partially frozen soil and the first date of frozen soil; R^2 ranged between 0.3 and 0.84 ($p < 0.05$, see Online Resource Table S2, Fig. S1). The highest correspondence was found between the first date of partially frozen soil and VAPend (Fig. 3a). The first date of partially frozen soil explained 84% of the variation in $VAPend_{10}$, and the transition date occurred on average, 15 days before the soil was partially frozen within the SMOS pixel. The first date of frozen soil to a depth of more than 10 cm over the whole SMOS pixel was detected much later than VAPend; it lagged behind $VAPend_5$ and $VAPend_{15}$ by 24 to 41 days, respectively.

There was a smaller delay between $VAPend_5$ and the first date of partially frozen soil (4 d) than for $VAPend_{10}$. The slope of their relationship was close to unity. However, there was higher scatter in the dates ($R^2 = 0.74$, Online Resource Fig S1a, Table S2) which could be partly due to higher uncertainties in $VAPend_5$. Due to the lower radiation levels during late autumn, there were less data available for calculating the daytime averages. If there were not enough data with PPFD $> 600\ \mu mol\ m^{-2}\ s^{-1}$, data at lower radiation

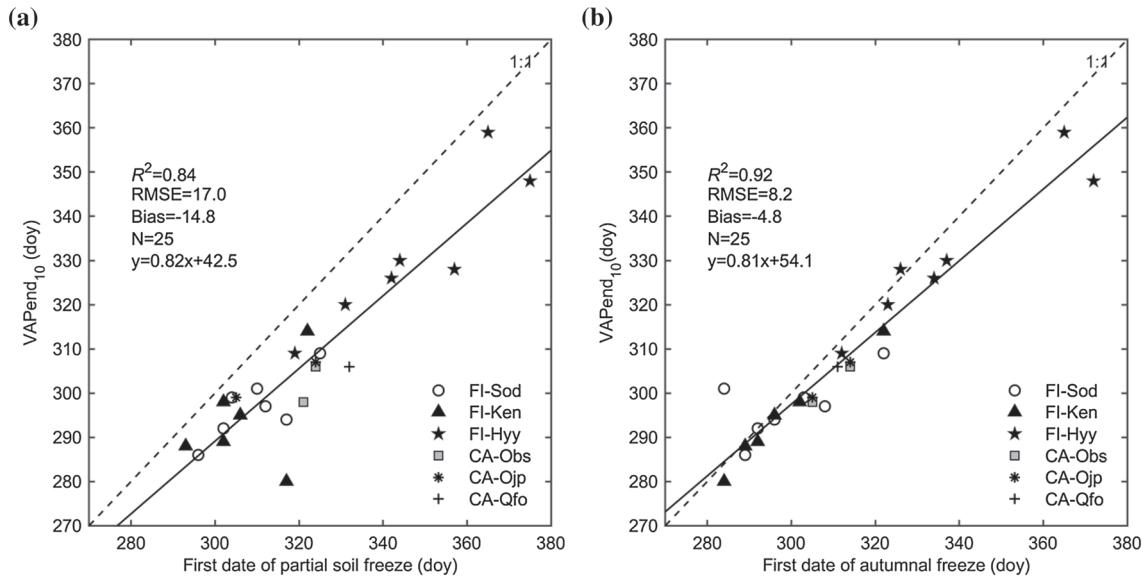**Fig. 3** Scatterplot of the end of vegetation active period, VAPend$_{10}$, versus the satellite-derived first date of partially frozen soil (**a**), and air temperature-derived autumnal freeze (**b**). The black lines show the linear regression line between VAPend$_{10}$ and the respective indicators.

Doy is day of year starting from 1 January. When the transition date occurred in the following year the doy is added to the last day of the previous year (31 December)

levels were used with a scaling factor. If there were still not enough daytime data, the GPI values were interpolated between nearest observations. For some years, the determination of VAPend$_5$ relied on interpolated values of the GPI (e.g. Fig. 2). Particularly large discrepancies between VAPend$_5$ and the date of partially frozen soil were observed in FI-Hyy in 2013 and 2016 when the VAPend$_5$ lagged behind the first date of partially frozen soil by 20 and 27 days, respectively. In both years, there was a large gap in the GPI time series (1 month in 2013 and 10 days in 2016) leading to high uncertainty in the estimated date. Therefore, we consider VAPend$_5$ a less reliable indicator than VAPend$_{10}$.

The progress of the GPI and satellite soil freeze is illustrated for 2 years with different temperature development in autumn at FI-Sod (Figs. 4 and 5). In 2013, temperature declined fast and GPI$_{15}$ to GPI$_5$ thresholds occurred within a few days, starting on 18 October and ending on 20 October (doy 291–293, Fig. 4). Due to the absence of snow, soil temperature changes followed closely the air temperature, and soil temperatures at the CO_2 flux site reached below-zero a few days days before GPI$_{15}$ was attained. Dry soils (Haplic Arenosols) in open and forested areas froze first. The latest soil freeze date was detected in forested areas with wetter soil type (Umbric Gleysol), and in wetlands with organic soil (Fig. 4). Soil freeze started within the SMOS pixel, i.e. partially frozen soil was detected, on doy 302. The mean soil frost date from soil temperature observation was observed 12 days before, on doy 290 (Online Resource Table S3). Soil freeze for the whole SMOS pixel was detected for the first

time on 3 November (doy 307). Except for one wetland site, in situ soil temperature measurements remained below the freezing point after 21 November (doy 325). This coincided well with the time of the continuous period of soil freeze detected from the SMOS pixel.

In contrast to 2013, autumn 2015 was characterized by alternating air temperature values (Fig. 5). A short frost period around doy 283 resulted in a reduction of photosynthetic carbon uptake that exceeded GPI$_{15}$ and GPI$_{10}$ for some days. Photosynthetic capacity recovered during the following warmer period until the subsequent frost period during which VAPend$_{15}$ was determined on 27 October (doy 300). This was again followed by above zero temperature and slightly increased photosynthetic capacity. Similarly, soil temperature measurements indicated soil freeze–thaw cycles and large variations of more than a month in the date when soil temperature dropped below the freezing point for the first time in areas with different vegetation cover and soil type (Online Resource Table S3). Again, soil freeze occurred first in dry mineral soils in open areas and latest in organic soils in wetland areas (Histosol). Thus, there were areas within the SMOS pixel for which the soil was frozen over the depth of 10–15 cm whereas other areas remained non-frozen for longer time. Satellite-observed soil freeze over the whole pixel was detected only after mid-December. Difference in soil wetness may also explain later (16 d) satellite soil freeze at CA-Ojp in 2010 compared to neighbouring site CA-Obs, while VAPend$_{10}$ took place only one day later than at CA-Obs.

Fig. 4 Time series of the gross photosynthesis index (GPI), air and soil temperature (5-cm depth), snow depth and satellite-derived soil freeze/thaw state at Sodankylä in 2013. Red vertical lines indicate the end of the vegetation active period based on the GPI thresholds at the CO_2 flux measurement site FI-Sod. The black vertical line indicates first date of autumnal freeze from ERA-Interim reanalysis air temperature data. *HA* haplic arenosol, *UG* umbric gleysol, *His* histosol
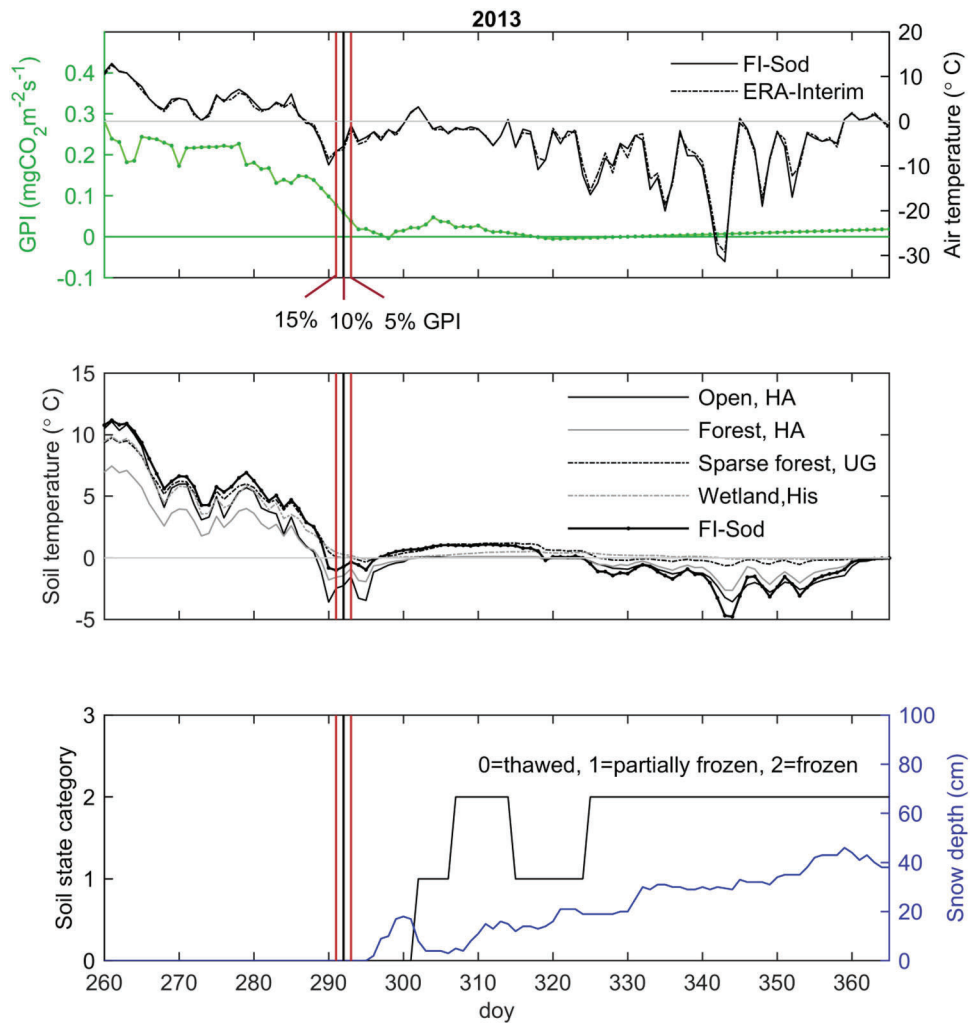
We compared the performance of the satellite-derived soil freeze state proxy for VAPend with the date of autumnal freeze from ERA-Interim reanalysis air temperature data. For all three VAPend dates, the agreement was better than that for the satellite soil freeze (Online Resource Table S2, Fig. S1 c, f, i). Again, the date of autumnal freeze showed the highest correspondence with VAPend$_{10}$ (Fig. 3b). VAPend$_{10}$, on average, occurred 5 days before the autumnal freeze.

The slope of the linear regression lines of the two interrelated freeze indicators with VAPend$_{10}$ was almost identical (~ 0.8). Autumn freeze reduced the carbon uptake. During warm winters, the time difference between VAPend and air and soil freeze increased. The mean time lag between VAPend$_{10}$ and first date of air freeze and satellite-observed partially frozen soil was 3 days longer for the warmest site FI-Hyy than for sites in northern Finland (2010–2016, Online Resource Table S4). For example, in 2011, the autumnal freeze was observed 24 days after VAPend$_{10}$ in FI-Hyy. During the warm winter, T_{10} did not drop below $-1\ °C$ until

7 January 2012. Instead, the photosynthetic capacity of the forest decreased below GPI$_{10}$ by mid-December. Low CO_2 uptake above GPI$_5$ was observed until the end of 2011, and VAPend$_5$ occurred 2 days after the first date of the autumnal freeze. This suggests that other factors, such as short photoperiod, also exert control on VAPend.

However, there was considerable year-to-year variation in VAPend$_{10}$ (see Table 2). For the Finnish sites, air temperature-derived autumn freeze and the satellite-derived first date of partially frozen soil explained well the deviations from the multi-year mean (2010–2016) with $R^2 = 0.82$ and 0.60 ($N = 20$, $p < 0.001$), respectively. Autumnal freeze from T_{10} took place considerably earlier than VAPend$_{10}$ once during the period 2010–2016. This was the case in 2015 at FI-Sod when it was observed early on 15 October (doy 288) during the first cold period with sub-zero temperature (Fig. 5).

ERA-Interim global atmospheric reanalysis air temperature data used to derive the air temperature proxy (Fig. 3b)

Fig. 5 Time series of the gross photosynthesis index (GPI), air and soil temperature (5-cm depth), snow depth and satellite-derived soil freeze/thaw at Sodankylä in 2015. Red vertical lines indicate the end of the vegetation active period based on the GPI thresholds at the CO_2 flux measurement site FI-Sod. The black vertical line indicates first date of autumnal freeze from ERA-Interim reanalysis air temperature data. *HA* haplic arenosol, *UG* umbric gleysol, *His* histosol
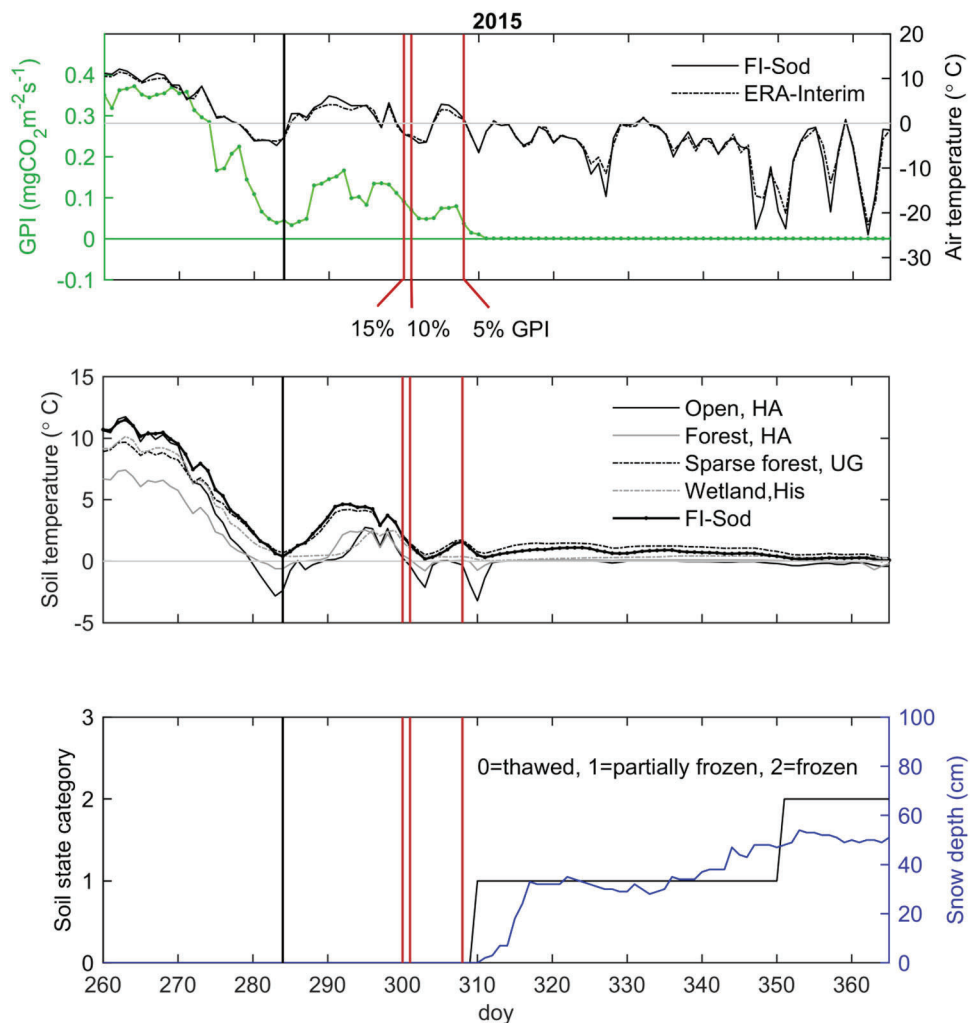
were also used as ancillary information to avoid false detections of soil freeze in summer from SMOS. During the retrieval of soil state, partially frozen soil and frozen soil are only assigned when a summer temperature flag has been released (Rautiainen et al. 2016). In consequence, it is possible that partially frozen or even frozen soil state detections are not independent of air temperature data, and soil freeze is detected only one day after the summer flag has been released. This phenomenon was observed in our study during 2010–2011 for FI-Ken and during 2015 for FI-Hyy. However, when removing these three points from the data the quality of the linear regression equation between satellite soil freeze with VAPend$_{10}$ remained the same ($N = 22$, $R^2 = 0.83$, $p < 0.001$).

3.3 Mapping of the End of Vegetation Active Period Using Proxy Indicators

The spatial distribution of VAPend$_{10}$ in the boreal forest zone in Finland and Canada was determined from the satellite-observed first date of partially frozen soil and the first date of autumnal freeze. For that, the linear regression equations in Fig. 3 were used to model VAPend$_{10}$. The RMSE of the linear regression model for the calibration was 7.5 days for the satellite-based and 5.2 days for the air temperature-based proxy (Online resource Fig. S2). For the average period 2010–2016, VAP ended before 10 October in the northwestern part of Canada and shifted to 20 November to 9 December in Southern Quebec and the island of Newfoundland (Fig. 6a). In northwest Finland, VAPend$_{10}$ occurred in mid-October and shifted to 10 December in the most southern parts (Fig. 6b). In general, the estimations based on the autumnal freeze produced a similar but smoother spatio-temporal gradient in the timing of VAPend$_{10}$ as satellite soil freeze. Despite the fact that the proxy indicator from autumnal freeze produced more accurate estimates for the CO_2 flux measurement sites, the satellite-derived soil freeze allows the mapping of VAPend with higher spatial detail at a global scale.
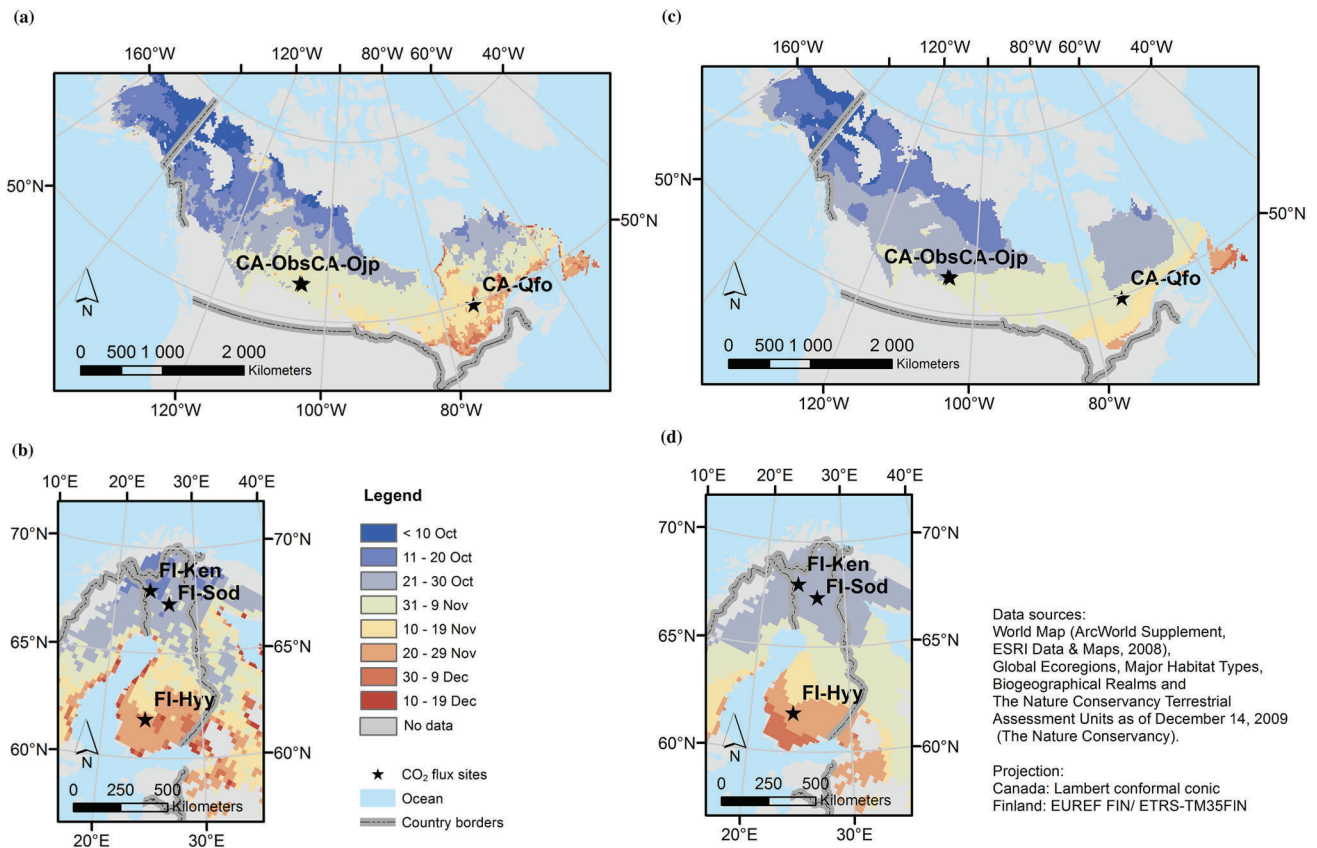
Fig. 6 Maps of the end of the vegetation active period, VAPend$_{10}$, in boreal evergreen needle-leaved forest for the average period 2010–2016 in Canada (**a**, **c**) and Finland (**b**, **d**). The maps were calculated from SMOS satellite observations of the first date of partially frozen soil (**a**, **b**) using the equation presented in Fig. 3a, and from the indicator for autumnal freeze (**c**, **d**; when 10-day moving average air temperature $\leq -1\ °C$) by applying the equation presented in Fig. 3b

4 Discussion

In our analysis of CO_2 flux measurement sites in the boreal zone, we found a strong connection between satellite-derived soil freeze and autumnal freeze from air temperature with VAPend. Our results are supported by Barr et al. (2009) who found a strong relationship of the first date of freeze with the end of photosynthetic activity at CA-Obs and CA-Ojp for an earlier period. In previous comparisons with satellite observations, only low correspondence of VAPend with estimates of landscape freeze from the SeaWinds scatterometer was observed for evergreen forests in northern America, including CA-Obs. This might be attributed to the low sensitivity of the K_u-band radar to freeze–thaw processes in autumn (Kimball et al. 2004). In contrast to the SMOS L-Band, the SeaWinds radar signal is not directly sensitive to the soil processes, thus observing landscape freeze from vegetation and the very skin of the soil surface or snow cover during winter (Kimball et al. 2004). In the study by Barichivich et al. (2013) also, only a weak link between the end of growing season with the timing of autumn freeze from satellite observations and the end of thermal growing season was found on the continental and global scale. The correlation between daily landscape freeze from Special Sensor Microwave Imager (SSM/I) and the end of growing season from the NDVI was not significant. The authors suggested, therefore, a decoupling between autumn phenology and thermal conditions for the northern high latitudes. This difference, relative to our study, may be due to the fact that the end of season indicator from NDVI describes changes related to leaf senescence of deciduous vegetation that precedes VAPend$_{10}$ in boreal evergreen forest ecosystems.

In almost all observations, the GPI$_{10}$ was reached days or weeks before T$_{10}$ dropped below $-1\ °C$ and before satellite soil freeze, suggesting that the relationship between autumnal soil freezing and decline of photosynthetic capacity is correlative rather than causal. The strong correlation found between autumn freeze and VAPend$_{10}$ is probably due to the fact that both processes, soil freezing and transition of plants towards a dormant state, are causally driven by a cumulative effect of declining temperature, similar to the effects of rising temperature in spring (Mäkelä et al. 2004; Pulliainen et al.

2017). Furthermore, the slope of the regression is < 1 (Fig. 3), such that delay time between $VAPend_{10}$ and the autumnal freeze is longer, the warmer the autumn. This suggests that other factors, such as photoperiod, also affect the change in photosynthetic capacity and that they become relatively more important during warmer autumns. The importance of the freeze-based proxy indicators could, therefore, be reduced in the future as autumn frost and soil freeze will likely occur later in a warming climate.

In our comparison of GPI threshold values, time of year (or photoperiod) rather than time of autumn freeze was more important when the threshold percentage used was higher, as shown by the slopes of the regression of $VAPend_{th}$ against the autumnal freezing date (Online resource Figure S1). However, for high percentage GPI thresholds, this could simply be linked with the strongly reduced light levels after the equinox, rather than marking a transition towards a dormant state. Consistent with this, Suni et al. (2003) found for the FI-Hyy site that day length was a better predictor than temperature for the date when net ecosystem exchange of CO_2 fell below 20% of the maximum summer uptake. In contrast, we found that $VAPend_5$ usually coincided with or followed the date of autumnal freezing and that the slope of the regression was close to 1, suggesting that autumnal freezing may describe an actual temperature-related limitation to photosynthesis. This is further supported by the finding that the latest $VAPend_{10}$ date in our investigation was observed after the winter solstice on 25 December 2015 at FI-Hyy, showing that the GPI can remain even above the 10% level during days with the shortest period of light at this site. However, more research is needed to ascertain the relative significance of the different environmental drivers in the autumnal downregulation of photosynthesis.

Air temperature-based indicators were suggested earlier by Thum et al. (2009) as a proxy for VAPend in boreal forest ecosystems, including FI-Hyy and FI-Sod. In contrast to the uniquely defined temperature threshold that was used here, Thum et al. (2009) adapted the temperature-based indicators for each site, which hindered the application to wider areas. In agreement with other studies (e.g. Hollinger et al. 1999; Kimball et al. 2004), we observed a reduction of the photosynthetic carbon uptake with the freezing temperatures. The drop of T_{10} below − 1 °C does not necessarily lead to a sustained decrease in GPI. Photosynthetic activity can recover to a certain level when temperatures and other factors, such as photoperiod, are favourable (Fig. 5). This is not accounted for with the simple air temperature-based threshold. The method could be adjusted in a way that it indicates a more persistent air temperature decrease as, for example, done for the GPI-based VAPend (Fig. 2) or a cumulative frost sum.

The $VAPend_{10}$ transition date always occurred before the detection of the first date of partially frozen soil from SMOS (Fig. 3a). Soil temperature observations at FI-Sod and from sites with a similar soil type in the surrounding areas (Figs. 4 and 5) indicated an earlier occurrence of frozen soil than that determined for the SMOS pixel, but the GPI_{10} was in most years exceeded before the occurrence of in situ soil freeze at FI-Sod (four out of six, e.g. Figs. 2 and 5), implying that soil freeze is not a necessary condition for $VAPend_{10}$. There is a spatial mismatch between the footprint of the CO_2 flux measurement site, extending only several hundred meters from the site, and the SMOS footprint of 40–50 km in diameter. Soil freezing is strongly affected by the soil type (see Online Resources Table S3), snow conditions and the openness of the vegetation layer. As shown for the FI-Sod site, soils with finer texture and higher water content froze at a slower pace than dry coarse-textured soils with lower heat capacity (e.g. Fig. 5) and the delay time depended on air temperature development. At FI-Sod, the forested area on dry mineral soil, representing best the CO_2 flux footprint, covered only a small fraction (7%) of the SMOS pixel. Moreover, other land cover classes, such as large water bodies (e.g. CA-Obs 14% and CA-Qfo 23% of the pixel, see Online resources Table S1) and wetland areas (FI-Sod 13% of the pixel), affect the soil state retrieval. Thus, scaling errors lead to inevitable discrepancies between satellite soil freeze and site measurements and possibly higher scatter in results compared to autumnal freeze (Fig. 3). L-band active radar measurements could provide soil freeze and thaw state at higher spatial resolution (Derksen et al. 2017), but the NASA Soil Moisture Active Passive (SMAP) radar failed in 2015. The currently operating Advanced Land Observing Satellite-2 Phased Array L-Band Synthetic Aperture Radar (ALOS-2 PALSAR) has a narrow swath and, thus, a too long revisit time (14 days) for the soil freeze and thaw monitoring. For site-specific more detailed studies, tower-based L-Band radiometer instruments, such as the ELBARRA-II (ETH L-Band Radiometer) (Schwank et al. 2010) installed at Sodankylä, could be utilized.

In comparison to satellite-derived soil freeze, the global ERA-Interim air temperature data set with a coarser resolution appears to represent the condition at the CO_2 flux measurement sites rather well (Figs. 4 and 5). The spatial variation of air temperature is smaller than for soil temperature, and, additionally, in situ air temperature observations that are ingested in the data assimilation system to produce the ERA-Interim global reanalysis data (Dee et al. 2011) probably stem from nearby synoptic weather stations, for example at Sodankylä. However, the accuracy of the reanalysis temperature is expected to be lower for areas with lack of near-surface observations and especially at high latitudes, because of difficulties in modelling surface temperatures over snow cover (Simmons et al. 2010).

We presented maps of the timing of VAPend in evergreen needle-leaved forest in the boreal region based on proxy indicators from air temperature and satellite-derived soil freeze

(Fig. 6). We selected VAPend$_{10}$ as a reference value for the model calibration, although VAPend$_5$ may be closest to the dormant state of vegetation from the three tested GPI threshold values. This was done since, the calculation of VAPend$_5$ from CO_2 fluxes has higher uncertainty than the determination of VAPend$_{10}$ because of lower light levels and resulting gaps in the GPI time series. The model parameterization for the calculation of VAPend$_{10}$ from the two freeze indicators is based on a limited number of observation sites and years. Future work is, therefore, needed to validate the results throughout the boreal forest region, especially for areas that are not well represented by the sites in this study, such as the northern boreal zone in North America and the southernmost part of the boreal zone in Europe (Fig. 6). However, publicly available eddy covariance data are scarce and sites are not well distributed in this region (Falge et al. 2017).

Furthermore, the possibilities for comparison with other independent data sets are limited. Recently, maps of the end of growing season for the northern hemisphere (1999–2013) based on a vegetation index (Phenological Index) were provided by Gonsamo and Chen (2016). For the evergreen needle-leaved boreal forest sites, the correspondence with gross primary production (GPP)-based autumn phenology indicators was only moderate ($r = 0.34$, RMSE 16 days) due to the time delay between greenness decrease and cessation of photosynthesis, and noise in the satellite observation during the transition period (Gonsamo et al. 2012). In our study, the multi-year mean VAPend dates (Table 2) occurred when solar elevation at solar noon was below 30° at all sites; hence, uncertainties in reflectance retrievals from optical satellite observations increase due to a longer atmospheric path length and shadowing effects of the canopy (Gutman 1991; Privette et al. 1995). A cutoff threshold of the solar zenith angle > 70 degrees is applied for satellite retrievals of SIF from GOME-2 (Joiner et al. 2014) and also for operational snow cover products (Metsämäki et al. 2015) that could otherwise provide complementary information.

5 Conclusion

We investigated whether a new satellite-derived soil freeze prototype product from SMOS can be used as a proxy indicator for the mapping of the end of the vegetation active period in boreal evergreen needle-leaved forest. Our results showed that the "partially frozen" soil state derived from satellite observations can be utilized to infer the date when the photosynthetic capacity of the forest decreases below 10% of the growing season maximum with good accuracy ($R^2 = 0.84$, RMSE = 7.5 days) at six CO_2 flux measurement sites in the boreal forest zone in Finland and Canada. Results for an air temperature-based indicator, defined as the day when 10-day average air temperature decreased below − 1 °C, were

consistent with satellite-derived soil freeze. Nevertheless, air freeze showed a stronger correlation with the end of vegetation active period than satellite-derived soil freeze ($R^2 = 0.92$, RMSE 5.2 days). Lower accuracy for the satellite-based proxy may be due to contributions to the SMOS signal from land cover and soil types, other than those dominant at the CO_2 flux measurement sites. Although further studies covering more sites and observation years are recommended, the results suggest that autumnal air temperature and satellite-based soil freeze can be utilized for the mapping of the start of the dormant season in boreal evergreen needle-leaved forest at continental to global scale. The maps complement existing satellite-based data on the end of the growing season in deciduous forests in the boreal region from vegetation indices and provide spatially explicit information that could help in monitoring the end of the vegetation active period and in the calibration and validation of biosphere models.

References

Al Bitar A, Mialon A, Kerr YH et al (2017) The global SMOS Level 3 daily soil moisture and brightness temperature maps. Earth Syst Sci Data 9:293–315. https://doi.org/10.5194/essd-9-293-2017

Arino O, Ramos Perez JJ, Kalogirou V, Bontemps S, Defourny P, Van Bogaert E (2012) Global land cover map for 2009 (GlobCover 2009). PANGAEA. https://doi.org/10.1594/pangaea.787668. Accessed 17 Mar 2018

Aubinet M, Vesala T, Papale D (eds) (2012) Eddy covariance—a practical guide to measurement and data analysis. Springer, Dordrecht. https://doi.org/10.1007/978-94-007-2351-1

Aurela M, Lohila A, Tuovinen J-P et al (2009) Carbon-dioxide exchange on a northern boreal fen. Boreal Environ Res 14:699–710

Aurela M, Lohila A, Tuovinen J-P, Hatakka J, Penttilä T, Laurila T (2015) Carbon dioxide and energy flux measurements in four northern-boreal ecosystems at Pallas. Boreal Environ Res 20:455–473

Baldocchi DD (2003) Assessing the eddy covariance technique for evaluating carbon dioxide exchange rates of ecosystems: past, present and future. Glob Chang Biol 9:479–492. https://doi.org/10.1046/j.1365-2486.2003.00629.x

Barichivich J, Briffa KR, Myneni RB et al (2013) Large-scale variations in the vegetation growing season and annual cycle of atmospheric CO2 at high northern latitudes from 1950 to 2011. Glob Chang Biol 19:3167–3183. https://doi.org/10.1111/gcb.12283

Barr AG, Black TA, Hogg EH, Kljun N, Morgenstern K, Nesic Z (2004) Inter-annual variability in the leaf area index of a boreal aspen-hazelnut forest in relation to net ecosystem production. Agric For Meteorol 126:237–255. https://doi.org/10.1016/j.agrformet.2004.06.011

Barr AG, Black TA, McCaughey H (2009) Climatic and phenological controls of the carbon and energy balances of three contrasting boreal forest ecosystems in western Canada. In: Noormets A (ed) Phenology of ecosystem processes, applications in global change research. Springer, Dordrecht. https://doi.org/10.1007/978-1-4419-0026-5_1

Bartsch A, Kidd RA, Wagner W, Bartalis Z (2007) Temporal and spatial variability of the beginning and end of daily spring freeze/thaw cycles derived from scatterometer data. Remote Sens Environ 106:360–374

Bauerle WL, Oren R, Way DA et al (2012) Photoperiodic regulation of the seasonal pattern of photosynthetic capacity and the implications for carbon cycling. Proc Natl Acad Sci 109:8612–8617. https://doi.org/10.1073/pnas.1119131109

Bergeron O, Margolis HA, Black TA, Coursolle C, Dunn AL, Barr AG, Wofsy SC (2007) Comparison of carbon dioxide fluxes over three boreal black spruce forests in Canada. Glob Chang Biol 13:89–107. https://doi.org/10.1111/j.1365-2486.2006.01281.x

Black TA (1999a) AmeriFlux CA-Obs Saskatchewan—Western Boreal, mature black spruce. Carbon dioxide fluxes and climate data 1999–2011, University of British Columbia, Canada. https://doi.org/10.17190/amf/1375198. Accessed 11 Mar 2018

Black TA (1999b) AmeriFlux CA-Ojp Saskatchewan—Western Boreal, mature jack pine. Carbon dioxide fluxes and climate data 1999–2011, University of British Columbia, Canada. https://doi.org/10.17190/amf/1375199. Accessed 11 Mar 2018

Black TA, Chen WJ, Barr AG et al (2000) Increased carbon sequestration by a boreal deciduous forest in years with a warm spring. Geophys Res Lett 27:1271–1274. https://doi.org/10.1029/1999GL011234

Böttcher K, Aurela M, Kervinen M et al (2014) MODIS time-series-derived indicators for the beginning of the growing season in boreal coniferous forest—a comparison with CO2 flux measurements and phenological observations in Finland. Remote Sens Environ 140:625–638. https://doi.org/10.1016/j.rse.2013.09.022

Brodzik MJ, Billingsley B, Haran T, Raup B, Savoie MH (2012) EASE-Grid 2.0: incremental but significant improvements for earth-gridded data sets. ISPRS Int J Geo Inf 1:32

Coursolle C, Margolis HA, Giasson MA et al (2012) Influence of stand age on the magnitude and seasonality of carbon fluxes in Canadian forests. Agric For Meteorol 165:136–148. https://doi.org/10.1016/j.agrformet.2012.06.011

Dee DP, Uppala SM, Simmons AJ et al (2011) The ERA-Interim reanalysis: configuration and performance of the data assimilation system. Q J R Meteorol Soc 137:553–597. https://doi.org/10.1002/qj.828

Derksen C, Xu X, Scott Dunbar R et al (2017) Retrieving landscape freeze/thaw state from soil moisture active passive (SMAP) radar and radiometer measurements. Remote Sens Environ 194:48–62. https://doi.org/10.1016/j.rse.2017.03.007

Drebs A, Nordlund A, Karlsson P, Helminen J, Rissanen P (2002) Climatological statistics of Finland 1971–2000. Climatic statistics of Finland 2002:1. Finnish Meteorological Institute, Helsinki

Falge E, Aubinet M, Bakwin PS et al (2017) FLUXNET research network site characteristics, investigators, and bibliography, 2016, ORNL DAAC, Oak Ridge, Tennessee, USA. https://doi.org/10.3334/ORNLDAAC/1530. Accessed 8 Dec 2018

Frankenberg C, O'Dell C, Guanter L, McDuffie J (2012) Remote sensing of near-infrared chlorophyll fluorescence from space in scattering atmospheres: implications for its retrieval and interferences with atmospheric CO2 retrievals. Atmos Meas Tech 5:2081–2094. https://doi.org/10.5194/amt-5-2081-2012

Frankenberg C, O'Dell C, Berry J et al (2014) Prospects for chlorophyll fluorescence remote sensing from the Orbiting Carbon Observatory-2. Remote Sens Environ 147:1–12. https://doi.org/10.1016/j.rse.2014.02.007

Fronzek S, Carter TR, Jylha K (2012) Representing two centuries of past and future climate for assessing risks to biodiversity in Europe. Global Ecol Biogeogr 21:19–35. https://doi.org/10.1111/j.1466-8238.2011.00695.x

Gamon JA, Huemmrich KF, Wong CYS et al (2016) A remotely sensed pigment index reveals photosynthetic phenology in evergreen conifers. Proc Natl Acad Sci USA 113:13087–13092. https://doi.org/10.1073/pnas.1606162113

Gonsamo A, Chen JM (2016) Circumpolar vegetation dynamics product for global change study. Remote Sens Environ 182:13–26. https://doi.org/10.1016/j.rse.2016.04.022

Gonsamo A, Chen JM, Price DT, Kurz WA, Wu C (2012) Land surface phenology from optical satellite measurement and CO2 eddy covariance technique. J Geophys Res 117:G03032. https://doi.org/10.1029/2012jg002070

Griffis TJ, Black TA, Morgenstern K et al (2003) Ecophysiological controls on the carbon balances of three southern boreal forests. Agric For Meteorol 117:53–71. https://doi.org/10.1016/S0168-1923(03)00023-6

Gu L, Post WM, Baldocchi D (2009) Characterizing the seasonal dynamics of plant community photosynthesis across a range of vegetation types. In: Noormets A (ed) Phenology of ecosystem processes, applications in global change research. Springer, Dordrecht, pp 35–58. https://doi.org/10.1007/978-1-4419-0026-5

Gutman GG (1991) Vegetation indices from AHVRR: an update and future prospects. Remote Sens Environ 35:121–136

Hollinger DY, Goltz SM, Davidson EA, Lee JT, Tu K, Valentine HT (1999) Seasonal patterns and environmental control of carbon dioxide and water vapour exchange in an ecotonal boreal forest. Glob Change Biol 5:891–902. https://doi.org/10.1046/j.1365-2486.1999.00281.x

Hölttä T, Lintunen A, Chan T, Mäkelä A, Nikinmaa E (2017) A steady-state stomatal model of balanced leaf gas exchange, hydraulics and maximal source–sink flux. Tree Physiol 37:851–868. https://doi.org/10.1093/treephys/tpx011

Ikonen J, Vehviläinen J, Rautiainen K, Smolander T, Lemmetyinen J, Bircher S, Pulliainen J (2016) The Sodankylä in situ soil moisture observation network: an example application of ESA CCI soil

moisture product evaluation. Geosci Instrum Method Data Syst 5:95–108. https://doi.org/10.5194/gi-5-95-2016

Jarvis P, Linder S (2000) Constraints to growth of boreal forests. Nature 405:904. https://doi.org/10.1038/35016154

Jeong SJ, Ho CH, Gim HJ, Brown ME (2011) Phenology shifts at start vs. end of growing season in temperate vegetation over the northern hemisphere for the period 1982–2008. Glob Chang Biol 17:2385–2399. https://doi.org/10.1111/j.1365-2486.2011.02397.x

Jin H, Eklundh L (2014) A physically based vegetation index for improved monitoring of plant phenology. Remote Sens Environ 152:512–525. https://doi.org/10.1016/j.rse.2014.07.010

Joiner J, Yoshida Y, Vasilkov AP et al (2014) The seasonal cycle of satellite chlorophyll fluorescence observations and its relationship to vegetation phenology and ecosystem atmosphere carbon exchange. Remote Sens Environ 152:375–391. https://doi.org/10.1016/j.rse.2014.06.022

Karlsen SR, Hogda KA, Wielgolaski FE, Tolvanen A, Tommervik H, Poikolainen J, Kubin E (2009) Growing-season trends in Fennoscandia 1982–2006, determined from satellite and phenology data. Clim Res 39:275–286. https://doi.org/10.3354/cr00828

Kim Y, Kimball JS, McDonald KC, Glassy J (2011) Developing a global data record of daily landscape freeze/thaw status using satellite passive microwave remote sensing. IEEE Trans Geosci Remote Sens 49:949–960. https://doi.org/10.1109/TGRS.2010.2070515

Kim Y, Kimball JS, Zhang K, McDonald KC (2012) Satellite detection of increasing northern hemisphere non-frozen seasons from 1979 to 2008: implications for regional vegetation growth. Remote Sens Environ 121:472–487. https://doi.org/10.1016/j.rse.2012.02.014

Kimball JS, McDonald KC, Running SW, Frolking SE (2004) Satellite radar remote sensing of seasonal growing seasons for boreal and subalpine evergreen forests. Remote Sens Environ 90:243–258. https://doi.org/10.1016/j.rse.2004.01.002

Kljun N, Black TA, Griffis TJ et al (2006) Response of net ecosystem productivity of three boreal borest stands to drought. Ecosystems 9:1128–1144. https://doi.org/10.1007/s10021-005-0082-x

Köhler P, Guanter L, Joiner J (2015) A linear method for the retrieval of sun-induced chlorophyll fluorescence from GOME-2 and SCIAMACHY data. Atmos Meas Tech 8:2589–2608. https://doi.org/10.5194/amt-8-2589-2015

Kolari P, Pumpanen J, Rannik Ü et al (2004) Carbon balance of different aged Scots pine forests in Southern Finland. Glob Change Biol 10:1106–1119. https://doi.org/10.1111/j.1529-8817.2003.00797.x

Kolari P, Chan T, Porcar-Castell A, Bäck J, Nikinmaa E, Juurola E (2014) Field and controlled environment measurements show strong seasonal acclimation in photosynthesis and respiration potential in boreal Scots pine. Front Plant Sci. https://doi.org/10.3389/fpls.2014.00717

Kozlowski T (2004) Soil freezing point as obtained on melting. Cold Reg Sci Technol 38:93–101. https://doi.org/10.1016/j.coldregions.2003.09.001

Kozlowski T (2016) A simple method of obtaining the soil freezing point depression, the unfrozen water content and the pore size distribution curves from the DSC peak maximum temperature. Cold Reg Sci Technol 122:18–25. https://doi.org/10.1016/j.coldregions.2015.10.009

Krishnan P, Black TA, Barr AG, Grant NJ, Gaumont-Guay D, Nesic Z (2008) Factors controlling the interannual variability in the carbon balance of a southern boreal black spruce forest. J Geophys Res Atmos. https://doi.org/10.1029/2007JD008965

Kulmala L, Launiainen S, Pumpanen J, Lankreijer H, Lindroth A, Hari P, Vesala T (2008) H_2O and CO_2 fluxes at the floor of a boreal pine forest. Tellus B Chem Phys Meteorol 60:167–178. https://doi.org/10.1111/j.1600-0889.2007.00327.x

Laapas M, Jylha K, Tuomenvirta H (2012) Climate change and future overwintering conditions of horticultural woody-plants in Finland. Boreal Environ Res 17:31–45

Mäkelä A, Hari P, Berninger F, Hänninen H, Nikinmaa E (2004) Acclimation of photosynthetic capacity in Scots pine to the annual cycle of temperature. Tree Physiol 24:369–376. https://doi.org/10.1093/treephys/24.4.369

Mäkelä A, Kolari P, Karimäki J, Nikinmaa E, Perämäki M, Hari P (2006) Modelling five years of weather-driven variation of GPP in a boreal forest. Agric For Meteorol 139:382–398. https://doi.org/10.1016/j.agrformet.2006.08.017

Mammarella I, Launiainen S, Gronholm T et al (2009) Relative humidity effect on the high frequency attenuation of water vapour flux measured by a closed path eddy covariance system. J Atmos Oceanic Tech 26:1856–1866

Margolis HA (2003) AmeriFlux CA-Qfo Quebec—Eastern Boreal, mature black spruce. Carbon dioxide fluxes and climate data 2003–2010, Université Laval, Canada. https://doi.org/10.17190/amf/1081. Accessed 11 Mar 2018

Mätzler C, Ellison W, Thomas B, Sihvola A, Schwank M (2006) Dielectric properties of natural media. In: Mätzler C (ed) Thermal microwave radiation: applications for remote sensing. The Institution of Engineering and Technology (IET), Stevenage, pp 427–506. https://doi.org/10.1049/PBEW052E_ch5

Menzel A, Fabian P (1999) Growing season extended in Europe. Nature 397:659

Metsämäki S, Pulliainen J, Salminen M et al (2015) Introduction to GlobSnow snow extent products with considerations for accuracy assessment. Remote Sens Environ 156:96–108. https://doi.org/10.1016/j.rse.2014.09.018

Öquist G, Huner NPA (2003) Photosynthesis of overwintering evergreen plants. Annu Rev Plant Biol. https://doi.org/10.1146/annurev.arplant.54.072402.115741

Piao S, Ciais P, Friedlingstein P et al (2008) Net carbon dioxide losses of northern ecosystems in response to autumn warming. Nature 451:49–52. https://doi.org/10.1038/nature06444

Piao S, Wang X, Ciais P, Zhu B, Wang TAO, Liu JIE (2011) Changes in satellite-derived vegetation growth trend in temperate and boreal Eurasia from 1982 to 2006. Glob Chang Biol 17:3228–3239. https://doi.org/10.1111/j.1365-2486.2011.02419.x

Privette JL, Fowler C, Wick GA, Baldwin D, Emery WJ (1995) Effects of orbital drift on advanced very high resolution radiometer products: normalized difference vegetation index and sea surface temperature. Remote Sens Environ 53:164–171

Pudas E, Leppälä M, Tolvanen A, Poikolainen J, Venäläinen A, Kubin E (2008) Trends in phenology of *Betula pubescens* across the boreal zone in Finland. Int J Biometeorol 52:251–259. https://doi.org/10.1007/s00484-007-0126-3

Pulliainen J, Aurela M, Laurila T et al (2017) Early snowmelt significantly enhances boreal springtime carbon uptake. Proc Natl Acad Sci USA 114:11081–11086. https://doi.org/10.1073/pnas.1707889114

Rautiainen K, Lemmetyinen J, Pulliainen J et al (2012) L-band radiometer observations of soil processes in boreal and subarctic environments. IEEE Trans Geosci Remote Sens 50:1483–1497. https://doi.org/10.1109/TGRS.2011.2167755

Rautiainen K, Parkkinen T, Lemmetyinen J et al (2016) SMOS prototype algorithm for detecting autumn soil freezing. Remote Sens Environ 180(SMOS special issue):346–360

Reich PB, Rich RL, Lu X, Wang Y-P, Oleksyn J (2014) Biogeographic variation in evergreen conifer needle longevity and impacts on boreal forest carbon cycle projections. Proc Natl Acad Sci 111:13703–13708. https://doi.org/10.1073/pnas.1216054110

Richardson AD, Black TA, Ciais P et al (2010) Influence of spring and autumn phenological transitions on forest ecosystem productivity.

Philos Trans R Soc Lond B Biol Sci 365:3227–3246. https://doi.org/10.1098/rstb.2010.0102

Richardson AD, Keenan TF, Migliavacca M, Ryu Y, Sonnentag O, Toomey M (2013) Climate change, phenology, and phenological control of vegetation feedbacks to the climate system. Agric For Meteorol 169:156–173. https://doi.org/10.1016/j.agrformet.2012.09.012

Roy A, Royer A, Derksen C, Brucker L, Langlois A, Mialon A, Kerr YH (2015) Evaluation of spaceborne L-band radiometer measurements for terrestrial freeze/thaw retrievals in Canada. IEEE J Sel Top Appl Earth Obs Remote Sens 8:4442–4459. https://doi.org/10.1109/JSTARS.2015.2476358

Schwank M, Wiesmann A, Werner C et al (2010) ELBARA II, an L-band radiometer system for soil moisture research. Sensors (Basel, Switz) 10:584–612. https://doi.org/10.3390/s100100584

Schwartz MD (1998) Green-wave phenology. Nature 394:839–840

Sevanto S, Suni T, Pumpanen J et al (2006) Wintertime photosynthesis and water uptake in a boreal forest. Tree Physiol 26:749–757. https://doi.org/10.1093/treephys/26.6.749

Simmons AJ, Willett KM, Jones PD, Thorne PW, Dee DP (2010) Low-frequency variations in surface atmospheric humidity, temperature, and precipitation: Inferences from reanalyses and monthly gridded observational data sets. J Geophys Res Atmos. https://doi.org/10.1029/2009jd012442

Smith NV, Saatchi SS, Randerson JT (2004) Trends in high northern latitude soil freeze and thaw cycles from 1988 to 2002. J Geophys Res Atmos. https://doi.org/10.1029/2003jd004472

Soldo Y, Cabot F, Khazaal A, Miernecki M, Słomińska E, Fieuzal R, Kerr YH (2015) Localization of RFI sources for the SMOS mission: a means for assessing SMOS pointing performances. IEEE J Sel Top Appl Earth Obs Remote Sens 8:617–627. https://doi.org/10.1109/JSTARS.2014.2336988

Suni T, Berninger F, Markkanen T, Keronen P, Rannik Ü, Vesala T (2003) Interannual variability and timing of growing-season CO_2 exchange in a boreal forest. J Geophys Res Atmos. https://doi.org/10.1029/2002JD002381

Thum T, Aalto T, Laurila T, Aurela M, Hatakka J, Lindroth A, Vesala T (2009) Spring initiation and autumn cessation of boreal coniferous forest CO_2 exchange assessed by meteorological and biological variables. Tellus B 61:701–717

Ulsig L, Nichol C, Huemmrich K et al (2017) Detecting inter-annual variations in the phenology of evergreen conifers using long-term MODIS vegetation index time series. Remote Sens 9:49

Vesala T, Suni T, Rannik Ü et al (2005) Effect of thinning on surface fluxes in a boreal forest. Global Biogeochem Cycles. https://doi.org/10.1029/2004gb002316

Vesala T, Launiainen S, Kolari P et al (2010) Autumn temperature and carbon balance of a boreal Scots pine forest in Southern Finland. Biogeosciences 7:163–176. https://doi.org/10.5194/bg-7-163-2010

Vogg G, Heim R, Hansen J, Schäfer C, Beck E (1998) Frost hardening and photosynthetic performance of Scots pine (Pinus sylvestris L.) needles. I. Seasonal changes in the photosynthetic apparatus and its function. Planta 204:193–200. https://doi.org/10.1007/s004250050246

Walther S, Voigt M, Thum T et al (2016) Satellite chlorophyll fluorescence measurements reveal large-scale decoupling of photosynthesis and greenness dynamics in boreal evergreen forests. Glob Chang Biol 22:2979–2996. https://doi.org/10.1111/gcb.13200

Wu C, Chen JM, Gonsamo A, Price DT, Black TA, Kurz WA (2012) Interannual variability of net carbon exchange is related to the lag between the end-dates of net carbon uptake and photosynthesis: evidence from long records at two contrasting forest stands. Agric For Meteorol 164:29–38. https://doi.org/10.1016/j.agrformet.2012.05.002

Xu L, Myneni RB, Chapin Iii FS et al. (2013) Temperature and vegetation seasonality diminishment over northern lands. Nature Clim Chang 3:581–586. https://doi.org/10.1038/nclimate1836

Evaluating Biosphere Model Estimates of the Start of the Vegetation Active Season in Boreal Forests by Satellite Observations

Kristin Böttcher [1,*]**, Tiina Markkanen** [2]**, Tea Thum** [2]**, Tuula Aalto** [2]**, Mika Aurela** [2]**, Christian H. Reick** [3]**, Pasi Kolari** [4]**, Ali N. Arslan** [2] **and Jouni Pulliainen** [2]

[1]   Data and Information Centre, Finnish Environment Institute, 00251 Helsinki, Finland
[2]   Finnish Meteorological Institute, 00560 Helsinki, Finland; tiina.markkanen@fmi.fi (T.M.);
       tea.thum@fmi.fi (T.T.); tuula.aalto@fmi.fi (T.A.); mika.aurela@fmi.fi (M.A.); ali.nadir.arslan@fmi.fi (A.N.A.);
       jouni.pulliainen@fmi.fi (J.P.)
[3]   Max Planck Institute for Meteorology, 20146 Hamburg, Germany; christian.reick@mpimet.mpg.de
[4]   Department of Physics, University of Helsinki, 00014 Helsinki, Finland; pasi.kolari@helsinki.fi
*   Correspondence: kristin.bottcher@environment.fi; Tel.: +358-295-251-092

Abstract: The objective of this study was to assess the performance of the simulated start of the photosynthetically active season by a large-scale biosphere model in boreal forests in Finland with remote sensing observations. The start of season for two forest types, evergreen needle- and deciduous broad-leaf, was obtained for the period 2003–2011 from regional JSBACH (Jena Scheme for Biosphere–Atmosphere Hamburg) runs, driven with climate variables from a regional climate model. The satellite-derived start of season was determined from daily Moderate Resolution Imaging Spectrometer (MODIS) time series of Fractional Snow Cover and the Normalized Difference Water Index by applying methods that were targeted to the two forest types. The accuracy of the satellite-derived start of season in deciduous forest was assessed with bud break observations of birch and a root mean square error of seven days was obtained. The evaluation of JSBACH modelled start of season dates with satellite observations revealed high spatial correspondence. The bias was less than five days for both forest types but showed regional differences that need further consideration. The agreement with satellite observations was slightly better for the evergreen than for the deciduous forest. Nonetheless, comparison with gross primary production (GPP) determined from CO_2 flux measurements at two eddy covariance sites in evergreen forest revealed that the JSBACH-simulated GPP was higher in early spring and led to too-early simulated start of season dates. Photosynthetic activity recovers differently in evergreen and deciduous forests. While for the deciduous forest calibration of phenology alone could improve the performance of JSBACH, for the evergreen forest, changes such as seasonality of temperature response, would need to be introduced to the photosynthetic capacity to improve the temporal development of gross primary production.

Keywords: start of season; boreal forest; MODIS; JSBACH; fractional snow cover; NDWI; evergreen needle-leaf forest; deciduous broad-leaf forest

1. Introduction

The boreal zone is characterized by strong seasonality of vegetation. Climate change is expected to influence this seasonal cycle and thus annual carbon balances of terrestrial vegetation are also subject to change [1]. In Finland, the growing season is predicted to lengthen in a warming climate with an earlier start in spring and a later cessation in autumn [2]. Rising temperature enhances both carbon uptake from the atmosphere by photosynthesis (Gross Primary Production, GPP) and

release of carbon to the atmosphere from biomass and soil carbon by autotrophic and heterotrophic respiration. Higher temperatures will enhance the forest carbon uptake in spring [3,4], while in autumn the ecosystem respiration may continue longer at a high level, reducing the annual net uptake of carbon by vegetation [5]. Winter temperatures have been projected to rise even more than the mean annual temperatures [6], which may disturb the dormancy development of trees [7]. The decrease in the number of frost days is most pronounced in the southern boreal zone, while, especially in the northerly regions, alternating freezing and melting periods may become more frequent [8], increasing the risk of frost damage [9]. Correspondingly, frequent severe springtime night frosts that constrain photosynthetic recovery may counteract the positive response of photosynthesis and phenological development to warmer spring temperatures and may have a long-term effect on the forest carbon balances [10]. Snow depth and snow-covered area will decrease in the warming climate [8,11].

In process-based modelling of the carbon cycle of vegetation, photosynthesis is constrained by the Leaf Area Index (LAI), whose development follows a modelled phenological cycle. Thus, any shortcomings in the modelled phenological cycle have marked impact on the predicted GPP [12–14]. Currently, the description of the seasonal development of LAI needs improvement in global earth system models [15] and more validation and calibration for the boreal zone, especially for deciduous broad-leaf forests (DBF) [14,16]. While local comparisons can be made with micrometeorological measurements of the CO_2 exchange at the ecosystems scale [14,16–18], a regional approach is needed to capture the spatial variability, and remote sensing is a useful tool for studying vegetation phenology over large areas [19]. Benchmarking biosphere models e.g., [20], with remotely sensed phenology would provide steps to a more accurate presentation of the annual carbon balance and its response to climate variability [15,21].

Remote sensing of the vegetation phenology in the boreal region is hindered by frequent prolonged overcast periods, low sun elevation in autumn and winter and a short vegetation period with rapid phenological changes [22]. Furthermore, a remote sensing method suitable for extracting the start of season of canopy photosynthesis capacity and GPP in one ecosystem does not necessarily work for all vegetation types [23]. In DBF, the leaf development in spring is a prerequisite for the start of photosynthetic activity and strong correlations are observed between early season phenology (leaf out date, start of LAI development) and the onset of daily net carbon uptake [16,24]. In contrast to DBF, photosynthesis in evergreen needle-leaf forests (ENF) increases gradually already before the production of new foliage and thus the seasonal recovery of photosynthesis has been difficult to observe in remote sensing observations [25,26].

Several remote sensing methods have been developed for detecting the start of the growing season in boreal areas [22,27–29]. These methods track the greening of the vegetation within the footprint of the satellite pixel and have been evaluated against in situ phenological observations of deciduous trees [27,28,30] or phenological indicators determined from micrometeorological CO_2 flux measurements [29]. Because in ENF the onset of photosynthesis occurs before the production of new foliage, remotely sensed start of season, tracking the development of new leaves and shoots at the land surface scale, showed a delay of several weeks when compared to the onset of photosynthesis [16,23,29,31]. Large shifts, of up to three months, between the greening phase from three global remotely sensed data sets of fraction of absorbed photosynthetically active radiation (fAPAR) were obtained for ENF in the boreal region [32]. Instead, a proxy indicator of start of season, determined from satellite time series of Fractional Snow Cover (FSC), was found suitable for this forest type in boreal areas [33].

In this study, we use simulations by the biosphere model JSBACH (Jena Scheme for Biosphere-Atmosphere Coupling in Hamburg) [34] to determine the start of season in DBF and ENF during the past decade in Finland. The start of season is here defined as the beginning of the photosynthetically active period of vegetation. JSBACH is the biosphere component of an Earth system model with a global scope and has, therefore, not been validated for regional applications. Evaluating such a model regionally is challenging, as there are hardly any suitable datasets available at this scale.

Even though these large-scale models have been targeted to global scale, it is important to assess their performance at a regional scale to gain understanding about their applicability and characteristics that require further development. The carbon and water cycle of vegetated areas are modelled in JSBACH by considering the physiological response of vegetation to the climatic variables. In this work, JSBACH is run with climatic variables from a regional climate model. Moreover, to assess the sensitivity of the model to the climate drivers, JSBACH is run also with observed meteorological data from micrometeorological measurement sites in Finland.

We use remote sensing observations for the evaluation of JSBACH-modelled start of season of boreal forests. Because of structural and functional differences in the photosynthetic recovery in DBF and ENF, specific methods will be employed to extract the start of season date from remote sensing data in the respective forest type. We apply the method developed by Delbart et al. [27] and the method based on snow cover [33] for DBF and ENF, respectively. Both methods have been used previously for the mapping of the start of season in boreal areas. For DBF, we also assess here the accuracy of the remote sensing observations against ground observations of bud break of birch trees in Finland. We assess the spatial and temporal correspondence of JSBACH results at the regional scale with these satellite observations. In addition, we evaluate the simulated start of season dates for ENF locally with micrometeorological CO_2 flux measurements.

2. Materials and Methods

2.1. Study Area

The study area covers Finland and ranges from 19° E to 32° E, and from 59° N to 71° N (Figure 1). According to Köppen's climate classification, the area belongs to the temperate coniferous-mixed forest zone with cold and wet winters. The average temperature of the warmest month exceeds 10 $^\circ$C and the average temperature of the coldest month is below -2 $^\circ$C [35]. Finland's vegetation can be divided into four phytogeographical zones: the hemiboreal, southern, middle and northern boreal zones [36] (Figure 1). The main land cover type is forest (with 44% coverage of evergreen, deciduous and mixed forest), followed by shrubs and herbaceous vegetation, inland waters and wetlands (Supplementary Materials, Table S1). ENF is the dominant forest type, except for areas north of 68° N where DBF is dominating (Figure 1b). The main tree species of forests are Scots pine (*Pinus sylvestris*) (67%), Norway spruce (*Picea abies*) (22%), and birch (10%), including silver birch (*Betula pendula*) and downy birch (*Betula pubescens*). More than half of the forests are pure stands (55%); stands with some mixing cover 31% of the forested area, and 13% of forest stands are mixed [37].
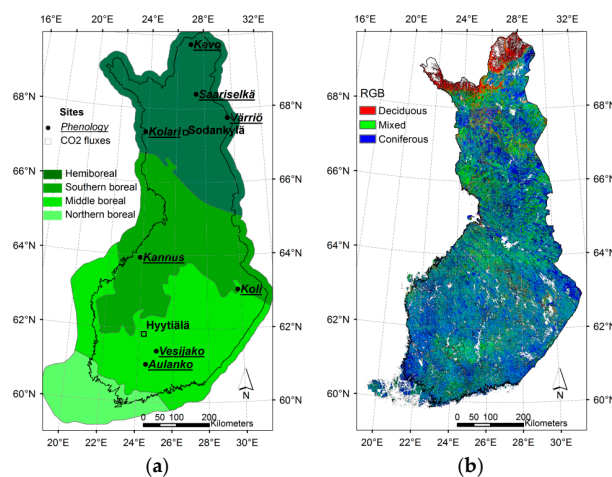

Figure 1. (**a**) CO_2 flux measurement sites, phenological sites and phytogeographical zones in Finland according to Ahti et al. (1968) (**b**) Red-Green-Blue (RGB) image of forest cover fractions determined from CORINE land cover 2000.

2.2. Carbon Dioxide Flux Measurements

The net ecosystem CO_2 exchange (NEE) between atmosphere and vegetation can be directly measured by the micrometeorological eddy covariance (EC) method [38]. The 30-min GPP value was here obtained by subtracting the modelled respiration (R) value from the NEE observation (GPP = NEE-R) utilizing standard flux partitioning procedures [39,40]. By the same parameterisation, the NEE and GPP time series were gap-filled for comparison with the model results. In this study, we used EC data from two boreal Scots pine forests, Sodankylä in northern Finland ($67°21'$N, $26°38'$E) [41] and Hyytiälä in southern Finland ($61°51'$N, $24°17'$E) [42] (Figure 1a), from years 2001–2010. Supporting meteorological data from both flux sites were used in the site level JSBACH model simulations (Section 2.4.4). The starting date of the vegetation active season (ENF_SOS$_{EC}$) was determined for the two sites from the continuous EC data. ENF_SOS$_{EC}$ was obtained as the day on which the CO_2 uptake permanently exceeds 15% of the growing season maximum uptake level. The method has been described in more detail in a previous study by Böttcher et al. [33].

2.3. Phenological Observations of Bud Break of Birch

We used phenological observations of the bud break of birch (*Betula pubescens* Ehrh.) from 8 sites for the evaluation of satellite observations of start of season in DBF (DBF_SOS$_{sat}$) in Finland. The sites are located in the southern (3), middle (1) and northern boreal zone (4) (Figure 1, Table 1). Bud break observations were obtained from the Finnish Forest Research Institute (now the Natural Resource Institute Finland) for the period from 2001 to 2008. The phenological observations at Aulanko and Saariselkä had already stopped in 2006. According to the observer's instructions [43], bud break is observed when at least 50% of buds have broken throughout the tree crown. Phenological observations were carried out twice a week at the respective sites. The monitored trees (five) are of local provenance and were preferably naturally regenerated. The microclimate of the site must be representative for the local climate conditions. Monitored trees may have been changed from year to year until 2007. Further details on observations are given in Kubin et al. [43].

Table 1. Phenological observation sites for the evaluation of DBF_SOS$_{sat}$ and characteristics of MODIS pixels at $0.05°$ by $0.05°$ resolution that were used in the comparison.

Site Name	Location		Phytogeographical Zone	Altitude m a.s.l.			Number of Pixels [1]
				Site	Median for Pixels [2]	SD [3]	
Aulanko	$61°01'$N	$24°27'$E	Southern boreal	145	99.8	20.5	10
Vesijako	$61°23'$N	$25°03'$E	Southern boreal	110	109.6	9.3	12
Koli	$63°06'$N	$29°49'$E	Southern boreal	135	139.1	56.1	17
Kannus	$63°54'$N	$23°57'$E	Middle boreal	40	43.7	2.8	12
Värriö	$67°45'$N	$29°37'$E	Northern boreal	350	382.9	39.4	62
Kolari	$67°21'$N	$23°50'$E	Northern boreal	150	151.5	4.9	26
Saariselkä	$68°24'$N	$27°23'$E	Northern boreal	300	303.4	27.4	38
Kevo	$69°45'$N	$27°01'$E	Northern boreal	100	130.5	52.6	41

[1] Pixels with the sum of deciduous and mixed forest fractions >50% at the original spatial resolution of $0.005°$ were used for the averaging of the Normalized Difference Water Index time series to the coarser grid; [2] Altitude was calculated from a digital elevation model provided by the National Land Survey of Finland with a grid size of 25 m by 25 m and a height precision of 2 m; [3] SD, standard deviation.

2.4. JSBACH Simulations

2.4.1. The JSBACH Model

The biosphere model JSBACH [34,44] is used for the modelling of GPP. It is part of the Max Planck Institute's (MPI) Earth System Model and implemented as a subroutine of its atmospheric component ECHAM [45]. JSBACH is used in global simulations, but it can also be applied at regional [46–48] and at site level scales [49], as is done in this work. JSBACH is a process-based model and calculates the exchanges of carbon, water and energy between the land surface and the atmosphere.

The phenology model (Logistic Growth Phenology; LoGro-P) of JSBACH provides leaf area index (LAI) at each time step to compute photosynthetic production. The model describes the phenological dynamics based on three subsequent phases; a growth (spring), a vegetative (summer) and a rest phase (autumn and winter). For evergreen and deciduous forest, the phenological cycle is dependent on air temperature. For the shift from dormancy to the growth phase in spring, the "alternating model" of Murray et al. [50] is employed in JSBACH. It consists of a heat sum approach (also often referred to as growing degree day approach) combined with a chilling condition. The counting of chilling days starts from the last autumn event (shift from vegetative phase to dormancy phase). The critical temperature, above which temperature contributes to heat sum and below which chilling days are counted, was set to 4 °C in both forest types. A detailed description of the JSBACH LoGro-P phenological model and the parameter values used in this work is given in Appendix A. The shift to the growth phase corresponds to the start of development of new shoots in ENF and to bud break in DBF. Because ENF have needles present throughout the year (and non-zero LAI in the model), photosynthesis can start before the shift to the growth phase and defines the start of season in ENF. The photosynthetic uptake increases with temperature and is enhanced by the increase of LAI after the beginning of the growth phase.

The photosynthesis model in JSBACH is based on the biochemical model developed by Farquhar et al. [51], as are many of the large-scale models. The temperature responses of photosynthesis model parameters describing the potential electron transport rate and maximum carboxylation rate stay the same throughout the year. The photosynthesis is coupled to the stomatal conductance, which is constrained at low soil water content [52]. As a part of the water and energy balances, the model simulates snow cover. Fractional Snow Cover is calculated according to Roesch et al. [53].

Different vegetation types are described as Plant Functional Types (PFTs). Each PFT has specific physiological and physical properties, such as photosynthesis parameters, aerodynamic roughness and canopy albedo. Four different PFTs were described for each grid cell in our simulations and based on the Coordinated Information on the European Environment (CORINE) Land Cover data. In this work, only the tiles containing ENF and DBF are considered. As ENF is the most abundant PFT in Finland, for the vast majority of grid cells there was representation of ENF, and thus an estimate was available for the whole Finnish territory except for the very northern areas. Nevertheless, the cover of grid cells with DBF representation was even more complete than that of ENF because it is everywhere among the four most abundant PFT's and the distribution of DBF extends further in northern Finland.

2.4.2. Preparation of Meteorological Driving Data for Regional Runs

In the set-up used, JSBACH requires seven mutually consistent meteorological variables (2-m air temperature and specific humidity, 10-m wind velocity, short-wave and long-wave radiation, potential short-wave radiation and precipitation) in hourly time resolution. In order to produce such a data set for a regional domain it is necessary to use a climate model of suitable scale. For the JSBACH regional driving data production we used the regional climate model REMO [54,55] with an implementation of surface properties by Gao et al. [56]. REMO resolves three-dimensional (3D) atmospheric variables such as air temperature, specific humidity and wind speed in a hybrid vertical coordinate system [57]. The model also produces surface layer values of the atmospheric variables (2-m air temperature and 10-m wind velocity) as well as surface and soil variables such as snow cover and soil moisture. In this study, REMO was run for a domain covering Fennoscandia, with a grid resolution of $0.167°$, corresponding approximately to 18 km. ERA-Interim, a global atmospheric re-analysis produced by the European Centre for Medium-Range Weather Forecasts (ECMWF) [58], was used as lateral boundary data for the 3D atmospheric variables. The forward run covered the period from 1979 to 2011. The forward run was preceded by a 10-year spin-up to equilibrate soil moisture and temperature.

Model-specific biases for distinct regions are inherent for regional climate models [59,60]. REMO exhibits colder temperatures than observed in winter and spring in Eastern Europe [61], and the area of cold bias covers most of Finland [56]. In summer and autumn the temperatures are too warm

compared to observations. REMO overestimates precipitation in northern Europe throughout the year [56]. In order to remove the biases, we corrected air temperature and precipitation against gridded homogenized weather data for 1980–2011 provided by the Finnish Meteorological Institute (FMI) [62]. A quantile–quantile type bias correction algorithm was applied for daily mean temperature [63], while daily cumulative precipitation was corrected using parametric quantile mapping [64]. Finally, the daily corrections were applied to the hourly modelled air temperature and precipitation values. To differentiate between the original REMO data and the bias-corrected REMO data, we will use the term regional climate model data when referring to the bias-corrected meteorological drivers in the following.

2.4.3. Regional JSBACH Runs

JSBACH was driven using hourly regional climate model data obtained from REMO for the years 1980–2011. A spin-up period of 30 years was applied before the forward run to equilibrate soil water and soil temperature. The spatial domain of JSBACH is the same as that of the driving model, REMO, covering Fennoscandia. For the present study only Finnish territory is investigated.

2.4.4. Site-Level JSBACH Runs

Additionally, JSBACH was run at site level for the two Scots pine EC flux sites, Sodankylä and Hyytiälä, using both regional climate model data and local site observations as meteorological input data. Regional climate model data, described in the previous section, was taken from the closest grid point to the site in the regional domain for the site-level simulations. The local meteorological data set, including the same variables, were gap-filled from the in situ meteorological measurements, except for the theoretically derived potential short-wave radiation. The site-level simulations for ENF were done with the PFT coniferous evergreen trees prescribed at both EC flux sites. The PFT for DBF was not considered in the site-level runs, because there are no continuous EC measurements in deciduous forest in Finland.

2.4.5. Model-Derived Indicators for the Start of Season

The start of season in ENF for the regional JSBACH run (ENF_SOS$_{mod}$) as well as for the local site-level runs (ENF_SOS$_{mod,loc}$) was calculated from the canopy GPP of the respective PFT fraction. The method of calculating the ENF_SOS$_{mod}$ was similar to that for ENF_SOS$_{EC}$ (see Section 2.2). The JSBACH modelled start of season of DBF (DBF_SOS$_{mod}$) was the first day of the year when the LAI exceeded the tiny threshold of 0.01 $m^2 \cdot m^{-2}$. This date typically coincides with the transition to the growth phase in LoGro-P.

Since we used a proxy indicator from satellite time series of FSC for ENF_SOS$_{sat}$, we also included JSBACH modelled daily FSC in our assessment and calculated the proxy indicator from it using the method described in Section 2.5.2. The JSBACH FSC of fully snow-covered ground is by definition smaller or equal to 0.95 [53] and depends on terrain variation within the grid cell, whereas the FSC from satellite observation equals one in the case of fully snow-covered ground. Thus, to apply the remote sensing method, we scaled the modelled FSC based on the maximum simulated value for each grid cell during the period from 2003 to 2010, which is considered to correspond to full snow cover.

In addition to ENF_SOS$_{mod}$ and DBF_SOS$_{mod}$ described above, the date of the start of the JSBACH "growth phase" (Section 2.4.1) of DBF and ENF was used in this study. We compared the JSBACH growth phase date of DBF simulated with a regional climate model and FMI gridded temperature for the analysis of remaining bias in the start of season due to the driving temperature. For this comparison, the grid cells at the edge of the area with FMI temperature observations were excluded.

2.5. Remote Sensing Data

We used daily Moderate Resolution Imaging Spectrometer (MODIS) time series for the detection of the start of season in ENF and DBF. The pre-processing of the MODIS time series and the extraction of start of season dates will be described in the following sections.

2.5.1. Pre-Processing of MODIS Time Series

Terra MODIS Level-1B data were obtained from the National Aeronautics and Space Administration (NASA)'s Level 1 and Atmosphere Archive and Distribution System (LAADS) and from the receiving station of the FMI in Sodankylä for the period from February to October in 2003 to 2010. The pre-processing consisted of calculation of Top-of-Atmosphere (TOA) reflectance and geometric projection of images into a latitude/longitude grid (datum WGS-84). MODIS observations with solar zenith angles greater than 73 degrees and sensor zenith angles greater than 50 degrees were excluded.

For the detection of DBF_SOS$_{sat}$, we calculated the Normalized Difference Water Index (NDWI) from MODIS TOA reflectance data at 0.005° spatial resolution (corresponding approximately to a pixel size of 280–190 m (at 60° N and 70° N) by 550 m) as:

$$\text{NDWI} = \frac{\text{R}_{\text{NIR}} - \text{R}_{\text{MIR}}}{\text{R}_{\text{NIR}} + \text{R}_{\text{MIR}}} \tag{1}$$

where R$_{\text{NIR}}$ and R$_{\text{MIR}}$ refer to near-infrared and mid-infrared reflectance in MODIS band 2 (841–876 nm) and MODIS band 6 (1628–1652 nm), respectively.

For the detection of ENF_SOS$_{sat}$, we calculated the FSC based on the SCAmod algorithm by Metsämäki et al. [65,66] at the same spatial resolution as the NDWI. Clouds in daily FSC and NDWI products were masked based on an automatic cloud masking algorithm developed at the Finnish Environment Institute.

2.5.2. Satellite-Observed Start of Season for JSBACH Model Evaluation

For the later comparison of satellite observations with modelled start of season, we spatially aggregated the daily time series of FSC and NDWI to a grid resolution of 0.25° by 0.25°. Because the heterogeneity of land cover is one main factor for discrepancies between satellite-observed phenology and ground observations [67,68], we focussed on satellite pixels with dominant cover of ENF and DBF according to CORINE Land Cover data of the year 2000 [69] (see also Figure 1b). In the aggregation, the FSC time series were averaged for MODIS pixels with a dominant fraction (⩾70%) of coniferous forest. NDWI time series were averaged for pixels with dominance of deciduous and mixed forest (sum of both vegetation types was ⩾70%).

A sigmoid function was fitted to the FSC time series and ENF_SOS$_{sat}$ was detected when the fraction of snow cover decreased from full snow cover, FSC = 1, to FSC = 0.99 as follows:

$$\text{ENF\_SOS}_{\text{sat}} = x_1 - \ln(99)\, x_2 \tag{2}$$

where x$_1$ is the inflection point (day when FSC reaches 0.5) and x$_2$ controls the rate of change of the sigmoid function. The full details of the method are given in Böttcher et al. [33]. The accuracy of ENF_SOS$_{sat}$ has been evaluated with ENF_SOS$_{EC}$ at three CO_2 flux measurement sites in Finland. The root mean square error (RMSE) was 5.3 days and the bias 1 day (late) [33]. The quality of the estimate was similar for the southern and the northern boreal sites, but it may be less reliable for the hemiboreal zone in winters with low snow depth [33].

For the detection of the DBF_SOS$_{sat}$, we followed the method by Delbart et al. [27], which is based on the NDWI. This index is useful for the detection of the start of season in boreal areas, because snow melt and greening-up of vegetation can be differentiated from the time series [70], whereas the observed spring increase in the widely applied Normalized Difference Vegetation Index (NDVI) can be

largely influenced by reflectance change in the visible range due to the melting of snow, and thus the increase in NDVI corresponds actually to the time of snow melt in boreal areas [71,72]. The method for determination of DBF_SOS$_{sat}$ from NDWI was first applied in central Siberia [27] and later to boreal Eurasia [73]. DBF_SOS$_{sat}$ is the date when the vegetation within the footprint of the satellite pixel is greening up, which corresponds to the time of NDWI increase after snow melt [27]. Comparison with in situ observations of leaf appearance of birch, larch and aspen in central Siberia with estimates from SPOT-VEGETATION NDWI time series showed an RMSE of 6.7 days and a negligible bias [70].

In this study, we smoothed averaged daily NDWI time series (spatial resolution 0.25°) with the adaptive Savitzky-Golay filter [74,75] that is implemented in the software TimeSat [76]. DBF_SOS$_{sat}$ was then determined from the smoothed time series as the last day when NDWI is lower than the minimum annual NDWI increased by 5% of the NDWI spring amplitude:

$$\text{DBF\_SOS}_{sat} = \arg \max_{t \in [32,200]} f(t) := \{t \mid \text{NDWI}(t) < \text{NDWI}_{min} + \varepsilon\} \tag{3}$$

where NDWI$_{min}$ is the minimum NDWI and ε equals 5%. The original threshold value ε of 20% that accounts for the noise level in the time series [27] was reduced to 5% because of the lower noise level in the averaged and smoothed NDWI time series here.

Satellite-observed start of season dates were not determined for areas with scarce coverage of the respective vegetation type within a MODIS pixel. Furthermore, long temporal gaps in satellite time series in spring increase the uncertainty in the detection of SOS from satellite observations. Therefore, we excluded grid cells with a temporal gap larger than two weeks around the estimated start of season date for the comparison with JSBACH model results.

2.6. Evaluation of DBF_SOS$_{sat}$ against Bud Break Observations

As described in the previous section, the method for the detection of DBF_SOS$_{sat}$ was validated earlier in Siberia [70] for boreal forests with a different species composition than in Finland. As described in Section 2.5.2, we made small changes to the original method. Therefore, we used bud break observations of birch from phenological sites (Section 2.3) for evaluation of DBF_SOS$_{sat}$ in Finland. The DBF_SOS$_{sat}$ at the coarse grid for the evaluation of JSBACH model results is not appropriate for comparison with ground observation. Thus, the original MODIS NDWI time series with a pixel size of 0.005° by 0.005° were aggregated to 0.05° by 0.05° taking into account pixels with a dominance of deciduous and mixed forest (>50% coverage, according to National CORINE Land Cover) and excluding pixels that were partially (≥10%) covered by water bodies. DBF_SOS$_{sat}$ was extracted from the nearest grid cell (at 0.05° resolution) to the phenological observation sites. The number of MODIS pixels that were used in the averaging of the NDWI time series is given in Table 1. The difference between the median of elevation within the grid cell and the elevation of the phenological site was less than 50 m (Table 1). For only two sites, Kevo and Koli, the variation in elevation within the pixel was larger than 50 m.

We analysed the correspondence between satellite and ground observations for all site-years, for each site and for the southern, middle and northern boreal zone, separately. Furthermore, we investigated the correspondence of the year-to-year anomalies between DBF_SOS$_{sat}$ and the bud break observations. The statistical metrics used in the comparison were the coefficient of determination (R^2), the root mean square error (RMSE) and the bias. The equations are given in Appendix B (Table B1). We excluded year 2002, because of missing data in the MODIS archive during the spring period. In addition, due to long periods of cloud cover, the DBF_SOS$_{sat}$ observations were not available for the following site-years: Aulanko 2001, Kolari 2005, Saariselkä 2001 and Kevo 2007 and 2008.

2.7. Evaluation of JSBACH-Modelled Start of Season

For the comparison of model- and satellite-derived start of season dates, JSBACH results were projected to the same grid as the satellite SOS (0.25°, see Section 2.5.2). We investigated correspondence

between the dates for the whole of Finland and for the boreal sub-regions: the southern, middle and northern boreal zone (Figure 1a), and calculated Pearson correlations, RMSE and bias for the period from 2003 to 2010 separately for the two forest types (ENF, DBF). In order to assess correspondence regarding spatial patterns, we used the multi-year mean dates for the whole period for each grid cell. In addition, agreement in temporal patterns was investigated based on the year-to-year anomalies.

For site-level comparisons at Sodankylä and Hyytiälä, the ENF_SOS_{mod} was extracted from the closest JSBACH grid cell. We calculated Pearson correlations, the RMSE and bias between ENF_SOS_{EC} and $ENF\_SOS_{mod,loc}$, and between ENF_SOS_{EC} and ENF_SOS_{mod}. We also assessed the agreement between the respective year-to-year anomalies for the period 2001 to 2010.

3. Results

3.1. Evaluation of DBF_SOS_sat with Phenological Observations of Bud Break

Comparisons of DBF_SOS_{sat} with bud break observations including all site-years resulted in an RMSE of one week and an early bias of 0.13 days ($R^2 = 0.75$, probability $p < 0.001$, Number of observations $N = 48$) (Figure 2a). The site-wise correlation between DBF_SOS_{sat} and in situ observations were not significant (Table 2), but the number of observations (4–7 per site) was also very small. RMSE and bias ranged between 4 to 10 days and 0 to 5 days, respectively. The smallest RMSE and bias were obtained for northern sites, Saariselkä and Kevo, in Lapland. The largest RMSE (10 days) and bias (5 days early) were both found for Kannus in western Finland. Large deviations (>two weeks) between satellite and in situ observations were observed for Vesijako in 2005 (15 days) and Kannus in 2007 (19 days).

For the southern boreal zone, including sites Aulanko, Vesijako and Koli, the correlation of DBF_SOS_{sat} with bud break observations was weak ($R^2 = 0.32$, $p = 0.012$, $N = 19$). The RMSE was 6.4 days and the bias 1.8 days (early). For the four sites in northern Finland: Värriö, Saariselkä, Kolari and Kevo, the correlation was higher than for the sites in the southern boreal zone ($R^2 = 0.62$, $p < 0.001$, $N = 22$), but the RMSE (6.9 days) and the bias (2.8 days late) were larger. The correlation between interannual anomalies of DBF_SOS_{sat} and bud break was significant (Figure 2b), but could explain only less than 30% of the interannual variation in the field observations.
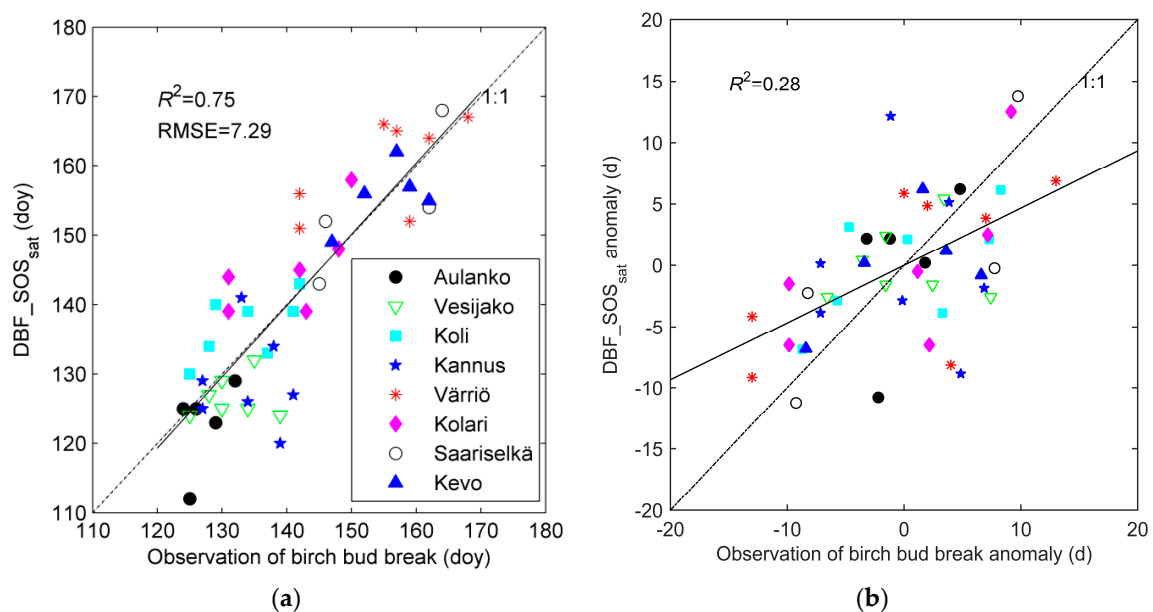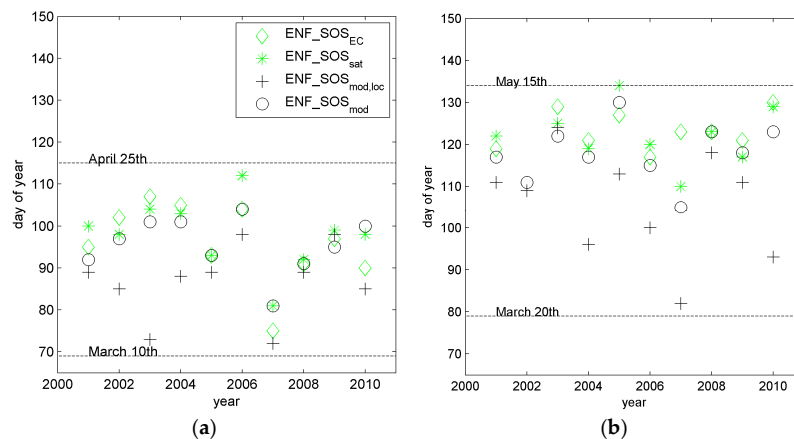

Figure 2. Relationship of the start of season in deciduous broad-leaf forests (DBF_SOS_{sat}) with phenological observations of birch bud break for the period from 2001 to 2008: (**a**) for all site-years and (**b**) for the year-to-year anomalies.

Table 2. Comparison between DBF_SOS$_{sat}$ and phenological observations of bud break of birch for sites in Finland. A positive bias means that the detected SOS is late compared to observations.

Site Name	Number of Observations	Mean Bud Break (Doy)	Mean DBF_SOS$_{sat}$ (Doy)	R^2	p	RMSE (d)	Bias (d)
Aulanko	5	127.2	122.8	0.28	0.362	6.6	−4.4
Vesijako	7	131.6	126.6	0.01	0.807	7.0	−5.0
Koli	7	133.7	136.8	0.40	0.127	5.7	3.1
Kannus	7	134.1	128.9	0.01	0.832	10.1	−5.3
Värriö	7	155.0	160.1	0.43	0.111	8.6	5.1
Kolari	6	140.8	145.5	0.46	0.137	7.3	4.7
Saariselkä	4	154.3	154.3	0.66	0.191	5.5	0.0
Kevo	5	155.4	155.8	0.35	0.294	4.4	−0.4
Site-means	8	141.5	141.4	0.94	0.001	4.4	0.2

3.2. Site-Level Start of Season in Evergreen Needle-Leaf Forest

We compared ENF_SOS$_{EC}$ in Sodankylä and Hyytiälä with JSBACH-simulated dates based on the two different sets of meteorological drivers: ENF_SOS$_{mod,loc}$ and ENF_SOS$_{mod}$ (Figure 3). ENF_SOS$_{EC}$ ranged from mid-March to mid-April (33 days) at Hyytiälä, and from the end of April to the beginning of May (14 days) at Sodankylä. The ENF_SOS$_{mod,loc}$ was too early in comparison with observations (Table 3). The bias was twice as large for Sodankylä as compared to Hyytiälä and correlations between ENF_SOS$_{mod,loc}$ and ENF_SOS$_{EC}$ were not significant.

Figure 3. Comparison of the start of season in evergreen needle-leaf forest determined from eddy covariance measurements (ENF_SOS$_{EC}$) and satellite observations (ENF_SOS$_{sat}$), together with JSBACH model-derived dates for 2001 to 2010 in (**a**) Hyytiälä, southern Finland and (**b**) Sodankylä, northern Finland. The start of season from JSBACH was determined from model runs using both REMO-generated bias-corrected meteorological data (ENF_SOS$_{mod}$) and local site observations (ENF_SOS$_{mod,loc}$).

Table 3. Start of season in evergreen needle-leaf forest for the period 2001–2010 at Hyytiälä and Sodankylä as defined from CO_2 flux measurements (ENF_SOS$_{EC}$) and based on JSBACH model simulations with local (ENF_SOS$_{mod,loc}$) and regional driving data (ENF_SOS$_{mod}$). A negative bias means that the simulated date is early compared to observations.

Site	Number of Years	ENF_SOS$_{EC}$	ENF_SOS$_{mod,loc}$				ENF_SOS$_{mod}$			
		Mean (Doy)	Mean (Doy)	R^2	p	Bias (d)	Mean (Doy)	R^2	p	Bias (d)
Hyytiälä	10	95.9	86.6	0.11	0.336	−9.3	95.5	0.75	0.001	−0.4
Sodankylä	9 [1]	123.3	105.3	0.02	0.696	−18.0	118.9	0.27	0.153	−4.4

[1] ENF_SOS$_{EC}$ was not available for 2002 at Sodankylä, therefore only 9 years were used in the analysis.

The bias between ENF_SOS$_{EC}$ and the start of season from the regional run, ENF_SOS$_{mod}$, was much smaller than the bias between ENF_SOS$_{EC}$ and ENF_SOS$_{mod,loc}$. Again, the early bias was larger for Sodankylä than for Hyytiälä. Correlations between ENF_SOS$_{mod}$-modelled dates with ENF_SOS$_{EC}$ were significant only for Hyytiälä (Table 3), whereas the year-to-year anomalies correlated significantly for both sites (R^2 = 0.51, *p* = 0.001, *N* = 19).

An investigation of the reasons for differences in ENF_SOS$_{mod}$ and ENF_SOS$_{mod,loc}$ in Sodankylä showed that GPP simulated with JSBACH followed closely the development of air temperature during the springs, 2004 and 2008 (Figures 4 and 5). However, the simulated GPP showed a higher increase during warm spells in spring than the GPP from CO$_2$ flux measurements. This was even more pronounced for the JSBACH GPP simulations with the local driving data than for simulations with regional climate data (Figure 4a,b). The local temperature observations indicated warm spells in 2004 around the day of year (doy) 96, 108 and 119. Therefore, the simulated GPP exceeded the threshold for the start of season earlier than the observed GPP. Consequently, the JSBACH-simulated ENF_SOS$_{mod,loc}$ and ENF_SOS$_{mod}$ occurred earlier than ENF_SOS$_{EC}$, on doy 96 and 117, respectively. Instead, ENF_SOS$_{EC}$ was delayed by cold spells that occurred around doy 110 and 115, and it was only observed on doy 121. Modelled snow depth from JSBACH simulations with both local and regional meteorological drivers was lower than the observed snow depth and the snow melted earlier in the model (Figures 4 and 5c).

The difference between JSBACH ENF_SOS$_{mod}$ and ENF_SOS$_{mod,loc}$ was smaller in 2008 than in 2004 (only 5 days) (Figures 3 and 5). ENF_SOS$_{mod}$ occurred on the same day as ENF_SOS$_{EC}$ observations (doy 123). Again, the local mean daily air temperatures were higher around the time of the start of season than the regional climate model temperatures, thus resulting in a higher GPP increase in JSBACH simulations with local drivers. Similarly to 2004, the snow melted earlier in JSBACH model simulations than indicated by snow depth measurements at Sodankylä (Figure 5c). The simulated GPP seemed to follow more closely the observed GPP at the site after the observed start of season date than during the time of spring recovery of photosynthesis.
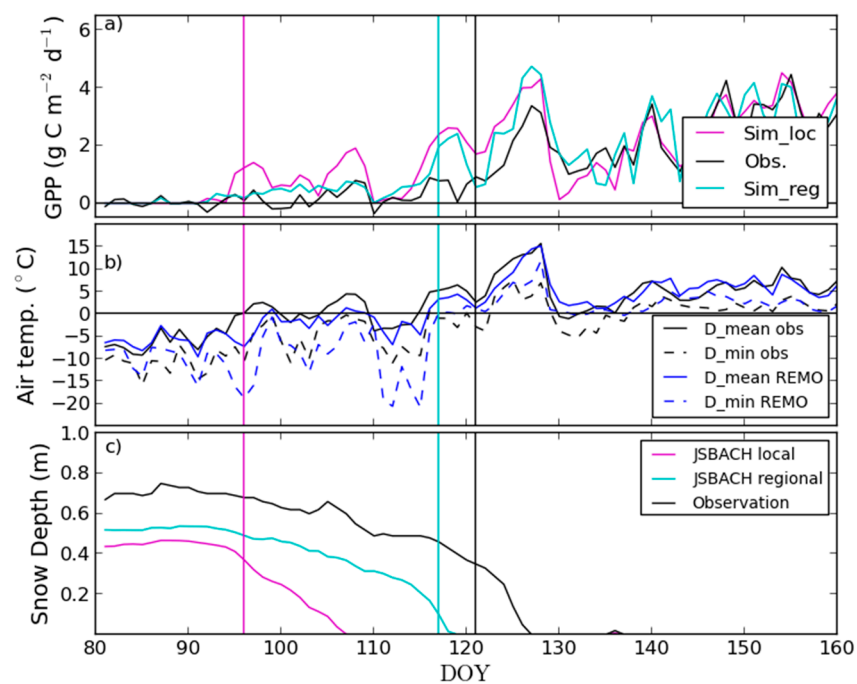
Figure 4. (**a–c**) Daily GPP (Gross Primary Production), mean and minimum air temperature and snow depth for Sodankylä in spring 2004. Vertical lines indicate the start of season (ENF_SOS): JSBACH local (magenta) refers to ENF_SOS$_{mod,loc}$; JSBACH regional (cyan) is ENF_SOS$_{mod}$, and observation refers to ENF_SOS$_{EC}$ (black).
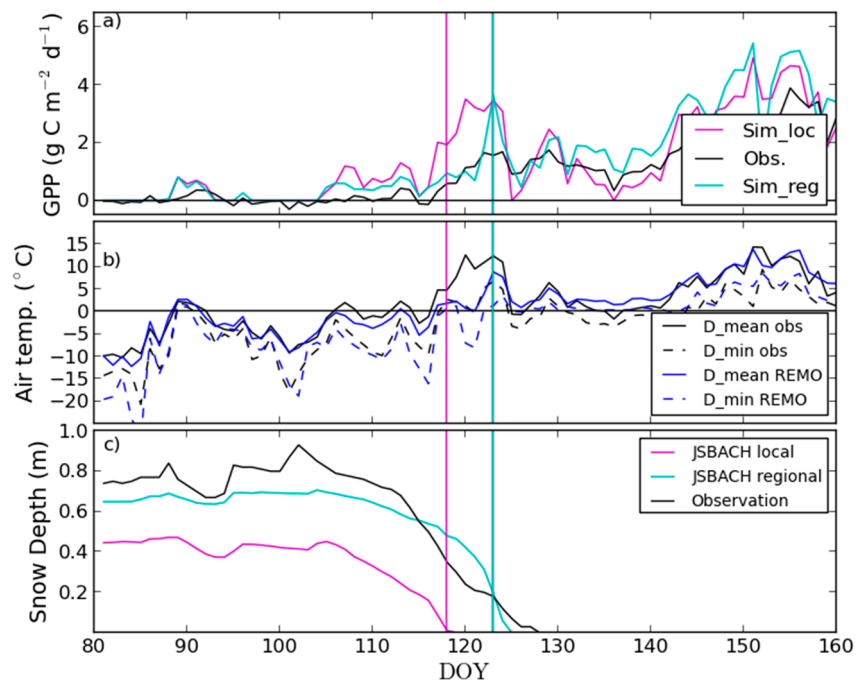
Figure 5. (**a**–**c**) Daily GPP, mean and minimum air temperature and snow depth for Sodankylä in spring 2008. Vertical lines indicate the start of season date: JSBACH local (magenta) refers to ENF_SOS$_{mod,loc}$; JSBACH regional (cyan) is ENF_SOS$_{mod}$. Note that ENF_SOS$_{EC}$ occurred on the same day as ENF_SOS$_{mod}$ shown with cyan line.

3.3. Regional Assessment of JSBACH-Modelled Start of Season against Satellite Observations

The earliest dates of ENF_SOS$_{sat}$ occurred in the south-western coastal areas and the latest dates were found in the north-east, ranging from the end of March to the beginning of May (Figure 6). DBF_SOS$_{sat}$ occurred about one month later than ENF_SOS$_{sat}$ and ranged from the beginning of May to mid-June. For the regional assessment of JSBACH SOS, we first investigated the spatial agreement between the multi-year averages of ENF_SOS$_{mod}$ and DBF_SOS$_{mod}$ for the period 2003–2010 with satellite observations. The modelled mean dates were highly correlated with the respective remote sensing observations (Figure 7, Supplementary Materials: Table S2) showing, however, an early bias for ENF_SOS$_{mod}$ and a late bias for DBF_SOS$_{mod}$. The RMSEs were five and six days for ENF_SOS$_{mod}$ and DBF_SOS$_{mod}$, respectively. For DBF_SOS$_{mod}$, this is a bit larger than the accuracy of the remote sensing estimates when considering the site-means (Table 2).

For the boreal sub-regions, the highest spatial correlations between the mean start of season dates for the period 2003–2010 was observed in the middle boreal zone (R^2 values $\geqslant$ 0.79) for both, ENF_SOS$_{mod}$ and DBF_SOS$_{mod}$, while R^2 was low in the northern boreal zone (<0.5). The bias varied regionally; it increased for ENF_SOS$_{mod}$ and decreased for DBF_SOS$_{mod}$ from the southern to the northern boreal zone (Supplementary Materials: Table S2). For ENF, it was largest ($\geqslant$10 days) in the south-western coastal areas (hemiboreal zone, late bias of ENF_SOS$_{mod}$) and south-western Lapland (early bias of ENF_SOS$_{mod}$) (Figure 8a). It has to be noted that the satellite estimate based on FSC may be less reliable for the hemiboreal zone in winters with low snow depth [33].

Only a few grid cells in the hemiboreal zone and the most northern grid cells showed a larger bias than 10 days for DBF_SOS$_{mod}$ (Figure 8b) and the bias was smallest for the transient region between the middle boreal and northern boreal zone.

Throughout Finland, the multi-year average ENF_SOS$_{mod}$ took place 20–40 days earlier than the simulated date of the JSBACH start of "growth phase" of ENF. The time lag between these two

phenological events decreased from south-west to north-east and increased again for northern areas of Lapland.

In the second step, we looked into year-wise comparisons of the start of season dates (Figure 9, Supplementary Materials: Table S3). The correspondence between the annual dates from JSBACH and from satellite observations showed large variations in R^2, RMSE and bias. As shown in Figure 9a,c, for many adjacent grid cells ENF_SOS_{mod} occurred on the same day (clumping), whereas we found a more gradual change from south to north in ENF_SOS_{sat}. In order to assess the reasons for clumping, we analysed the change in 5-day mean temperature, which is a good predictor of spring recovery in ENF, according to Suni et al. [18], and the 5-day mean temperature often exceeded zero degrees concurrent with ENF_SOS_{mod}. Thus, a change in weather pattern may simultaneously trigger the start of season in a large area. Clumping was not observed for DBF_SOS_{mod} (Figure 9; lower panel).
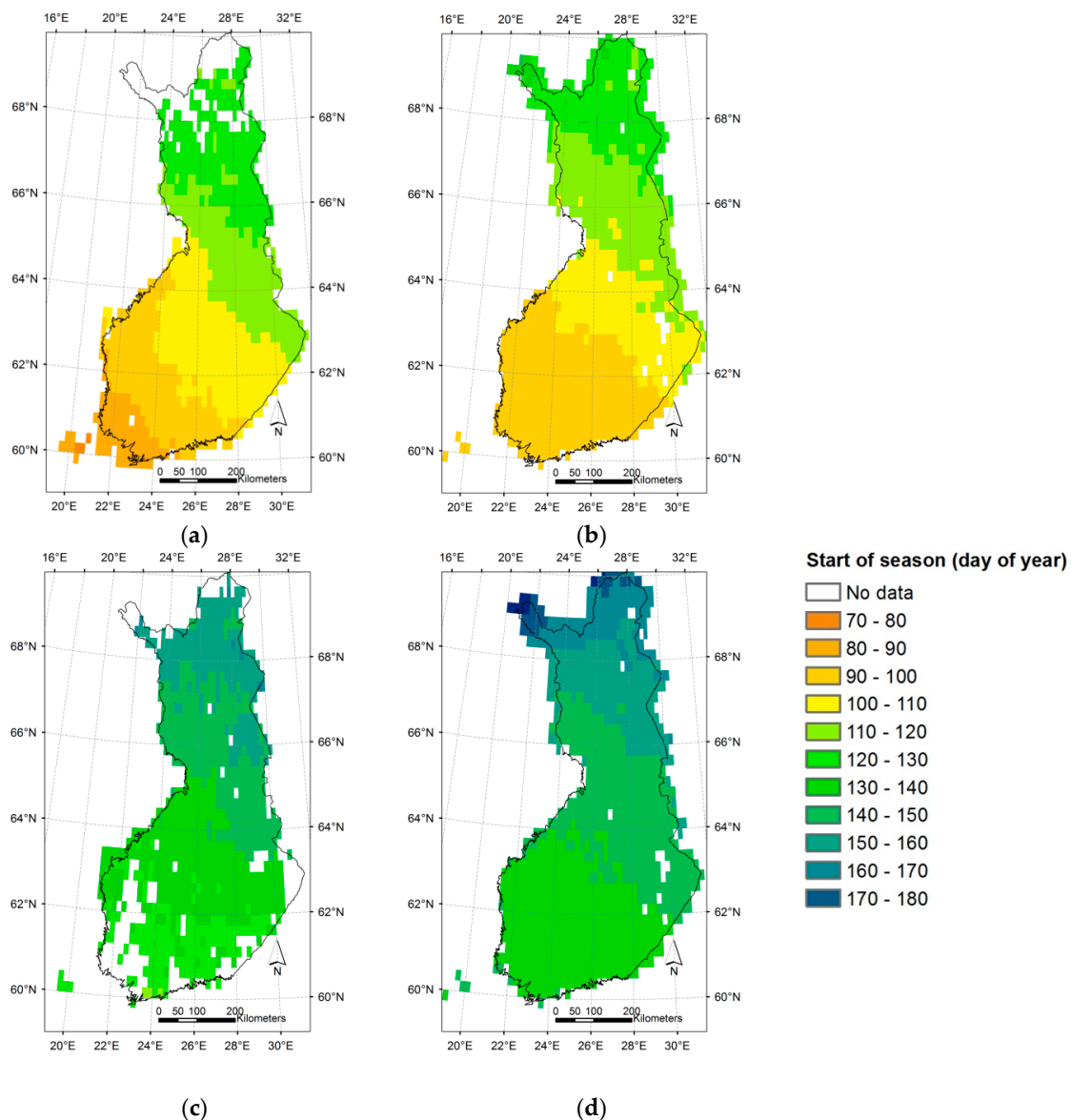
Figure 6. Spatial distribution of mean start of season dates in Finland for the period 2003–2010. The upper panel shows estimates for evergreen needle-leaf forest: (**a**) determined from satellite observation, and (**b**) determined from JSBACH simulations. The lower panel shows estimates for deciduous broad-leaf forest: (**c**) determined from satellite observations and (**d**) from JSBACH simulations.
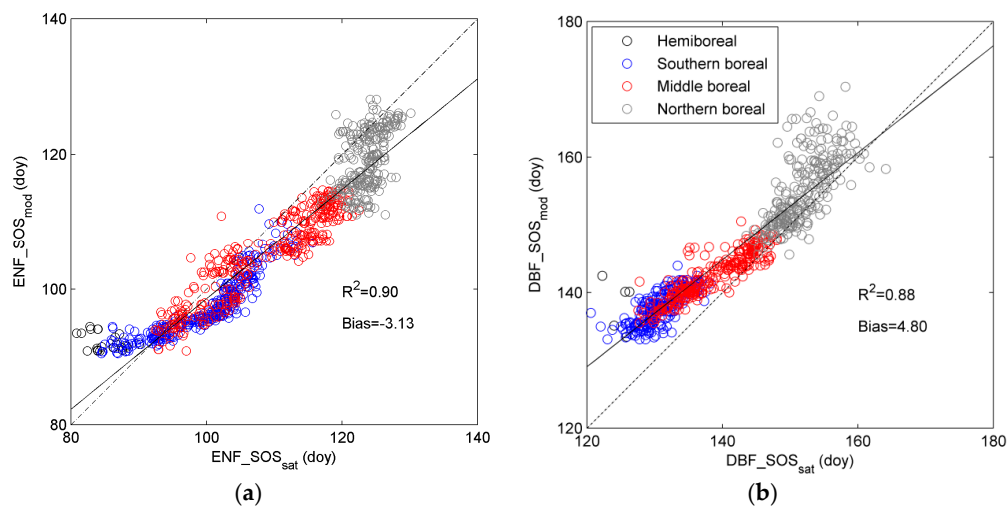
Figure 7. Scatterplots of mean satellite- and JSBACH model-derived start of season for forested areas in Finland for the period 2003–2010 for: (**a**) evergreen needle-leaf forest (ENF_SOS); and (**b**) deciduous broad-leaf forest (DBF_SOS). The dotted line gives the 1:1 line and the black line the linear fit between JSBACH-modelled and satellite-observed dates.
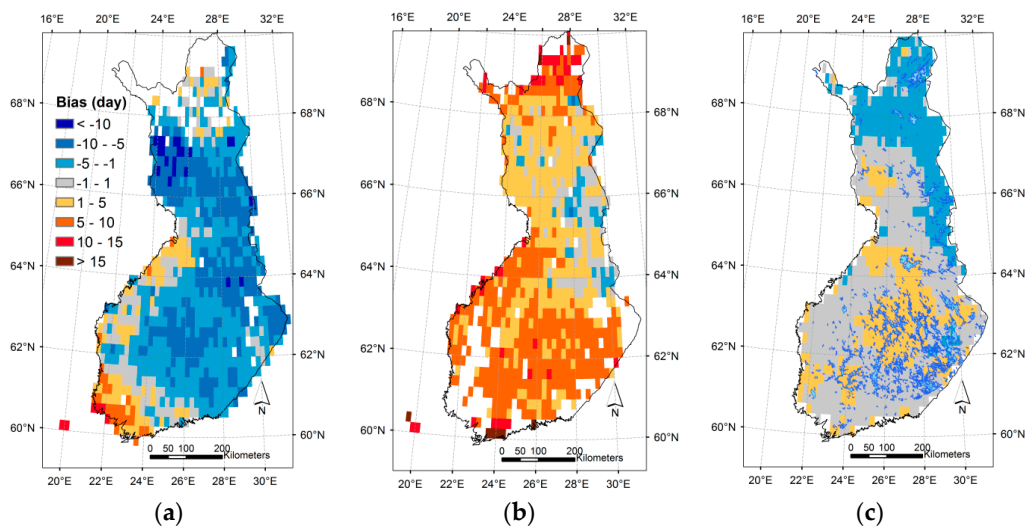
Figure 8. Grid cell-wise bias between start of season derived from the JSBACH model and remote sensing in Finland for the period 2003–2010: (**a**) in evergreen needle-leaf forest; and (**b**) in deciduous broad-leaf forest; (**c**) Bias in JSBACH-modelled starting date of the "growth phase" of DBF because of the driving temperature data. The bias was calculated as the difference in the start date of the "growth phase" simulated by running the LoGro-P-model with regional climate model data and with gridded temperature observations. Red colours show areas with a late bias and blue areas indicate an early bias of the modelled date.

The application of the method used for detection of ENF_SOS$_{sat}$ (Section 2.5.2) relating to the JSBACH-simulated snow cover was not possible for many years (2005, 2007, 2008 and 2009) in the hemiboreal, southern boreal zone and partly also in the middle boreal zone, because the simulated scaled FSC was below 1 during the whole spring period. For the remaining areas with sufficient snow cover, the modelled decrease of FSC occurred in mean earlier than ENF_SOS$_{sat}$ (8 days) for the period 2003–2010, which is also confirmed by local comparison to snow depth observations in Sodankylä (Figures 4c and 5c).
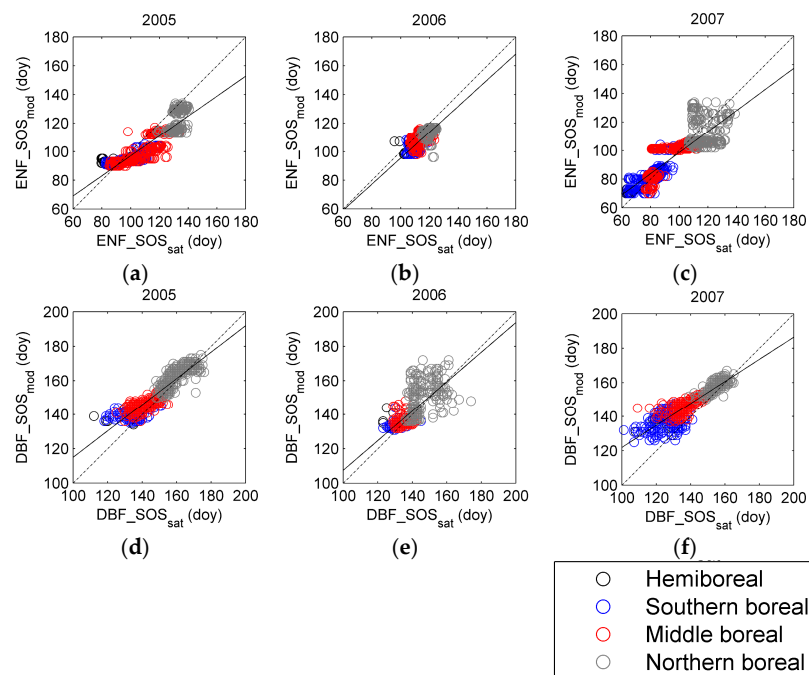
Figure 9. (**a**–**f**) Scatterplots of satellite-observed and JSBACH-simulated start of season for individual years 2005–2007. Upper panel: evergreen needle-leaf forest (ENF_SOS); Lower panel: deciduous broad-leaf forest (DBF_SOS). The dotted line gives the 1:1 line and the black line the linear fit between satellite- and JSBACH-modelled estimates.

We verified whether the driving temperature contributed to the differences between DBF_SOS$_{sat}$ and DBF_SOS$_{mod}$. Correlations between the multi-year average dates of the start of the "growth phase" of DBF for the period 2003–2010 from LoGro-P simulations with two temperature drivers (regional climate model and FMI gridded temperature) were very high and the remaining bias for the whole of Finland was very small (R^2 = 0.98, RMSE = 1.66, Bias = −0.05 days). Nevertheless, the bias varied spatially (Figure 8c); late biases (1–2 days) occurred in central Finland and early biases were observed in north-eastern Finland (−2−−4 days).

The last part of this Section focuses on the inter-annual variations in the start of season dates. On the whole, inter-annual variations of JSBACH model-derived dates were in agreement with satellite observations (Figure 10), except in 2007, when DBF_SOS$_{mod}$ was 8 days delayed compared to DBF_SOS$_{sat}$. The deviation from the respective mean date (period 2003–2010) at individual locations (grid cell) ranged in average between −14 and 10, and −12 and 8 days for ENF_SOS$_{sat}$ and ENF_SOS$_{mod}$ throughout Finland. Regarding DBF_SOS, inter-annual variations at one location were slightly smaller than for ENF_SOS, ranging in mean from −8 to 9, and −8 to 7 days for DBF_SOS$_{sat}$ and DBF_SOS$_{mod}$, respectively. The inter-annual variations of mean air temperature for Finland in May correlated with the inter-annual variations in DBF_SOS$_{mod}$; that is, higher May temperatures lead to an earlier start of season, (R^2 = 0.71). Instead, for the evergreen forest, April temperatures are more important: the mean air temperature in April was correlated with the ENF_SOS$_{mod}$ time series (R^2 = 0.56). The inter-annual differences between DBF_SOS$_{mod}$ and ENF_SOS$_{mod}$ can be largely explained by the differences in the mean air temperature in April and May (R^2 = 0.70).

We observed an early anomaly in the start of season in ENF in 2007, both from satellite observations and JSBACH simulations (Figures 10 and 11c,f). The yearly anomaly for ENF_SOS$_{sat}$ was larger than −20 days in south-western coastal areas and in central Finland (Figure 11c). The ENF_SOS$_{mod}$ anomaly agreed in many parts of Finland with the satellite-observed anomaly, but not for western areas at Bothnian Bay and areas in the northern boreal zone (Figure 11f).
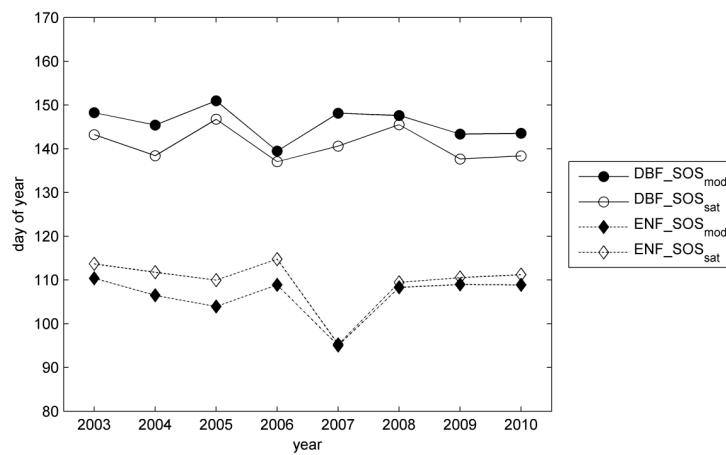
Figure 10. Interannual variations of the start of season in evergreen coniferous forest and deciduous broad-leaf forest in Finland derived from the JSBACH model and from remote sensing observations.
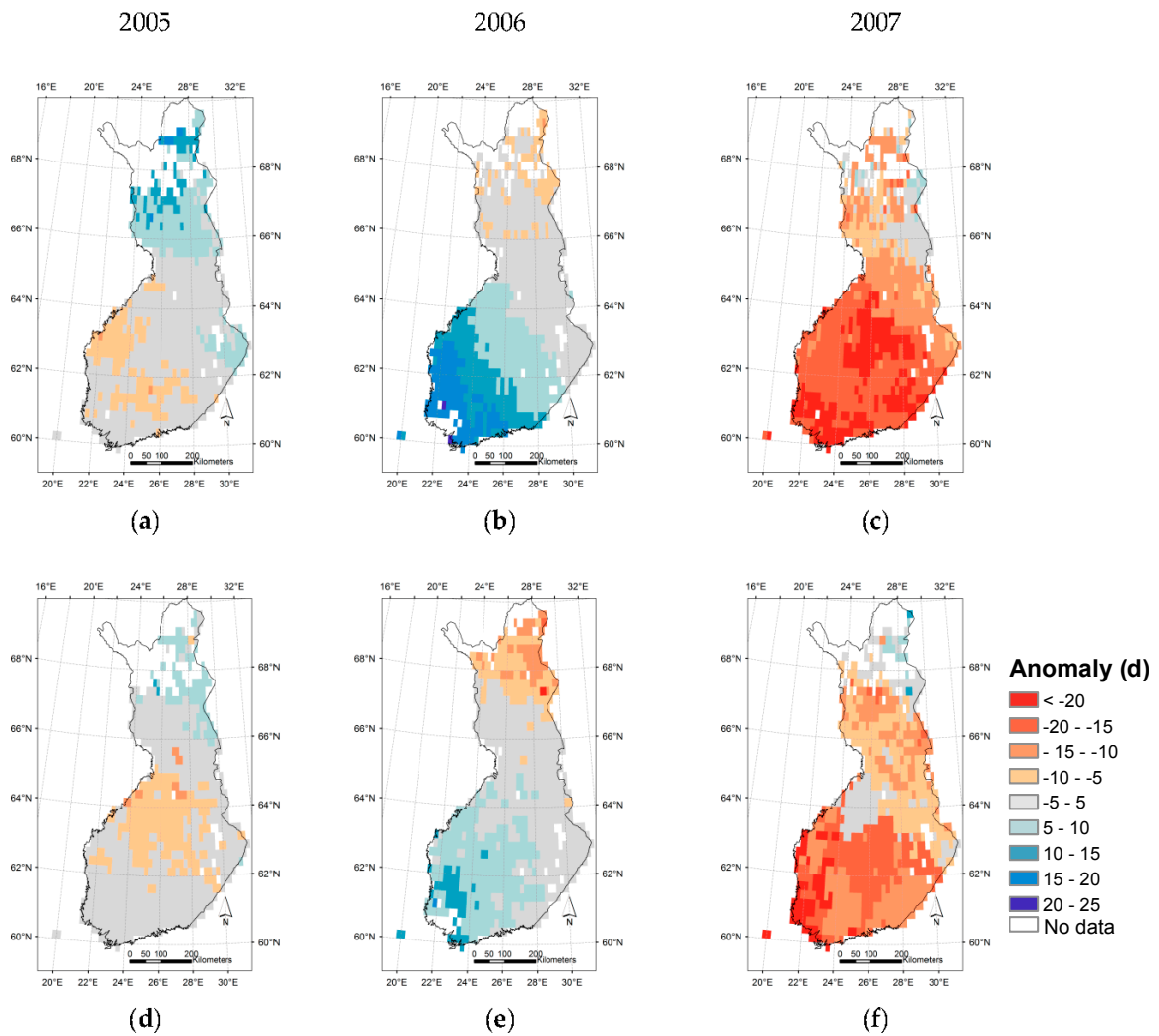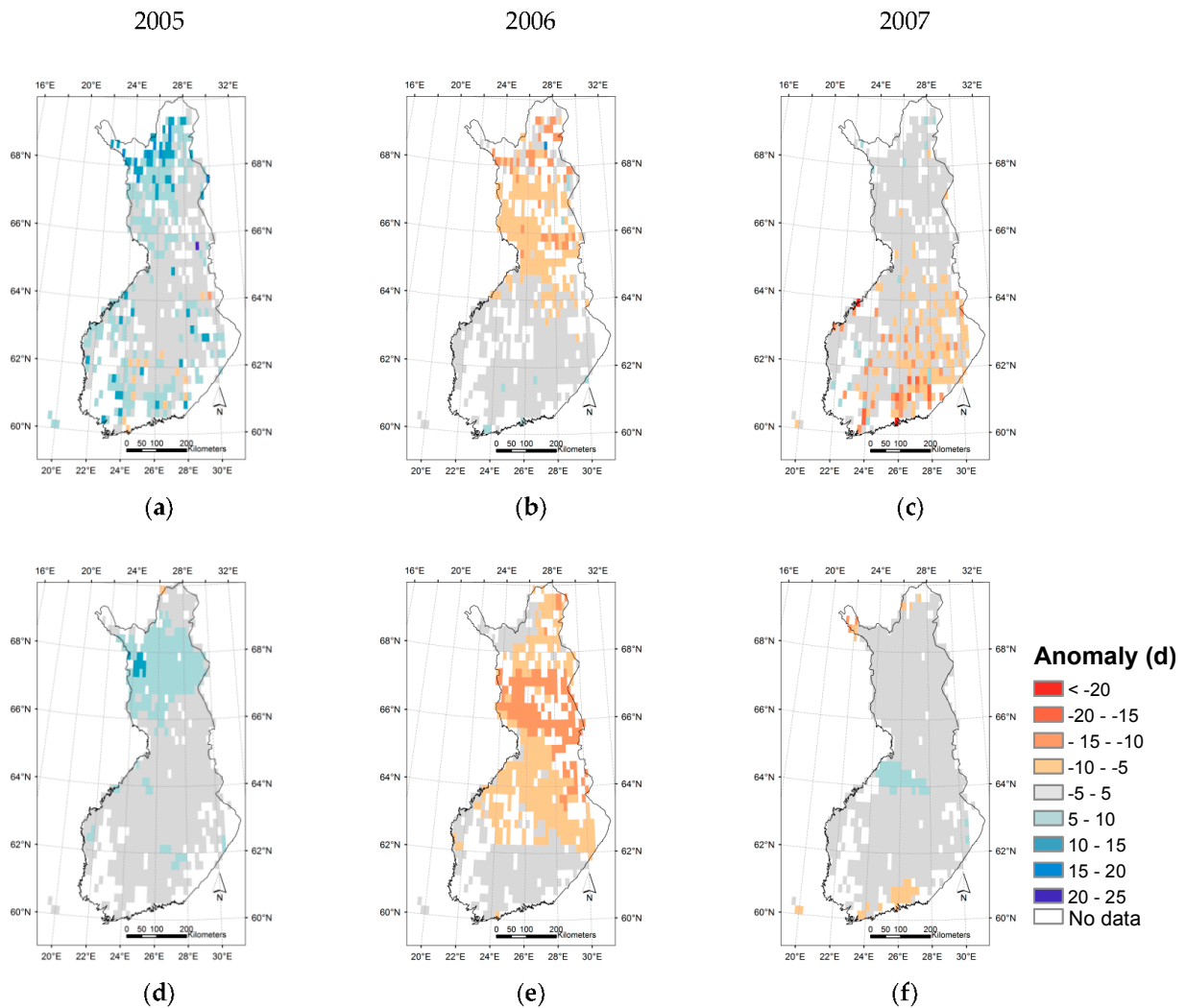

Figure 11. (**a**–**f**) Spatial distribution of yearly anomalies, the deviations (in days) from grid cell mean for 2003–2010, of start of season in evergreen needle-leaf forest. Upper panel: remote sensing estimate (ENF_SOS$_{sat}$). Lower panel: model-derived estimate (ENF_SOS$_{mod}$).

Furthermore, agreement was found for parts of central and northern Finland regarding the early anomaly of DBF_SOS in 2006 (Figure 12b,e); although DBF_SOS$_{mod}$ indicated a stronger early anomaly than shown by DBF_SOS$_{sat}$. Some disagreement between the anomalies was observed in 2007; an early anomaly (up to 15 days) occurred in the south-eastern parts of Finland, according to DBF_SOS$_{sat}$, but this was not the case for DBF_SOS$_{mod}$ (Figure 12c,f).

Figure 12. (**a**–**f**) Spatial distribution of yearly anomalies, the deviations (in days) from grid cell mean 2003–2010, of the start of season of deciduous broad-leaf forest. Upper panel: remote sensing estimate (DBF_SOS$_{sat}$). Lower panel: model-derived estimate (DBF_SOS$_{mod}$).

4. Discussion

4.1. Quality of Remote Sensing Observations of the Start of Season

The accuracy of DBF_SOS$_{sat}$ was about one week for Finnish sites, which is in line with results obtained in Siberia [70]. Moreover, our observations are in agreement with a map of satellite-derived greening-up of vegetation in Fennoscandia for the period 1982–2002 by Karlsen et al. [77] Figure 2a, but DBF_SOS$_{sat}$ occurred slightly later in the northern boreal zone than in the map for a relatively warmer period (2000–2006) [28] Figure 5. The sites Aulanko, Kevo, Saariselkä and Värriö were also used for evaluation of the NDVI-based method in studies by Karlsen et al. [28,78] that showed higher

correlation between field observations and the NDVI-based start of season in Aulanko and Kevo, but larger RMSE and bias for all four sites than in our results (Table 2).

For the evaluation of DBF_SOS$_{sat}$, we compared visual observation of bud break of birch on a few trees with the satellite signal on green-up for many pixels covering an area of several kilometres. As described by Badeck et al. [67], several factors could cause deviations between the in situ observation and DBF_SOS$_{sat}$: (a) the inter-individual variability in bud break, (b) systematic time lags between bud break and the date derived from the satellite signal and (c) the heterogeneity in terrain and land cover. Concerning (a), no information on the observer error was given with the ground observations, but the visual observations at Finnish sites were carried out twice a week and we therefore assumed an observers error of about three days. The within-population variation in the date of bud break can range between a few days to up to four weeks and varies from year to year depending on weather patterns [79]. The variation of microclimate for areas covering several kilometres and elevation differences lower than 50 m was estimated with 2.5 days in Badeck et al. [67]. Regarding (b), satellite-observed start of season of DBF did not show a systematic time lag to bud break observations in this study for the whole of Finland. According to Delbart et al. [27,70], the timing of the NDWI minimum in spring after snowmelt corresponds to the time of greening-up of vegetation. Because of noise in the satellite time series, due to cloud cover and atmospheric influences, a threshold value was applied to avoid false detection of the start date (see Equation (3)). We minimized the effect of land cover heterogeneity (c) by selecting MODIS pixels with a dominance of deciduous and mixed forest cover. However, differences in forest structure and the contribution of the understorey to the satellite signal may be one reason for the different biases in DBF_SOS$_{sat}$ when looking at the southern and northern boreal sites separately (Section 3.1). More investigations are needed on a possible inherent regional bias in the remote sensing estimate for the start of season date in deciduous broad-leaf forest. Information on the forest structure and the understorey phenology, e.g., from web-camera observations, could be helpful in this respect.

In this study, we use the timing of the beginning of snow melt as a proxy indicator for the start of season in ENF that showed good correspondence with ENF_SOS$_{EC}$ for flux measurement sites in Finland. The quality of the estimate has been discussed in Böttcher et al. [33]. Recent studies suggest that the photochemical reflectance index (PRI) can be used as a direct indicator of spring photosynthetic activation in boreal ENF [25] and can potentially be applied to satellite observations, e g., MODIS [80]. However, satellite-based monitoring with the PRI will need to take into account, among other things, the varying background [25], and this is especially relevant for the spring recovery in evergreen boreal forest when the ground is still snow-covered. Alternatively, the Plant Phenological Index (PPI) seems insensitive to noise and snow and follows well the seasonal development of GPP in boreal ENF [81]. In addition, new space-borne instruments, such as those for the Global Ozone Monitoring Experiment (GOME-2), the Greenhouse Gases Observing Satellite (GOSAT) and the Orbiting Carbon Observatory-2 (OCO-2), provide the opportunity of measuring solar-induced fluorescence and, therefore, ways to directly assess photosynthetic activity [26,82,83], and could be considered in future work.

The presence of long and frequent periods of cloud cover increases the uncertainty of the phenological dates extracted from optical satellite observations. In this study, we applied temporal interpolation of the daily FSC and NDWI time series, but excluded cases of continuous cloud cover longer than two weeks. Including the spatial dimension in the gap-filling based on geostatistical techniques [84–86] could improve the completeness of the time series. The quality of the gap-filled time series may still depend on the pattern of missing data in time and space [85]. Another possibility would be the use of the all-weather capabilities of satellite radar and microwave observations alone [87] or in combination with optical observations. For ENF, our method relies on observations of snow cover. Microwave retrievals of the Snow Water Equivalent (SWE), such as provided by the GlobSnow project [88], could be used in combination with the optical observations to gain information on the snow during periods of cloud cover. Currently, the SWE time series covering the period from 1979–2012 is

only available at a grid resolution of 25 km $\times$ 25 km, but a higher resolution SWE product (augmented using the optical FSC data) is under development at the FMI.

4.2. Modelling of Springtime Development and the Start of Season in JSBACH

The inspection of the modelled GPP time series (Figures 4 and 5) showed that the JSBACH model instantaneously responds to the increase of air temperature above zero $^\circ$C resulting in a higher GPP than obtained from the CO_2 flux measurements and, consequently, earlier ENF_SOS$_{mod}$ than ENF_SOS$_{EC}$. The photosynthesis module in JSBACH has the same temperature response for parameters describing the potential electron transport rate and maximum carboxylation rate for the whole year, thus indicating that the simulated vegetation is ready to immediately photosynthesize in spring with increasing air temperatures without any recovery period required, providing there is foliage present as in the case of ENF. However, the boreal coniferous forests have a recovery period in spring after the winter dormancy before they reach their full summertime photosynthetic capacity [89,90]. This may explain the differences between observed GPP at Sodankylä and simulated GPP using local weather observations (Figures 4 and 5). Overestimation of the spring carbon uptake (a too large GPP) by JSBACH was also found by Dalmonech and Zaehle [21] in a study that evaluated, among others, the phenology of the JSBACH model. Furthermore, because of generally lower air temperatures from the regional climate model than from the site measurements, the ENF_SOS$_{mod,loc}$ was earlier than ENF_SOS$_{mod}$.

The observed early bias of three days in ENF_SOS$_{mod}$ from JSBACH is relatively small in comparison to results by Richardson et al. [14] for the simulated start of photosynthetic uptake from 14 biosphere models (mean bias of -11 ± 15 days) and is in the same range as for the best-performing models in the evaluation. The increase in the negative bias of ENF_SOS$_{mod}$ from south to north (Figure 8, Supplementary Materials: Table S2) found here, agrees with higher temperatures observed at time of ENF_SOS at northern sites compared to southern boreal sites [4,18,33] and suggests that the response of air temperature for ENF follows a climate gradient in the boreal zone.

For the performance of the JSBACH model regarding the estimation of ENF_SOS, the photosynthesis model plays the dominant role and deviations from ENF_SOS$_{sat}$ are not due to the LoGro-P model. Improvements to the model performance during the start of season of ENF could be achieved by implementing seasonality to temperature response of JSBACH photosynthesis parameters, and possibly also accounting for photoinhibition in coniferous forests, a phenomenon observed during spring at high light levels and freezing temperatures [91]: the light receiving apparatus in chloroplast gets damaged at high light levels, and for low temperature conditions the photosynthetic capacity may be notably reduced. The description of effects of soil water freeze on carbon uptake could also be improved. According to observations [18,92], the coniferous trees are able to photosynthesize before the soil thaw, but lack of liquid water from soil soon reduces the carbon uptake. In the model, the actual simulated proportions of liquid and frozen water in soil layers could be used to limit the carbon exchange. There are advances related to expressing frozen soil in JSBACH northern permafrost regions [93].

The modelled FSC by JSBACH does not serve as a reliable predictor of ENF_SOS (Section 3.3), as too little snow and too early snow melt is simulated for our study area. Having bias-corrected temperature and precipitation data does not guarantee precise snow cover, as the formulation of snow accumulation relies on a universal temperature threshold and parameterizations of snow processes are not adjusted for region and drivers.

In contrast to results for ENF, we found a late bias of DBF_SOS$_{mod}$ (Figure 7, Supplementary Materials: Table S2). This agrees with findings by Dalmonech and Zaehle for southern Finland [21], but due to the higher temporal resolution of the remote sensing data set used here, we can quantify the bias better and also give results for the northern parts of Finland that were masked out in the study above. As regards other biosphere models from the study by Richardson et al. [14], the bias for

JSBACH DBF_SOS$_{mod}$ turned out to be relatively small, although direct comparisons are difficult due to differences in the environmental drivers for the model runs.

It has to be noted that the definition of DBF_SOS$_{mod}$ does not correspond exactly to DBF_SOS$_{sat}$. While DBF_SOS$_{mod}$ is defined based on a minimal change in LAI, the visual observation of bud break may indicate a later stage of development. An optimized parameterization of the LoGro-P model for the boreal zone would allow an improvement of the overall bias for DBF_SOS$_{mod}$; variation in parameter values, such as the alternating temperature (T_{alt}) and the minimum value of the critical heat sum (S_{crit}^{min}) can reduce the mean bias (Appendix A, Tables A1 and A2). A proper tuning of the LoGro-P parameters for our area of interest was outside the scope of this study and needs further investigation, but could be performed using satellite observations and Bayesian optimization techniques.

Similar to ENF, the bias in DBF_SOS$_{mod}$ showed a regional gradient; that is, the bias decreased from south to north (Figure 7, Supplementary Materials: Table S2). According to field observations, the heat sum requirement for bud break of birch decreases from south to north in the boreal region [94,95] and also the temperature threshold for the NDVI-based greening-up decreases [28,77]. This seems to be in contradiction to our results for JSBACH DBF_SOS$_{mod}$. The same critical temperature and heat sum requirement was used in the LoGro-P model for the whole study area. According to the above, one would expect a gradient with earlier bias in southern areas compared to northern areas. We observed the opposite, except for the northernmost parts of the study area (Figure 8b). Reasons for this could be an insufficient chilling predicted by the LoGro-P model, a regional gradient in bias in the bias-corrected driving temperature, or in the remote sensing estimate of DBF_SOS$_{sat}$. Under the current climate, the chilling requirement is typically fulfilled in the boreal region [96] and this was also the case in our study area. Therefore, the chilling requirement cannot be used for a better calibration of the south–north gradient, and since the start date of the chilling decay follows a climate gradient, an increase in the decay parameter (C_{decay}) would further pronounce the delay in the DBF_SOS$_{mod}$ in southern regions. The S_{crit}^{min} parameter plays a role as well, but while the overall bias could be reduced with a lower parameter value, the regional gradient would still remain and this may suggest that optimal parameters for the boreal region are zone-specific.

Despite a very small temperature bias in the start date of the "growth phase" of DBF for the whole of Finland (Figure 8c), the slope of the regression line between DBF_SOS$_{sat}$ and the modelled date from LoGro-P was slightly higher (0.9 compared to 0.79) when FMI gridded temperatures were used instead of temperature data from the regional climate model. This indicates a small influence of the driving data to the regional gradient. Likewise, the late bias in DBF_SOS$_{sat}$ for phenological sites in northern, and early bias in southern Finland (Section 3.1) need further investigations and may partly explain differences in bias in JSBACH DBF_SOS$_{mod}$ in the different boreal sub-zones.

5. Conclusions

In this study, we evaluated the timing of the start of the photosynthetically active season in evergreen needle- and deciduous broad-leaf forest in Finland in the biosphere model JSBACH against satellite observations. The differences between the two forest types with respect to photosynthetic recovery in spring were taken into account. The accuracy of the satellite-derived dates for the deciduous forest was assessed with bud break observations. The NDWI-based method is applicable for deciduous forest in Finland and the estimated dates can be used for the evaluation of model results at a regional scale. The inaccuracy of the satellite-observed date was one week and the bias was small (Figure 2), but regional differences in bias need further evaluation.

The comparisons between JSBACH-simulated and satellite-observed start of season at the regional scale showed that the general spatial and temporal dynamics were rather well captured by JSBACH, for both ENF and DBF (Figures 7 and 10). The performance was slightly better for evergreen forest. We found an early bias of three days and a late bias of five days in the start of season of evergreen needle- and deciduous broad-leaf forest, respectively. The bias showed a south–north gradient for both forest types. While in the deciduous forest the start of the vegetation active season is determined by

the phenological model LoGro-P, the photosynthesis model is more important for the evergreen forest type. The date of the predicted "growth phase" in evergreen forest occurred about one month after the start of the vegetation active season. Therefore, an improved calibration of the phenology model would not be sufficient for this plant functional type. Instead, JSBACH photosynthesis parameters would need to be adjusted to limit too strong early photosynthesis and hence to improve the behaviour of gross primary production in early spring (Figures 4 and 5). In the deciduous broad-leaf case, results could be slightly improved with different JSBACH phenology parameters, but the model formulation seems not optimal with respect to the south–north gradient in Finland. In further work, one could optimize the phenological parameters with a Bayesian method using the remote sensing observations to better understand the effectiveness of individual parameters and the relationships between them. Furthermore, using in situ measurements such as chlorophyll fluorescence observations and greenness change from phenology cameras could be used to improve the photosynthesis and phenology descriptions of the model.

Author Contributions: Kristin Böttcher, Tiina Markkanen, Jouni Pulliainen, Tuula Aalto, Tea Thum and Ali N. Arslan conceived and designed the study; Tiina Markkanen and Tea Thum performed the regional and local JSBACH model runs; Kristin Böttcher analysed the remote sensing data and made the comparison with model results; Kristin Böttcher, Tiina Markkanen and Tea Thum analysed the results; Christian H. Reick developed the phenology model and took part in the discussions on some aspects of the design of the study, Mika Aurela determined the ENF_SOS$_{EC}$ dates from the EC measurements and provided the EC and meteorological data from Sodankylä forest, Pasi Kolari provided Hyytiälä data; Kristin Böttcher wrote the draft of the manuscript and prepared the final version; Tiina Markkanen, Tuula Aalto, Tea Thum, Mika Aurela, Christian H. Reick, Jouni Pulliainen and Pasi Kolari contributed to the writing of the paper. Ali N. Arslan acted as project manager for the projects SnowCarbo and Monimet.

Conflicts of Interest: The authors declare no conflict of interest.

Abbreviations

The following abbreviations are used in this manuscript:

3D	Three-dimensional
CORINE	Coordinated Information on the European Environment
C_{decay}	Decay parameter in the LoGro-P model
DBF	Deciduous broad-leaf forest
DBF_SOS	Starting date of the vegetation active season of DBF
DBF_SOS$_{mod}$	Starting date of the vegetation active season of DBF determined from JSBACH regional runs
DBF_SOS$_{sat}$	Starting date of the vegetation active season of DBF determined from satellite observations
doy	Day of year
EC	Eddy covariance
ECMWF	European Centre for Medium-Range Weather Forecasts
ENF	Evergreen needle-leaf forest
ENF_SOS	Starting date of the vegetation active season in ENF
ENF_SOS$_{EC}$	Starting date of the vegetation active season determined from continuous EC measurements
ENF_SOS$_{mod,loc}$	Starting date of the vegetation active season of ENF determined from JSBACH local runs at CO_2 flux measurement sites
ENF_SOS$_{mod}$	Starting date of the vegetation active season of ENF determined from JSBACH regional runs
ENF_SOS$_{sat}$	Starting date of the vegetation active season of ENF determined from satellite observations
fAPAR	Fraction of absorbed photosynthetically active radiation
FMI	Finnish Meteorological Institute
FSC	Fractional Snow Cover
GOME-2	Global Ozone Monitoring Experiment
GOSAT	Greenhouse Gases Observing Satellite
GPP	Gross Primary Production
JSBACH	Jena Scheme for Biosphere–Atmosphere Hamburg
LAADS	Level-1 & Atmosphere Archive and Distribution System
LAI	Leaf Area Index
LoGro-P	Logistic Growth Phenology
MODIS	Moderate Resolution Imaging Spectrometer
MPI	Max Planck Institute
NASA	National Aeronautics and Space Administration
NDVI	Normalized Difference Vegetation Index
NDWI	Normalized Difference Water Index
NEE	Net ecosystem CO_2 exchange
OCO-2	Orbiting Carbon Observatory
N	Number of observations
p	Probability
PFT	Plant Functional Type
PPI	Plant Phenological Index
PRI	Photochemical Reflectance Index
R	Respiration
R^2	Coefficient of determination
REMO	Regional climate model
RMSE	Root mean square error
R_{MIR}	Mid-infrared reflectance
R_{NIR}	Near-infrared reflectance
SCAmod	Algorithm for the retrieval of FSC from optical satellite observations
S_{crit}^{min}	Heat sum parameter in LoGro-P model
T_{alt}	Alternating temperature in LoGro-P model
TOA	Top-of-Atmosphere

Appendix A.

A1. The JSBACH Phenology for Extra-Tropical Forests

The JSBACH phenology model, called LoGro-P (Logistic Growth Phenology), distinguishes five phenology types: evergreen, summergreen, raingreen, grasses, and crops. Each PFT is linked to one of these phenology types. Here, only those two phenologies relevant for the present study are described, namely the evergreen phenology that applies to the PFTs "temperate broad-leaf evergreen trees" and "coniferous evergreen trees", and the summergreen phenology that applies to the PFTs "temperate broad-leaf deciduous trees" and "coniferous deciduous trees".

A2. General Dynamics

The key variable of LoGro-P is the LAI (Leaf Area Index), denoted by the symbol Λ, developing in time according to logistic growth dynamics

$$\frac{d\Lambda}{dt} = k\Lambda \left(1 - \frac{\Lambda}{\Lambda_{max}}\right) - p\Lambda \tag{A1}$$

For small Λ, this equation describes exponential growth at rate k reduced by leaf shedding at rate p. The term in brackets reduces growth when Λ approaches the maximum LAI Λ_{max} of the particular PFT. Equation (A1) has the solution

$$\Phi\left(t + \tau\right) = (k - p)\, \frac{\Phi\left(t\right)}{k\Phi\left(t\right) + \left(k - p - k\Phi\left(t\right)\right)\exp\left(-\left(k - p\right)\tau\right)} \tag{A2}$$

where

$$\phi\left(t\right) = \frac{\Lambda\left(t\right)}{\Lambda_{max}} \tag{A3}$$

is called the "phenological state". To simulate the development of the LAI Equation (A2) is iterated at a daily time step τ.

The logistic dynamics (Equation (A1)) is such that whenever Λ fell to zero it could never recover. Plants solve this problem by growing seeds or leaf buds containing biochemical resources sufficient to grow a leaf until they can grow further by carrying out photosynthesis. In LoGro-P, this is modelled by assuming a minimum value of Λ called "seed value"—when conditions are favourable for starting growth.

Environmental conditions enter the dynamics only via the growth and shedding rates *k* and *p*. Hence, the more complicated part of LoGro-P is the modelling of plant's dependence on temperature, soil moisture etc., which is different for the various phenology types, as explained below.

A3. Evergreen Phenology

Basic to the phenology model for evergreens is the assumption that the phenological dynamics can be divided into two subsequent phases, a "growth phase" (spring), characterized by non-zero k and absence of leaf shedding ($p = 0$); and a "rest phase" (all other seasons), where growth is zero ($k = 0$) and leaf shedding p is non-zero. If not zero anyway, growth and shedding rates are prescribed parameters.

A4. Summer-Green Phenology

The summer-green phenology assumes three phases: "growth phase" (spring), characterized by non-zero k and absence of leaf shedding ($p = 0$); a "vegetative phase" (summer), where growth is zero ($k = 0$) and leaf shedding p is small; and a "rest phase" (all other seasons), where growth is zero ($k = 0$) and leaf shedding p is non-zero.

Vegetative phase and rest phase differ only by the magnitude of the shed rate. The introduction of three phases instead of only those two of the evergreens is suggested by fAPAR data of summer-green vegetation, where typically, after a short time of rapid growth, a reduction of fAPAR is seen, much before the leaves are shed in autumn—also, here, if not anyway zero, growth and shedding rates are prescribed parameters.

A5. Spring and Autumn Events

A main issue in modelling the phenological phases is to determine when the vegetation shifts from one phase to the next. For the transition from the growth to the subsequent phase it is assumed that the growth phase lasts only for a fixed time, so that after that time the next phase automatically starts. However, for the shift from the rest phase to the growth phase (called spring event) and the shift from the vegetative phase to the rest phase (autumn event), the dependence on environmental conditions cannot be neglected. This is the topic of the following sections.

A6. The Spring Event

To determine the spring event, the alternating model of Murray et al. [50] is used (see also Botta et al. [97]): Let $S(d)$ denote the value of the heat sum at day d:

$$S(d) = \sum_{d'=d_0}^{d} \max\left(0, T(d') - T_{alt}\right) \tag{A4}$$

where $T(d)$ is the mean day temperature at day d, T_{alt} is a parameter called alternating temperature (which has the function of a cut-off temperature in the heat sum), and d_0 is the starting date for temperature summation. In the model, it is taken care that this starting date falls in times after the buds have already experienced chilling (see below).

Another key quantity of the alternating model is the number of chill days, $C(d)$: this is the number of days with a mean day temperature below the alternating temperature T_{alt}, where counting starts at the day d_a of the last autumn event:

$$C(d) = \sum_{d'=d_a}^{d} \theta\left(T_{alt} - T(d)\right) \tag{A5}$$

where θ is the Heaviside step function. To prevent that under bad climate conditions $C(d)$ influences the phenological behaviour of the next growing season, the number of chill days is limited to 365 days. From $C(d)$ a critical heatsum $S_{crit}(d)$ is computed:

$$S_{crit}(d) = S_{crit}^{min} + S_{crit}^{range} \exp\left(-\frac{C(d)}{C_{decay}}\right) \tag{A6}$$

where S_{crit}^{min}, S_{crit}^{range} and C_{decay} are parameters of the alternating model. Finally, the spring event happens at the first day d for which during the rest phase

$$S(d) \geqslant S_{crit}(d) \tag{A7}$$

is fulfilled—if at the spring event Λ is less than the above mentioned seed value, Λ is set to this seed value to allow for sufficiently fast growth.

A7. The Autumn Event

At the autumn event the vegetative phase of summer-greens switches to the rest phase with rapid leaf shedding. The autumn event is calculated from a smoothed air temperature $T_s(n)$ at every time step n (see below). The smoothing is performed to prevent "false" autumn events upon short periods of coldness. The autumn event happens when during the vegetative phase T_s falls below a critical temperature T_s^{crit}. To prevent that this event is detected in spring, the condition is added that the mean day air temperature $T(d)$ should be smaller than T_s, i.e., the autumn event happens at the first day d when

$$T(d) < T_s(n) < T_s^{crit} \tag{A8}$$

Heat summation starts in the northern hemisphere always on 1 January (day 1), and in the southern hemisphere on day 183.

A8. Calculation of Smoothed Air Temperature

The smoothed temperature T_s at time step n is calculated as

$$T_s(n) = \frac{1}{N} \sum_{n'=-\infty}^{n} T(n) \exp\left(-(n-n')\frac{\tau}{\tau_s}\right) \qquad (A9)$$

where $T(n)$ is the air temperature, τ the length of a time step, τ_s the characteristic time for memory loss and N the normalization constant

$$N = \sum_{n'=-\infty}^{n} \exp\left(-(n-n')\frac{\tau}{\tau_s}\right) = \left(1-\exp\left(-\frac{\tau}{\tau_s}\right)\right)^{-1} \qquad (A10)$$

The calculation of the smoothed temperature is simplified by noting that from Equation (A9) it follows that its computation can be done iteratively:

$$T_s(n+1) = \frac{T_s(n)}{N} + T_s(n)\exp\left(-(n-n')\frac{\tau}{\tau_s}\right) \qquad (A11)$$

A9. Parameter Values

The following tables give an overview on values for the parameters of the evergreen and summer-green phenology models of LoGro-P that were used in this study. The maximum LAI values are PFT-specific.

Table A1. Parameters of the evergreen and summer-green phenological models of LoGro-P used in this study. Parameter values for the alternating temperature (T_{alt}), the characteristic time for memory loss for computation of the pseudo soil temperature ($\tilde{T}s$) and the minimum value of the critical heat sum (S_{crit}^{min}) were varied for sensitivity tests. Parameter values that produced zero bias in the start date of season for deciduous forest when compared to satellite observation of DBF_SOS$_{sat}$ in Finland are given in brackets.

Parameter	Units	Summergreen	Evergreen
seed LAI	m^2/m^2	0.4	0.4
τ_s	d	10	10
k	d^{-1}	0.087	0.015
T_{alt}	°C	4.0 (2.0)	4.0
T_s^{crit}	°C	10.0 (15.0)	-
S_{crit}^{min}	d·°C	30 (30)	10
S_{crit}^{range}	d·°C	200	150
C_{decay}	d	25	15
growth phase length	d	60	60
p (rest phase)	d^{-1}	0.1	0.0008
p (vegetative phase)	d^{-1}	0.004	-

Table A2. The maximum LAI values in our simulations.

PFT	Λ_{max}
temperate broad-leaf evergreen trees	6.0
coniferous evergreen trees	5.0
temperate broad-leaf deciduous trees	5.0
coniferous deciduous trees	5.0

To agree with the yearly amplitude of GPP from EC measurements, the maximum LAI for coniferous evergreen trees in site-level runs in Sodankylä and Hyytiälä were set to 9 and 16, respectively.

Appendix B.

Table B1. Statistical metrics that were used in the evaluation of satellite-derived start of season in deciduous broad-leaf forest (DBF_SOS$_{sat}$) and JSBACH simulations of the start of season in deciduous forest (DBF_SOS$_{mod}$) and evergreen forest (ENF_$_{SOSmod,loc}$; ENF_SOS$_{mod}$).

Statistical Measure	Equation
Root mean squared error	$\text{RMSE} = \sqrt{\sum_{i=1}^{N} (y_i - \hat{y}_i)^2 / N}$
Bias	$Bias = \sum_{i=1}^{N} (\hat{y}_i - y_i) / N$
Coefficient of determination	$R^2 = \dfrac{\sum_{i=1}^{N} (\hat{y}_i - \bar{y})^2}{\sum_{i=1}^{N} (y_i - \bar{y})^2}$

y_i is the reference observation. In the evaluation of satellite-observed DBF_SOS$_{sat}$ in situ observations of birch bud break are used as reference. For the evaluation of ENF_SOS$_{mod}$ and DBF_SOS$_{mod}$, the satellite-observed DBF_SOS$_{sat}$ and ENF_SOS$_{sat}$ were used as reference. $\hat{y}_i$ is the estimated or simulated value of the start of season, $\bar{y}$ is the arithmetic average of y values, and N is the number of observations.

References

1. Bonan, G.B. Forests and climate change: Forcings, feedbacks, and the climate benefits of forests. *Science* **2008**, *320*, 1444–1449. [CrossRef] [PubMed]
2. Ruosteenoja, K.; Raisanen, J.; Pirinen, P. Projected changes in thermal seasons and the growing season in Finland. *Int. J. Climatol.* **2011**, *31*, 1473–1487. [CrossRef]
3. Delpierre, N.; Soudani, K.; François, C.; Köstner, B.; Pontailler, J.Y.; Nikinmaa, E.; Misson, L.; Aubinet, M.; Bernhofer, C.; Granier, A.; et al. Exceptional carbon uptake in European forests during the warm spring of 2007: A data–model analysis. *Glob. Chang. Biol.* **2009**, *15*, 1455–1474. [CrossRef]
4. Thum, T.; Aalto, T.; Laurila, T.; Aurela, M.; Hatakka, J.; Lindroth, A.; Vesala, T. Spring initiation and autumn cessation of boreal coniferous forest CO$_2$ exchange assessed by meteorological and biological variables. *Tellus B* **2009**, *61*, 701–717. [CrossRef]
5. Vesala, T.; Launiainen, S.; Kolari, P.; Pumpanen, J.; Sevanto, S.; Hari, P.; Nikinmaa, E.; Kaski, P.; Mannila, H.; Ukkonen, E.; et al. Autumn temperature and carbon balance of a boreal Scots pine forest in Southern Finland. *Biogeosciences* **2010**, *7*, 163–176. [CrossRef]
6. Jylhä, K.; Ruosteenoja, K.; Räisänen, J.; Venäläinen, A.; Tuomenvirta, H.; Ruokolainen, L.; Saku, S.; Seitola, T. *Arvioita Suomen Muuttuvasta Ilmastosta Sopeutumistutkimuksia Varten. ACCLIM-Hankkeen Raportti 2009 (Changing Climate in Finland: Estimates for Adaptation Studies. ACCLIM Project Report 2009)*; Finnish Meteorological Institute: Helsinki, Finland, 2009.
7. Kaduk, J.; Los, S. Predicting the time of green up in temperate and boreal biomes. *Clim. Chang.* **2011**, *107*, 277–304. [CrossRef]
8. Räisänen, J.; Eklund, J. 21st Century changes in snow climate in Northern Europe: A high-resolution view from ENSEMBLES regional climate models. *Clim. Dyn.* **2012**, *38*, 2575–2591.
9. Rammig, A.; Jönsson, A.M.; Hickler, T.; Smith, B.; Bärring, L.; Sykes, M.T. Impacts of changing frost regimes on Swedish forests: Incorporating cold hardiness in a regional ecosystem model. *Ecol. Modell.* **2010**, *221*, 303–313. [CrossRef]
10. Ensminger, I.; Sveshnikov, D.; Campbell, D.A.; Funk, C.; Jansson, S.; Lloyd, J.; Shibistova, O.; Öquist, G. Intermittent low temperatures constrain spring recovery of photosynthesis in boreal Scots pine forests. *Glob. Chang. Biol.* **2004**, *10*, 995–1008. [CrossRef]
11. Jylhä, K.; Fronzek, S.; Tuomenvirta, H.; Carter, T.; Ruosteenoja, K. Changes in frost, snow and Baltic sea ice by the end of the twenty-first century based on climate model projections for Europe. *Clim. Chang.* **2008**, *86*, 441–462. [CrossRef]
12. Picard, G.; Quegan, S.; Delbart, N.; Lomas, M.R.; Le Toan, T.; Woodward, F.I. Bud-burst modelling in Siberia and its impact on quantifying the carbon budget. *Glob. Chang. Biol.* **2005**, *11*, 2164–2176. [CrossRef]

13. Jeong, S.-J.; Medvigy, D.; Shevliakova, E.; Malyshev, S. Uncertainties in terrestrial carbon budgets related to spring phenology. *J. Geophys. Res.: Biogeosci.* **2012**, *117*, G01030. [CrossRef]

14. Richardson, A.D.; Anderson, R.S.; Arain, M.A.; Barr, A.G.; Bohrer, G.; Chen, G.; Chen, J.M.; Ciais, P.; Davis, K.J.; Desai, A.R.; et al. Terrestrial biosphere models need better representation of vegetation phenology: results from the North American Carbon Program Site Synthesis. *Glob. Chang. Biol.* **2012**, *18*, 566–584. [CrossRef]

15. Mahowald, N.; Lo, F.; Zheng, Y.; Harrison, L.; Funk, C.; Lombardozzi, D. Leaf area index in earth system models: Evaluation and projections. *Earth Syst. Dyn. Discuss.* **2015**, *6*, 761–818. [CrossRef]

16. Melaas, E.K.; Richardson, A.D.; Friedl, M.A.; Dragoni, D.; Gough, C.M.; Herbst, M.; Montagnani, L.; Moors, E. Using FLUXNET data to improve models of springtime vegetation activity onset in forest ecosystems. *Agric. For. Meteorol.* **2013**, *171–172*, 46–56. [CrossRef]

17. Baldocchi, D.; Falge, E.; Gu, L.; Olson, R.; Hollinger, D.; Running, S.; Anthoni, P.; Bernhofer, C.; Davis, K.; Evans, R.; et al. FLUXNET: A new tool to study the temporal and spatial variability of ecosystem–scale carbon dioxide, water vapor, and energy flux densities. *Bull. Am. Meteorol. Soc.* **2001**, *82*, 2415–2434. [CrossRef]

18. Suni, T.; Berninger, F.; Vesala, T.; Markkanen, T.; Hari, P.; Mäkelä, A.; Ilvesniemi, H.; Hänninen, H.; Nikinmaa, E.; Huttula, T.; et al. Air temperature triggers the recovery of evergreen boreal forest photosynthesis in spring. *Glob. Chang. Biol.* **2003**, *9*, 1410–1426.

19. Yang, X.; Mustard, J.F.; Tang, J.; Xu, H. Regional-scale phenology modeling based on meteorological records and remote sensing observations. *J. Geophys. Res.: Biogeosci.* **2012**, *117*, G3. [CrossRef]

20. Luo, Y.Q.; Randerson, J.T.; Abramowitz, G.; Bacour, C.; Blyth, E.; Carvalhais, N.; Ciais, P.; Dalmonech, D.; Fisher, J.B.; Fisher, R.; et al. A framework for benchmarking land models. *Biogeosciences* **2012**, *9*, 3857–3874. [CrossRef]

21. Dalmonech, D.; Zaehle, S. Towards a more objective evaluation of modelled land-carbon trends using atmospheric CO_2 and satellite-based vegetation activity observations. *Biogeosciences* **2013**, *10*, 4189–4210. [CrossRef]

22. Beck, P.S.A.; Atzberger, C.; Høgda, K.A.; Johansen, B.; Skidmore, A.K. Improved monitoring of vegetation dynamics at very high latitudes: A new method using MODIS NDVI. *Remote Sens. Environ.* **2006**, *100*, 321–334. [CrossRef]

23. Shen, M.; Tang, Y.; Desai, A.R.; Gough, C.; Chen, J. Can EVI-derived land-surface phenology be used as a surrogate for phenology of canopy photosynthesis? *Int. J. Remote Sens.* **2014**, *35*, 1162–1174. [CrossRef]

24. Baldocchi, D.D.; Black, T.A.; Curtis, P.S.; Falge, E.; Fuentes, J.D.; Granier, A.; Gu, L.; Knohl, A.; Pilegaard, K.; Schmid, H.P.; et al. Predicting the onset of net carbon uptake by deciduous forests with soil temperature and climate data: A synthesis of FLUXNET data. *Int. J. Biometeorol.* **2005**, *49*, 377–387. [CrossRef] [PubMed]

25. Wong, C.Y.S.; Gamon, J.A. The photochemical reflectance index provides an optical indicator of spring photosynthetic activation in evergreen conifers. *New Phytol.* **2015**, *206*, 196–208. [CrossRef] [PubMed]

26. Walther, S.; Voigt, M.; Thum, T.; Gonsamo, A.; Zhang, Y.; Koehler, P.; Jung, M.; Varlagin, A.; Guanter, L. Satellite chlorophyll fluorescence measurements reveal large-scale decoupling of photosynthesis and greenness dynamics in boreal evergreen forests. *Glob. Chang. Biol.* **2015**. [CrossRef] [PubMed]

27. Delbart, N.; Kergoat, L.; Le Toan, T.; L'Hermitte, J.; Picard, G. Determination of phenological dates in boreal regions using normalized difference water index. *Remote Sens. Environ.* **2005**, *97*, 26–38. [CrossRef]

28. Karlsen, S.R.; Tolvanen, A.; Kubin, E.; Poikolainen, J.; Høgda, K.A.; Johansen, B.; Danks, F.S.; Aspholm, P.; Wielgolaski, F.E.; Makarova, O. MODIS-NDVI-based mapping of the length of the growing season in northern Fennoscandia. *Int. J. Appl. Earth Observ. Geoinf.* **2008**, *10*, 253–266. [CrossRef]

29. Gonsamo, A.; Chen, J.M.; Price, D.T.; Kurz, W.A.; Wu, C. Land surface phenology from optical satellite measurement and CO_2 eddy covariance technique. *J. Geophys. Res.* **2012**, *117*, G3. [CrossRef]

30. Beck, P.S.A.; Jönsson, P.; Høgda, K.-A.; Karlsen, S.R.; Eklundh, L.; Skidmore, A.K. A ground-validated NDVI dataset for monitoring vegetation dynamics and mapping phenology in Fennoscandia and the Kola Peninsula. *Int. J. Remote Sens.* **2007**, *28*, 4311–4330. [CrossRef]

31. Richardson, A.D.; Black, A.T.; Ciais, P.; Delbart, N.; Friedl, M.A.; Gobron, N.; Hollinger, D.Y.; Kutsch, W.L.; Longdoz, B.; Luyssaert, S.; et al. Influence of spring and autumn phenological transitions on forest ecosystem productivity. *Philos. Trans. R. Soc. B: Biol. Sci.* **2010**, *365*, 3227–3246. [CrossRef] [PubMed]

32. Dahlke, C.; Loew, A.; Reick, C. Robust identification of global greening phase patterns from remote sensing vegetation products. *J. Clim.* **2012**, *25*, 8289–8307. [CrossRef]

33. Böttcher, K.; Aurela, M.; Kervinen, M.; Markkanen, T.; Mattila, O.-P.; Kolari, P.; Metsämäki, S.; Aalto, T.; Arslan, A.N.; Pulliainen, J. MODIS time-series-derived indicators for the beginning of the growing season in boreal coniferous forest—A comparison with CO_2 flux measurements and phenological observations in Finland. *Remote Sens. Environ.* **2014**, *140*, 625–638. [CrossRef]

34. Raddatz, T.J.; Reick, C.H.; Knorr, W.; Kattge, J.; Roeckner, E.; Schnur, R.; Schnitzler, K.G.; Wetzel, P.; Jungclaus, J. Will the tropical land biosphere dominate the climate-carbon cycle feedback during the twenty-first century? *Clim. Dyn.* **2007**, *29*, 565–574. [CrossRef]

35. Pirinen, P.; Simola, H.; Aalto, J.; Kaukoranta, J.-P.; Karlsson, P.; Ruuhela, R. *Tilastoja Suomen Ilmastosta 1981–2010 (Climatological Statistics of Finland 1981–2010)*; Finnish Meteorological Insitute: Helsinki, Finland, 2012.

36. Ahti, T.; Hämet-Ahti, L.; Jalas, J. Vegetation zones and their sections on northwestern Europe. *Ann. Bot. Fennica* **1968**, *5*, 169–211.

37. Parviainen, J.; Västilä, S. *5a/2011 State of Finland´s Forests 2011 Based on the Criteria and Indicators of Sustainable Forest Management*; Ministry of Agriculture and Forestry: Helsinki, Finlandia, 2011.

38. Baldocchi, D.D. Assessing the eddy covariance technique for evaluating carbon dioxide exchange rates of ecosystems: Past, present and future. *Glob. Chang. Biol.* **2003**, *9*, 479–492. [CrossRef]

39. Kolari, P.; Kulmala, L.; Pumpanen, J.; Launiainen, S.; Ilvesniemi, H.; Hari, P.; Nikinmaa, E. CO_2 exchange and component CO_2 fluxes of a boreal Scots pine forest. *Boreal Environ. Res.* **2009**, *14*, 761–783.

40. Reichstein, M.; Falge, E.; Baldocchi, D.; Papale, D.; Aubinet, M.; Berbigier, P.; Bernhofer, C.; Buchmann, N.; Gilmanov, T.; Granier, A.; et al. On the separation of net ecosystem exchange into assimilation and ecosystem respiration: Review and improved algorithm. *Glob. Chang. Biol.* **2005**, *11*, 1424–1439. [CrossRef]

41. Thum, T.; Aalto, T.; Laurila, T.; Aurela, M.; Kolari, P.; Hari, P. Parametrization of two photosynthesis models at the canopy scale in a northern boreal Scots pine forest. *Tellus B* **2007**, *59*, 874–890. [CrossRef]

42. Vesala, T.; Suni, T.; Rannik, Ü.; Keronen, P.; Markkanen, T.; Sevanto, S.; Grönholm, T.; Smolander, S.; Kulmala, M.; Ilvesniemi, H.; et al. Effect of thinning on surface fluxes in a boreal forest. *Glob. Biogeochem. Cycles* **2005**, *19*, GB2001. [CrossRef]

43. Kubin, E.; Kotilainen, E.; Poikolainen, J.; Hokkanen, T.; Nevalainen, S.; Pouttu, A.; Karhu, J.; Pasanen, J. *Fenologisen Havaintoverkon Seurantaohjeet*; Finnish Forest Research Institute: Muhos, Finland, 2007.

44. Reick, C.H.; Raddatz, T.; Brovkin, V.; Gayler, V. Representation of natural and anthropogenic land cover change in MPI-ESM. *J. Adv. Model. Earth Syst.* **2013**, *5*, 459–482. [CrossRef]

45. Stevens, B.; Giorgetta, M.; Esch, M.; Mauritsen, T.; Crueger, T.; Rast, S.; Salzmann, M.; Schmidt, H.; Bader, J.; Block, K.; et al. Atmospheric component of the MPI-M Earth System Model: ECHAM6. *J. Adv. Model. Earth Syst.* **2013**, *5*, 146–172. [CrossRef]

46. Beer, C.; Weber, U.; Tomelleri, E.; Carvalhais, N.; Mahecha, M.; Reichstein, M. Harmonized European Long-Term Climate Data for Assessing the Effect of Changing Temporal Variability on Land-Atmosphere CO_2 Fluxes. *J. Clim.* **2014**, *27*, 4815–4834. [CrossRef]

47. Van Oijen, M.; Balkovič, J.; Beer, C.; Cameron, D.; Ciais, P.; Cramer, W.; Kato, T.; Kuhnert, M.; Martin, R.; Myneni, R.; et al. Impact of droughts on the C-cycle in European vegetation: A probabilistic risk analysis using six vegetation models. *Biogeosci. Discuss.* **2014**, *11*, 8325–8371. [CrossRef]

48. Peltoniemi, M.; Markkanen, T.; Härkönen, S.; Muukkonen, P.; Thum, T.; Aalto, T.; Mäkelä, A. Consistent estimates of gross primary production of Finnish forests—Comparison of estimates of two process models. *Boreal Environ. Res.* **2015**, *20*, 196–212.

49. Gao, Y.; Markkanen, T.; Thum, T.; Aurela, M.; Lohila, A.; Mammarella, I.; Kämäräinen, M.; Hagemann, S.; Aalto, T. Assessing various drought indicators in representing summer drought in boreal forests in Finland. *Hydrol. Earth Syst. Sci.* **2016**, *20*, 175–191. [CrossRef]

50. Murray, M.B.; Cannell, G.R.; Smith, R.I. Date of budburst of fifteen tree species in Britain following climate warming. *J. Appl. Ecol.* **1989**, *26*, 693–700. [CrossRef]

51. Farquhar, G.D.; Caemmerer, S.; Berry, J.A. A biochemical model of photosynthetic CO_2 assimilation in leaves of C3 species. *Planta* **1980**, *149*, 78–90. [CrossRef] [PubMed]

52. Knorr, W. Annual and interannual CO_2 exchanges of the terrestrial biosphere: Process-based simulations and uncertainties. *Glob. Ecol. Biogeogr.* **2000**, *9*, 225–252. [CrossRef]

53. Roesch, A.; Wild, M.; Gilgen, H.; Ohmura, A. A new snow cover fraction parametrization for the ECHAM4 GCM. *Clim. Dyn.* **2001**, *17*, 933–946. [CrossRef]

54. Jacob, D.; Podzun, R. Sensitivity studies with the regional climate model REMO. *Meteorol. Atmos. Phys.* **1997**, *63*, 119–129. [CrossRef]

55. Jacob, D. A note to the simulation of the annual and inter-annual variability of the water budget over the Baltic Sea drainage basin. *Meteorol. Atmos. Phys.* **2001**, *77*, 61–73. [CrossRef]

56. Gao, Y.; Weiher, S.; Markkanen, T.; Pietikäinen, J.-P.; Gregow, H.; Henttonen, H.M.; Jacob, D.; Laaksonen, A. Implementation of the CORINE land use classification in the regional climate model REMO. *Boreal Environ. Res.* **2015**, *20*, 261–282.

57. Simmons, A.J.; Burridge, D.M. An Energy and angular-momentum conserving vertical finite-difference scheme and hybrid vertical coordinates. *Mon. Weather Rev.* **1981**, *109*, 758–766. [CrossRef]

58. Dee, D.P.; Uppala, S.M.; Simmons, A.J.; Berrisford, P.; Poli, P.; Kobayashi, S.; Andrae, U.; Balmaseda, M.A.; Balsamo, G.; Bauer, P.; et al. The ERA-Interim reanalysis: Configuration and performance of the data assimilation system. *Q. J. R. Meteorol. Soc.* **2011**, *137*, 553–597. [CrossRef]

59. Christensen, J.H.; Boberg, F.; Christensen, O.B.; Lucas-Picher, P. On the need for bias correction of regional climate change projections of temperature and precipitation. *Geophys. Res. Lett.* **2008**, *35*, L20709. [CrossRef]

60. Teutschbein, C.; Seibert, J. Bias correction of regional climate model simulations for hydrological climate-change impact studies: Review and evaluation of different methods. *J. Hydrol.* **2012**, *456–457*, 12–29. [CrossRef]

61. Pietikäinen, J.P.; O'Donnell, D.; Teichmann, C.; Karstens, U.; Pfeifer, S.; Kazil, J.; Podzun, R.; Fiedler, S.; Kokkola, H.; Birmili, W.; et al. The regional aerosol-climate model REMO-HAM. *Geosci. Model Dev.* **2012**, *5*, 1323–1339. [CrossRef]

62. Aalto, J.; Pirinen, P.; Heikkinen, J.; Venalainen, A. Spatial interpolation of monthly climate data for Finland: Comparing the performance of kriging and generalized additive models. *Theor. Appl. Climatol.* **2013**, *112*, 99–111. [CrossRef]

63. Räisänen, J.; Räty, O. Projections of daily mean temperature variability in the future: Cross-validation tests with ENSEMBLES regional climate simulations. *Clim. Dyn.* **2013**, *41*, 1553–1568. [CrossRef]

64. Räty, O.; Räisanen, J.; Ylhäsi, J.S. Evaluation of delta change and bias correction methods for future daily precipitation: Intermodel cross-validation using ENSEMBLES simulations. *Clim. Dyn.* **2014**, *42*, 2287–2303. [CrossRef]

65. Metsämäki, S.J.; Anttila, S.T.; Markus, H.J.; Vepsäläinen, J.M. A feasible method for fractional snow cover mapping in boreal zone based on a reflectance model. *Remote Sens. Environ.* **2005**, *95*, 77–95. [CrossRef]

66. Metsämäki, S.; Mattila, O.-P.; Pulliainen, J.; Niemi, K.; Luojus, K.; Böttcher, K. An optical reflectance model-based method for fractional snow cover mapping applicable to continental scale. *Remote Sens. Environ.* **2012**, *123*, 508–521. [CrossRef]

67. Badeck, F.-W.; Bondeau, A.; Böttcher, K.; Doktor, D.; Lucht, W.; Schaber, J.; Sitch, S. Responses of spring phenology to climate change. *New Phytol.* **2004**, *162*, 295–309. [CrossRef]

68. Doktor, D.; Bondeau, A.; Koslowski, D.; Badeck, F.-W. Influence of heterogeneous landscapes on computed green-up dates based on daily AVHRR NDVI observations. *Remote Sens. Environ.* **2009**, *113*, 2618–2632. [CrossRef]

69. Härmä, P.; Teiniranta, R.; Törmä, M.; Repo, R.; Järvenpää, E.; Kallio, E. *CLC2000 Finland: Final Report*; Finnish Environment Institute, Geoinformatics and Land Use Division: Helsinki, Finland, 2005.

70. Delbart, N.; Le Toan, T.; Kergoat, L.; Fedotova, V. Remote sensing of spring phenology in boreal regions: A free of snow-effect method using NOAA-AVHRR and SPOT-VGT data (1982–2004). *Remote Sens. Environ.* **2006**, *101*, 52–62. [CrossRef]

71. Moulin, S.; Kergoat, L.; Viovy, N.; Dedieu, G. Global-scale assessment of vegetation phenology using NOAA/AVHRR satellite measurements. *J. Clim.* **1997**, *10*, 1154–1155. [CrossRef]

72. Jönsson, A.M.; Eklundh, L.; Hellström, M.; Bärring, L.; Jönsson, P. Annual changes in MODIS vegetation indices of Swedish coniferous forests in relation to snow dynamics and tree phenology. *Remote Sens. Environ.* **2010**, *114*, 2719–2730. [CrossRef]

73. Delbart, N.; Picard, G.; Le Toan, T.; Kergoat, L.; Quegan, S.; Woodward, I.A.N.; Dye, D.; Fedotova, V. Spring phenology in boreal Eurasia over a nearly century time scale. *Glob. Chang. Biol.* **2008**, *14*, 603–614. [CrossRef]

74. Savitzky, A.; Golay, M.J.E. Smoothing and differentiation of data by simplified least squares procedures. *Anal. Chem.* **1964**, *36*, 1627–1639. [CrossRef]

75. Chen, J.; Jönsson, P.; Tamura, M.; Gu, Z.; Matsushita, B.; Eklundh, L. A simple method for reconstructing a high-quality NDVI time-series data set based on the Savitzky-Golay filter. *Remote Sens. Environ.* **2004**, *91*, 332–344. [CrossRef]

76. Jönsson, P.; Eklundh, L. TIMESAT-a program for analyzing time-series of satellite sensor data. *Comput. Geosci.* **2004**, *30*, 833–845. [CrossRef]

77. Karlsen, S.; Solheim, I.; Beck, P.; Høgda, K.; Wielgolaski, F.; Tømmervik, H. Variability of the start of the growing season in Fennoscandia, 1982–2002. *Int. J. Biometeorol.* **2007**, *51*, 513–524. [CrossRef] [PubMed]

78. Karlsen, S.R.; Elvebakk, A.; Høgda, K.A.; Johansen, B. Satellite-based mapping of the growing season and bioclimatic zones in Fennoscandia. *Glob. Ecol. Biogeogr.* **2006**, *15*, 416–430. [CrossRef]

79. Rousi, M.; Heinonen, J. Temperature sum accumulation effects on within-population variation and long-term trends in date of bud burst of European white birch (*Betula pendula*). *Tree Physiol.* **2007**, *27*, 1019–1025. [CrossRef] [PubMed]

80. Drolet, G.G.; Huemmrich, K.F.; Hall, F.G.; Middleton, E.M.; Black, T.A.; Barr, A.G.; Margolis, H.A. A MODIS-derived photochemical reflectance index to detect inter-annual variations in the photosynthetic light-use efficiency of a boreal deciduous forest. *Remote Sens. Environ.* **2005**, *98*, 212–224. [CrossRef]

81. Jin, H.; Eklundh, L. A physically based vegetation index for improved monitoring of plant phenology. *Remote Sens. Environ.* **2014**, *152*, 512–525. [CrossRef]

82. Houborg, R.; Fisher, J.B.; Skidmore, A.K. Advances in remote sensing of vegetation function and traits. *Int. J. Appl. Earth Observ. Geoinf.* **2015**, *43*, 1–6. [CrossRef]

83. Joiner, J.; Yoshida, Y.; Vasilkov, A.P.; Schaefer, K.; Jung, M.; Guanter, L.; Zhang, Y.; Garrity, S.; Middleton, E.M.; Huemmrich, K.F.; et al. The seasonal cycle of satellite chlorophyll fluorescence observations and its relationship to vegetation phenology and ecosystem atmosphere carbon exchange. *Remote Sens. Environ.* **2014**, *152*, 375–391. [CrossRef]

84. Poggio, L.; Gimona, A.; Brown, I. Spatio-temporal MODIS EVI gap filling under cloud cover: An example in Scotland. *ISPRS J. Photogr. Remote Sens.* **2012**, *72*, 56–72. [CrossRef]

85. Weiss, D.J.; Atkinson, P.M.; Bhatt, S.; Mappin, B.; Hay, S.I.; Gething, P.W. An effective approach for gap-filling continental scale remotely sensed time-series. *ISPRS J. Photogr. Remote Sens.* **2014**, *98*, 106–118. [CrossRef] [PubMed]

86. Zhang, C.; Li, W.; Travis, D.J. Restoration of clouded pixels in multispectral remotely sensed imagery with cokriging. *Int. J. Remote Sens.* **2009**, *30*, 2173–2195. [CrossRef]

87. Jones, M.O.; Jones, L.A.; Kimball, J.S.; McDonald, K.C. Satellite passive microwave remote sensing for monitoring global land surface phenology. *Remote Sens. Environ.* **2011**, *115*, 1102–1114. [CrossRef]

88. Finnish Meteorological Institute. GlobSnow. Available online: http://www.globsnow.info (accessed on 5 July 2016).

89. Kolari, P.; Chan, T.; Porcar-Castell, A.; Bäck, J.; Nikinmaa, E.; Juurola, E. Field and controlled environment measurements show strong seasonal acclimation in photosynthesis and respiration potential in boreal Scots pine. *Front. Plant Sci.* **2014**, *5*. [CrossRef] [PubMed]

90. Thum, T.; Aalto, T.; Laurila, T.; Aurela, M.; Lindroth, A.; Vesala, T. Assessing seasonality of biochemical CO_2 exchange model parameters from micrometeorological flux observations at boreal coniferous forest. *Biogeosciences* **2008**, *5*, 1625–1639. [CrossRef]

91. Robakowski, P. Susceptibility to low-temperature photoinhibition in three conifers differing in successional status. *Tree Physiol.* **2005**, *25*, 1151–1160. [CrossRef] [PubMed]

92. Sevanto, S.; Suni, T.; Pumpanen, J.; Grönholm, T.; Kolari, P.; Nikinmaa, E.; Hari, P.; Vesala, T. Wintertime photosynthesis and water uptake in a boreal forest. *Tree Physiol.* **2006**, *26*, 749–757. [CrossRef] [PubMed]

93. Ekici, A.; Beer, C.; Hagemann, S.; Boike, J.; Langer, M.; Hauck, C. Simulating high-latitude permafrost regions by the JSBACH terrestrial ecosystem model. *Geosci. Model Dev.* **2014**, *7*, 631–647. [CrossRef]

94. Pudas, E.; Leppälä, M.; Tolvanen, A.; Poikolainen, J.; Venäläinen, A.; Kubin, E. Trends in phenology of *Betula pubescens* across the boreal zone in Finland. *Int. J. Biometeorol.* **2008**, *52*, 251–259. [CrossRef] [PubMed]

95. Bennie, J.; Kubin, E.; Wiltshire, A.; Huntley, B.; Baxter, R. Predicting spatial and temporal patterns of bud-burst and spring frost risk in north-west Europe: The implications of local adaptation to climate. *Glob. Chang. Biol.* **2010**, *16*, 1503–1514. [CrossRef]

96. Linkosalo, T.; Lappalainen, H.K.; Hari, P. A comparison of phenological models of leaf bud burst and flowering of boreal trees using independent observations. *Tree Physiol.* **2008**, *28*, 1873–1882. [CrossRef] [PubMed]

97. Botta, A.; Viovy, N.; Ciais, P.; Friedlingstein, P.; Monfray, P. A global prognostic scheme of leaf onset using satellite data. *Glob. Chang. Biol.* **2000**, *6*, 709–725. [CrossRef]

IV

ORIGINAL RESEARCH

Predictive power of remote sensing versus temperature-derived variables in modelling phenology of herbivorous insects

Juha Pöyry[1] (iD), Kristin Böttcher[1], Stefan Fronzek[1], Nadine Gobron[2], Reima Leinonen[3], Sari Metsämäki[1] & Raimo Virkkala[1]

[1]Finnish Environment Institute (SYKE), P.O. Box 140, Helsinki, FI-00251, Finland
[2]European Commission Joint Research Centre, Directorate D Sustainable Resources, Via E. Fermi 2749, TP 440, Ispra (VA) 210207, Italy
[3]Kainuu Centre for Economic Development, Transport and the Environment, P.O. Box 115, Kajaani FI-87101, Finland

Abstract

Application of remote sensing datasets in modelling phenology of heterotrophic animals has received little attention. In this work, we compare the predictive power of remote sensing versus temperature-derived variables in modelling peak flight periods of herbivorous insects, as exemplified by nocturnal moths. Moth phenology observations consisted of weekly observations of five focal moth species (*Orthosia gothica*, *Ectropis crepuscularia*, *Cabera exanthemata*, *Dysstroma citrata* and *Operophtera brumata*) gathered in a national moth monitoring scheme in Finland. These species were common and widespread and had peak flight periods in different seasons. Temperature-derived data were represented by weekly accumulating growing degree days (GDD) calculated from gridded temperature observations. Remote sensing data were obtained from three sources: (1) snow melt-off date from the MODIS daily snow maps, (2) greening date using the NDWI from MODIS data and (3) dates of start, maximum and end of growing season based on the JRC FAPAR products. Peak phenology observations of moths were related to different explanatory variables by using linear mixed effect models (LMM), with 70% of the data randomly selected for model calibration. Predictive power of models was tested using the remaining 30% of the data. Remote sensing data (snow melt-off and vegetation greening date) showed the highest predictive power in two moth species flying in the early and late spring, whereas in the three other species none of the variables showed reasonable predictive power. Flight period of the spring species coincides with natural events such as snow melt or vegetation greening that can easily be observed using remote sensing techniques. We demonstrate the applicability of our methodology by predictive spatial maps of peak flight phenology covering the entire Finland for two of the focal species. The methods are applicable in situations that require spatial predictions of animal activity, such as the management of populations of insect pest species.

Introduction

Remote sensing data have been used to observe vegetation phenology (White et al. 2009; Ganguly et al. 2010; Gonsamo and Chen 2016; Vrieling et al. 2017) or the amount of annual net primary productivity across continents (Myneni et al. 1997; Running et al. 2004; Liu et al. 2013), and their change over time (Ivits et al. 2012; Zhang et al., 2014; Zhao et al. 2015). While modelling of the phenology of plants and vegetation has utilized both temperature-derived and remote sensing data, modelling the phenology of animals has typically relied on using temperature-derived measures such as growing degree days as predictor variables (e.g. Roy et al. 2001; Nietschke et al.

2007; Hodgson et al. 2011), but very few studies have used remote sensing data. By contrast, most studies combining animals and remote sensing data have focused on predicting species occurrence in space (Leyequien et al. 2007; Pettorelli et al. 2011, 2014), with only some exceptions focusing on temporal occurrence of insect abundance (Jepsen et al. 2009a; Trierweiler et al. 2013; Sweet et al. 2015; Olsson et al. 2016).

Several different satellite-based remote sensing indices have been developed and used in studies of vegetation phenology in recent years. These include the Normalized Difference Vegetation Index (NDVI) (Badeck et al. 2004; Karlsen et al. 2006; White and Nemani 2006; Pettorelli et al. 2011), the Normalized Difference Water Index (NDWI) (Delbart et al. 2005, 2008) and the Fraction of Absorbed Photosynthetically Active Radiation (FAPAR) (Verstraete et al. 2008). Thus, it is now possible to explore if such variables could be used in addition to temperature-derived variables to model phenology of animals. Developing such methodologies is also timely as they will support the global targets of conserving biodiversity set by the Convention of Biological Diversity at the Aichi conference (CBD, 2014; O'Connor et al. 2015). One of these targets is development of novel methods for monitoring phenology of terrestrial ecosystems. Therefore, novel initiatives of using earth observation techniques in monitoring changes in ecosystems, including phenology of animal species, at both regional and global scales are urgently needed (e.g. Lausch et al. 2016; Vihervaara et al. 2017).

In this study we test if the phenology of heterotrophic animals, as exemplified by nocturnal moths, can be modelled using remote sensing variables and temperature-derived variables (growing degree days), and compare the predictive power of models fitted using different sets of variables. Firstly, we are particularly interested in understanding under what circumstances do models based on remote sensing data show reasonable power in predicting insect phenology and how they compare to models using variables derived from temperature observations. Secondly, and building on the first aim, we derive predictive spatial models that can be used as phenological indicators to describe the seasonal progress of flight periods of herbivorous insects. As the focal group we selected nocturnal moths, for which we use an extensive monitoring dataset collected between 1993 and 2012 across one country, Finland. Moths comprise a particularly suitable species group for a comparison of predictive power between remote sensing and temperature-derived measures, as they are widespread and abundant enough to allow collecting phenological observations across large geographic areas by using standard methods.

Materials and Methods

Study area

The study area covers the total land area of Finland (338 400 km^2), which largely belongs to the boreal forest zone, with some deciduous-dominated forests in the southern parts of the country. Forests dominate the landscape throughout the country all the way to the very northern parts, which are characterized by subarctic tundra and open bogs. Agricultural areas are concentrated in the south-western parts. Finland's climate is intermediate, combining characteristics of both a maritime and a continental climate. According to Köppen's climate classification most of Finland belongs to the subarctic (or boreal) climate zone (Dfc), whereas the southernmost parts of the country are situated in the warm-summer humid continental zone (Dfb). Snow cover typically covers the whole country, arriving in October–December, melting in April–June, depending on the year. In mild winters the southern parts of the country may lack a continuous seasonal snow cover.

Moth phenology data

The observations of moth phenology gathered through the Finnish national moth monitoring scheme (Nocturna) constitute the basic phenology data in this work (Leinonen et al. 2016). Moths are observed using light traps that are equipped with Hg bulbs and run every night from the early spring to the late autumn, typically between April and October. The traps are usually emptied weekly and the moth specimens identified by voluntary observers. During the period 1993–2012, altogether 208 trap sites were included in the monitoring network (Leinonen et al. 2016). Of these sites, 51 traps with the least temporal gaps and altogether consisting of 810 trapping years with continuous moth observations were selected for data extraction (Fig. S1).

The focal moth species were selected for phenology modelling based on the following criteria: wide distributional area, high abundance and timing of the peak flight period spread in different parts of the season. The selected five focal species are: *Orthosia gothica* (family Noctuidae, peak flight in late April–early May), *Ectropis crepuscularia* (Geometridae, late May–early June), *Cabera exanthemata* (Geometridae, late June–early July), *Dysstroma citrata* (Geometridae, mid-August) and *Operophtera brumata* (Geometridae, late September–early October). Stages of life cycle of the five focal species in relation to the phenological events detected using remote sensing methods and used in this work are presented in Figure 1. Of the five focal species, *O. brumata* has been subject to considerable research as the species is a forest pest in parts of its range, whereas the four other species have been subject to very few or no
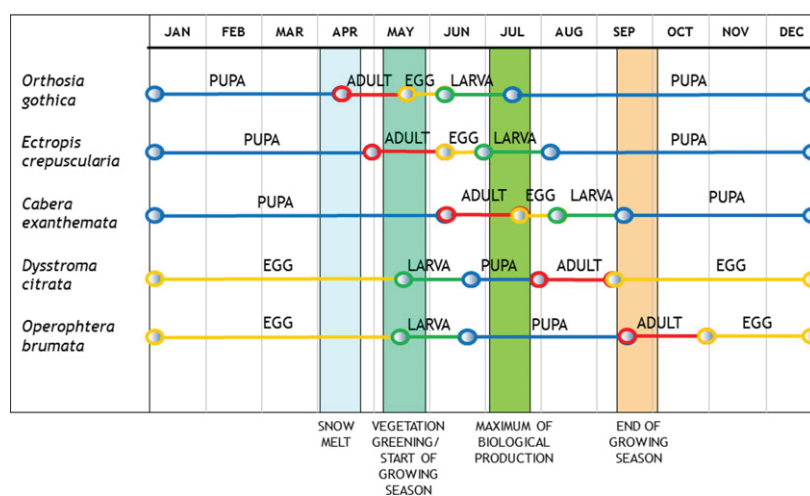
Figure 1. Annual life cycle of the five focal moth species (*Orthosia gothica*, *Ectropis crepuscularia*, *Cabera exanthemata*, *Dysstroma citrata* and *Operophtera brumata*) and timing of natural phenomena observed with remote sensing and used in this work. The figure represents a typical phenological sequence during an average year in the southern part of Finland.

ecological studies at all. In *O. brumata*, timing of egg hatching and larval development have been topics of studies due to their high importance to population growth rate and development of defoliations (Jepsen et al. 2009b; van Asch et al. 2013). The nomenclature of moths follows Aarvik et al. (2017).

Peak flights were selected to represent timing of the flight periods because they are less affected by inter-annual abundance variation than other descriptors of the flight period such as start, end and length (e.g. Roy and Sparks 2000). This is because the length of a species' flight period may appear longer in years of high abundance compared to years of low abundance. Peak flights were calculated based on the median occurrence of individuals per year and trap site. Mid-day of the median observation period was used as the peak flight date. Although moth traps are typically emptied weekly, there is some variation in the lengths of observational periods for logistic reasons. Therefore, inaccuracy (expressed as the average length of observational period divided by two) in the mid-day values of the peak flight periods varies slightly across the focal species (due to slight variations in the length of the observational period): *Orthosia gothica* (±3.83 days), *Ectropis crepuscularia* (±3.67 days), *Cabera exanthemata* (±3.81 days), *Dysstroma citrata* (±3.85 days) and *Operophtera brumata* (±4.26 days).

Explanatory variables

Geographical variables

Location of each trap site is represented by the latitudinal coordinate of the Finnish national uniform grid system in

metres (YKJ) to account for a potential latitudinal trend in timing of the peak flight. Two of the five focal species (*Orthosia gothica* and *Operophtera brumata*) showed a marked latitudinal gradient in timing of their peak flight period (Fig. S2a, S2e).

Climatic variables

Time series of daily mean temperatures for the grid cells containing the moths trap locations were extracted from daily gridded temperature dataset in 10 km × 10 km resolution (Venäläinen et al. 2005; updated). If the location of a moth trap was exactly on the edge between two 10-km grid cells, the cell to the east and north of that point was used. Accumulated temperature sums (growing degree days, GDD) above a base temperature were calculated for the locations of moth traps for each year of the period 1993 to 2012. A total of 18 different summation periods were calculated, all starting on 1 January of each year and ending between 1 April (or 31 March in leap years) and 29 July (28 July in leap years) in weekly intervals. GDDs were calculated using 16 different base temperatures between −5°C and 10°C with intervals of one degree. This range of base temperatures was selected because previous empirical and modelling studies on insect phenology have shown that the base temperature of accumulated temperature sum affecting adult phenology varies at least from −5°C to 10°C (Pritchard et al. 1996; Valtonen et al. 2011). This resulted in 288 different GDD indices (16 base temperature times 18 summation periods).

Previous modelling studies focusing on moth phenology that included the focal species of our work have

reported variable base temperatures used in calculations of the temperature sums. For example, Valtonen et al. (2011) reported the base temperatures of −5°C and 2°C for *Dysstroma citrata* and *Orthosia gothica*, respectively. By contrast, Valtonen et al. (2014) reported the following base temperatures: −5.8°C and −6.0°C for *Orthosia gothica*, 1.9°C and 2.4°C for *Ectropis crepuscularia*, and 3.2°C for *Cabera exanthemata*. Thus, base temperatures that produce the best model fit vary from model to model and are also dependent on what variables are included in the model.

Remote sensing variables

Three kinds of remote sensing products were used in the phenology modelling:

(1) Date of snow melt in spring was derived for each trap site from time series of daily Pan-European Fractional Snow Cover (FSC) products from CryoLand (Copernicus Service Snow and Land Ice, http://www.cryoland.eu/), available for the years 2001–2016 (Nagler et al. 2015). A particular method for extraction of melt-off day despite the gaps in the FSC time series (due to cloudiness that prevent the observations) was developed at the Finnish Environment Institute (SYKE) (Metsämäki et al. 2017). The actual method for FSC retrieval from satellite imagery (NASA Terra/MODIS, Moderate Resolution Imaging Spectroradiometer, in the case of CryoLand) was also developed at SYKE (Metsämäki et al. 2005, 2012), and complemented by a latitude-dependent adjustment related to snow-free ground detection rules within the CryoLand project. Temporal resolution of the snow melt date is 1 day, but days missing due to cloudiness cause some uncertainty in the estimate. Our investigations covering CryoL and FSC time series and the corresponding in situ observations on snow depth for 2001–2016 show that for Finland the mean absolute difference (melt-off day based on FSC–melt-off day from in situ) is less than 5 days, with bias of ~2.7 days. The positive bias indicates that CryoLand FSC-based melt-off day is slightly overestimated (i.e. delayed) compared to the in situ-observed melt-off day, the latter indicated by the first day of 0 cm snow depth starting the snow-free season.

(2) We selected the NDWI for the determination of the greening date of deciduous species in Finland because its detection from NDVI can be affected by snow melt in boreal areas (Moulin et al. 1997; Delbart et al. 2006). Instead, the NDWI decreases during snow melt and increases during the greening up (Delbart et al. 2005), and thus the effect of snow on the observed greening date can be reduced. The date of

greening of the vegetation in Finland was determined from MODIS-derived time series of the NDWI following the method of Delbart et al. (2005) and further described in Böttcher et al. (2016). The greening date was calculated for MODIS pixels with vegetation cover. The vegetation cover per MODIS pixel was estimated from the national CORINE Land Cover 2006 raster product with a spatial resolution of 25 m provided by the Finnish Environment Institute (2009). We took into account all vegetated land cover types. Both understory growth and canopy phenology contribute to the land surface greening observed from the NDWI. Their respective contributions depend on canopy closure, sun and view angles and understory type. At a southern boreal site in Finland the contribution of the understory reflectance was below 30% in the near infrared at the beginning of the growing season in May for different stand types (Rautiainen and Lukes 2015). The vegetation development in spring in boreal forests Finland occurs during a very short time interval and there is no mismatch in the seasonal development of understory and the forest canopy (Rautiainen et al. 2011). The resolution of the greening date maps is $0.05° \times 0.05°$. Temporal resolution of the NDWI is 1 day, but days missing due to cloudiness cause some uncertainty in the estimate of the greening date. For years 2001–2012, depending on the location, in average 34–73% of daily observations were missing during the period of April–July. The greening date was then extracted in the satellite map from the closest pixel to the trap site. These data are available for the years 2001–2012. The greening date in deciduous forests shows good correspondence (RMSE 1 week) with the date of birch bud break in Finland (Böttcher et al. 2016).

(3) Fraction of Absorbed Photosynthetically Active Radiation (FAPAR)-derived dates of start (FSGS), peak (FMD) and end (FEGS) of growing season were acquired from the Joint Research Centre (JRC) datasets (Gobron et al. 2006; Jung et al. 2008; Ceccherini et al. 2013b, 2014), and extracted at each trap site. The FAPAR used in this study covers the period from January 1998 to December 2012 using harmonized SeaWiFS and MERIS datasets with a nominal spatial resolution of 1.5 km (Gobron et al. 2006; Ceccherini et al. 2013a). The FAPAR values correspond to the 10-day time composite products spatially averaged over 3 x 3 pixels around the trap sites for FSGS and FEGS. For FMD, FAPAR values were derived for the pixel overlapping with the trap site.

Examples of timing of the peak flight periods of the focal moth species, snow melt-off dates (SMD), vegetation greening dates derived from the NDWI and dates of

Table 1. The number of peak flight observations in the selected 51 sites and across the five focal moth species with different limitations of data.

Species	Total number of flight period observations in 1993–2012	Number of peak flight observations in 1993–2012	Peak flight observations in 2003–2011 with remote sensing data
Orthosia gothica	3644	790	282
Ectropis crepuscularia	2291	608	220
Cabera exanthemata	4176	704	231
Dysstroma citrata	5890	829	520
Operophtera brumata	2130	709	449

FAPAR start (FSGS), peak (FMD) and end (FEGS) of the growing season are presented in Figure S3. In order to compare the predictive power of models built using different variables, datasets of moth phenology, climatic variables and remote sensing variables were combined for the period 2003–2011. The impact of data availability on the amount of peak flight observations in the five focal species is shown in Table 1. Cross-correlations among the explanatory variables in all five focal species are shown in Table S1.

Modelling methods

An overview of datasets used and analysis steps conducted for deriving predictive models of moth phenology is presented in Figure 2. Details of modelling methods are described in the following paragraphs.

Comparing predictive power of different variables

Peak flight dates of each focal moth species were related to explanatory variables using linear mixed effect models (LMM) (Venables and Ripley 2002). Explanatory variables tested for all focal species included latitude and thermal sum (GDD), whereas the inclusion of remote sensing variables differed depending on timing of the peak flight period of the species in question (Table 2). A single GDD index for each species was selected by minimizing the value for the Akaike Information Criterion (AIC; Burnham and Anderson 2002) in univariate LMMs of the 288 GDD indices as explanatory variable.

The performance of LMMs was evaluated for both total models including all explanatory variables and for univariate models, that is, models including one variable at a time.

This was done in order to determine the proportion of variation in timing of the peak flight periods that may be explained by all variables and the explanatory power of individual variables, respectively (e.g. Guisan and Zimmerman 2000). For this purpose, data were randomly divided into two sets in each five focal species: model fitting (70% of the data) and model validation (30%). This was done in order to allow for independent evaluation of model performance (i.e. predictive power). Predictive power was calculated here as the proportion of explained variance (r^2) in the model testing part (30%) of the data (Guisan and Zimmerman 2000). Calculation of predictive power was done with models either excluding (i.e. producing an average prediction across sites by setting 'level = 0', see Pinheiro et al. 2014) or including site information as a random effect term. This was done in order to get an estimate of what proportion of the predictive power is due to the observational site and what proportion is due to the variation in the explanatory variable; with higher proportion of the latter expected to produce more reliable spatial predictions. This choice was done because calculation of an average prediction across large spatial scales is often more useful so that the general trend in phenology patterns will not be masked by local variation that is due to, for example, microclimatic factors. All LMMs were fitted as implemented in the nlme library, version 3.1-121 (Pinheiro et al. 2014) within the R statistical environment, version 3.2.2 (R Core Team, 2015).

Producing spatial predictive maps of peak flight period

In order to produce spatial predictive maps of timing of the peak flight period for the focal species, we selected the total model including all variables and the single variable which showed reasonable predictive power ($r^2 > 0.3$) in each respective species, that is, snow melt-off date in one species (*Orthosia gothica*) and vegetation greening date in another species (*Ectropis crepuscularia*) (Table 2). Spatial predictions were derived with the models excluding site information (Table S2), as described above. Maps showing the spatial distribution of the peak flight date in Finland were produced for the average period 2001–2013, an example year for an early peak flying period (2007) and an example late year (2006), chosen on the basis of a high and a low March–May mean temperature, respectively. In addition, an average prediction for 2001–2013 based on weekly accumulating thermal sum (i.e. GDD index with summation period starting on 1 January) was produced for both species. Thus, seven prediction maps are presented for both species.

To produce maps based on all variables, the input datasets were re-sampled to a common latitude–longitude grid at a spatial resolution of 0.05 × 0.05 degrees. The
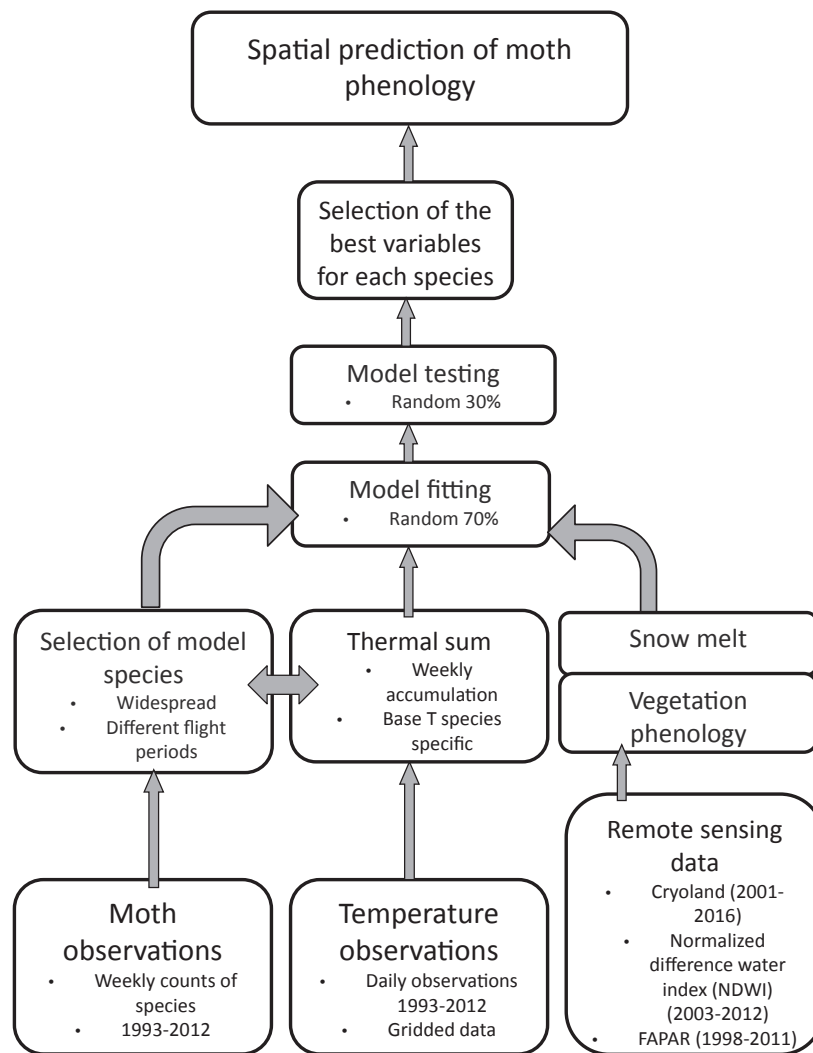
Figure 2. Flowchart of datasets used and analysis steps conducted for deriving predictive models of moth phenology.

maps of the greening date were smoothed and gap filled with a median filter with a kernel size of 3 × 3 pixels prior to the application of the multivariate model. For FSGS the mean of the period 2001–2011 was used for the calculation of the average prediction maps for 2001–2013. Selection of the GDD index is explained above (see the section 'Comparing predictive power of different variables'). Peak flight dates were transformed into periods of 5 days in length to facilitate drawing the maps.

Results

Comparison of variables

The predictive power (r^2) of total LMMs (i.e. models including all corresponding explanatory variables)

calculated for the five focal species varied between 0.05 and 0.60 when site information was excluded and between 0.14 and 0.69 when site information was included (Table 2, Fig. S4). In univariate LMMs there was large variation in predictive power between species and variables but in most cases predictive power decreased markedly when site information was excluded (Table 2, Fig. 3, Fig. S4). In the early spring species (*Orthosia gothica*) snow melt-off date showed the highest predictive power that was retained after exclusion of site information (from $r^2 = 0.68$ to $r^2 = 0.59$) (Fig. 3A). Peak flight of the late spring species (*Ectropis crepuscularia*; Fig. 3B) was associated equally strongly with GDD and the greening date of vegetation ($r^2 = 0.34$, site information excluded), whereas in the late autumn species (*Operophtera brumata*, Fig. 3E), the strongest predictor of the peak

Table 2. Predictive power (r^2) of linear mixed effect models (LMM) for the peak flight date in the randomly selected validation part (30%) of the data.

Species	Total model (all variables)	Latitude (Lat)	Weekly accumulating growing degree days (GDD)	Snow melt date (SMD)	Greening date (GD)	FAPAR start of growing season (FSGS)	FAPAR maximum date (FMD)	FAPAR end of growing season (FEGS)
Orthosia gothica	0.60[1]	0.38	0.42[1]	0.59	0.38	0.05	—	—
	(0.69[1])	(0.58)	(0.60[1])	(0.68)	(0.58)	(0.54)		
Ectropis crepuscularia	0.46[2]	0.17	0.34[2]	0.19	0.34	0.00	—	—
	(0.46[2])	(0.12)	(0.31[2])	(0.19)	(0.39)	(0.05)		
Cabera exanthemata	0.05[3]	0.05	0.01[3]	—	0.03	0.01	0.00	—
	(0.14[3])	(0.19)	(0.12[3])		(0.18)	(0.13)	(0.16)	
Dysstroma citrata	0.07[4]	0.00	0.03[4]	—	—	—	0.01	0.00
	(0.27[4])	(0.15)	(0.27[4])				(0.20)	(0.19)
Operophtera brumata	0.48[5]	0.51	0.04[5]	—	—	—	0.01	0.01
	(0.56[5])	(0.57)	(0.55[5])				(0.56)	(0.55)

The weekly accumulating GDDs depict the base threshold temperature (T_b) used in the calculation as well as the date (DOY) that was selected for model calibration on the basis of Akaike Information Criterion (AIC) (see the superscripts). Predictive power is calculated for models both by excluding (i.e. by producing predictions averaged across sites) and by including site information (as a random effect term, in brackets). – indicates that the variable was not included in the respective model.
Weekly accumulating GDD parameters:
[1]Base temperature (T_b) = −5°C, summation period day-of-the-year (DOY) = 1–210.
[2]T_b = 9°C, DOY = 1–133.
[3]T_b = 10°C, DOY = 1–133.
[4]T_b = 10°C, DOY = 1–210.
[5]T_b = 6°C, DOY = 1–112.

flight was latitude (r^2 = 0.51, site information excluded). Peak flight periods of the mid and late summer species (*Cabera exanthemata*, *Dysstroma citrata*, Fig. 3C–D) were only weakly associated with the inspected explanatory variables (r^2 < 0.1, site information excluded).

Spatial predictive models

Spatial prediction maps were produced for the two species (*Orthosia gothica* and *Ectropis crepuscularia*) for which remote sensing variables and GDD showed meaningful predictive power (Figs. 4 and 5). Separate predictions are presented for a total model including all variables, a model including one remote sensing variable with the highest predictive power (snow melt-off date in *Orthosia* (Fig. 4) and vegetation greening date in *Ectropis* (Fig. 5)) and a model based on an alternative variable (GDD). Under each model, example predictions are given for an average period of 2001–2013, a phenologically late year (2006) and a phenologically early year (2007). For the alternative variable (GDD) model, only an average prediction of 2001–2013 is given.

In *Orthosia gothica*, the peak flight starts on 25–29 April in south-western Finland and shifts by 20–24 May to the northernmost part of the country according to average predictions for the period 2001–2013 (Fig. 4A, D,

G). In an early example year (2007) the predicted peak flight occurred already on 15–19 April in south-western Finland (Fig. 4C and F), whereas in a late year (2006) the peak flight period was postponed to 30 April–4 May in the south of the country (Fig. 4B, E). However, in 2006 the latitudinal shift in timing of the peak flight period occurred faster than in 2007. In general, models based on all variables (Fig. 4A–C) and models based on a single variable (Fig. 4D–G) produced qualitatively similar spatiotemporal gradients for the occurrence of the peak flight period of *O. gothica*.

In *Ectropis crepuscularia*, the peak flight starts on 15–19 May in south-western Finland and shifts by 30 May–3 June to the northernmost part of the species range according to average predictions for the period 2001–2013 (Fig. 5A, D, G). In an early example year (2007) the predicted peak flight occurred on 10–14 May in southern Finland (Fig. 5C, F), whereas in a late year (2006) the peak flight period was postponed to 20–24 May in southern Finland but occurred then by 25–29 May across the entire distributional range in Finland (Fig. 5B, E). In contrast to *O. gothica*, in *E. crepuscularia* models based on all variables (Fig. 5A–C) predicted longer spatiotemporal gradients for the occurrence of the peak flight period than did models based on a single variable (Fig. 5D–G).
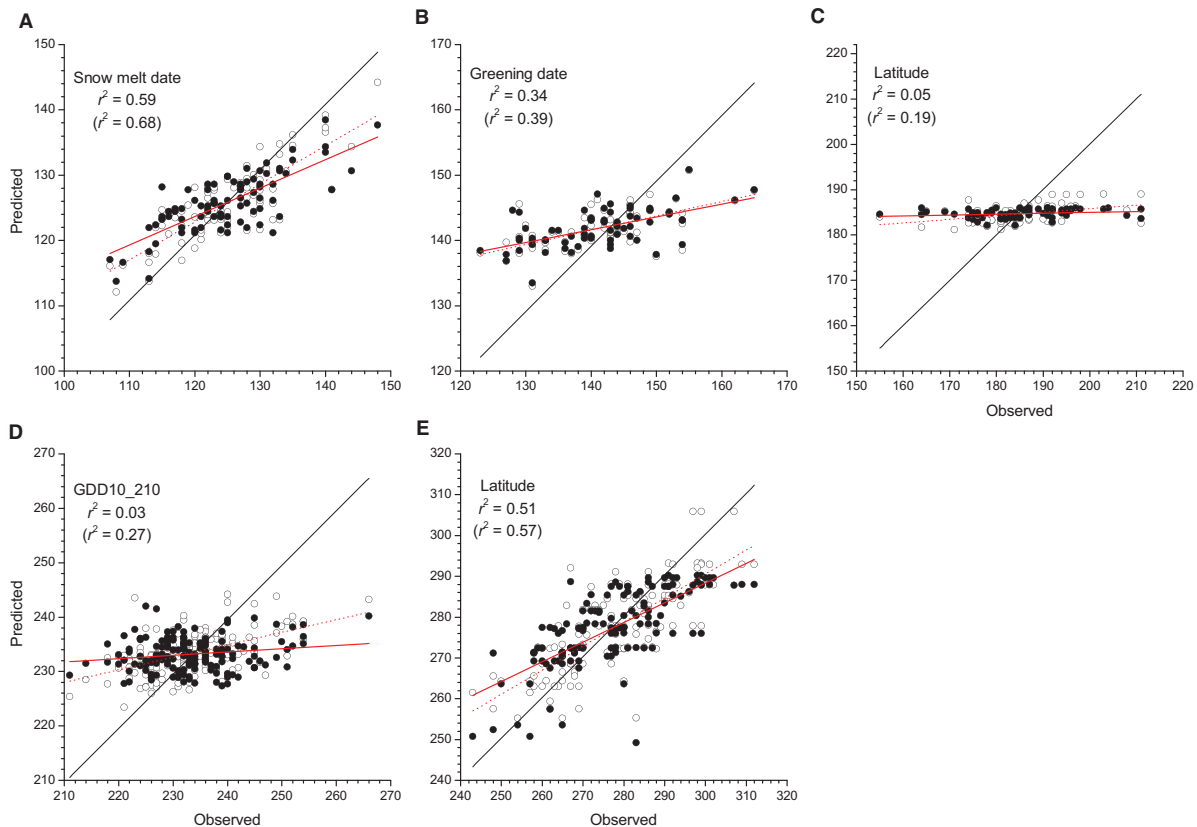
Figure 3. Predictive power of linear mixed effect models (LMM) including the single explanatory variable that showed the highest r^2 value in the randomly selected 30% of the data across the five focal species: (A) *Orthosia gothica*, (B) *Ectropis crepuscularia*, (C) *Cabera exanthemata*, (D) *Dysstroma citrata* and (E) *Operophtera brumata*. All panels show dots for observed versus predicted values of peak flight dates, with black dots excluding (i.e. average prediction where level = 0) and open dots including site location in predictions. Red solid lines and dotted lines depict the model fits when site location is excluded (upper r^2 value) and included (r^2 value in parentheses), respectively, and black line depicts the identity line y = x.

Discussion

The feasibility of remote sensing data in modelling and predicting phenology of animal species has received only little attention (cf. Roy et al. 2001; Nietschke et al. 2007; Hodgson et al. 2011). This is surprising considering that such methods are potentially very useful in the field of applied ecological sciences, including management of natural resources (White and Nemani 2006). Previously, earth observation products have been used to detect forest defoliations caused by pest species such as gypsy moth (*Lymantria dispar*; de Beurs and Townsend 2008; Spruce et al. 2011; Foster et al. 2013) and autumnal moth (*Epirrita autumtata*; Jepsen et al. 2009a; Babst et al. 2010; Olsson et al. 2016). Based on similar methodology, Trierweiler et al. (2013) and Sweet et al. (2015) developed NDVI-based models predicting overall temporal abundance of canopy arthropod biomass of grasshoppers and defoliation of birch trees, respectively, but they did not attempt predicting phenology of individual species. With

our work, we provide first tools towards a more widespread application of remote sensing datasets in modelling phenology of heterotrophic animal species and producing practical applications of spatial predictions.

According to our results, predictive ability of different variables is strongly affected by species identity. Notably, only in the species flying in early spring (*Orthosia gothica*) and late spring (*Ectropis crepuscularia*), remote sensing variables show good predictive power. In the three other species, however, none of the temperature-derived (i.e. thermal sum) and remote sensing variables showed meaningful predictive power. This result indicates that remote sensing variables are more clearly correlated with phenological patterns of those species in which the flight period coincides with distinguishable natural events such as snow melt or vegetation greening, which can easily be observed using remote sensing techniques. Thus, flight periods of these species also show potential in monitoring the impacts of climate change. For species that have their activity period in other parts of the season, it may be
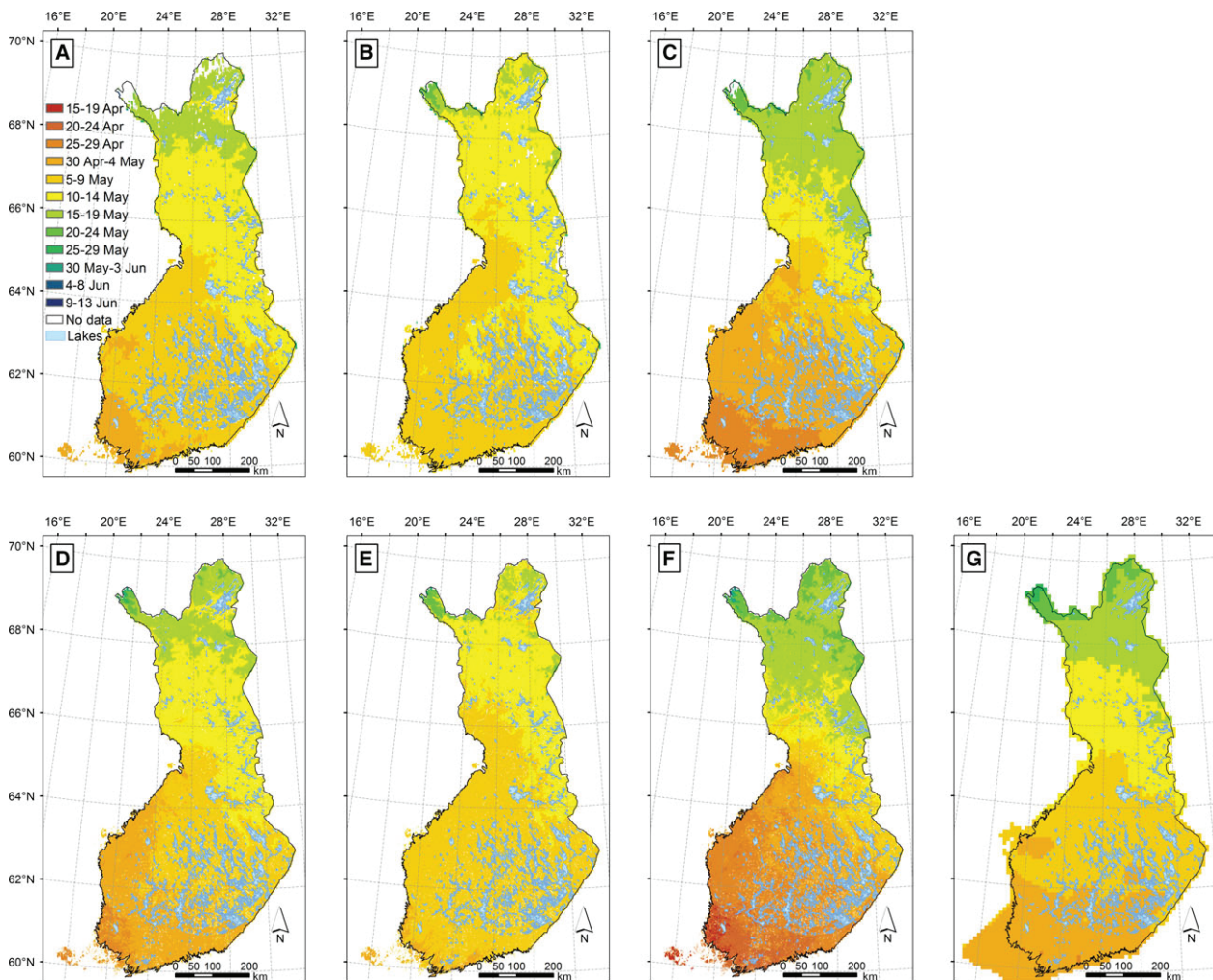
Figure 4. Maps of the peak flight periods for *Orthosia gothica*: predictions made on the basis of the total model including all variables for (A) an average period of 2001–2013, (B) a phenologically late year (2006), (C) a phenologically early year (2007); predictions made on the basis of snow melt-off date for (D) an average period of 2001–2013, (E) a phenologically late year (2006), (F) a phenologically early year (2007) and (G) an average prediction for 2001–2013 based on an alternative variable (weekly accumulating growing degree days). Model formulas are presented in Table S2. Data sources: Country borders © ESRI, Lakes © SYKE, Biogeographical provinces ©LUOMUS and SYKE.

necessary to develop novel indicators based on remote sensing.

In general, it appears that predictive models do not fully describe the spatial gradient of moth peak flight. Model predictions generally showed a smaller range of values compared to observations, as can be seen by too late predictions of peak flight date for the south of Finland and too early predictions in northern Finland (Fig. 3, Fig. S4). Moreover, predictive power of the majority of investigated models decreased considerably after excluding the site information (represented as the random effect term) from the predictions (cf. Pinheiro et al. 2014). This indicates that the variables included in such models were not useful for making spatial predictions for the whole country, but instead their predictive power was more closely related to the knowledge about exact locations of sites used in the model calibration. The choice of calculating an average prediction across large spatial scales was justifiable here because we were interested in the general trend in phenology patterns, which is not masked by local variation caused by, for example, microclimatic factors.

The predictive power of thermal sum, measured as GDD with varying base temperatures and summation periods, showed less variation across species when compared to remote sensing variables, but only when site information was included in spatial predictions. This indicates that temperature controls a large proportion of variation in timing
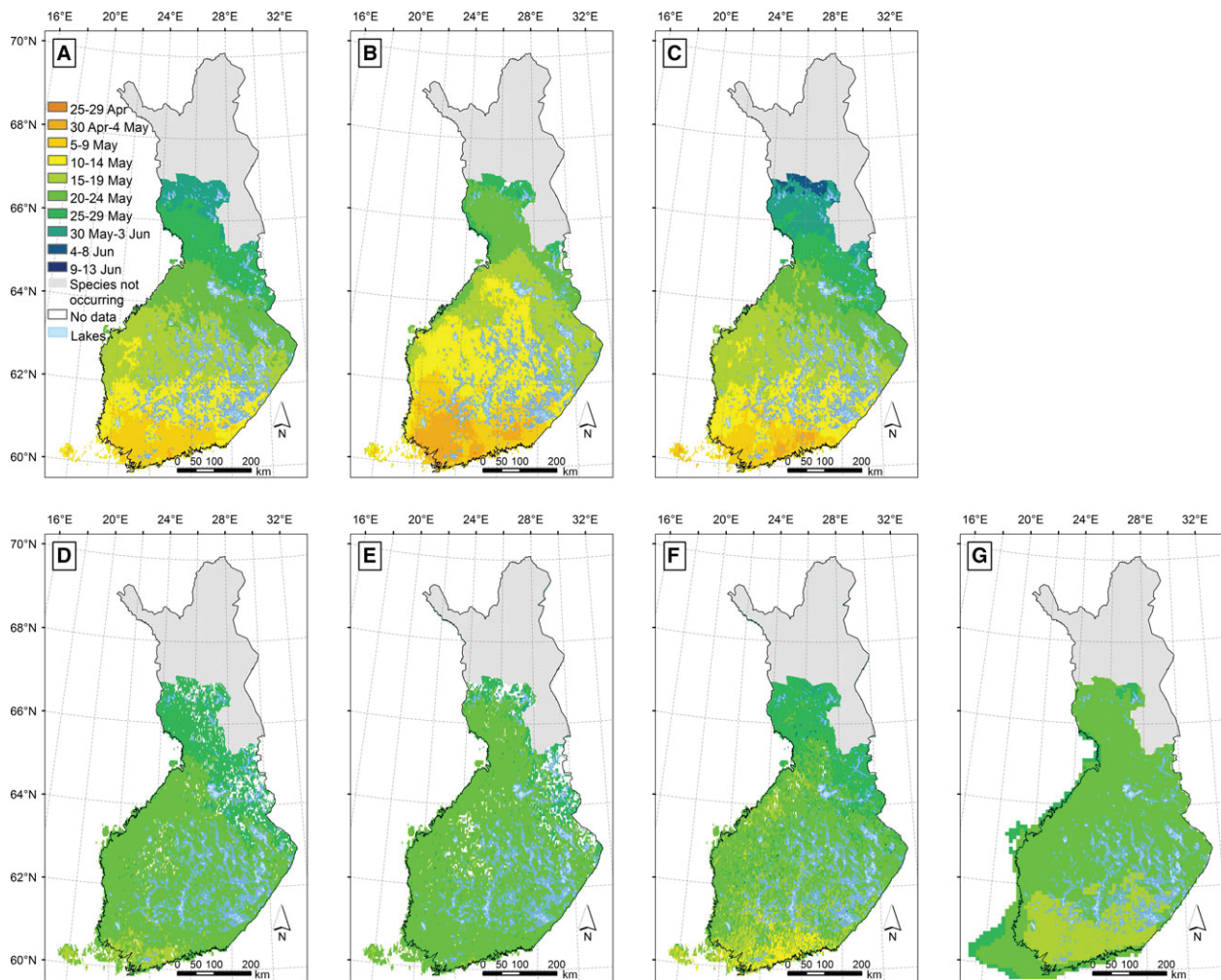
Figure 5. Maps of the peak flight periods for *Ectropis crepuscularia*: predictions made on the basis of the total model including all variables for (A) an average period of 2001–2013, (B) a phenologically late year (2006), (C) a phenologically early year (2007); predictions made on the basis of the vegetation greening date for (D) an average period of 2001–2013, (E) a phenologically late year (2006), (F) a phenologically early year (2007); and (G) an average prediction for 2001–2013 based on an alternative variable (weekly accumulating growing degree days). Model formulas are presented in Table S2. Data sources: Country borders © ESRI, Lakes © SYKE, Biogeographical provinces ©LUOMUS and SYKE.

of the flight period in these species, but this effect is also strongly dependent on local climatic variation. This is a clear drawback in using temperature-derived variables in spatial predictions because large-scale spatial predictions are typically done without site information to avoid the general latitudinal trend being masked by the local variation. Previous studies have suggested that thermal controls determine timing of the flight period in a majority of moth species, and thus our results are only partly consistent with earlier studies (Valtonen et al. 2011, 2014).

The uncertainty of model predictions may stem from different sources, one of which being the differences in the temporal accuracy between the datasets deployed in the modelling, a factor that applies to both moth observational data and explanatory variables. The light traps used

in collecting moth observational data are emptied usually once a week, but for logistic reasons there is some additional variation in the length of the observational period. Thus, the temporal inaccuracy around the mid-day of the peak flight period calculated as average length of observational period divided by two varies between 3.67 and 4.26 days depending on the species identity. GDD indices defined with weekly varying summation periods were tested, but the spatial resolution (10 km × 10 km) and the representativeness of the underlying meteorological station network maybe too coarse to capture some of the microclimatic conditions at the trap sites. However, it is difficult to estimate this exactly. Onsite temperature observations made at the trap sites would probably increase predictive power of GDD indices, but such data

were not available in this study. In the future, more fine-grained gridded temperature products may become available and in part alleviate the shortcomings caused by too coarse scale of the gridded datasets.

By contrast, all the remote sensing datasets show an inherent temporal uncertainty. Snow melt and greening dates are estimated with the precision of 1 day, but in both cases missing observations stemming mainly from cloudiness cause some uncertainty that varies from year to year and by region depending on weather conditions. This is estimated to be ca. 5 days for snow melt date (Metsämäki et al. 2017), depending on the general snow cover conditions, that is, whether the area has a consistent seasonal snow cover or only sporadic snow occurrences. However, Metsämäki et al. (2017) demonstrate that compared with microwave data-based melt-off day information (which is not affected by such data gaps), the year-to-year trend of melt-off day is very similar. We can therefore expect that the inaccuracies obtained by using optical data such as MODIS do not have a remarkable effect on the results presented in this study. For the greening date, NDWI time series were interpolated at a daily time step and time series with a temporal gap larger than 2 weeks were discarded in the detection (Böttcher et al. 2016). The FAPAR dates for the start, maximum date and end of the growing season are obtained from 10-day products, and thus uncertainty is 5 days. Greening date and FAPAR growing season start date showed low correlation for the trap site locations in Finland (Table S1), although both satellite indices track the development of new foliage in the footprint of the satellite pixel. The satellite-based detection of the greening up of vegetation in Finland is challenging due to long periods of snow and cloud cover, fast vegetation development in spring and dominance of evergreen coniferous forest (e.g. Beck et al. 2006). The daily temporal resolution of the NDWI time series may be an advantage in this respect. Furthermore, the method for the greening date detection was targeted at and evaluated in boreal areas previously (see Delbart et al. 2006; Böttcher et al. 2016).

Data availability limits the applicability of using remote sensing variables when compared to temperature-derived variables. In the case of our work, all the remote sensing variables were available only for a part of the period (2003–2011) for which moth phenology data would be available (1993–2012). Although lack of datasets may be a major shortcoming in older time periods, the importance of this factor will diminish by time and continuing collection of data by satellites. The longer satellite data time series provided by TM (Thematic Mapper, 1984–2013) ETM+ (Enhanced Thematic Mapper Plus, 1999–present) and OLI (Operational Land Imager, 2013–present) on-board Landsat 5, Landsat 7 and Landsat 8, respectively,

can be used in estimating the vegetation phenology and with higher spatial resolution than moderate-resolution sensors such as MODIS. Despite the temporally sparse and spatially scarce nature of TM and ETM+ acquisitions, for example, a Bayesian approach introduced by Senf et al. (2017) maps the variation and temporal year-to-year changes in phenological events in a way that overcomes these deficiencies. Although their study was limited to a restricted area, such a technique is worth further investigation with longer phenological time series.

The impact of latitude was observed in the two species flying either in spring (O. gothica) or late autumn (O. brumata). This is not surprising as both species show a clear latitudinal gradient in timing of their peak flight period (Fig. S2). It has not been analysed how widespread latitudinal gradients in timing of the flight periods are in European moths, but in butterflies a majority of species show a shift towards later timing in the north (Roy and Asher 2003). However, it may be expected that moth species that have their flight season in the autumn will shift their flight period later towards the south (e.g. Pöyry et al. 2011).

The species sample included in this study was temporally representative, including one species flying at different times of the North European warm season, but yet quite limited in numbers. Thus, future studies focusing on a larger species set are required to verify the tentative observations made in this study. Moreover, previous studies have shown that in certain moth species, phenology is predominantly controlled by photoperiod (i.e. day length), or thermal controls are modified by photoperiod (see Valtonen et al. 2014). Although day length was included in models indirectly through latitude, it would be interesting to explore if predictive power of phenology models might be increased by accounting explicitly for photoperiod.

The spatial prediction methods demonstrated in this work allow for the prediction of timing of the peak flight periods of herbivorous insects, as exemplified here by moths, on the basis of both earth observation data and temperature observations. Such methodology has potential for application in other insect groups and extension to larger geographical areas. This enables also effective use of remote sensing variables (snow melt, greening) over large geographic areas in explaining phenology, when species-specific characteristics such as timing of flight period are taken into account. There are also widespread practical applications, for example, in supporting the achievement of the Aichi targets of biodiversity conservation, one of which being the development of new methodologies for monitoring of phenology in terrestrial ecosystems (CBD, 2014) and the monitoring, prediction and management of populations of insect pest species (e.g. Olsson et al. 2016).

Acknowledgements

Data Accessibility

The data used in this study is placed on the Knowledge Network for Biocomplexity (KNB) digital repository Poyry, J. et al. (2017) Moth phenology modelling data from Finland 1993–2012. *Knowledge Network for Biocomplexity.* https://doi.org/10.5063/f1542kks).

References

Aarvik, L., B. Å. Bengtsson, H. Elven, P. Ivinskis, U. Jürivete, O. Karsholt, et al. 2017. Nordic-Baltic checklist of Lepidoptera. *Norw. J. Entomol. Suppl.* **3**, 1–236.

van Asch, M., L. Salis, L. J. M. Holleman, B. van Lith, and M. E. Visser. 2013. Evolutionary response of the egg hatching date of a herbivorous insect under climate change. *Nat. Clim. Chang.* **3**, 244–248.

Babst, F., J. Esper, and E. Parlow. 2010. Landsat TM/ETM+ and tree-ring based assessment of spatiotemporal patterns of the autumnal moth (Epirrita autumnata) in northernmost Fennoscandia. *Remote Sens. Environ.* **114**, 637–646.

Badeck, F.-W., A. Bondeau, K. Böttcher, D. Doktor, W. Lucht, J. Schaber, et al. 2004. Responses of spring phenology to climate change. *New Phytol.* **162**, 295–309.

Beck, P. S. A., C. Atzberger, K. A. Høgda, B. Johansen, and A. K. Skidmore. 2006. Improved monitoring of vegetation dynamics at very high latitudes: a new method using MODIS NDVI. *Remote Sens. Environ.* **100**, 321–334.

de Beurs, K. M., and P. A. Townsend. 2008. Estimating the effect of gypsy moth defoliation using MODIS. *Remote Sens. Environ.* **112**, 3983–3990.

Böttcher, K., T. Markkanen, T. Thum, T. Aalto, M. Aurela, C. Reick, et al. 2016. Evaluating biosphere model estimates of the start of the vegetation active season in boreal forests by satellite observations. *Remote Sens.* **8**, 580.

Burnham, K. B., and D. R. Anderson. 2002. *Model selection and multimodel inference. A practical information-theoretic approach*, 2nd ed.Springer, New York.

CBD (Convention on Biological Diversity). 2014. *Earth observation for biodiversity monitoring: a review of current approaches and future opportunities for tracking progress towards the aichi biodiversity targets.* Pp 183. Secretariat of the Convention on Biological Diversity, Canada. Technical Series No. 72.

Ceccherini, G., N. Gobron, and M. Robustelli. 2013a. Harmonization of FAPAR from SeaWiFS and MERIS instruments. *Remote Sens.* **5**, 3357–3376.

Ceccherini, G., N. Gobron, M. Migliavacca, and M. Robustelli. 2013b. Long-term measurements of plant phenology over Europe derived from SeaWiFS and Meris. In: L. Ouwehand (ed.) *Proceedings of the 2013 ESA Living Planet Symposium, 9-13 September 2013*, Edinburgh, UK. ESA, Noordwijk, The Netherlands, Issue SP-722, ISBN 978-92-9221-286-5.

Ceccherini, G., N. Gobron, and M. Migliavacca. 2014. On the response of european vegetation phenology to hydroclimatic anomalies. *Remote Sens.* **6**, 3143–3169.

Delbart, N., L. Kergoat, T. Le Toan, J. L'Hermitte, and G. Picard. 2005. Determination of phenological dates in boreal regions using normalized difference water index. *Remote Sens. Environ.* **97**, 26–38.

Delbart, N., T. Le Toan, L. Kergoat, and V. Fedotova. 2006. Remote sensing of spring phenology in boreal regions: a free of snow-effect method using NOAA-AVHRR and SPOT-VGT data (1982-2004). *Remote Sens. Environ.* **101**, 52–62.

Delbart, N., G. Picard, T. Le Toan, L. Kergoat, S. Quegan, I. A. N. Woodward, et al. 2008. Spring phenology in boreal Eurasia over a nearly century time scale. *Glob. Change Biol.* **14**, 603–614.

Finnish Environment Institute. 2009. CLC2006 Finland. Final technical report. Available at: http://www.syke.fi/download/noname/%7BC7C849EB-3F4D-42AE-9A94-5B8069FFDFFB%7D/37641 (accessed 14 June 2017)

Foster, J. R., P. A. Townsend, and D. J. Mladenoff. 2013. Mapping asynchrony between gypsy moth egg-hatch and forest leaf-out: putting the phenological window hypothesis in a spatial context. *For. Ecol. Manage.* **287**, 67–76.

Ganguly, S., M. A. Friedl, B. Tan, X. Zhang, and M. Verma. 2010. Land surface phenology from MODIS: characterization of the collection 5 global land cover dynamics product. *Remote Sens. Environ.* **114**, 1805–1816.

Gobron, N., B. Pinty, M. Taberner, F. Mélin, M. M. Verstraete, and J. L. Widlowski. 2006. Monitoring the photosynthetic activity of vegetation from remote sensing data. *Adv. Space Res.* **38**, 2196–2202.

Gonsamo, A., and J. M. Chen. 2016. Circumpolar vegetation dynamics product for global change study. *Remote Sens. Environ.* **182**, 13–26.

Guisan, A., and N. E. Zimmerman. 2000. Predictive habitat distribution models in ecology. *Ecol. Model.* **135**, 147–186.

Hodgson, J. A., C. D. Thomas, T. H. Oliver, B. J. Anderson, T. M. Brereton, and E. E. Crone. 2011. Predicting insect phenology across space and time. *Glob. Change Biol.* **17**, 1289–1300.

Ivits, E., M. Cherlet, G. Tóth, S. Sommer, W. Mehl, J. Vogt, et al. 2012. Combining satellite derived phenology with climate data for climate change impact assessment. *Global Planet. Change* **88–89**, 85–97.

Jepsen, J. U., S. B. Hagen, K. A. Høgda, R. A. Ims, S. R. Karlsen, H. Tømmervik, et al. 2009a. Monitoring the spatio-temporal dynamics of geometrid moth outbreaks in birch forest using MODIS-NDVI data. *Remote Sens. Environ.* **113**, 1939–1947.

Jepsen, J. U., S. B. Hagen, S.-R. Karlsen, and R. A. Ims. 2009b. Phase-dependent outbreak dynamics of geometrid moth linked to host plant phenology. *Proc. R. Soc. B: Biol. Sci.* **276**, 4119–4128.

Jung, M., M. Verstraete, N. Gobron, M. Reichstein, D. Papale, A. Bondeau, et al. 2008. Diagnostic assessment of European gross primary production. *Glob. Change Biol.* **14**, 2349–2364.

Karlsen, S. R., A. Elvebakk, K. A. Høgda, and B. Johansen. 2006. Satellite-based mapping of the growing season and bioclimatic zones in Fennoscandia. *Glob. Ecol. Biogeogr.* **15**, 416–430.

Lausch, A., L. Bannehr, M. Beckmann, C. Boehm, H. Feilhauer, J. M. Hacker, et al. 2016. Linking Earth Observation and taxonomic, structural and functional biodiversity: local to ecosystem perspectives. *Ecol. Ind.* **70**, 317–339.

Leinonen, R., J. Pöyry, G. Söderman, and L. Tuominen-Roto. 2016. Suomen yöperhosseuranta (Nocturna) 1993-2012 [The Finnish moth monitoring scheme (Nocturna) 1993-2012]. Suomen ympäristökeskuksen raportteja, 15/2016, 71 p.

Leyequien, E., J. Verrelst, M. Slot, G. Schaepman-Strub, I. M. A. Heitkönig, and A. Skidmore. 2007. Capturing the fugitive: applying remote sensing to terrestrial animal distribution and diversity. *Int. J. Appl. Earth Obs. Geoinf.* **9**, 1–20.

Liu, Y. Y., A. I. J. M. van Dijk, M. F. McCabe, J. P. Evans, and R. A. M. de Jeu. 2013. Global vegetation biomass change (1988–2008) and attribution to environmental and human drivers. *Glob. Ecol. Biogeogr.* **22**, 692–705.

Metsämäki, S. J., S. T. Anttila, H. J. Markus, and J. M. Vepsäläinen. 2005. A feasible method for fractional snow cover mapping in boreal zone based on a reflectance model. *Remote Sens. Environ.* **95**, 77–95.

Metsämäki, S., O.-P. Mattila, J. Pulliainen, K. Niemi, K. Luojus, and K. Böttcher. 2012. An optical reflectance model-based method for fractional snow cover mapping applicable to continental scale. *Remote Sens. Environ.* **123**, 508–521.

Metsämäki, S. J., K. Böttcher, J. Pulliainen, K. Luojus, O. P. Mattila, C. Derksen, et al. 2017. The accuracy of snow melt-off day derived from optical and microwave radiometer data and the relationship of snow water equivalent and fractional snow cover - a study for Europe. In review.

Moulin, S., L. Kergoat, N. Viovy, and G. Dedieu. 1997. Global-scale assessment of vegetation phenology using NOAA/AVHRR satellite measurements. *J. Clim.* **10**, 1154–1155.

Myneni, R. B., C. D. Keeling, C. J. Tucker, G. Asrar, and R. R. Nemani. 1997. Increased plant growth in the northern high latitudes from 1981 to 1991. *Nature* **386**, 698–702.

Nagler, T., G. Bippus, C. Schiller, S. Metsämäki, O.-P. Mattila, K. Luojus, et al. 2015. CryoLand - Copernicus Service Snow and Land Ice: Final Report. In p. 46

Nietschke, B. S., R. D. Magarey, D. M. Borchert, D. D. Calvin, and E. Jones. 2007. A developmental database to support insect phenology models. *Crop Prot.* **26**, 1444–1448.

O'Connor, B., C. Secades, J. Penner, R. Sonnenschein, A. Skidmore, N. D. Burgess, et al. 2015. Earth observation as a tool for tracking progress towards the Aichi Biodiversity Targets. *Remote Sens. Ecol. Conserv.* **1**, 19–28.

Olsson, P.-O., J. Lindström, and L. Eklundh. 2016. Near real-time monitoring of insect induced defoliation in subalpine birch forests with MODIS derived NDVI. *Remote Sens. Environ.* **181**, 42–53.

Pettorelli, N., S. Ryan, T. Mueller, N. Bunnefeld, B. Jedrzejewska, M. Lima, et al. 2011. The normalized difference vegetation index (NDVI): unforeseen successes in animal ecology. *Clim. Res.* **46**, 15–27.

Pettorelli, N., W. F. Laurance, T. G. O'Brien, M. Wegmann, H. Nagendra, and W. Turner. 2014. Satellite remote sensing for applied ecologists: opportunities and challenges. *J. Appl. Ecol.* **51**, 839–848.

Pinheiro, J., D. Bates, S. DebRoy, and D. Sarkar, & R Core Team. 2014. Nlme: Linear and Nonlinear Mixed Effects Models. R package, version 3.1-118.

Pöyry, J., R. Leinonen, G. Söderman, M. Nieminen, R. K. Heikkinen, and T. R. Carter. 2011. Climate-induced increase of moth multivoltinism in boreal regions. *Glob. Ecol. Biogeogr.* **20**, 289–298.

Pritchard, G., L. D. Harder, and R. A. Mutch. 1996. Development of aquatic insect eggs in relation to temperature and strategies for dealing with different thermal environments. *Biol. J. Lin. Soc.* **58**, 221–244.

R Core Team. 2015. R: A language and environment for statistical computing. R Foundation for Statistical Computing.

Rautiainen, M., and P. Lukes. 2015. Spectral contribution of understory to forest reflectance in a boreal site: an analysis of EO-1 Hyperion data. *Remote Sens. Environ.* **171**, 98–104.

Rautiainen, M., M. Mõttus, J. Heiskanen, A. Akujärvi, T. Majasalmi, and P. Stenberg. 2011. Seasonal reflectance dynamics of common understory types in a northern European boreal forest. *Remote Sens. Environ.* **115**, 3020–3028.

Roy, D. B., and J. Asher. 2003. Spatial trends in the sighting dates of British butterflies. *Int. J. Biometeorol.* **47**, 188–192.

Roy, D. B., and T. Sparks. 2000. Phenology of British butterflies and climate change. *Glob. Change Biol.* **6**, 407–416.

Roy, D. B., P. Rothery, D. Moss, E. Pollard, and J. A. Thomas. 2001. Butterfly numbers and weather: predicting historical trends in abundance and the future effects of climate change. *J. Anim. Ecol.* **70**, 201–217.

Running, S. W., R. R. Nemani, F. A. Heinsch, M. Zhao, M. Reeves, and H. Hashimoto. 2004. A Continuous Satellite-Derived Measure of Global Terrestrial Primary Production. *Bioscience* **54**, 547–560.

Senf, C., D. Pflugmacher, M. Heurich, and T. Krueger. 2017. A Bayesian hierarchical model for estimating spatial and temporal variation in vegetation phenology from Landsat time series. *Remote Sens. Environ.* **194**, 155–160.

Spruce, J. P., S. Sader, R. E. Ryan, J. Smoot, P. Kuper, K. Ross, et al. 2011. Assessment of MODIS NDVI time series data products for detecting forest defoliation by gypsy moth outbreaks. *Remote Sens. Environ.* **115**, 427–437.

Sweet, S. K., A. Asmus, M. E. Rich, J. Wingfield, L. Gough, and N. T. Boelman. 2015. NDVI as a predictor of canopy arthropod biomass in the Alaskan arctic tundra. *Ecol. Appl.* **25**, 779–790.

Trierweiler, C., W. C. Mullié, R. H. Drent, K.-M. Exo, J. Komdeur, F. Bairlein, et al. 2013. A Palaearctic migratory raptor species tracks shifting prey availability within its wintering range in the Sahel. *J. Anim. Ecol.* **82**, 107–120.

Valtonen, A., M. P. Ayres, H. Roininen, J. Pöyry, and R. Leinonen. 2011. Environmental controls on the phenology of moths: predicting plasticity and constraint under climate change. *Oecologia* **165**, 237–248.

Valtonen, A., R. Leinonen, J. Pöyry, H. Roininen, J. Tuomela, and M. P. Ayres. 2014. Is climate warming more consequential towards poles? The phenology of Lepidoptera in Finland. *Glob. Change Biol.* **20**, 16–27.

Venables, W. N., and B. D. Ripley. 2002. *Modern Applied Statistics with S*, 4th ed.. Springer-Verlag, New York.

Venäläinen, A., H. Tuomenvirta, P. Pirinen, and A. Drebs. 2005. A basic Finnish climate data set 1961–2000 — description and illustrations. *Finnish Meteorol. Inst. Rep.* **5**, 1–27.

Verstraete, M. M., N. Gobron, O. Aussedat, M. Robustelli, B. Pinty, J.-L. Widlowski, et al. 2008. An automatic procedure to identify key vegetation phenology events using the JRC-FAPAR products. *Adv. Space Res.* **41**, 1773–1783.

Vihervaara, P., A.-P. Auvinen, L. Mononen, M. Törmä, P. Ahlroth, S. Anttila, et al. 2017. How Essential Biodiversity Variables and remote sensing can help national biodiversity monitoring. *Glob. Ecol. Conserv.* **10**, 43–59.

Vrieling, A., A. K. Skidmore, T. Wang, M. Meroni, B. J. Ens, K. Oosterbeek, et al. 2017. Spatially detailed retrievals of spring phenology from single-season high-resolution image time series. *Int. J. Appl. Earth Obs. Geoinf.* **59**, 19–30.

White, M. A., and R. R. Nemani. 2006. Real-time monitoring and short-term forecasting of land surface phenology. *Remote Sens. Environ.* **104**, 43–49.

White, M. A., K. M. De Beurs, K. Didan, D. W. Inouye, A. D. Richardson, O. P. Jensen, et al. 2009. Intercomparison, interpretation, and assessment of spring phenology in North America estimated from remote sensing for 1982–2006. *Glob. Change Biol.* **15**, 2335–2359.

Zhang, X., B. Tan, & Y. Yu. 2014. Interannual variations and trends in global land surface phenology derived from enhanced vegetation index during 1982–2010. *Int. J. Biometeorol.* **58**, 547–564.

Zhao, J. J., H. Y. Zhang, Z. X. Zhang, X. Y. Guo, X. D. Li, and C. Chen. 2015. Spatial and temporal changes in vegetation phenology at middle and high latitudes of the Northern Hemisphere over the past three decades. *Remote Sens.* **7**, 10973–10995.

Supporting Information

Additional supporting information may be found online in the supporting information tab for this article.

Figure S1. Locations of the moth monitoring trap sites that produced the phenological observations used in building the models.

Figure S2. Latitudinal gradient in timing of the peak flight period across the five focal species.

Figure S3. Two examples of timing of the peak flight periods of the focal moth species, snow melt-off dates (SMD), vegetation greening dates and dates of start (FSGS), peak (MD) and end (EGS) of the growing season derived from the FAPAR data. Both examples are from the year 2007, and situated in southern (Espoo) and northern (Kolari) part of Finland.

Figure S4. Model predictive power across the five focal species and different sets of explanatory variables.

Table S1. Pearson correlation coefficients among the explanatory variables for each focal species.

Table S2. Linear mixed effect models (LMM) fitted using randomly selected 70% of the phenological data using different sets of explanatory variables for the five focal species.

Supplementary Materials

S II

Böttcher, K., Rautiainen, K., Aurela, M., Kolari, P., Mäkelä, A., Arslan, A.N., Black, T.A., Koponen, S. (2018). Proxy indicators for mapping the end of the vegetation active period in boreal forests inferred from satellite-observed soil freeze and ERA-Interim reanalysis air temperature. *Journal of Photogrammetry, Remote Sensing and Geoinformation Science*, 86 (3-4), 169-185.

Proxy indicators for mapping the end of the vegetation active period in boreal forests inferred from satellite-observed soil freeze and ERA-Interim reanalysis air temperature

Kristin Böttcher [1], Kimmo Rautiainen[2], Mika Aurela[2], Pasi Kolari[3], Annikki Mäkelä[4], Ali N. Arslan[2], T. Andrew Black[5], Sampsa Koponen[1]

[1] Finnish Environment Institute, Geoinformatics Research, FI-00251 Helsinki, Finland, Email: kristin.bottcher@environment.fi, sampsa.koponen@environment.fi

[2] Finnish Meteorological Institute, FI-00560 Helsinki, Finland, Email: mika.aurela@fmi.fi, kimmo.rautiainen@fmi.fi, ali.nadir.arslan@fmi.fi

[3] University of Helsinki, Institute for Atmospheric and Earth System Research/Physics, FI-00014 University of Helsinki, Finland, Email: pasi.kolari@helsinki.fi

[4] University of Helsinki, Department of Forest Sciences, FI-00014 University of Helsinki, Finland, Email: annikki.makela@helsinki.fi

[5] University of British Columbia, Faculty of Land and Food Systems, Canada, Email: andrew.black@ubc.ca

*Corresponding author, Tel. +358-401-876447; Fax: +358-9-40300690, Email: kristin.bottcher@environment.fi

Supplementary material

Table S 1 Proportions (%) of land cover within the SMOS 25 km x 25 km pixels covering in situ sites based on GlobCover 2009 (Global Land Cover Map, © ESA 2010 and UCLouvain). Land cover classes with proportions lower than 1% are not reported and proportions higher than 10% are shown in bold letters.

| Site	FI-Hyy	FI-Ken	FI-Sod	CA-Obs	CA-Ojp	CA-Qfo
Class 50: Closed (>40%) broadleaved deciduous forest (>5m)	7.63	1.47	2.15	-	-	-
Class 70: Closed (>40%) needle-leaved evergreen forest (>5m)	-	-	-	9.63	2.05	5.89
Class 90: Open (15-40%) needle-leaved deciduous or evergreen forest (>5m)	**59.76**	**58.80**	**47.95**	**63.79**	**83.89**	**42.41**
Class 100: Closed to open (>15%) mixed broadleaved and needle-leaved forest (>5m)	**25.42**	5.37	**23.97**	7.44	1.67	**17.37**
Class 110: Mosaic forest or shrubland (50-70%)/ grassland (20-50%)	-	6.63	2.93	2.15	5.09	2.01
Class 120: Mosaic grassland (50-70%) / forest or shrubland (20-50%)	1.02	8.09	3.98	1.41	4.45	2.84
Class 140: Closed to open (>15%) herbaceous vegetation (grassland, savannas or lichens/mosses)					1.70	3.38
Class 150: Sparse (<15%) vegetation	2.07	7.02	5.46	-	1.09	-
Class 180: Closed to open (>15%) grassland or woody vegetation on regularly flooded or waterlogged soil - Fresh, brackish or saline water	2.39	7.42	**13.06**	-		-
Class 210: Water bodies	-	4.83	-	**14.44**	-	**23.90**
Other classes	1.71	0.37	0.50	1.14	0.06	2.20
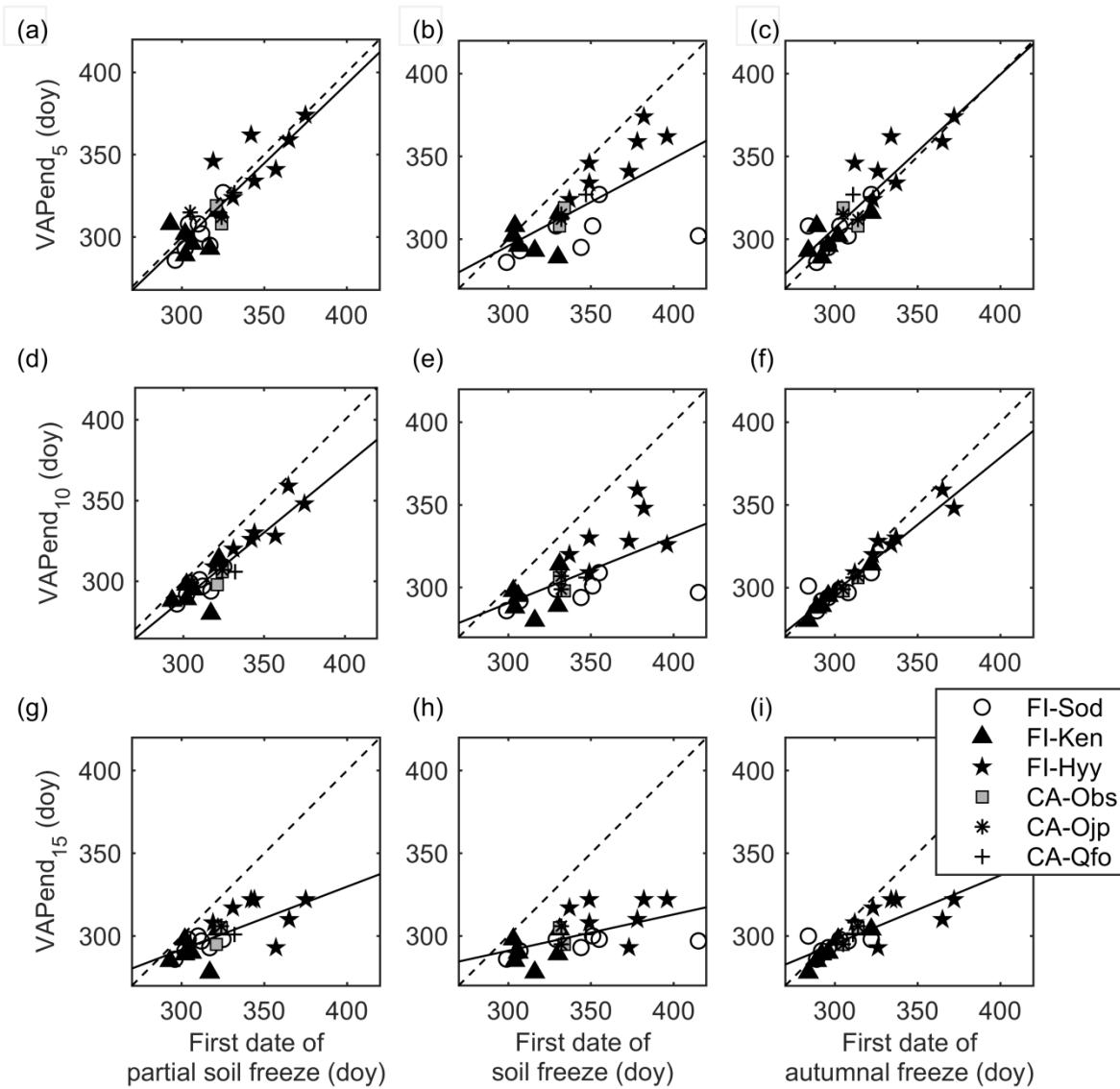
Fig. S 1 Scatterplots of the end of the vegetation active period (VAPend) from CO$_2$ flux measurements versus the first date of partial soil freeze from satellite observations (left), the first date of soil freeze (middle) and first date of autumnal freeze from ERA-Interim reanalysis air temperature data (right). VAPend is based on thresholds 5% (a, b, c); 10% (d, e, f) and 15% (g, h, i) of the gross photosynthesis index (GPI)

Table S 2 Statistical measures for the comparison of the end of the vegetation active period based on different threshold of the gross photosynthesis index (GPI$_{th}$) versus the first date of partially soil freeze and soil freeze from SMOS satellite observations and the first date of autumnal freeze from air temperature for the period 2010−2016

	GPI$_{th}$	N	R^2	RMSE (d)	Bias (d)
Satellite-derived first date of partially frozen soil	5%	25	0.74**	12.6	-4.1
	10%	25	0.84**	17.0	-14.8
	15%	25	0.47**	26.7	-21.8
Satellite-derived first date of frozen soil up to depth > 10 cm	5%	25	0.44**	32.4	-23.8
	10%	25	0.39**	41.0	-34.1
	15%	25	0.30*	48.0	-41.1
First date of autumnal freeze from air temperature	5%	25	0.78**	12.6	5.9
	10%	25	0.92**	8.2	-4.8
	15%	25	0.63**	18.9	-11.8

N, Number of observations, R^2, Coefficient of determination, *significant p<0.05, ** p<0.001, RMSE, Root Mean Square Error.

Table S 3 Soil freeze dates from soil temperature measurements of the distributed network at Sodankylä covering different soil and land cover types. The given date is a mean of three sensors for one measurement site. Light grey and grey colours indicate that only two, respectively, one sensor was available for the site

First time when soil temperature is below freezing point (doy)

	Open, Haplic Arenosol	Forest, Haplic Arenosol	Forest, Haplic Arenosol	Forest, Haplic Podzol	Sparse forest, Umbric Gleysol	Sparse forest, Umbric Gleysol	Wetland, Histosol	Wetland, Histosol
2011	312	318			323		332	332
2012	294	294			335	334	336	392
2013	288	288			293	289		294
2014	287	287	287	293	294	293		296
2015	279	280	280	282	370	363	378	388
2016	309	309	310	312	311	311	386	314

Date when soil temperature remained below the freezing point (doy)

	Open, Haplic Arenosol	Forest, Haplic Arenosol	Forest, Haplic Arenosol	Forest, Haplic Podzol	Sparse forest, Umbric Gleysol	Sparse forest, Umbric Gleysol	Wetland, Histosol	Wetland, Histosol
2011	317	318			387		336	345
2012	333	332			335	334	336	392
2013	318	323			325	324		382
2014	302	287	302	303	353	303		357
2015	336	356	341	368	370	368	378	388
2016	309	309	310	367	358	337	386	314

Table S 4 Correspondence of the date of autumnal freeze from air temperature and partially frozen soil from SMOS with the end of the vegetation active period, VAPend$_{10,}$ for Finnish flux measurement sites for the period 2010−2016

Site	*In situ*			Date of autumnal freeze					Date of satellite partial soil freeze				
	Mean (doy)	SD	# y	Mean (doy)	SD	R^2	Bias (d)	RMSE (d)	Mean (doy)	SD	R^2	Bias (d)	RMSE (d)
Hyytiälä	331	16.9	7	338	22.2	0.90*	-7	10.3	348	19.5	0.80*	-16	18.0
Kenttärova	294	11.6	6	298	13.5	0.98**	-4	4.2	307	10.7	0.16	-13	17.1
Sodankylä	297	7.3	7	299	13.0	0.44	-2	10.8	309	9.8	0.64*	-13	13.7

#y, number of years for comparison. SD, standard deviation, Doy, day of year. R^2 coefficient of determination, * significant p<0.05, ** p<0.001.
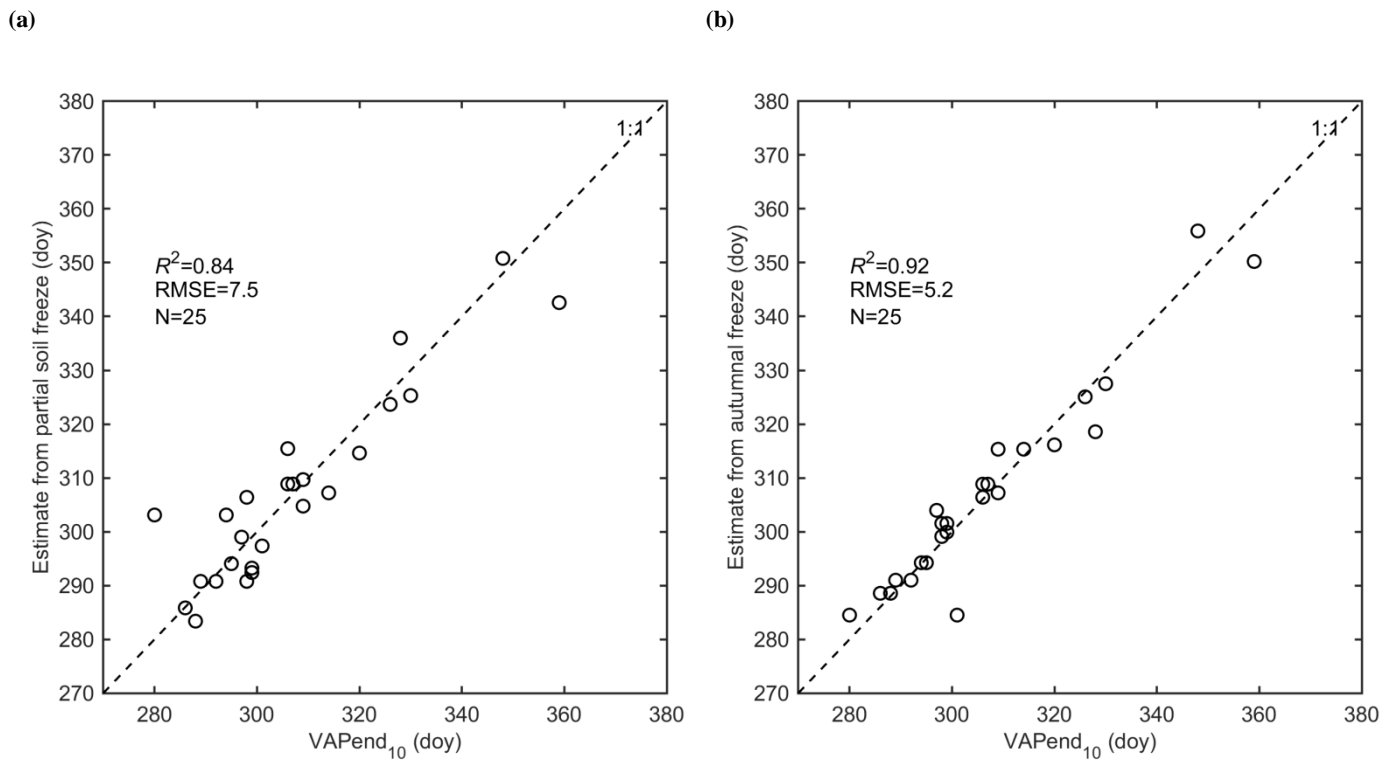
(a)　　　　　　　　　　　　　　　　　　　　　　(b)

Fig. S 2 Scatterplots of the end of the vegetation active period (VAPend$_{10}$) from CO$_2$ flux measurements versus (a) satellite- and (b) air- temperature-derived estimates. The satellite-based estimate of VAPend$_{10}$ was determined from the first date of partially frozen soil from SMOS observations by applying the linear regression equation shown in Fig. 3a. The air-temperature-based estimate of VAPend$_{10}$ was calculated from the date of autumnal freeze by applying the linear regression equation given in Fig.3b

S III

Böttcher, K., Markkanen, T., Thum, T., Aalto, T., Aurela, M., Reick, C., Kolari, P., Arslan, A., Pulliainen, J. (2016). Evaluating biosphere model estimates of the start of the vegetation active season in boreal forests by satellite observations. *Remote Sensing*, 8, 580.

Supplementary Materials:

Table S 1. Proportions of land cover classes in Finland determined from CORINE land cover 2000 (Härmä et al. 2005).

Land cover class	Proportion (%)[1]
Evergreen needle-leaf forest	23.6
Deciduous broad-leaf forest	4.4
Mixed Forest	15.8
Shrubs and/or herbaceous vegetation	17.4
Inland waters	8.5
Inland wetlands	7.0
Arable land	5.8
Urban fabric	1.5

[1]Only land cover classes with proportions higher than 1% were included here.

Table S 2. Relationship between the mean of start of season from remote sensing and determined from JSBACH modelling for evergreen needle-leaf forest (ENF_SOSmod) and deciduous broad-leaf forest (DBF_SOSmod) for whole Finland and the three boreal sub-zones. The mean start of season was calculated for the period 2003- 2010. All correlations were significant ($p<0.0001$). A positive bias means that the simulated date is late compared to observations.

Forest type	Boreal zone	N	R^2	RMSE(d)	Bias (d)
(a) ENF	Finland	922	0.90	5.00	-3.13
	Southern	326	0.81	4.10	-2.47
	Middle	336	0.86	4.96	-3.58
	Northern	251	0.25	5.76	-4.33
(b) DBF	Finland	741	0.88	5.95	4.80
	Southern	246	0.58	7.18	6.89
	Middle	257	0.79	4.78	3.94
	Northern	239	0.48	4.91	3.18

Table S 3. Relationship between start of season derived from remote sensing and from JSBACH simulations for evergreen needle-leaf forest (ENF) and deciduous broad-leaf forest (DBF) for different years in Finland. All correlations were significant ($p<0.0001$). A positive bias means that the simulated date is late compared to observations.

Forest type	Year	R^2	RMSE (d)	Bias (d)
(a) ENF				
N=958	2003	0.63	8.28	-3.30
N=973	2004	0.65	10.14	-5.28
N=880	2005	0.83	9.45	-6.03
N=948	2006	0.63	6.77	-5.90
N=904	2007	0.77	8.70	-0.28
N=959	2008	0.77	8.11	-1.15
N=973	2009	0.85	3.86	-1.58
N=956	2010	0.89	6.91	-2.33
(b) DBF				
N=778	2003	0.43	8.05	5.02
N=740	2004	0.63	10.96	7.01
N=840	2005	0.86	6.32	4.24
N=705	2006	0.56	6.48	2.41
N=874	2007	0.84	9.52	7.52
N=824	2008	0.83	6.35	2.10
N=975	2009	0.80	7.36	5.67
N=1002	2010	0.29	10.12	5.16

S IV

Pöyry, J., Böttcher, K., Fronzek, S., Gobron, N. Leinonen, R., Metsämäki, S., Virkkala, R. (2018). Predictive power of remote sensing versus. temperature-derived variables in modelling of herbivorous insects. *Remote sensing in Ecology and Conservation*, 4, 113-126.

Supplementary material

Supplementary figure S1. Locations of the moth monitoring trap sites that produced the phenological observations used in building the models.

Supplementary figure S2. Latitudinal gradient in timing of the peak flight period across the five focal species.

Supplementary figure S3. Two examples of timing of the peak flight periods of the focal moth species, snow melt-off dates (SMD), vegetation greening dates and dates of start (FSGS), peak (MD) and end (EGS) of the growing season derived from the FAPAR data. Both examples are from the year 2007, and situated in southern (Espoo) and northern (Kolari) part of Finland.

Supplementary figure S4. Model predictive power across the five focal species and different sets of explanatory variables.

Supplementary table S1. Pearson correlation coefficients among the explanatory variables for each focal species.

Supplementary table S2. Linear mixed effect models (LMM) fitted using randomly selected 70% of the phenological data using different sets of explanatory variables for the five focal species.
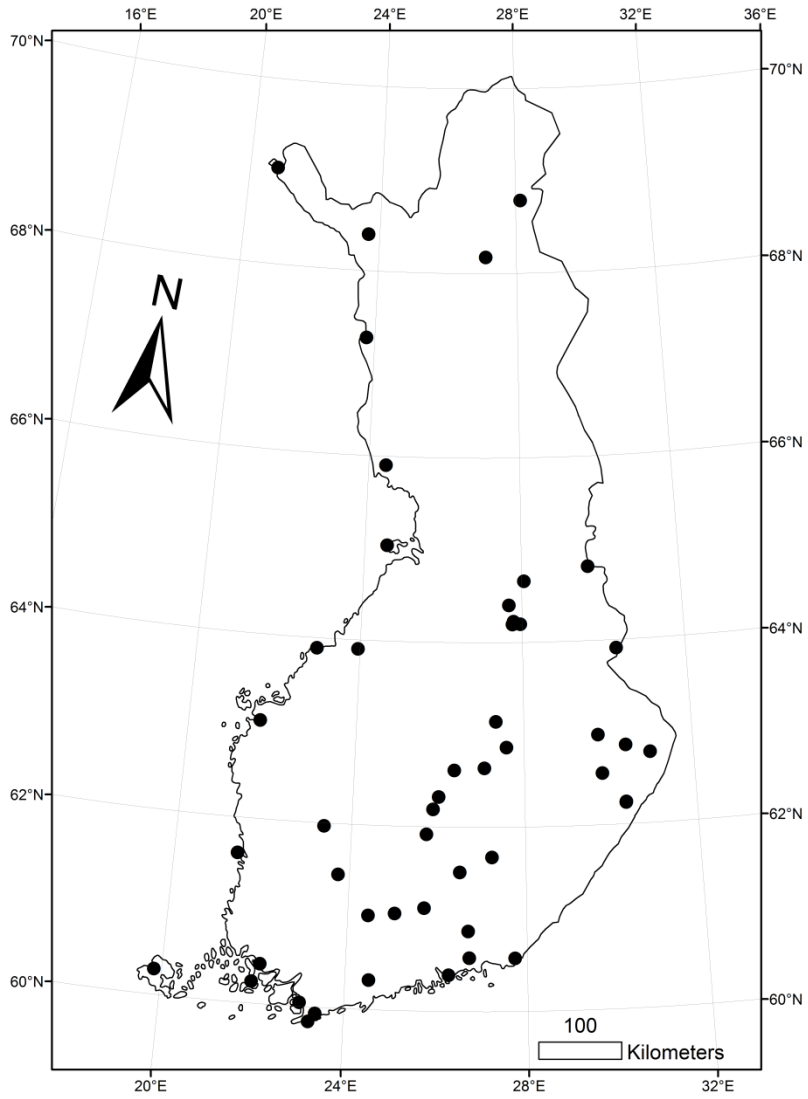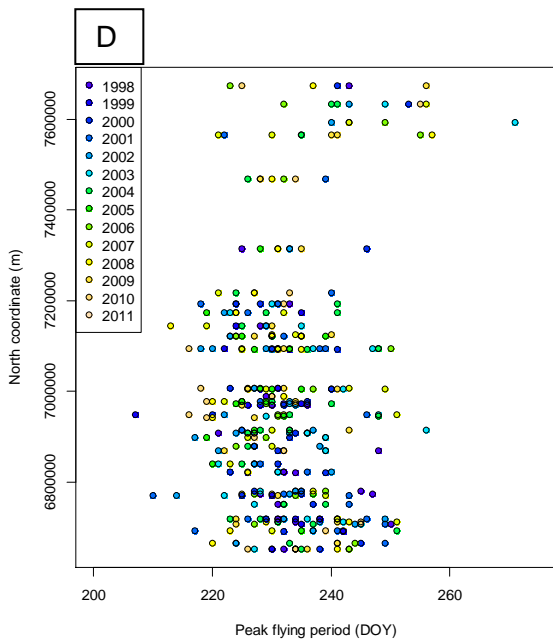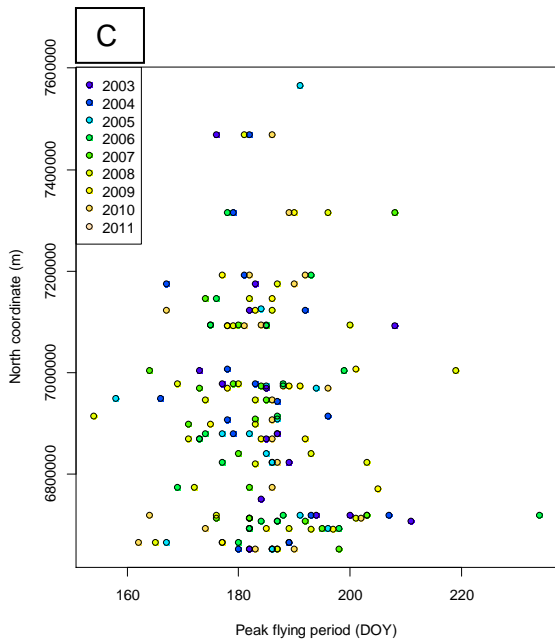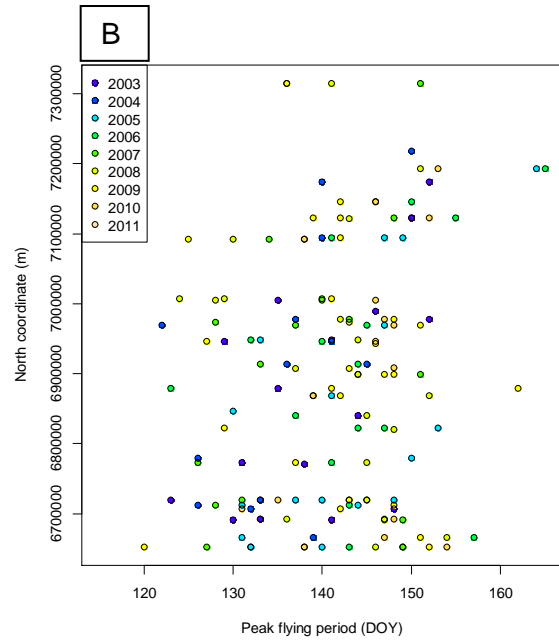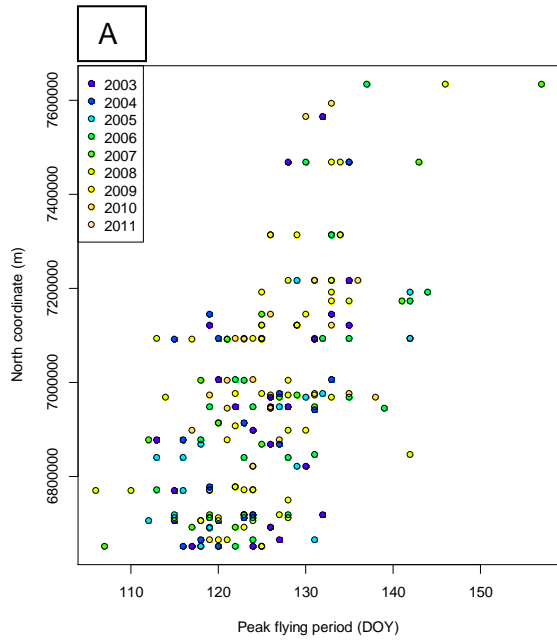
Fig. S1. Locations of the moth monitoring trap sites that produced the phenological observations used in building the models.
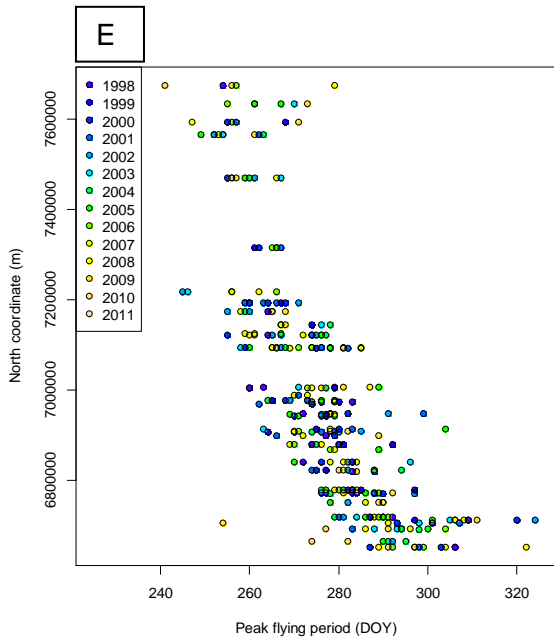
Fig. S2. Latitudinal gradient in timing of the peak flight period across the five focal species: (a) *Orthosia gothica*, (b) *Ectropis crepuscularia*, (c) *Cabera exanthemata*, (d) *Dysstroma citrata* and (e) *Operophtera brumata*. Dot colour depicts one year during the period 2003–2011. Data points included in each randomly selected 70% of the total data are shown. Peak flying period (DOY) depicts day of the peak flight period counted from the beginning of a year and North coordinate (m) depicts the latitude in metres according to the Finnish national uniform grid system (YKJ).
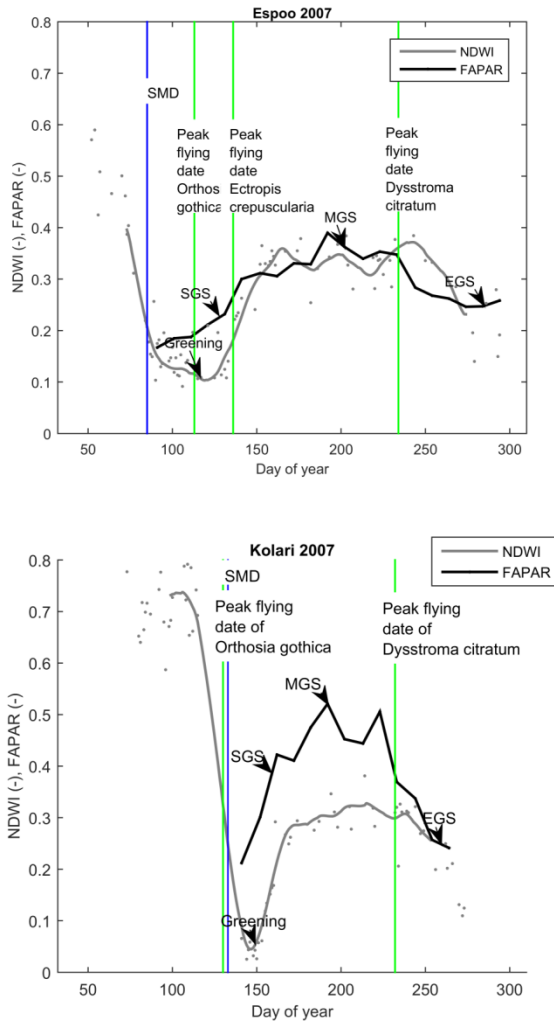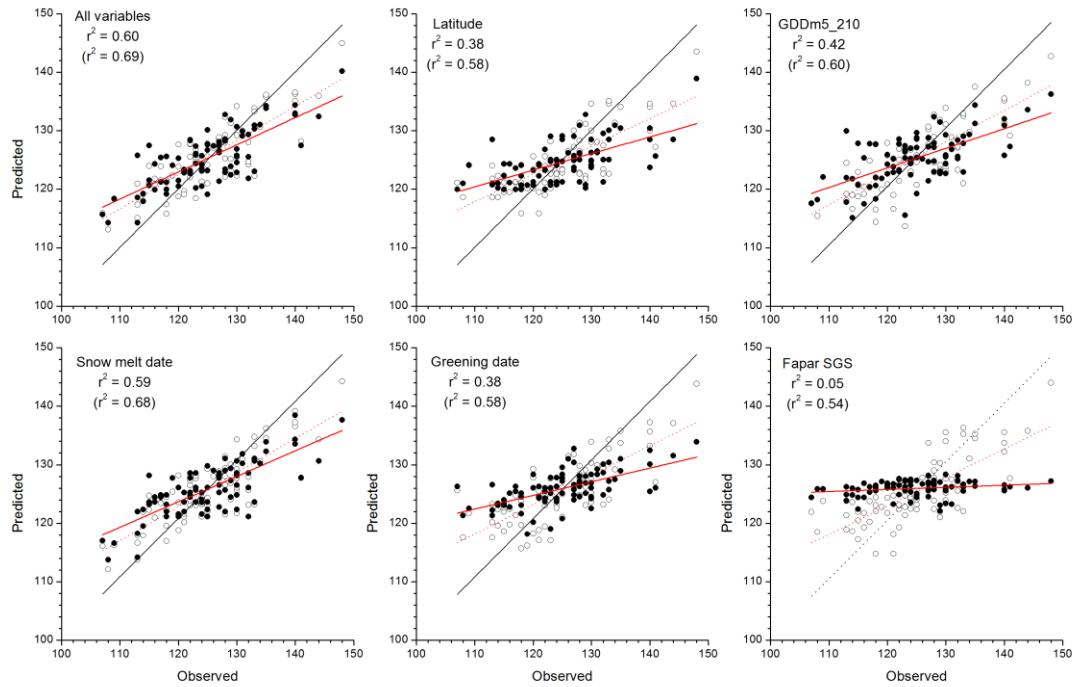
Fig. S3. Two examples of timing of the peak flight periods of the focal moth species, snow melt-off dates (SMD), vegetation greening dates and dates of start (FSGS), peak (MD) and end (EGS) of the growing season derived from the FAPAR data. Both examples are from the year 2007, and situated in southern (Espoo) and northern (Kolari) part of Finland.
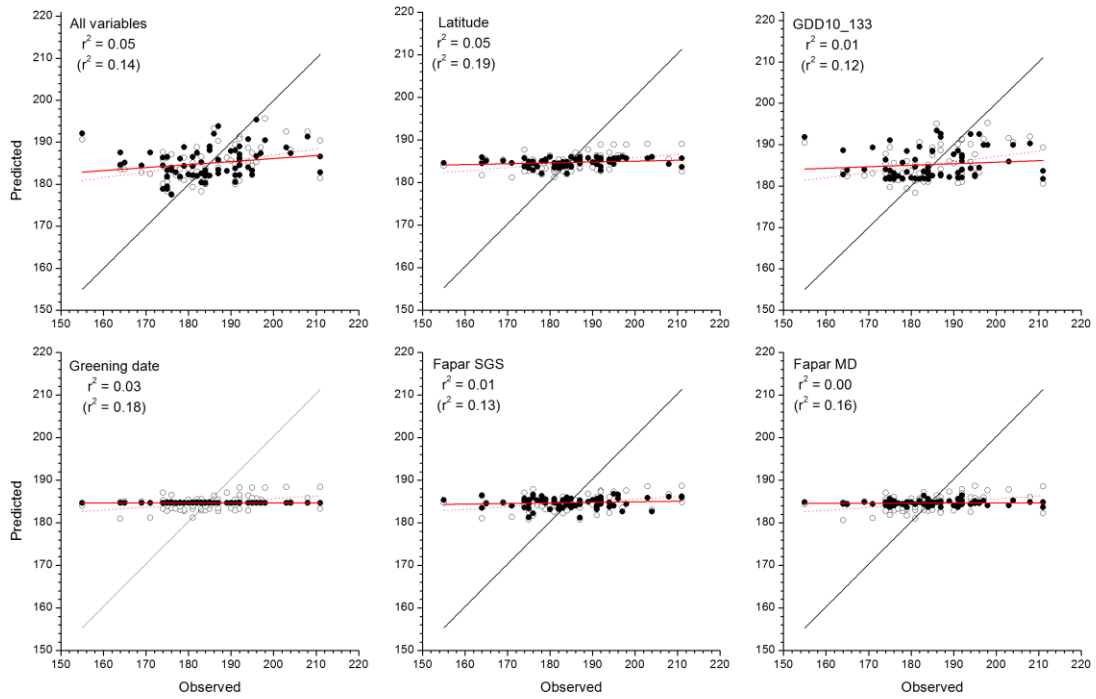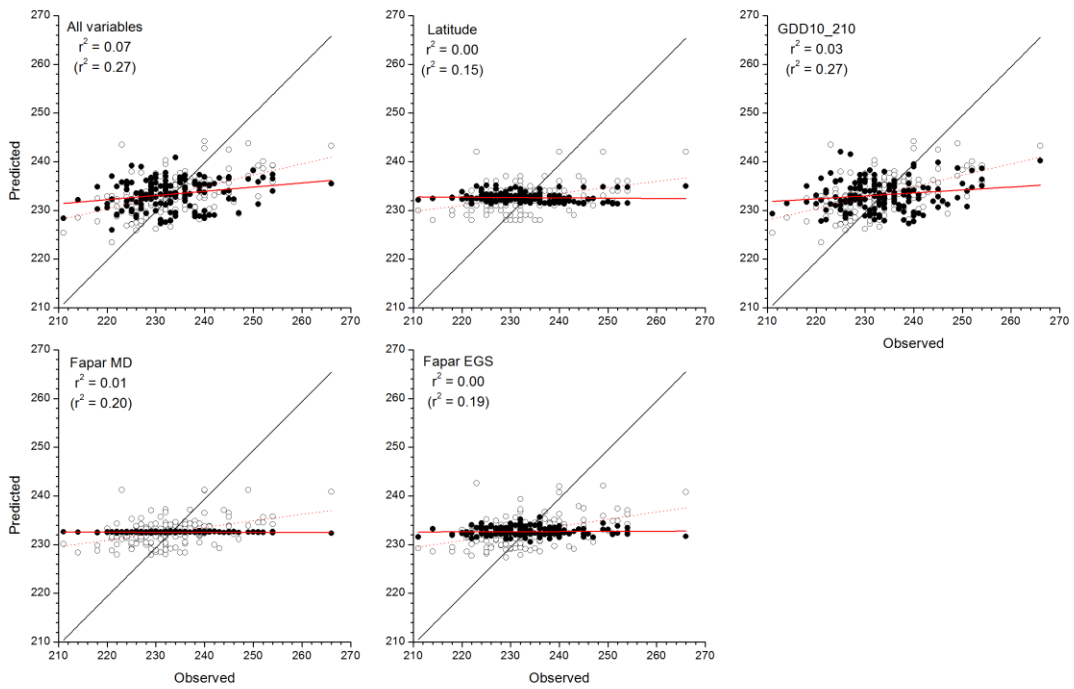
Orthosia gothica:

Ectropis crepuscularia:
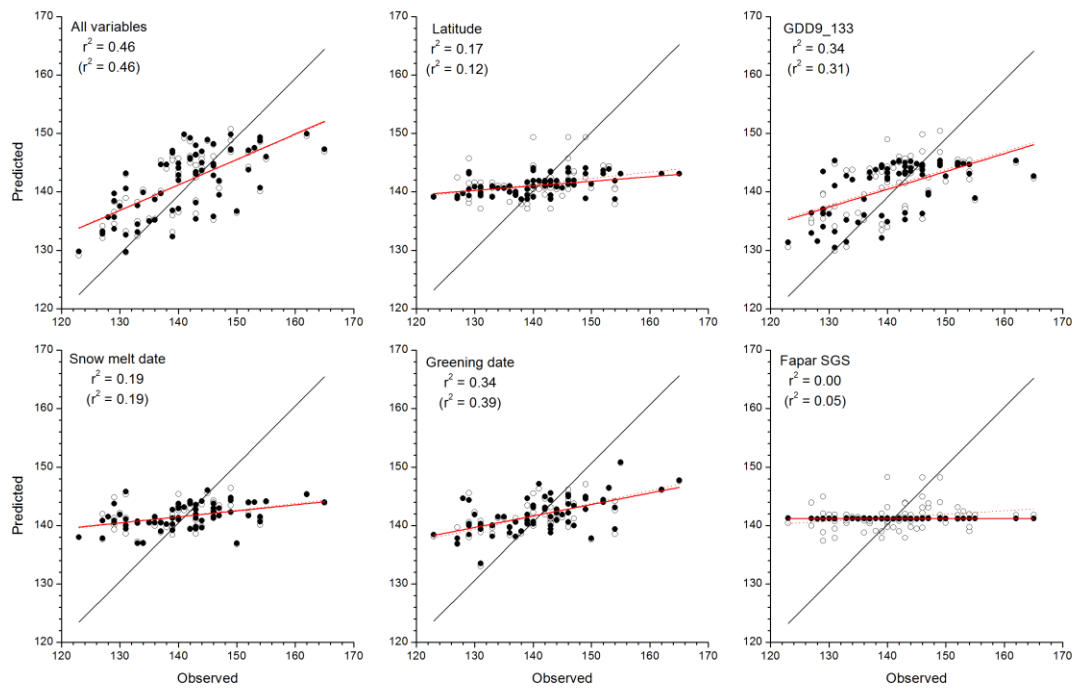
Cabera exanthemata:

Dysstroma citrata:
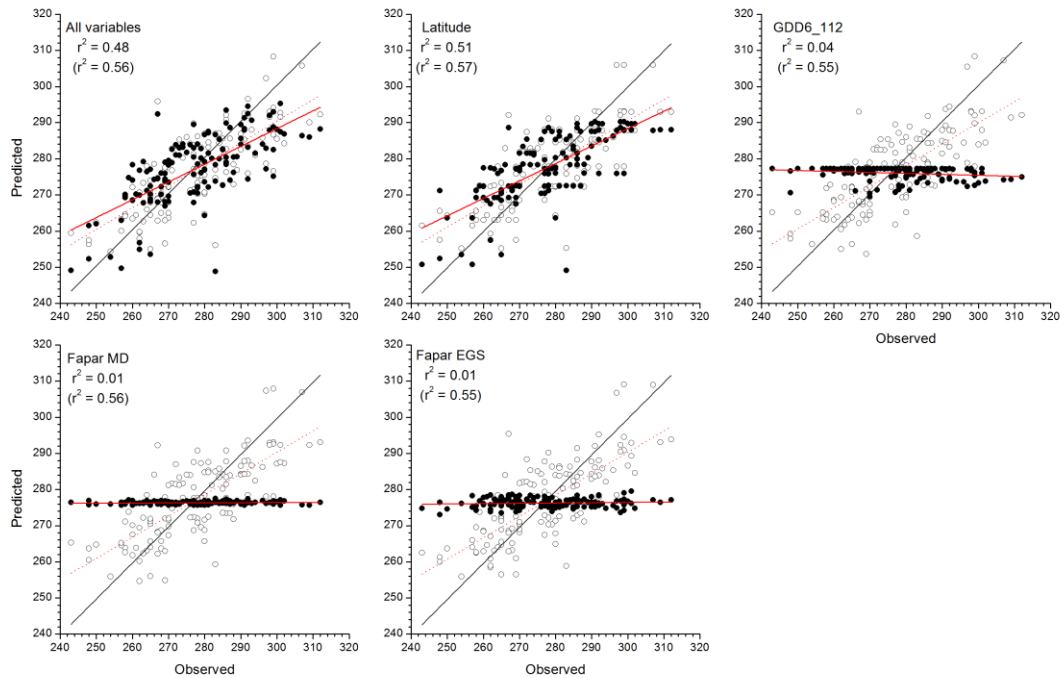
Operophtera brumata:

Fig. S4. Predictive power of linear mixed effect models (LMM) measured as r^2 in the randomly selected 30% of the data across the five focal species and different sets of explanatory variables: *Orthosia gothica*, *Ectropis crepuscularia*, *Cabera exanthemata*, *Dysstroma citrata* and *Operophtera brumata*. All panels show dots for observed vs. predicted values, with black dots excluding (i.e. average prediction where level = 0) and open dots including site location in predictions. Red solid lines and dotted lines depict the model fits when site location is excluded and included, respectively, and black line for the identity line y = x.

Table S1. Pearson correlation coefficients among the explanatory variables for each focal species.

Orthosia gothica:

	Latitude	GDDm5_210	Snow melt date	Greening date	FAPAR SGS
GDDm5_210	-0.852	1.000	-	-	-
Snow melt date	0.690	-0.803	1.000	-	-
Greening date	0.745	-0.809	0.767	1.000	-
FAPAR SGS	0.376	-0.350	0.231	0.207	1.000

Ectropis crepuscularia:

	Latitude	GDD9_133	Snow melt date	Greening date	FAPAR SGS
GDD9_133	-0.309	1.000	-	-	-
Snow melt date	0.607	-0.079	1.000	-	-
Greening date	0.673	-0.278	0.684	1.000	-
FAPAR SGS	0.339	-0.022	0.156	0.085	1.000

Cabera exanthemata:

	Latitude	GDD10_133	Greening date	FAPAR SGS	FAPAR MD
GDD10_133	-0.318	1.000	-	-	-
Greening date	0.698	-0.286	1.000	-	-
FAPAR SGS	0.440	-0.101	0.217	1.000	-
FAPAR MD	-0.038	0.109	0.018	0.012	1.000

Dysstroma citrata:

	Latitude	GDD10_210	FAPAR MD	FAPAR EGS
GDD10_210	-0.671	1.000	-	-
FAPAR MD	0.067	-0.146	1.000	-
FAPAR EGS	-0.019	-0.033	0.106	1.000

Operophtera brumata:

	Latitude	GDD6_112	FAPAR MD	FAPAR EGS
GDD6_112	-0.330	1.000	-	-
FAPAR MD	0.065	-0.058	1.000	-
FAPAR EGS	-0.020	-0.084	0.113	1.000

Table S2. Linear mixed effect models (LMM) fitted using randomly selected 70% of the phenological data using different sets of explanatory variables for the five focal species: *Orthosia gothica*, *Ectropis crepuscularia*, *Cabera exanthemata*, *Dysstroma citrata* and *Operophtera brumata*. Coefficients ± standard errors are shown for each model term and intercept.

Species	Total model (all variables)	Latitude (Lat)	Weekly accumulating growing degree days (GDD)	Snow melt date (SMD)	Greening date (GD)	Fapar start of growing season (FSGS)	Fapar maximum date (FMD)	Fapar end of growing season (FEGS)
Orthosia gothica[1]	$4.7*10^{-6}\pm3.4*10^{-6}$ * Lat - 0.009 ± 0.004 * GDDm5_210 + 0.244 ± 0.061 * SMD - 0.003 ± 0.060 * GD + 0.003 ± 0.035 * FSGS + 84.078 ± 30.922	$19.3*10^{-6}\pm2.8*10^{-6}$ * Lat - 8.687 ± 19.280	-0.022 ± 0.002 * GDDm5_210 $+170.307\pm4.897$	0.412 ± 0.040 * SMD $+79.080\pm4.594$	0.292 ± 0.046 * GD $+88.055\pm6.011$	0.095 ± 0.044 * FSGS $+112.634\pm6.353$	-	-
Ectropis crepuscularia[2]	$1.8*10^{-6}\pm5.2*10^{-6}$ * Lat - 0.264 ± 0.039 * GDD9_133 + 0.153 ± 0.082 * SMD + 0.230 ± 0.089 * GD - 0.018 ± 0.049 * FSGS + 182.746 ± 28.703	$9.9*10^{-6}\pm4.7*10^{-6}$ * Lat + 72.811 ± 32.240	-0.263 ± 0.038 * GDD9_133 $+145.370\pm0.948$	0.206 ± 0.067 * SMD $+118.182\pm7.488$	0.310 ± 0.067 * GD $+101.586\pm8.565$	-0.002 ± 0.060 * FSGS $+141.526\pm8.433$	-	-
Cabera exanthemata[3]	$-9.0*10^{-6}\pm6.7*10^{-6}$ * Lat + 0.270 ± 0.063 * GDD10_133 + 0.148 ± 0.103 * GD + 0.136 ± 0.070 * FSGS + 0.005 ± 0.032 * FMD +	$-4.7*10^{-6}\pm4.7*10^{-6}$ * Lat + 217.727 ± 32.632	0.268 ± 0.061 * GDD10_133 $+181.733\pm1.232$	-	0.001 ± 0.081 * GD $+184.535\pm10.573$	0.093 ± 0.063 * FSGS $+171.660\pm8.846$	0.025 ± 0.034 * FMD 179.866 ± 6.688	-

Dysstroma citrata[4]	204.691 ± 38.114 $-6.7*10^{-6}\pm2.9*10^{-6} * Lat -$ $0.040\pm0.006 * GDD10\_210 -$ $0.017\pm0.017 * FMD -$ $0.104\pm0.050 * FEGS -$ 323.901 ± 25.662	$3.8*10^{-6}\pm2.6*10^{-6} *$ $Lat +$ 206.387 ± 18.059	$0.025\pm0.002 * GDD$ $+171.240\pm4.720$	-	-	-	$-0.004\pm0.018 *$ FMD 233.287 ± 3.519	$-0.096\pm0.053 *$ $FEGS$ $+257.750\pm13.999$
Operophtera brumata[5]	$-42.2*10^{-6}\pm3.5*10^{-6} * Lat +$ $0.026\pm0.002 * GDD6\_112 +$ $0.019\pm0.018 * FMD +$ $0.130\pm0.054 * FEGS +$ 535.021 ± 28.767	$-40.2*10^{-6}\pm3.5*10^{-6}$ $* Lat +$ 557.379 ± 24.363	$-0.327\pm0.089 *$ $GDD6\_112$ $+277.307\pm1.905$	-	-	-	$0.016\pm0.019 *$ FMD 273.238 ± 4.057	$0.139\pm0.057 *$ $FEGS$ $+239.733\pm15.288$

Weekly accumulating GDD-parameters: [1]GDDm5_210, [2]GDD9_133, [3]GDD10_133, [4]GDD10_210 and [5]GDD6_112. For example, GDDm5_210 means GDD calculated using base temperature of -5 °C for the week starting on day 210.

Eidesstattliche Erklärung / *Declaration under Oath*

Ich erkläre an Eides statt, dass ich die Arbeit selbstständig und ohne fremde Hilfe verfasst, keine anderen als die von mir angegebenen Quellen und Hilfsmittel benutzt und die den benutzten Werken wörtlich oder inhaltlich entnommenen Stellen als solche kenntlich gemacht habe.

I declare under penalty of perjury that this thesis is my own work entirely and has been written without any help from other people. I used only the sources mentioned and included all the citations correctly both in word or content.

26.06.2019

Datum / Date

Unterschrift des Antragstellers / *Signature of the applicant*

CURRICULUM VITAE

Name:	Kristin Böttcher
Postal address:	Finnish Environment Institute
	Latokartanonkaari 11
	00790 Helsinki
	Finland
E-Mail	Kristin.Bottcher (at) environment.fi

EDUCATION

04/2013 – 12/2018	Doctoral student at Martin Luther University Halle Wittenberg, Institute of Geosciences and Geography, Department Remote Sensing and Thematic Cartography, Halle (Germany)
10/1993 – 09/2000	Studies of Geoecology at Potsdam University (Germany) Specialisation in Biology and Remote Sensing / Geographic Information Systems

SCIENTIFIC CAREER

since 05/2009	Research scientist at the Finnish Environment Institute, Helsinki (Finland)
10/2004 – 04/2009	Scientific/ technical project officer at the Joint Research Centre of the European Commission, Institute for Environment and Sustainability, Ispra (Italy)
04/2004 – 07/2004	Marie Curie Fellowship at Nottingham University, Environmental Sciences, Nottingham (United Kingdom)
01/2001 – 07/2003	Research associate at Martin Luther University Halle Wittenberg, Institute of Geography, Halle (Germany)